



OPERATIONAL METHODS FOR THE ASSESSMENT AND MANAGEMENT OF AGING INFRASTRUCTURE

Pietro Croce, Milan Holický et al.





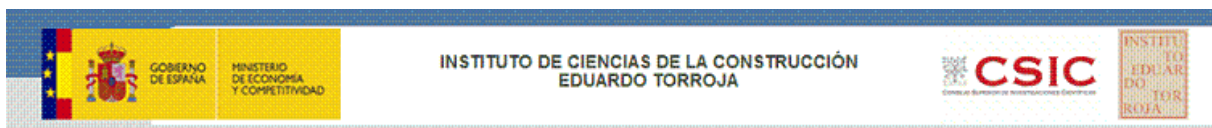
OPERATIONAL METHODS FOR THE ASSESSMENT AND MANAGEMENT OF AGING INFRASTRUCTURE

Editors:

Pietro Croce, University of Pisa, Department of Civil and Industrial Engineering
Milan Holický, Czech Technical University in Prague, Klokner Institute

Authors:

Milan Holický, Czech Technical University in Prague, Klokner Institute
Miroslav Sýkora, Czech Technical University in Prague, Klokner Institute
Dimitris Diamantidis, Ostbayerische Technische Hochschule Regensburg
Peter Tanner, E. Torroja Institute of Construction Sciences, CSIC, Madrid
Ana de Diego, E. Torroja Institute of Construction Sciences, CSIC, Madrid
Carlos Lara, E. Torroja Institute of Construction Sciences, CSIC, Madrid
Miguel Prieto, E. Torroja Institute of Construction Sciences, CSIC, Madrid
Ramon Hingorami, E. Torroja Institute of Construction Sciences, CSIC, Madrid
Antonio Menéndez Ondina, Civil Engineering School, Univ. Of Granada
Pietro Croce, University of Pisa, Department of Civil and Industrial Engineering
Raffaello Bartelletti, University of Pisa, Department of Civil and Industrial Engineering
Maria Luisa Beconcini, University of Pisa, Department of Civil and Industrial Engineering
Paolo Formichi, University of Pisa, Department of Civil and Industrial Engineering
Francesca Marsili, University of Pisa, Department of Civil and Industrial Engineering
Martina Muzzi, University of Pisa, Department of Civil and Industrial Engineering
Elisa Rosso, University of Pisa, Department of Civil and Industrial Engineering
Selcuk Toprak, Pamukkale University, Denizli
Mehmet Inel, Pamukkale University, Denizli
Cem Koc, Pamukkale University, Denizli
Engin Nacaroglu, Pamukkale University, Denizli
Sevket M. Senel, Pamukkale University, Denizli



This project has been funded with support from the European Commission.
This publication [communication] reflects the views only of the author, and the Commission cannot be held responsible for any use which may be made of the information contained therein.

**OPERATIONAL METHODS FOR THE ASSESSMENT
AND MANAGEMENT OF AGING INFRASTRUCTURE**

ISBN: 978-88-8250-147-1

Edited by:

Pietro Croce, University of Pisa, Department of Civil and Industrial Engineering
Milan Holický, Czech Technical University in Prague, Klokner Institute

Published by:

Tipografia editrice Pisana snc

Pages: 186

Printed by:

Tipografia Editrice Pisana snc

Via Trento, 26

56126 Pisa

tel. +39 050 503526

info@tepsnc – www.tepsnc.it

1st edition

FOREWORD

The Leonardo da Vinci Project, “Innovation Transfer in Risk Assessment and Management of Aging Infrastructures”, CZ/13/LLP-LdV/TOI/134014, addresses the urgent need to train students, young engineers and professionals in the assessment of existing infrastructures. The future of the construction industry lies in moving from new constructions towards the maintenance, repair and rehabilitation of existing structures, particularly of aging infrastructures. Risk management consisting of risk assessment and risk control of existing structure therefore plays thereby an important role.

The assessment of existing infrastructures is an imperative issue of great economic significance in most countries around the world, as more than 50 % of all construction activities concerns existing buildings, bridges and other civil engineering works. At present, the Eurocodes which will be used in all CEN Member countries are primarily focused on the design of new structures. Additional operational rules for existing structures are still missing. The international standard ISO 13822 provides only general principles for the assessment of existing structures which should be further developed for their effective operational use in practice.

The overall procedure of risk management of aging infrastructures is therefore an urgent issue of great economic significance in most countries around the world. This is primarily caused due to the fact that many infrastructures are affected by action effects, fatigue and environmental influences, and inevitably deteriorate. Moreover, available resources for the maintenance, repair or possible replacement of infrastructures are always limited. Typical questions and problems which must be solved in this context can be summarized as follows:

- What is the current state of a particular infrastructure?
- What is an acceptable level of the relevant risk?
- Which aspects are critical to sustainable performance?
- What is the optimum life-cycle cost?
- What is the best long-term funding strategy?

The proposed project highlights the above problems and focusses also on vocational training in risk management and assessment of aging infrastructure in the partner countries (CZ, DE, ES, IT and TR).

The current project addresses the urgent need for practical implementation of principles of the management and risk assessment of existing infrastructures in all the partner countries. The project is supported by the Czech Chamber of Chartered Engineers (ČKAIT). The project consortium, under the leadership of the Klokner Institute of the Czech Technical University in Prague (KI CTU), consists of five other partners, including research institutions and universities from three EU Member States (DE, ES, IT) as well as one associated country (TR), and also the Secondary Technical School of Civil Engineering in Ceske Budejovice (CZ). All researchers within the partnership are involved in research projects dealing with reliability assessment of existing structures. They participate in the national and international standardization activities within the international organizations CEN (European Committee for Standardisation) and ISO (International Standardization Organisation).

The project outcomes consist of vocational training materials based on international research and relevant standard committee’s activities, and on the significant experience gained from case studies, and on selected results obtained from the previous projects of the Leonardo da Vinci programme. In particular, the experience gained by the partners of the present consortium from the completed project on vocational training related to assessment of existing structures is utilized. Available innovations are transferred to undergraduate and graduate students, practising engineers

and local government representatives. The developed training materials are of practical use in offering illustrative examples and several case studies.

All the project outcomes are based on documents of the international research organization, Joint Committee on Structural Safety JCSS and international research projects, selected outcomes of the previous project of the Leonardo da Vinci programme (developed by five partners of the present consortium in 2013-2015) and also on background documents to the new European and international standards.

Particular outcomes of the proposed project include practical handbooks, software tools, web-sites, e-learning, courses and seminars organized in the partners' home countries. The project outcomes will also be offered to other European countries through code committees work, lectures and the project web-sites. It is foreseen that the outcomes being used by engineers, designers, technicians, and representatives of public authorities involved in planning and management will have an impact on the risk-based management of infrastructures.

One of the important project outcomes is the present Handbook 2 "Operational Methods for the Assessment and Management of Aging Infrastructure", which is focussed on operational techniques for the assessment of aging infrastructures supplemented by illustrative case studies developed according to ISO 13822 and Eurocodes for different structures and materials. From the mentioned project also result Handbook 1, where general procedures of risk-management and assessment of aging infrastructures are presented, and Handbook 3, where operational techniques for the assessment of aging infrastructures supplemented by illustrative case studies are presented with a more basic approach.

Handbook 2 consists of eleven chapters. Chapter 1 gives a brief introduction. Chapter 2 summarizes current applicable standards and codes for existing structures. Chapter 3 reviews survey methods. The remaining chapters are devoted to the illustration of relevant case studies, referring to the assessment of different existing infrastructures. In particular, chapter 4 refers to a commercial building, chapter 5 to a r.c. building damaged by corrosion, chapter 6 to silos, chapter 7 to pipelines and water supply systems, chapter 8 to tanks, chapter 9 to historical aqueducts, chapter 10 to bridges and chapter 11 to dams and flood protection systems. In each case studies the entire procedure of the assessment is illustrated step by step emphasizing references to relevant Codes and in particular to ISO 13822.

It is believed that the material of this handbook is presented in an understandable way, referring to several case studies. A number of references mentioned in each chapter provide additional background materials, further guidance and information useful to widen the significance and the field of application of the assessment methods illustrated for each case study.

Pisa and Prague, 2015

CONTENTS

CHAPTER 1: AIMS AND SCOPE	1
1 INTRODUCTION	1
2 AIMS AND SCOPE	1
REFERENCES	2
CHAPTER 2: CODES AND STANDARD	3
1 INTRODUCTION	3
2 HISTORICAL DEVELOPMENT OF STANDARDS	3
3 REQUIREMENTS AND POSSIBLE CONTENTS FOR AN ASSESSMENT CODE	4
4 EXAMPLE GUIDELINES AND STANDARDS	6
4.1 JCSS Recommendations	6
4.2 ISO standards	7
4.3 Other standards	6
5 CURRENT CODE AND GUIDELINE DEVELOPMENTS	8
6 VERIFICATION	8
7 CONCLUSIONS	10
REFERENCES	10
CHAPTER 3: SURVEY METHODS	13
1 INTRODUCTION	13
2 DETERMINATION OF DETERIORATION MODEL PARAMETERS	14
2.1 Corrosion parameters in reinforced concrete structures	14
2.1.1 Overview	14
2.1.2 Corrosion rate	14
2.1.3 Electrical resistivity	15
2.1.4 Potential	17
2.1.5 Environmental parameters	18
2.2 Detection and evaluation of other chemical attacks	19
2.2.1 Sulfate attack	19
2.2.2 Alkali-aggregate reaction	20
2.3 Structural surveys with ground penetrating radar	23
2.3.1 System description	23
2.3.2 Applications	24
2.3.3 Advantages and drawbacks compared to conventional techniques	25
3 REMOTE MONITORING AND CONTROL OF INFRASTRUCTURES	25
3.1 Overview	25
3.2 Remote radar interferometric measurement of displacement and vibrations	25
3.2.1 System description	25
3.2.2 Applications	26
3.2.3 Advantages and drawbacks compared to conventional techniques	27
4 DETECTION AND EVALUATION OF FATIGUE DAMAGE	27
4.1 Overview	27

Contents

4.2	Weigh-in-motion measurements	28
5	FINAL REMARKS	30
	REFERENCES	31

CHAPTER 4: STRUCTURAL FAILURE AND ASSESSMENT OF A DEPARTMENT STORE 35

1	INTRODUCTION	35
2	DESCRIPTION OF THE STRUCTURE	35
3	PERFORMANCE DEFECTS	36
4	ASSESSMENT	38
5	REPAIR	38
6	PUBLIC PERCEPTION	39
7	THEORETICAL MODEL OF PUBLIC PERCEPTION	39
8	EFFECTS OF EXPECTED CONSEQUENCES	41
9	CONCLUSIONS	42
	REFERENCES	42

CHAPTER 5: ASSESSMENT OF A CORROSION-DAMAGED REINFORCED CONCRETE STRUCTURE 45

1	INTRODUCTION	45
2	ASSESSMENT PROCEDURE	46
3	BASIS FOR EXAMINATION	47
3.1	Partial factor format for assessment	47
3.2	Load bearing capacity of corrosion-damaged structures	48
3.2.1	General	49
3.2.2	Resistance models	49
4	FIRST STAGE OF THE EVALUATION	49
4.1	Information	49
4.2	Updating of material strength	49
4.2.1	General	49
4.2.2	Concrete	50
4.2.3	Reinforcing steel	52
4.2.4	Updating of partial factors	52
4.3	Structural analysis and verification	53
4.4	Recommendations	54
5	SECOND STAGE OF THE EVALUATION	54
5.1	Improved information	54
5.2	Updating of material strength	55
5.2.1	General	55
5.2.2	Concrete	56
5.2.3	Reinforcing steel	56
5.2.4	Updating of partial factors	57
5.3	Structural analysis and verification	57
6	CONCLUDING REMARKS	58
	REFERENCES	58

CHAPTER 6: SILOS - A CASE STUDY	61
1 INTRODUCTION	61
2 THE AGRICULTURAL CONSORTIUM SILO IN GROSSETO	62
3 PRELIMINARY ASSESSMENT	64
3.1 Study of the available documentation.	64
3.2 Decision on immediate actions	66
4 DETAILED ASSESSMENT	66
4.1 Detailed documentary search and review	66
4.2 Detailed visual inspection	66
4.2.1 Ground Floor	68
4.2.2 Longitudinal Section BB'	71
4.2.3 The main façade survey	74
4.3 Structural analysis	77
4.3.1 Determination of actions	77
4.3.2 Stresses evaluation	80
4.4 Determination of properties of the structure	81
6 CONCLUSIONS	81
REFERENCES	82
ANNEX A - CALCULATION OF PRESSURES AND STRESSES IN THE SILO	83
A.1 DATA	83
A.2 EVALUATION OF THE PRESSURES	83
A.3 EVALUATION OF STRESSES	85
CHAPTER 7: PIPELINES AND WATER SUPPLY	89
1 INTRODUCTION	89
2 DENIZLI WATER SUPPLY SYSTEM	90
2.1 Introduction to Water Supply System of Denizli	90
2.2 Assessment of the Water Distribution System	91
2.3 Reviewing Network Operational Practices	92
2.3.1 Quantifying Water Loss	92
3 WATER BALANCE AND REPLACEMENT PROGRAM	93
3.1 The Water Balance	93
3.2 Replacement Program	94
4 CONCLUSIONS AND RECOMMENDATIONS	96
REFERENCES	97
CHAPTER 8: WATER TANKS – A CASE STUDY	99
1 INTRODUCTION	99
2 DESCRIPTION OF THE STRUCTURE	100
3 THE EXPERIMENTAL TEST CAMPAIGN	103
4 STRUCTURAL MODELING	108
4.1 Actions modelling	109
4.2 FEM model identification	111
4.3 Discussion about experimental and numerical values	110
6 CONCLUSIONS	111
REFERENCES	112

CHAPTER 9: AQUEDUCTS – A CASE STUDY	113
1 INTRODUCTION	113
2 PRELIMINARY ASSESSMENT	114
2.1 Study of available documentation. A brief history	114
2.2 Preliminary inspection	116
2.3 Preliminary checks	119
2.4 Decision on immediate actions and recommendations for detailed assessment	121
3 DETAILED ASSESSMENT	121
3.1 Detailed documentary search and review of accidental actions	122
3.2 Detailed inspection	123
3.2.1 Deteriorations and cracks classification	123
3.2.2 The survey of the Medicean Aqueduct	128
4 STRUCTURAL ANALYSIS	129
4.1 The case study	130
4.2 Characteristics of the models: properties of materials and soil	131
4.3 Evaluation of actions	132
4.4 Global analyses	134
4.4.1 Implemented model	134
4.4.2 Static analysis	135
4.4.3 Dynamic analysis	136
4.4.4 Seismic analysis	136
4.4.5 Soil-structure interaction and second order effects	138
4.5 Local analyses	140
4.5.1 Case A)	142
4.5.2 Case B): evaluation of the stabilizing forces	144
4.5.3 Case C)	144
5 CONCLUSIONS	146
REFERENCES	146
ANNEX A - MECHANICAL PROPERTIES OF STRUCTURAL MATERIALS	148
ANNEX B - ELASTIC RESPONSE SPECTRA	149
ANNEX C - SEISMIC VERIFICATIONS	150
ANNEX D - KINEMATIC ANALYSIS	151
D.1 INTRODUCTION	151
D.2 TYPES OF ANALYSIS AND BASIC ASSUMPTIONS	152
D.3 LINEAR KINEMATIC ANALYSIS	153
D.4 NON-LINEAR KINEMATIC ANALYSIS	153
D.5 CAPACITY CURVE	154
D.6 SAFETY VERIFICATIONS	155
ANNEX E - EVALUATION OF SOIL-STRUCTURE INTERACTION AND SECOND ORDER EFFECTS	157
E.1 MOMENT-CURVATURE DIAGRAMS	157
E.2 CALCULATION OF THE DEFORMED CONFIGURATION	158
E.3 DETERMINATION OF THE CAPACITY CURVE	158
ANNEX F - EVALUATION OF STABILIZING FORCES	160

CHAPTER 10: COLLAPSE OF THE RIVER VERDE VIADUCT SCAFFOLDING SYSTEM	163
1 INTRODUCTION	163
2 RIVER VERDE VIADUCT	163
3 THE MOVABLE SCAFFOLDING SYSTEM	164
4 THE ACCIDENT	165
5 EVALUATION PROCEDURE	166
6 QUALITATIVE RISK ANALYSIS	167
6.1 Situation	167
6.2 Hazard identification	167
6.3 Inspections, tests and analyses	168
6.4 Hazard classification	169
6.5 Hazard scenarios	170
7 QUANTITATIVE ASSESSMENT	171
8 CONCLUSIONS	172
REFERENCES	172
CHAPTER 11: PREDICTING FLOODS AND DAMAGE TO INFRASTRUCTURES	175
1 INTRODUCTION	175
2 STATISTICAL MODELING	177
2.1 Statistical evaluation of annual maximum flows	177
2.2 Probabilistic models	178
2.3 Parameter estimation	178
3 ESTIMATION OF EXTREMES	179
4 CAUSES OF STRUCTURAL FAILURES	180
5. RISK-BASED IMPLEMENTATION OF SAFETY MEASURES	183
6 CONCLUSIONS AND RECOMMENDATIONS	185
REFERENCES	185

CHAPTER 1: AIMS AND SCOPE

¹Pietro Croce

¹Department of Civil and Industrial Engineering – Structural Division – Univ. of Pisa, Italy

Summary

This chapter deals with introduction, aims and scope of the present Handbook 2, which is one of the outcomes of Leonardo da Vinci Project, “Innovation Transfer in Risk Assessment and Management of Aging Infrastructures”, CZ/13/LLP-LdV/TOI/134014.

1 INTRODUCTION

The present Handbook 2, which is one of the outcomes of Leonardo da Vinci Project, “Innovation Transfer in Risk Assessment and Management of Aging Infrastructures”, CZ/13/LLP-LdV/TOI/134014, is composed of eleven chapters and it is dedicated to the illustration of operational techniques for the assessment of aging infrastructures.

In the following the operational methods for the assessment of existing structures are illustrated in detail, referring to several case studies, where practical application of general procedures of risk-management and assessment of aging infrastructures illustrated in Handbook 1 [1] is explained in detail, systematically referring to relevant Codes and documents concerning existing structures [2], [3], [4].

The relevant case studies cover a wide field of existing infrastructures, spanning from industrial and commercial buildings to silos, tanks, pipelines, water supply systems, aqueduct, bridges and dams and water protection systems.

Since the preservation of cultural heritage is one of the most relevant challenge in the field of existing structures, in the choice of case studies, a particular attention have been devoted to heritage infrastructures.

2 AIMS AND SCOPE

The aims and scope of the Handbook is to provide designers with a general methodology for the assessment of existing structures, which is illustrated step by step, referring to the selected case studies.

The case studies have been chosen not only in order to cover as much as possible the actual variety of infrastructures and materials, but also different building periods, from the sixteenth century to the most recent past. In this way, it is possible to consider structures designed according to different approaches; in fact, while recent structures have been designed according to Codes, Standards, Guidelines or theoretical models, the most ancient ones have been designed according to empirical rules or architectural canons, therefore the understanding of original design ideas often requires that survey and in-situ measurements and investigations are supplement with historical studies.

In the presentation of case studies, beside the reference to the general procedures provided by modern Codes and ISO 13822 in particular, the above mentioned necessity of understanding original design ideas and the significance of the engineering judgement in the diagnosis of the structural decays are emphasized, aiming to communicate to the reader a correct way to approach existing structures.

The references mentioned in each chapter provide additional background materials, further guidance and information, allowing to widen the significance and the field of application of the assessment methods illustrated for each case study.

REFERENCES

- [1] Holický M., Diamantidis D. (eds.), *Methods for the risk assessment and risk based managements of aging infrastructures*, CTU Prague, 2014, ISBN: 978-80-01-05611-0.
- [2] International Standards Organization (ISO), 2003, Bases for design of structures – Assessment of existing structures, ISO 13822, corrected version.
- [3] ISO (International Standards Organization) 2394, General principles on reliability for structures, 1998.
- [4] Joint Committee on Structural Safety (JCSS), *Assessment of Existing Structures*, RILEM Publications S.A.R.L., 2000

CHAPTER 2: CODES AND STANDARDS

Dimitris Diamantidis¹

¹OTH Regensburg, Germany

Summary

This chapter deals with current standards for existing infrastructures. The historical development of standards is briefly provided first. Safety aspects for existing structures as described in national and international standards and guidelines are summarized and prenormative research is presented and reviewed. Recent developments are discussed together with concepts for verification.

1 INTRODUCTION

This chapter deals with current standards for existing infrastructures. In discussing codification related to existing infrastructures it appears useful and practical to distinguish between:

- prenormative research including for example code committee work, documents of international associations or organizations;
- guidelines and recommendations in use;
- code type documents.

Prenormative research has been performed within various scientific groups and committees dealing in general with the reassessment of existing structures or in countries subjected to earthquake actions focusing on safety of existing structures subjected to earthquake.

Guidelines and internationally accepted standards have been also developed on assessment of existing structures and will be described in more detail herein. The typical difference between a code and a guideline is that a code provides minimum requirements on the structural assessment, while guidelines give information on generally how to carry out a structural assessment or reassessment. These type of documents have been developed in many countries and for many categories of structures such as bridges, towers or normal buildings and also requirements associated to particular aspects such as seismic parameters remodeling and so on. For example in the USA, Canada, Switzerland, UK such guidelines have been prepared at a relatively detailed level. However at present only a few countries have a general applicable and real and direct code type document for the assessment of existing structures.

A historical development of the codes in general is given in section 2. Requirements and contents of standards are summarized in section 3. Prenormative research and standards such as ISO-standards are summarized in section 4. Developments are outlined in section 5. Finally conclusions are given in section 6.

2 HISTORICAL DEVELOPMENT OF STANDARDS

Standards provide the basis of good engineering practice and a framework of implementing safety in design rules. Until the 1960s, the safety criteria in standards were mainly based on allowable stress principles. Developments in computation methods and material technology as well as a number of structural damages led to a new philosophy of structural design in the USA, Canada and Europe. Conditions i.e. limit states that affect the performance of the structure were

defined and safety was implemented through the LFD (Load Factor Design) and later LRFD (Load and Resistance Factor Design) in the USA and Canada or through the similar partial safety factor method in Europe. The significant developments were manifested in a number of documents, standards and guidelines (NKB, [3] NaBau, [4] and later ISO [5] or the work by the JCSS [6]).

In the late 1990s a global concept for checking the structure was based on PBD (Performance Based Design) as opposed to Prescriptive design rules, leading to more freedom for the designer. This approach was particularly strongly developed in the USA in relation to seismic design.

The Eurocodes [1,2] coming now into power in many countries in as well as outside the European Union highlight advanced concepts for the design of civil engineering works, the most important being durability, reliability, robustness. The concepts are defined in EN 1990 [1]. The method behind has been developed in the last 20 to 30 years and includes reliability of members and systems as well as time dependent reliability. The basic reliability measures are thereby the probability of failure and reliability index as described for example in [2, 3, 4,]. In general the following advantages of the use of the Eurocodes have been stated [5,6]:

- Reliability of structural members and of the whole structure reflected in its robustness are major issues in the Eurocodes and are treated with specific provisions, which are based on modern risk analysis and risk appraisal criteria.
- A reliability class differentiation scheme is proposed in the Eurocodes with basically three different reliability classes. A measure of reliability is the probability of failure or the associated reliability index, which depends on the reliability class (type of structure, consequences of failure).
- Reliability in design (limit state design) is reflected through the design values of the design parameters and consequently through the partial safety factors and characteristic values for load and resistance parameters.
- Limit state design is based on the consideration of local and not global failure, since design equations are usually defined and applied on a local level only. The global reliability i.e. the reliability against collapse of the entire system is treated in the robustness requirements.
- Robustness requirements and associated design rules are given in the Eurocodes. Risk analyses are recommended for important structures associated to high consequences of failure.

Figure 1 shows the procedure adopted for the performance of risk analysis in the Eurocodes.

3 REQUIREMENTS AND POSSIBLE CONTENTS FOR AN ASSESSMENT CODE

The aforementioned codes deal mainly with new structures and the inherent reliability of those. The safety evaluation of existing structures and infrastructures may differ depending upon the type of structure, the reason for re-evaluation etc. Important requirements for a code related to the assessment of existing structures are [9]:

- Applicability: the code should be applicable to typical assessment cases.
- Compatibility to codes for new structures: the code should use the same philosophy as current codes for new structures (limit state analysis, safety factor format etc).
- Flexibility: the code should be flexible to include additional information gained by inspection.
- Ease of use: the code should be understandable to engineers and easy to use in practice.

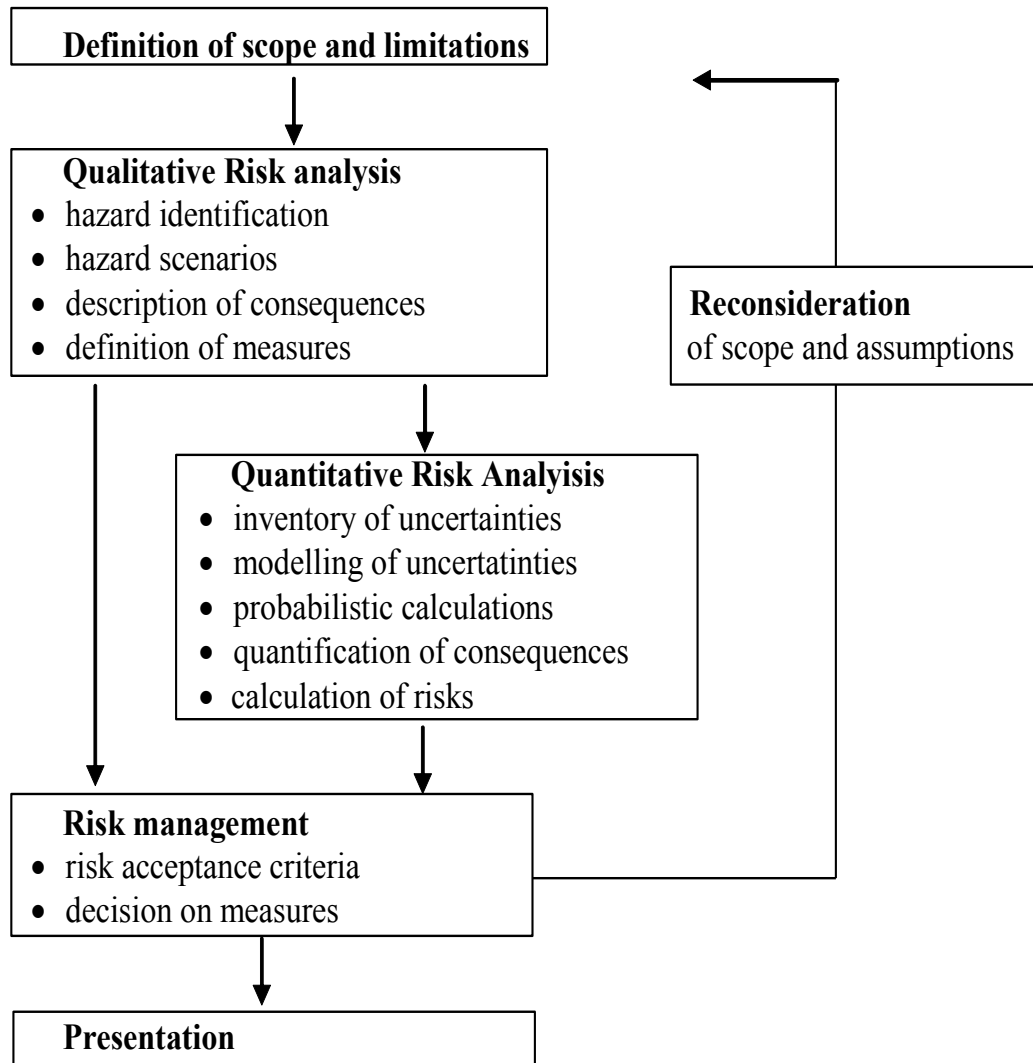


Figure 1. Risk analysis procedure as given in the Eurocodes

Some recommendations on the content of a code on assessment of existing structures are briefly described next:

The code should be applicable in the following characteristic cases:

- changes in the load-carrying (structural) system;
- change in the utilization of the structure (change of use);
- extension of the planned working life;
- deterioration and/or damage;
- reliability of the structure in doubt;
- inadequate serviceability.

Analysis and assessment of an existing structure shall be based on the same general principles as provided by current standards for the design of new structures. Older codes valid in the period when the original structure was designed, or based on other principles, should be used only as guidance documents.

Currently applied limit state formulations for the specified hazard scenarios should provide the basis for reassessment criteria. Limit states are basically classified as for design purposes in two categories:

- Ultimate Limit States (ULS), which concern the maximum load carrying capacity of the structure.
- Serviceability Limit States (SLS), which concern the normal use of the structure.

For the description and the formulation of the limit states the following groups of basic variables are taken into account:

- geometry properties (such as dimensions of structural members);
- load characteristics;
- material properties;
- model uncertainties.

The variability of such variables shall be analyzed based on the available information. Updating of information should be performed based on state-of-the art of reliability analysis. Two different routes can be distinguished:

- updating of individual random variables due to measurements, observations related to the individual variable based possibly on Bayesian techniques.
- updating of failure probability by conditioning i.e. conditional failure probabilities due to measured cracks, or due to survival of extreme loads, etc.

In updating procedures the POD (Probability of Detection) and accuracy of the measurements should be taken into account. The format of verification depends upon the degree of sophistication of the assessment analyses. Either a partial safety factor format or a full probabilistic format may be used.

Risk acceptance criteria should be derived based on:

- implementation of a safety class differentiation principle;
- limit state classification;
- consideration of the desired residual service life;
- current tendencies in target safety levels regarding existing structures;
- consideration of global failure of the structure.

If the degree verified of the reliability is too low, the code must require a decision either to:

- reduce the loads on the infrastructure,
- strengthen the infrastructure,
- demolish the infrastructure.

4 EXAMPLE GUIDELINES AND STANDARDS

4.1 JCSS Recommendations

In the 90s considerable prenormative work has been carried out from the JCSS (Joint Committee on Structural Safety [9]) and the respective publication is summarized next. The JCSS document on existing structures which is published under RILEM [9] has been worked out by the members of the working party of the JCSS. The document serves as a precodification document and is also referring to the JCSS probabilistic model code. It is noted here that the probabilistic model code and the associated stochastic models is published in the internet [6].

The JCSS document is of educational type and provides reliability methods to be used in the structural reassessment. Tutorial examples and practical case studies are included as shown in the contents, which are as follows:

Preface	
Part 1:	General Guidelines Codification
Part 2:	Reliability Updating and Decision Analysis Procedures
Part 3:	Acceptability and target criteria
Part 4:	Examples and case studies
Annex:	Reliability Analysis Principles

The document provides consequently relevant information on how to process specific information about an existing structure, how to update its reliability based on such information, how to base decisions regarding maintenance, strengthening, upgrading etc. It is generally applicable for various materials and various structure types.

4.2 ISO standards

General requirements and procedures for the assessment of existing structures based on the theory of structural reliability are provided in the International Standard ISO 13822 [14]. For practical applications, information on properties of various construction materials may be provided in National Annexes. Supplementary guidance on can also be found in ISO 2394 [5], ISO 15697 [14].

The safety evaluation of existing structures is different depending on, for instance, the type of structure and the reason for evaluation. In regions of high seismicity, for example, guidelines and standards, such as [16, 17, 18, 19] provide concepts and tools for the seismic evaluation of existing buildings. The evaluation procedures are based on a rigorous approach to determine whether existing buildings subject to ground motions associated with specific mean return periods suffer consequences that are within the definition of pre-specified acceptable performance levels. The performance is measured in terms of monetary losses, fatalities, and downtime.

The ISO 13822 provides general information and methodological background on how to perform a reassessment of an existing structure. It is independent on the material and the type of structure and it covers many important topics of the structural reassessment.

The contents of the document are as follows::

- Scope
- Normative references
- General Framework of assessment
- Data for assessment
- Structural analysis
- Verification
- Assessment based on pat performance
- Interventions
- Report
- Judgement and decisions
- Annexes A-J

4.3 Other standards

These topics and aspects have been dealt with in research work in order to develop standards on the reassessment of structures. The reader can find respective information for example in [10-13]. The safety evaluation of existing structures is different depending on, for instance, the type of structure and the reason for evaluation. In regions of high seismicity, for

example, guidelines and standards, such as [16, 17, 18, 19] provide concepts and tools for the seismic evaluation of existing buildings. The evaluation procedures are based on a rigorous approach to determine whether existing buildings subject to ground motions associated with specific mean return periods suffer consequences that are within the definition of pre-specified acceptable performance levels. The performance is measured in terms of monetary losses, fatalities, and downtime.

5 CURRENT CODE AND GUIDELINE DEVELOPMENTS

Safety aspects for existing structures are also provided in national and international standards and recommendations. The American Concrete Institute [20] guidelines and the Swiss note SIA [21] are typical examples. Another widely used code is the ICC [22] which contains requirements intended to encourage the use and reuse of existing buildings. The scope covers repair, alteration, addition and change of occupancy for existing buildings and historic buildings, while achieving appropriate levels of safety without requiring full compliance with the new construction requirements contained in the other ICC codes.

As mentioned earlier, criteria for safety acceptance of existing infrastructures should be based on present guidelines, standards and methodologies but allow for “discounts” in the level of safety. In fact, many organizations (e.g., FEMA and SEAOC) authorities set the precedent that the acceptable seismic performance objectives for existing buildings maybe somewhat lower than those for new ones. These allowances reflect a realistic recognition of the reduced cost-effectiveness of seismic retrofits versus new construction and implicitly account for legal considerations as well.

It can be concluded that, although the codification for assessment procedures for existing structures is a relatively new field of development, considerable work has been lately performed in this field and valuable documents have been issued by different national and international associations. Basic items are:

- general principles of assessment;
- procedures and different phases of assessment;
- methods for updating of additional information and appropriate evaluation of inspection results;
- format for verification;
- risk acceptance criteria.

In the Netherlands, together with the formal introduction of the Eurocodes, the NEN 8700 and NEN 8701 for Assessment and Renovation of Existing Structures were launched in 2012. The NEN 8700 gives for every clause in EN 1990 (Basis of Design) rules and indications on what is directly applicable for existing structures and what should be changed. The NEN 8701 does a similar job for EN 1991 (Actions). A comparable draft NEN 8702 for concrete is under development. The theoretical background can be found in [23]. Finally a new version of ISO 2394 has been developed and is currently at the finalization stage [25].

6 VERIFICATION

The verification of components of existing infrastructures can be performed based on the partial factor format given in the EUROCODES [1, 2]. Instead of using partial safety factors one may apply directly updated design values based on the well-known FORM results. Common verification methods take basis in design equations from which the reliability verification of a given design may be easily performed by a simple comparison of resistances and loads and/or load effects. Due to the fact that loads and resistances are subject to uncertainties, design values

for resistances and load effects are introduced in the design equations to ensure that the design is associated with an adequate level of reliability. When deriving design values one may consider:

- costs of safety measures
- remaining lifetime
- degree of information available

A verification is considered to be sufficient if the limit states are not reached when the design values are introduced into the analysis models. In symbolic notation this is expressed as :

$$e_d < r_d \quad (1)$$

This is the practical way to ensure that the reliability index β is equal to or larger than the target value.

The design values of action effects e_d and resistances r_d should be defined such that the probability of having a more unfavourable value is as follows :

$$P(E > e_d) = F_x(e_d) = \Phi(+\alpha_E\beta) \quad (2a)$$

$$P(R < r_d) = F_x(r_d) = \Phi(-\alpha_R\beta) \quad (2b)$$

where :

- F_x is the cumulative distribution function;
- β is the target reliability index;
- α_E and α_R are the sensitivity factors.

The design values are obtained as:

$$E_d = F_x^{-1}[\Phi(+\alpha_E\beta)] \quad (3a)$$

$$R_d = F_x^{-1}[\Phi(-\alpha_R\beta)] \quad (3b)$$

The expressions provided in the following table should be used for deriving the design values of variables with the given probability distribution.

Table 1 Design values for common distributions

Distribution	Design values
<i>Normal</i>	$\mu - \alpha \beta \sigma$
<i>Lognormal</i>	$\mu \exp(-\alpha \beta V)$ for $V = \frac{\sigma}{\mu} < 0,2$
<i>Gumbel</i>	$u - \frac{1}{a} \ln\{-\ln[\Phi(-\alpha \beta)]\}$ where $u = \mu - \frac{0,577}{a}$; $a = \frac{\pi}{\sigma\sqrt{6}}$

The reliability index β can be taken from the target values as recommended chapter 5 of Handbook 1. Examples for verification are shown in other chapters of the present Handbook. Aspects on the influence of the working life and on cost-optimization are also included in Handbook 1.

7 CONCLUSIONS

The following conclusions are drawn in this chapter:

- Assessment of existing structures is in many aspects different from designing a new structure
- Actual characteristics of structural material, action (permanent load), and geometric data should be considered.
- Currently valid codes should be considered (models for actions and resistances). Previously used codes as background documents.
- A number of specific codes exist and have been identified herein regarding the assessment of existing infrastructure.
- Target reliability level should be optimized taking into account residual life time, consequences and costs of safety measures.
- Partial factor method and probabilistic methods are recommended.
- Assessment based on satisfactory past performance may be used.
- Final report should include recommendations concerning intervention.

REFERENCES

- [1] EN 1990 Eurocode - *Basis of structural design*. European Committee for Standardisation, 04/2002.
- [2] EN 1991-1-1 Eurocode 1: *Actions on structures*. European Committee for Standardisation, 04/2002.
- [3] NaBau, *Grundlagen zur Festlegung von Sicherheitsanforderungen für bauliche Anlagen*, DIN Deutsches Institut für Normung, Berlin, Köln, Beuth Verlag, 1981.
- [4] NKB Nordic Committee on Building Regulations, *Recommendations for Loading and Safety Regulations for Structural Design*, NKB-Report No. 36, Copenhagen, Denmark, 1984.
- [5] ISO (International Standards Organization) 2394, *General principles on reliability for structures*, 1998.
- [6] Joint Committee on Structural Safety (JCSS), *Probabilistic Model Code, Parts 1 to 4, Basis of design, Load and resistance models, Examples*, JCSS, www.jcss.ethz.ch.
- [7] H. Gulvanessian, J.-A. Calgaro, M. Holický, M.: *Designer's Guide to EN 1990, Eurocode: Basis of Structural Design*; Thomas Telford, London, 2002, 192 pp.
- [8] D. Diamantidis “Structural Reliability and Robustness in the Eurocodes”, ICAMB Conference, Vellore, India, December 2009.
- [9] Joint Committee on Structural Safety (JCSS), *Assessment of Existing Structures*, RILEM Publications S.A.R.L., 2000.
- [10] CSA S6-1990, 1990, *Design of Highway Bridges: Supplement No. 1-Existing Bridge Evaluation*, Canadian Standards Association, Ottawa, Ontario.
- [11] Danish Technical Research Council, 1997, *Probabilistic Methods and Models for Reliability-based Reassessment*, Report No. 1.
- [12] Department of Energy (DOE), 2002, *Natural Phenomena Hazards Design and Evaluation Criteria for Department of Energy Facilities*, DOE-STD-1020-2002, U.S. Department of Energy, Washington D.C.

- [13] Ellingwood, B.R., 2005, Risk-informed condition assessment of civil infrastructure, state of practice and research issues, *Journal of Structural and Infrastructural Engineering* 1(1), pp. 7-18.
- [14] International Standards Organization (ISO), 2003, Bases for design of structures – Assessment of existing structures, ISO 13822, corrected version.
- [15] [15] ISO 16587: Condition Monitoring of Structures, General Guidelines
- [16] American Society of Civil Engineers (ASCE), 2003, *Seismic Evaluation of Existing Buildings*.
- [17] Federal Emergency Management Agency (FEMA), 1998, FEMA 310 – Handbook for the Seismic Evaluation of Buildings- A Pre-standard, Washington DC, USA
- [18] Federal Emergency Management Agency (FEMA), 2000, FEMA 350 – Recommended Seismic Design Criteria for New Steel Moment-Frame Buildings, Washington DC, USA
- [19] Federal Emergency Management Agency (FEMA), 2000, FEMA 352 – Recommended Post-earthquake Evaluation and Repair Criteria for Welded Steel Moment-Frame Buildings, Washington DC, USA
- [20] American Concrete Institute (ACI), 2003, *Strength Evaluation of Existing Concrete Buildings*, ACI 437R-03.
- [21] Schweizer Ingenieur und Architektenverein (SIA), 1994, *Beurteilung der Tragsicherheit bestehender Bauwerke*, Richtlinie 462.
- [22] ICC International Code Council (ICC) *Existing Buildings Code*, 2009.
- [23] Vrouwenvelder A.,and N. Scholten, *Assessment Criteria for Existing Structures*, *Structural Engineering International* 1/2010, pp 62-65,
- [24] Steenbergen R. and A.Vrouwenvelder, *Safety philosophy for existing structures and partial factors for traffic loads on bridges*, *HERON* 55, No 2, Delft, 2010, ISSN 1574-4078 (<http://heron.tudelft.nl>)
- [25] ISO (International Standards Organization) 2394, *General principles on reliability for structures*, draft, 2014.

CHAPTER 3: SURVEY METHODS

Carlos Lara¹, Peter Tanner¹, Ana de Diego¹

¹Eduardo Torroja Institute for Construction Science, IETcc-CSIC, Madrid, Spain

Summary

During their service life, infrastructures are subject to numerous environmental influences which over time may cause deterioration of their materials. Degradation usually influences both, resistance and appearance of an infrastructure. In order to efficiently assess and manage aging infrastructures, the most relevant operational methods for determination of model parameters for deterioration processes such as corrosion and other chemical attacks are briefly described in this chapter. Likewise, operational methods for detection and evaluation of fatigue damage are presented. Continuous monitoring of aging infrastructures could provide data to better understand its structural behaviour and to predict its deterioration and remaining service life. To that end, methods for remote monitoring and control of infrastructures are also provided.

1 INTRODUCTION

The structural assessment of an existing infrastructure and its risk-based management for the future use is based on the available information regarding the actions on the structure, structural behaviour and the resistance of its components. Usually established structural analysis methods are applied and the degree of detail of the analysis depends on the stage of the assessment process which has been described in Handbook 1 [1].

According to the risk assessment process reported in Handbook 1 Chapter 1 [1], the investigation involves the acquisition of all relevant information concerning:

- the original design and structural concept of the infrastructure, as well as the code rules used, if any;
- the sequence of structural modifications during its previous service period, addition or demolition of structural parts and/or deep maintenance interventions;
- actual material properties;
- actual damage and degradation;
- required performance level.

Time is a decisive factor within the framework of assessment and management of infrastructures, influencing residual service life, maintenance, inspection, repair or the life-cycle cost. The reliability level for important limit states has to be analysed frequently utilising mathematical models for prediction of degradation.

During their service life, infrastructures are subject to numerous environmental influences (e.g., moisture, temperature, chemical substances, biological processes, etc.) which, over time, may cause deterioration of their materials. Degradation usually influences both, resistance and appearance of an infrastructure. Serviceability and safety of the structure may be seriously compromised by degradation mechanisms. In order to efficiently assess and manage aging infrastructures, operational methods for determination of parameters of the models for deterioration processes are needed.

Furthermore, information is needed on whether the condition has stabilised or is progressing and, in case of the latter, at what rate. Monitoring of aging infrastructures could

provide data to better understand its structural behaviour and control the evolution of its deterioration. The relevant background documents for the operational methods for determination of the parameters needed for the modelling of deterioration processes, which are described in the following, are given in Chapter 3 of Handbook 1 (HB1) [1].

The present Chapter gives a short review of the operational methods for determination of model parameters for deterioration processes such as corrosion, chemical attacks and other environmental influences (section 2). The use of ground penetration radar for the inspection of damaged infrastructures is also described. Section 3 discusses the techniques that may be used for remote monitoring and control of the structural behaviour of aging infrastructures, particularly the use of microwave interferometry. Section 4 describes operational methods for detection and evaluation of fatigue damage. Some final remarks are presented in section 5.

2 DETERMINATION OF DETERIORATION MODEL PARAMETERS

2.1 Corrosion parameters in reinforced concrete structures

2.1.1 Overview

Corrosion of reinforcing steel in concrete due to the action of chlorides and atmospheric carbon dioxides is generally considered as the main degradation process for reinforced concrete (RC) infrastructures. The modelling of time-dependence of the corrosion process is described in Chapter 3 of HB1 [1] using a two-phase model, including the initiation and the propagation phases. Modelling of consequences of reinforcement corrosion such as reduction in bar cross section, change of reinforcing bar material properties and loss of load bearing capacity is also described in [1].

Operational methods for determination of corrosion parameters in RC structures that should be taken into consideration when assessing corrosion-deteriorated infrastructures and for the degradation modelling are described here. These parameters include corrosion rate, electrical resistivity and potential, as well as the chief environmental parameters.

2.1.2 Corrosion rate

The corrosion rate is defined as the amount of steel corroded per unit of surface and time [5]. The amount of oxides generated is directly related to concrete cover cracking and weakening of the steel/concrete bond, while any decline in the steel cross-section significantly affects the load bearing capacity of the structure. The corrosion rate is therefore a proxy measurement for the loss of load carrying capacity. In addition to calculating rebar cross-section losses, the corrosion current may be used to identify corroded zones and evaluate the efficacy of repair techniques [2].

The corrosion current, I_{corr} , is measured by a reference electrode which determines the electrical potential, in conjunction with a counter electrode, which supplies the current. In on-site measurements, in addition to the central circular counter electrode, a second electrode (guard ring) is used to confine the current to a limited area in the reinforcement. The aim of this guard ring is to balance the electrical field produced by the central auxiliary electrode (fig. 3.1).

The polarisation resistance, R_p , method is the most widespread of the various electrochemical methods proposed to measure corrosion-related electrical parameters. This method is based on the application of a small electrical current to the steel with a counter and a reference electrode. Providing the electrical signal is uniformly distributed across the reinforcement, R_p is defined as [3]:

$$R_p = (\Delta E / \Delta I)_{\Delta E < 20 \text{ mV}} \quad (1)$$

where ΔE denotes the corrosion potential-induced polarisation and ΔI the polarisation current. The corrosion current, I_{corr} , is inversely proportional to R_p :

$$I_{corr} = B / R_p \quad (2)$$

where B is a constant, for in-situ tests usually taken to be 26 mV [2].

In on-site measurements, the location of the measuring points is crucial, for they must be representative of the deterioration process. The location may be selected on the grounds of a hypothetical grid with fixed spacing, although supplementary techniques such as the corrosion potential or resistivity may be used prior to the grid procedure.

The corrosion rate meters used must be able to accurately determine current dispersion over a given distance. That calls for applying the modulated confinement technique (controlled guard ring, see fig. 3.1) or the potential attenuation method. One of these two operating modes must be used, for otherwise an error of one or two orders of magnitude may be incurred [2].

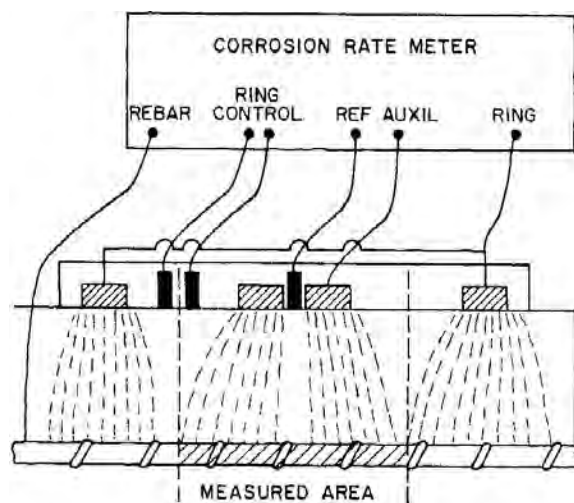


Figure 3.1 Modulated current confinement method [3]

When no electrochemical techniques are available, a mean corrosion rate value may be calculated by dividing the measured loss in rebar diameter by the number of years that corrosion has been propagating [3].

2.1.3 Electrical resistivity

Electrical resistivity, ρ ($\Omega \cdot m$), which is the inverse of conductivity, is a volumetric measurement of electrical resistance, R_e (Ω): according to Ohm's law, the ratio between voltage and current ($R_e = V / I$). Resistivity is the property whereby a porous medium is able to convey an electrical charge [4].

Since the potential difference or the current applied by two electrodes is carried across the aqueous phase of the concrete pore system by electrical carriers (ions), the electrical resistivity of water-saturated concrete is an indirect measure of concrete pore connectivity. Electrical resistivity provides insight into pore connectivity and therefore into the resistance of the material to penetration by fluids. In other words, resistivity indirectly measures the key properties that determine reinforcement durability [4].

Age, water saturation level and temperature are factors that affect resistivity values. Concrete resistivity increases with time due to pore structure refinement. Variations in concrete resistivity with changes in environmental factors such as moisture condition and temperature must consequently be taken into consideration in on-site measurements.

The most widely used techniques for direct on-site measurement of concrete resistivity are the four-probe method (four electrodes) and the disc method (one electrode). *The four-probe method* is based on Wenner’s technique [5], originally developed for geophysical prospecting but subsequently applied to concrete. This method uses four equally spaced point electrodes in contact with the concrete surface [6]. The electrode tips should be moistened with a conducting liquid to ensure good contact with the concrete. A known alternating current (generally with a frequency of 50 to 1000 Hz) is passed between the two outer electrodes while measuring the potential difference between the inner electrodes (fig. 3.2). Resistivity is found as a function of voltage, current and distance between tips:

$$\rho = 2 \cdot \pi \cdot a \cdot R \tag{3}$$

where a denotes the distance between electrode tips and R the resistance as directly measured.

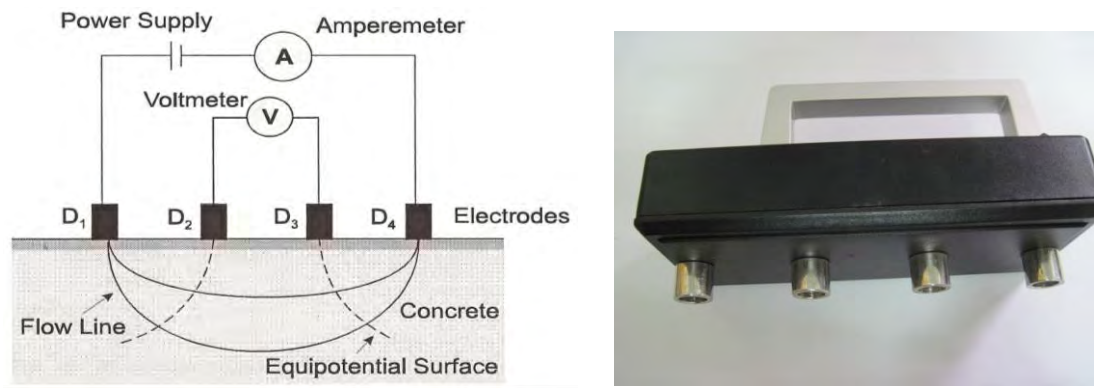


Figure 3.2 Wenner four-probe method resistivity measurement set-up and sensor [2]

The disc (one electrode) method, based on Newman’s studies, was fully developed by Feliú, González and Andrade [7] to estimate the ohmic drop between a small disc placed on the surface of an electrolyte and a much larger counter electrode placed at “infinity”. Theoretically, if the contribution by the counter electrode to the total resistance is negligible, the electrical resistance can be said to depend on electrode resistivity.

The device consists of a disc made of conductive material, a potentiostat and a reference electrode (fig. 3.3). Once good contact is made between the electrode and the concrete, a galvanostatic pulse is applied and the instantaneous ohmic drop is recorded. As in the Wenner four-probe method, disc and rebar must be at a certain distance, normally twice the disc diameter, to obtain an accurate measure of bulk resistance. The resistivity obtained is:

$$\rho = 2 \cdot R_e \cdot \phi \tag{4}$$

where ϕ is the disk diameter.

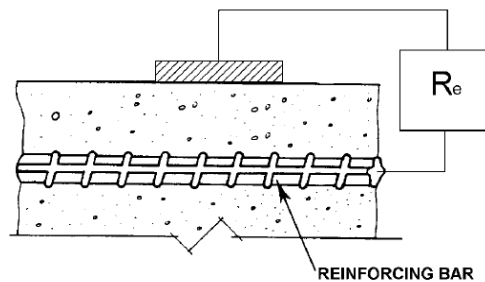


Figure 3.3: Disc method for measuring resistivity [2]

2.1.4 Potential

Steel corrosion leads to the coexistence of passive and corroding areas in the same bar, forming a short-circuited element in which the corroding area is the anode and the passive surface the cathode. The main purpose of measuring potential in a structure is to locate areas where the reinforcement has become depassivated and may corrode when suitable amounts of oxygen and moisture are present [2].

Before the areas where the reinforcement is corroding can be identified, a system of coordinates must be devised to correlate readings and measuring points. The accuracy of the measurements depends on the size of this grid. While a good electrical connection to the reinforcement must be established to measure the half-cell potentials in a structure, direct contact should not be made if the reinforcing steel is connected to an exposed steel member. An external reference electrode is positioned on the concrete surface (with a wet sponge between them to ensure good electrolytic contact) to furnish the high impedance voltmeter with further data (fig. 3.4). The electrical continuity of the reinforcing steel must be assured by measuring the resistance between separate sections of rebar. Resistance values of less than or equal to 0.3Ω denote electrical continuity.

Potential measurements can be performed with a single electrode or with one or several wheel electrodes. The latter are used to check potential in structures such as large bridge decks or car park deck slabs, for they can cover up to 300 m^2 per hour when connected to microprocessor-controlled data-loggers.

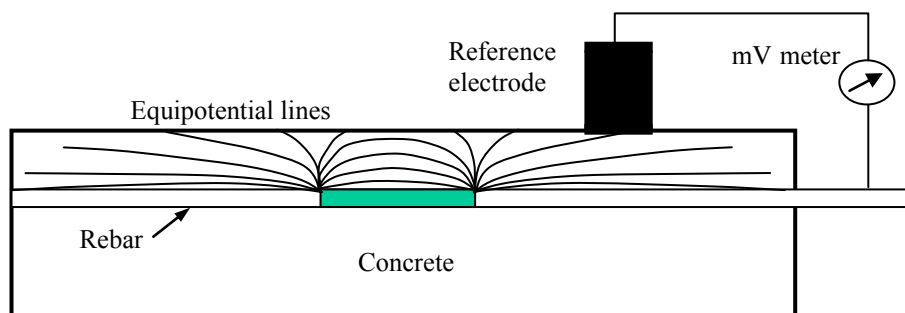


Figure 3.4 Measuring potential in concrete rebars with one reference electrode [2]

Once the data are gathered, optimal representation depends on the amount of data and structure type. The information may be set out in anything from tables to a coloured grid map of the potential field, where every individual potential reading can be identified as a small cell and a contour line map can be drawn with algorithms for interpolating values between measurement points. Potential measurements can also be represented with standard statistical tools, of course, such as frequency distributions or histograms. The representational design should be determined by the kind and depth of the study [2].

Corrosion potential measurements are affected by a wide range of factors, including: concrete moisture content, chloride content, concrete carbonation, cover thickness, polarisation effects, oxygen content and type of reference electrode used, and are very dependent on the environmental conditions, temperature and humidity, during measurements. For these reasons, corrosion rates determined with the abovementioned methods result generally very scattered. Therefore, additional investigations and suitable cross checks are necessary to improve the reliability of the predicted corrosion rate values.

2.1.5 *Environmental parameters*

The chief environmental parameters to be taken into consideration when assessing corrosion-deteriorated structures include moisture, temperature, chloride content and carbonation.

Concrete moisture content, the environmental parameter with the greatest impact on corrosion, depends on environmental humidity and affects electrical resistivity and oxygen availability around the rebar. A common denominator of most mechanisms of deterioration is access to concrete of moisture. Without water, with mechanical damage such as abrasion being an exception, no mechanism of deterioration can proceed. Examples of such processes are of both chemical (e.g. corrosion of reinforcement, alkali–silica reaction, sulfate attack) and physical (e.g. freezing–thawing) nature.

Temperature may hasten or retard corrosion. When it rises, pore water evaporates and oxygen is released from the pore solution. Consequently, although corrosion is stimulated by higher temperatures, that effect may be counterbalanced by the rise in resistivity (evaporation) and the decline in oxygen levels (oxygen is less soluble at higher temperatures). The opposite effect is induced by declines in temperature in semi-dry concrete due to the resulting condensation. In a nutshell, the effect of daily and seasonal variations in relative humidity and temperature on the corrosion rate cannot be easily quantified [2].

Chloride attack is the result of the presence of chloride ions in the concrete, either as a component of admixtures, water or aggregates, or, more commonly, as an outside agent in structures exposed to marine environments or de-icing salts. Chlorides induce local damage to the passive layer on the steel, generating pits or localised attacks. Cracking may or may not ensue, depending on whether the corrosion is widespread or localised. Rebar has been known to corrode in submerged members with no cover cracking. Chlorides penetrate submerged or fully saturated concrete by diffusion. In members exposed to the air or cyclical conditions (de-icing salts), by contrast, ingress may be governed primarily by capillary absorption.

A number of methods are in place to determine the total chloride content in hardened concrete. The samples for these tests may be taken from dust in core holes or scratched off the structure at different depths, measured from the surface. Fragments for chemical analysis may also be removed from cracks or spalled areas. The aim is to establish the chloride gradient or profile from the concrete surface inward and identify the chloride threshold that induces depassivation. Chloride profiles can be also obtained from cores drilled from the structure and subsequently scratched layer by layer [2]. The quantab- and rapid chloride (RCT) tests are the methods most often used to determine the total chloride content in field surveys. Other more accurate analytical methods can be performed under laboratory conditions.

In the absence of chlorides, carbonation is the agent that affects concrete most aggressively. Atmospheric carbon dioxide reacts with the calcium and alkaline hydroxides present in the cement phases, lowering the pore solution pH to values near neutrality. This process results in the depassivation of the steel in contact with the carbonated zones. The concrete moisture content is the factor with the greatest impact on the penetration rate of the carbonation front.

A freshly exposed concrete surface is needed to determine the carbonation depth. The depth of the carbonation front is found by spraying the concrete surface with an acid-base indicator (phenolphthalein) that changes colour with the pH value. At least four measurements of depth at which the indicator is colourless must be taken and the maximum and minimum values recorded to obtain a representative mean value. Carbonation depth can be measured on cores drilled for mechanical strength or in the drill holes. If no core can be drilled or concrete removed, a hammer drill can be used to obtain a freshly exposed concrete surface [2].

2.2 Detection and evaluation of other chemical attacks

2.2.1 Sulfate attack

As has been mentioned in HB1 Chapter 3 [1], sulfate attack is the result of the exposure of a concrete structure to an excessive amount of sulfate from internal or external sources. External sulfate attack is most common and typically occurs when water containing dissolved sulfates penetrates the concrete. Sulfate attack on concrete is primarily attributed to sodium, magnesium and calcium sulfate salts present in the soil, ground water or sea water which react with calcium hydroxide and, if enough water is present, result in expansion and irregular concrete cracking that can lead to a progressive loss of strength and mass. The parameters mentioned in this section are associated with modelling of degradation of concrete elements due to sulphate attack, whose recent advances are briefly described in Chapter 3 of HB1 [1].

Concrete structures subjected to attack from sulfates may suffer two types of damage: loss of strength of the matrix due to degradation and volumetric expansion leading to cracking. Loss of strength has been linked to decalcification of the cement paste hydrates upon sulfate ingress. Expansion, which leads to cracking is attributed to formation of expansive compounds such as ettringite [8].

Due to the complicated mechanisms involved in sulfate attack, no one parameter can be used to evaluate sulfate-related damage in all conditions. Deterioration of concrete by sulfates has been historically assessed in numerous ways, neither of which gives adequate results under all conditions. Such assessment techniques include visual evaluation and tests for determining wear rating, loss of mass, surface hardness, compressive or tensile strength, dynamic modulus of elasticity, and volume instability. Presently used tests are deemed to be indirect because they do not take into consideration the actual cause of deterioration but only measure the physical or mechanical consequence of the damage [9]. Although in many field studies, surface softening and loss of structural stability are seen to be the key damage indicators [10], because of the abovementioned complicated mechanisms it is advisable to use a combination of parameters to evaluate the degradation of concrete under sulfate attack.

Expansion is the most common parameter for determining concrete sulfate resistance. Two current test methods for assessing sulfate attack in laboratory conditions are ASTM C 1012 [11] and ASTM C 452 [12]. These methods use the expansion as the indicator of degradation. However, there exists a general lack of correlation between the performance of concrete subjected to standard test methods and concrete subjected to realistic field conditions [10]. Translating the effects observed in the laboratory to field situations is a challenging task because a complex interaction of physical and chemical factors occurs in field conditions. The added challenge to testing is the simulation of conditions like drying and wetting cycles, and temperature and humidity variations, among others. Therefore, the methods for condition surveys of concrete infrastructures, exposed to sulfates during its service life, need some development [13].

Determining the change in the *compressive strength* is another mean of detecting sulfate attack. Compression test on cores is considered as a semi-destructive technique. The concrete strength can be determined on cores when the health of a structure at a particular moment is at issue. If cores taken from an existing structure have a lower strength than the 28-day strength at the time of placing the concrete, then it is reasonable to conclude that the concrete has suffered damage, possibly owing to sulfate attack [14]. When strength change is used for assessing the sulfate resistance of concrete large amounts of specimens are necessary, especially for prolonged tests [15]. However, compression tests performed on samples cored from infrastructures may entail certain complexities and weakens the member. Such semi-destructive procedures consequently tend to be limited to a short number of samples [16].

The assessment of concrete infrastructures damaged by sulfate attack requires the use of test methods that give results within a reasonable time. With the improvement of Non-

Destructive Techniques (NDT) on site determination of concrete properties is becoming quicker and easier [10]. Some hints about the use of NDT for detection and evaluation of sulfate-related damage in concrete infrastructures are presented below.

The *dynamic modulus of elasticity* of concrete can be measured by ultrasonic pulse velocity (UPV) technique. Cores taken from affected structures are used for investigation by pulse velocity. Obtaining reliable results from pulse velocity measurements requires access to the structure from two opposite sides, which necessitates the use of cores if access to both sides of the structure is not available. With experimental modification and using sensitive transducers, the pulse velocity technique can be used for one-sided measurements. However, the use of this technique to quantify the depth of degradation (that results from the attack by sulfates) needs to be studied in detail, with sufficient data for calibration [17].

The formation of various reaction products in the initial stages of sulfate attack can lead to an increase in the compressive strength, due to the filling up of voids. A similar effect can be observed for the dynamic modulus of elasticity as measured by pulse velocity. However, this behavior is not always consistent, and sometimes, a steady drop in strength or modulus may be observed right from the beginning. For these reasons, the choice of such parameters for evaluating damage due to sulfate attack does not appear to be appropriate in some cases [17].

External sulfate attack produces weak zones near the surface of the concrete. The sulfates responsible for the damage migrate into the concrete from an outside source. Under this condition, an altered layer resulting from the action of sulfates develops on the surface in contact with the sulfate-containing water or soil, while as the material in deeper regions stays unaffected [9]. The spectral analysis of surface waves technique, which is used extensively to study the stiffness variations of layered structures such as pavements [18], may help to quantify the extent of damage. With this method surface waves containing a wide range in frequencies are generated by impacting the system surface. Propagation of the waves through the system is monitored with two receivers located on its surface. By analysis of the phase information for each frequency determined between receivers, Rayleigh wave velocities and wavelengths over the frequency range of interest are determined. Velocity versus wavelength information represents a dispersion curve that on inversion gives Young's modulus profiles along with the thicknesses of the layers.

Weakened surface zones can also be detected by using the rebound hammer to perform hardness tests. Despite all limitations and uncertainties using the rebound hammer test, it could be used to provide valuable information about the relative qualities of concrete in an infrastructure. Good training and adequate calibration of the technique are necessary to obtain reliable results using this test [10].

Microstructural observations by scanning electron microscopy (SEM) or X-ray diffraction (XRD) can be used to determine the extent of damage in concrete elements subjected to sulfate attack [17]. SEM and XRD provide information on: phases, phase composition, textural and morphological relationships and porosity. Particularly, SEM is used to establish whether sulfate attack had occurred by demonstrating the presence of ettringite (fig. 3.5).

The degradation of materials by expansive reactions, such as caused by the sulfate attack, can be detected unequivocally by microstructural analysis using the suitable techniques (e. g. SEM, XRD). By the microstructural observations is possible even identify the presence of other secondary deterioration processes or the overlap of degradation mechanisms. However, the main disadvantage of this type of analysis lies in that is a qualitative analysis and not easily allows evaluating the evolution of deterioration and the quantification of the studied mechanism [19].

2.2.2 Alkali-aggregate reaction

Concrete expansion and cracking with a concomitant loss of strength, stiffness, and durability, may be induced by the calcium alkali-silicate gel forming when alkaline ions present in portland cement react with calcium and hydroxyl ions and certain siliceous constituents in

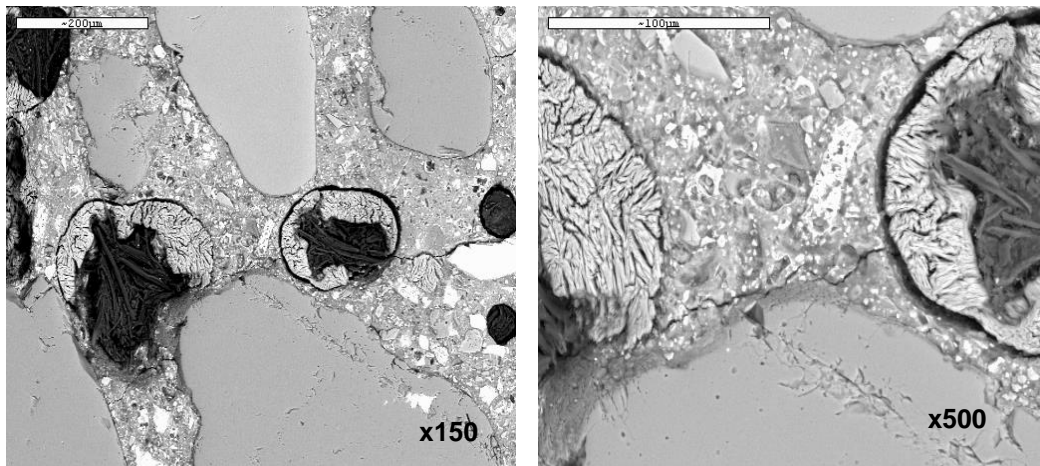


Figure 3.5 SEM images of a concrete sample. Left: ettringite induced micro-cracks (x150). Right: detailed view of ettringite formation (x500)

aggregates [20]. The evaluation of the current and future condition of existing structures damaged by alkali-aggregate reaction (AAR) requires that a wide range of effects be considered. These effects have been summarized in [1].

The assessment of infrastructures affected by AAR is a complex task which includes calculations of the structural effects, a thorough investigation of the steel detailing and the prediction and evaluation of the effects of future expansions. The determination of the current level of expansion of an affected element is difficult and normally can only be done indirectly. The mechanical properties of concrete in RC elements affected by AAR should be obtained from extracted cores [1]. As in the case of sulfate attack, due to the complicated mechanisms involved in AAR is advisable to use a combination of parameters to evaluate the degradation of concrete.

A detailed field survey is normally the first stage for identifying the possible presence of AAR, and the extent of deterioration. Visual survey is generally complemented by coring of selected components; laboratory tests need to be performed on these cores to confirm AAR as the major cause of deterioration. The most commonly reported field symptoms of AAR are discussed hereafter. It must be noted that presence of one or more of these features is not necessarily indicating AAR as the main or only factor responsible for the observed damage [21].

Deformations and displacements: the differential concrete swelling between adjacent members of a structure affected by AAR can cause misalignment, separation, or distortion of adjacent structural units and associated mechanical equipment, excessive deflection, closure of joints, and ultimately spalling of concrete. Concrete deformation and movements may also be caused by mechanisms such as excessive loading, thermal or moisture movements, differential shrinkage, foundation effects, hydraulic pressure, creep, impact, and vibrations.

Map-cracking: the pattern of cracking due to AAR is influenced by the geometry of the concrete element, the environmental conditions, the presence and the arrangement of reinforcement, and the load or stress applied to the concrete. The appearance of map cracking can vary from just a few cracks (fig. 3.6a) to isolated areas of pattern cracking to fairly severe, closely spaced extensive map cracking (figures 3.6b and 3.6c), i.e., the crack density on the surface may vary. It must be noted that it may be difficult to distinguish map cracking due to AAR from the one due to thaw-freezing process in concrete structures [22].

Presence of gel: surface gel exudation is a common and characteristic feature of AAR-affected concrete. However, in the early stages of the reaction, or under conditions where only small quantities of AAR gel are produced, the gel is not easily observed, and is revealed only by microscopy. Thus, AAR may go unrecognized in field structures for some period of time, possibly years, before associated severe distress develops to force its recognition, structure assessment and, possibly, rehabilitation. Moisture movement through pores and cracks in

concrete transports the AAR gel to the surface, where it exudes (see fig 3.7) [22].

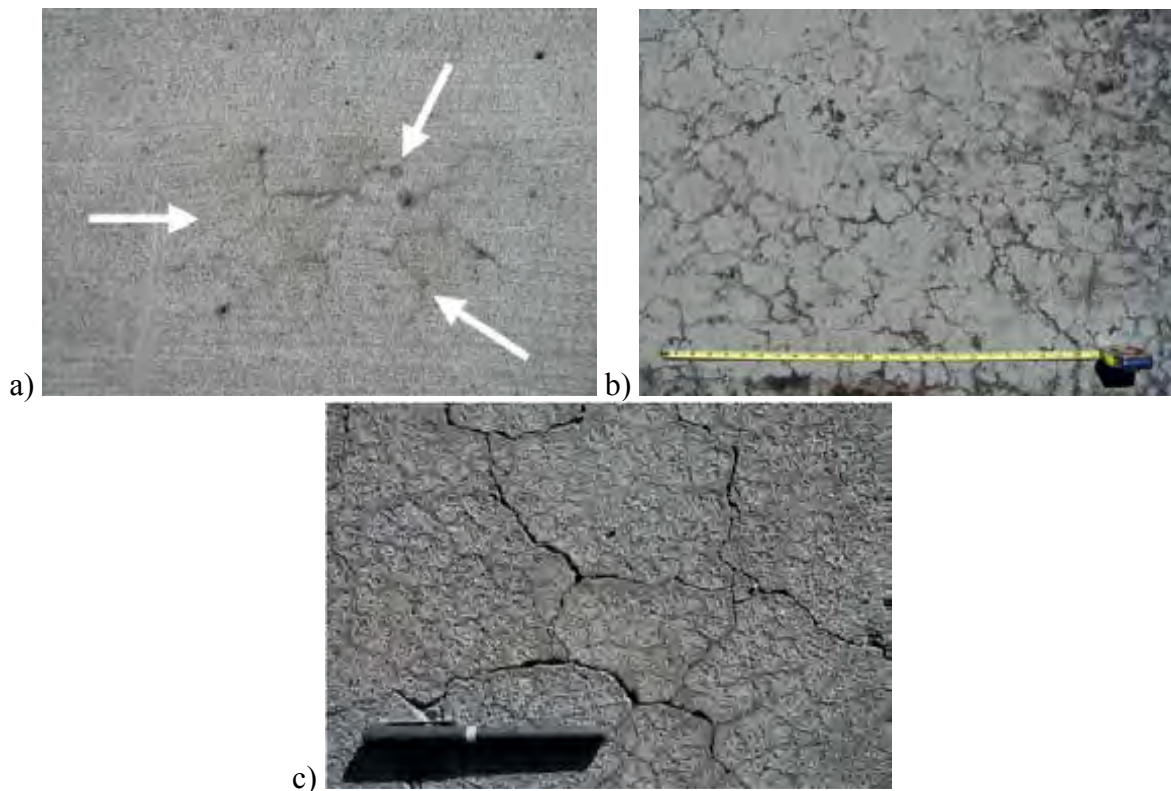


Figure 3.6 Examples of map-cracking on the concrete surface. a) Only a few cracks. b) Isolated areas of map-cracking. c) Severe map-cracking (Images taken from <http://www.faa.gov/>)

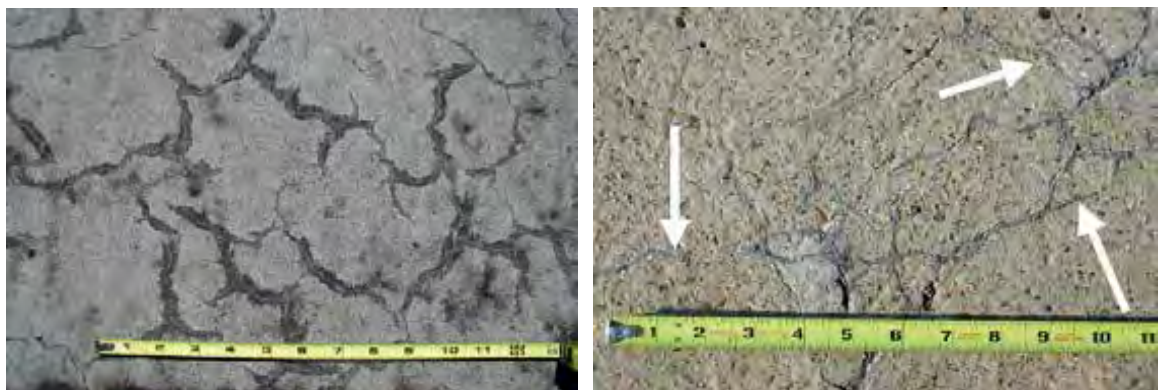


Figure 3.7 Examples of gel exudation through cracks [22]

Laboratory investigations can be carried out to help identify the presence of AAR in concrete and assess its current condition. The potential for future expansion and distress of the concrete due to AAR, as well as the structural effects of AAR can also be estimated by laboratory testing.

Microstructural observations can be used to identify the presence and distribution of AAR in concrete structures. This type of test is essential to diagnose AAR in concrete [21]. Several methods exist to show the microstructural evidence of the presence of AAR in concrete structures. Core samples are examined using tools such as ultra-violet light diagnosis, optical microscopic techniques and SEM.

Expansion: is the first structural effect observed in AAR damaged concrete elements. Due to the swelling process, the dimensions of AAR affected concrete increase. The dimension change of concrete elements is a function of time. According to [21], the dimension change is one of the most commonly used indirect methods for assessing the degree of concrete damage.

The most widely used indirect method for determination of the current level of expansion of an affected concrete element is the crack width summation method proposed in [23]. The measured strain is simply the resultant of strains arising from structural and non-structural (e. g. thermal, moisture movement, etc.) effects as well as AAR and represents the restrained expansion. The width of crack is measured along a number of lines drawn perpendicular to the principal crack orientation on the most severely affected face of each element of the concrete being assessed. The orientation of the intercepted crack with respect to the drawn lines is also recorded.

Expansion tests can be carried out on concrete cores extracted from concrete structures. These tests can be used for diagnosis of AAR; however, they are generally performed for prognosis purposes. Expansion testing is normally carried out after the cores had stabilised, that is, when any expansion due to release of restraint has practically ceased [24].

The mechanical properties of concrete in structural elements affected by AAR are normally obtained from extracted cores. Compressive strength, indirect tensile strength and static modulus of elasticity can be determined by testing of concrete specimens. The compressive strength of concrete decreases as the mechanical damage due to the AAR increases. The compressive strength is generally not sensitive to AAR until high expansions are reached. The reduction tends to approximately 40% at large expansions. As pointed out by Swamy [20] the compressive strength is not a good indicator for the beginning and the progress of AAR. Nevertheless, it is often used for concrete monitoring due to the simplicity of the measurement.

According to [22] it seems that tensile strength is more susceptible to AAR deterioration than the compressive strength, which has also been confirmed by measurements on concrete structures in service. The loss in tensile strength is due to the micro-cracking that occurs. This explains why much of the loss occurs before significant expansion is recorded [25].

AAR can also significantly reduce the elastic modulus of concrete, even at low level of expansion or when compressive strength is still increasing. This reduction is governed by the amount and orientation of the micro-cracking of the concrete. The expansion generally gives an indication of the extent of the micro-cracking and therefore the deterioration in the elastic modulus. Hence, when assessing the elastic modulus of a structural member the results from cores should be compared with the estimated expansion at the position from where the core was extracted [25].

The variation of other parameter such as UPV and dynamic modulus of elasticity can be determined with NDT for evaluating the concrete condition on cores drilled from infrastructures suffering from AAR. Several papers dealing with laboratory concrete specimens reported that UPV decreases with expansion. However, some others reported that UPV is slightly affected by AAR, except at very high expansion levels [26]. As is indicated in [20] the behaviour of the dynamic modulus is similar to that of the tensile strength. The dynamic modulus seems to be more sensitive to AAR than the UPV.

2.3 Structural surveys with ground penetrating radar

2.3.1 System description

Ground penetrating radar (GPR) is a non-destructive inspection method used world-wide in applications ranging from mining to geophysical or structural surveys. Basically, GPR is an electromagnetic technique based on the difference in the dielectric behaviour of materials. An antenna located on the surface of the structure emits a short pulse of electromagnetic energy. When that energy strikes an interface between layers of materials with different dielectric

properties, part of the wave is reflected and the rest continues to the next interface. The splitting rate of this energy is determined by the relative dielectric properties of the media. The energy reflected can be detected by an antenna and analysed to identify and characterise features not externally visible.

The equipment required for radar surveys normally comprises three elements (fig. 3.8). *The control unit* powers the antenna and receives and processes the reflected signals detected. The processed signal is subsequently transferred to the data-logger where it may be printed out in real-time if connected to a printer. *The antenna* is the key component in the radar system. A number of types of antenna can be used, depending on survey requirements. Smaller high frequency antennae (500 MHz-2,6 GHz) are useful for low depth (to 0,5 m), high-resolution work, such as the location of rebar. Low frequency units (200–900 MHz) penetrate more deeply into the structure surveyed (1–8 m) but afford much lower resolution. As a rule, the receiving and transmitting circuits are built into in the same antenna (monostatic mode), although bistatic systems with two antennas, one for transmission and the other for reception, are also used. *The data-logger* features real-time signal reception and display, as well as data recording. A video monitor is normally needed for signal adjustments.

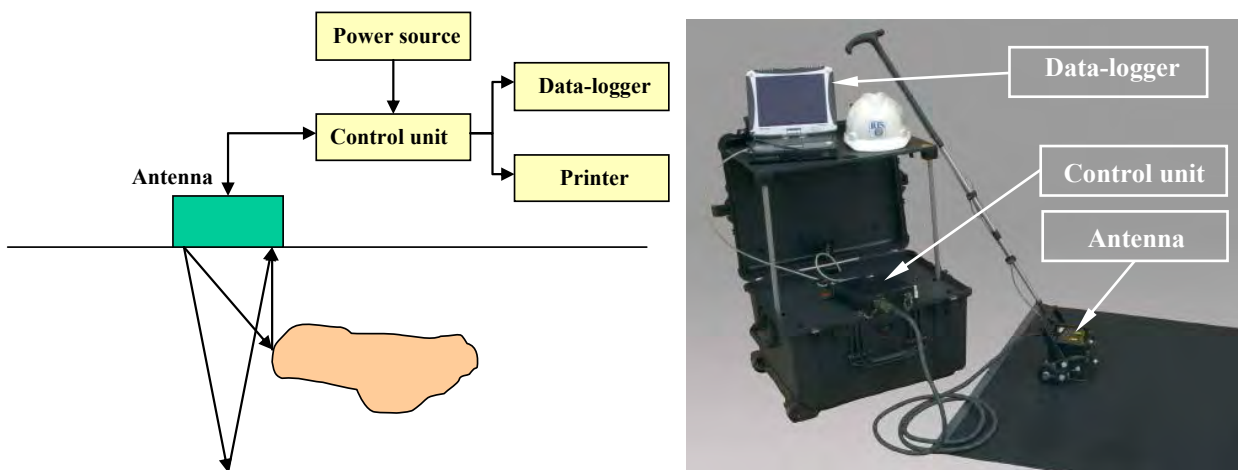


Figure 3.8 GPR flow chart (left) and radar equipment (right) used in non-destructive structural analysis

2.3.2 Applications

Radar systems can help solve many survey problems in a wide variety of fields, including structural engineering, railway engineering, road engineering, geological and environmental engineering, archaeology, the cultural heritage, forensic engineering, and reliability assessments. More specifically, in the non-destructive analysis of structures and buildings, GPR is used to:

- locate rebar and prestressing tendons in concrete structures;
- measure slab thickness;
- detect voids and other structural defects;
- identify wall cavities;
- detect the presence of water;
- explore the reconstruction of inner wall structures;
- locate pipes and other objects in walls and floors;
- inspect structural members in bridges, monuments, towers, tunnels, car park deck slabs and balconies.

2.3.3 Advantages and drawbacks compared to conventional techniques

The main advantages of GPR are:

- multiple applications;
- the innocuousness of wave frequencies for the subsurface, environment or people in the surrounds;
- multiple size options for convenient storage, shipping and use almost anywhere with scant limitations;
- wide range of antenna with frequencies of 200 to 2600 MHz to meet resolution and depth requirements.

Its most significant drawbacks are:

- performance limitations due to signal scattering in variable conditions;
- relatively high energy demand, which can pose problems in lengthy field surveys.

3 REMOTE MONITORING AND CONTROL OF INFRASTRUCTURES

3.1 Overview

Structural monitoring serves several purposes. Among others, monitoring of infrastructures over a long period can provide the opportunity to identify anomalies that may indicate unusual loading conditions, modified structural behaviour or deterioration, which can lead in the extreme case to its failure.

In general, a typical monitoring system includes three major components: a sensor system, a data processing system (including data acquisition, transmission and storage), and an evaluation system (including diagnostic algorithms and information management). The sensors utilized in structural monitoring are required to monitor not only the structural status, for instance stress, displacement, acceleration etc., but also influential environmental parameters, such as wind speed and temperature [27].

Infrastructures need a monitoring and control procedure which is reliable, inexpensive and easy to implement. The techniques used should be easy to adapt to different types of structures and structural parts since a large variety exists and adaptation is time consuming.

The development of non-contact systems for the measurement of static and dynamic response has recently drawn the attention of several researchers. Specially, the applications of laser-based systems, Global Positioning System, image analysis and vision systems are reported in the literature. A recently developed technology named microwave interferometer, capable to detecting the position of several points belonging to a large structure and simultaneously measuring the deflection of these points in both static and dynamic conditions is described in the next section [28].

3.2 Remote radar interferometric measurement of displacement and vibrations

3.2.1 System description

Microwave interferometry is an innovative technology for remote static and dynamic monitoring of bridges and structures such as buildings, historical monuments and towers. Interferometric radar equipment can be operated remotely and need not be in direct contact with the monitoring target. The radar generates an ongoing flow of deformation maps as opposed to the periodic information provided by current contact sensors. Measurement speeds and accuracy are also higher than in conventional techniques. The displacement response of several points on a

structure can be measured simultaneously with a precision on the order of 0.01 mm and a maximum sampling frequency of 100 Hz. Such high sensitivity is the result of interferometric techniques that measure displacement by comparing subsequent readings of the waves reflected off the object.

The system consists of the following elements (fig. 3.9):

- sensor module fitted with a signal transmitter and receiver, view finder and horn antenna;
- tripod and 3-D rotating head;
- processing unit;
- power supply.

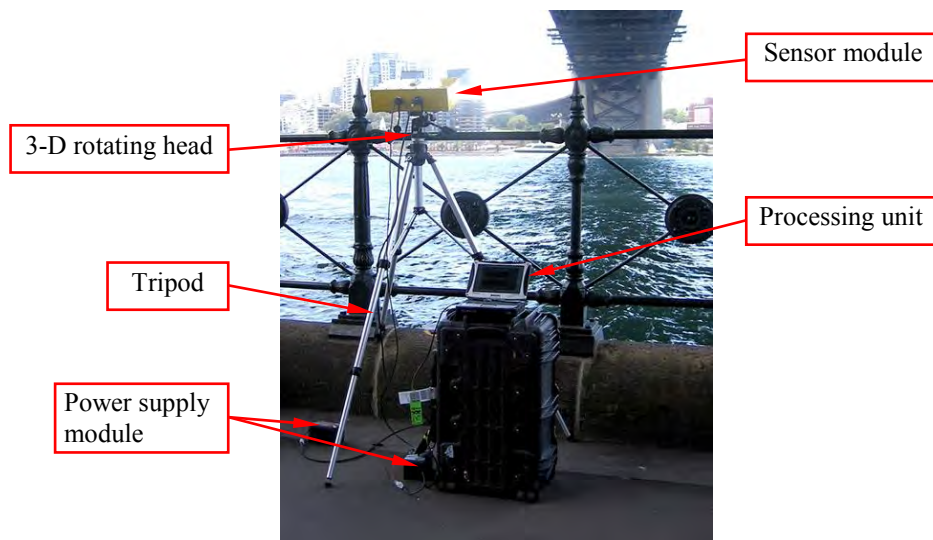


Figure 3.9 Microwave interferometer

The sensor module emits an electromagnetic wave that first strikes and is then reflected off all the targets radiated by the antenna. The information received from the reflected wave is used to record the variation in the position of the measuring point with respect to the preceding reading (fig. 3.10). Microwave interferometers measure line of sight displacement (d_{los}). Assessment of the actual displacement calls for information on the acquisition geometry and the real direction of movement.

3.2.2 Applications

The fields of application for remote monitoring based on radar interferometry include:

Static problems:

- structural load testing;
- structural displacement;
- conservation of the cultural heritage;

Dynamic problems:

- structural resonance frequency measurement;
- modal shape analysis of the structure;
- deformation monitoring in real time.

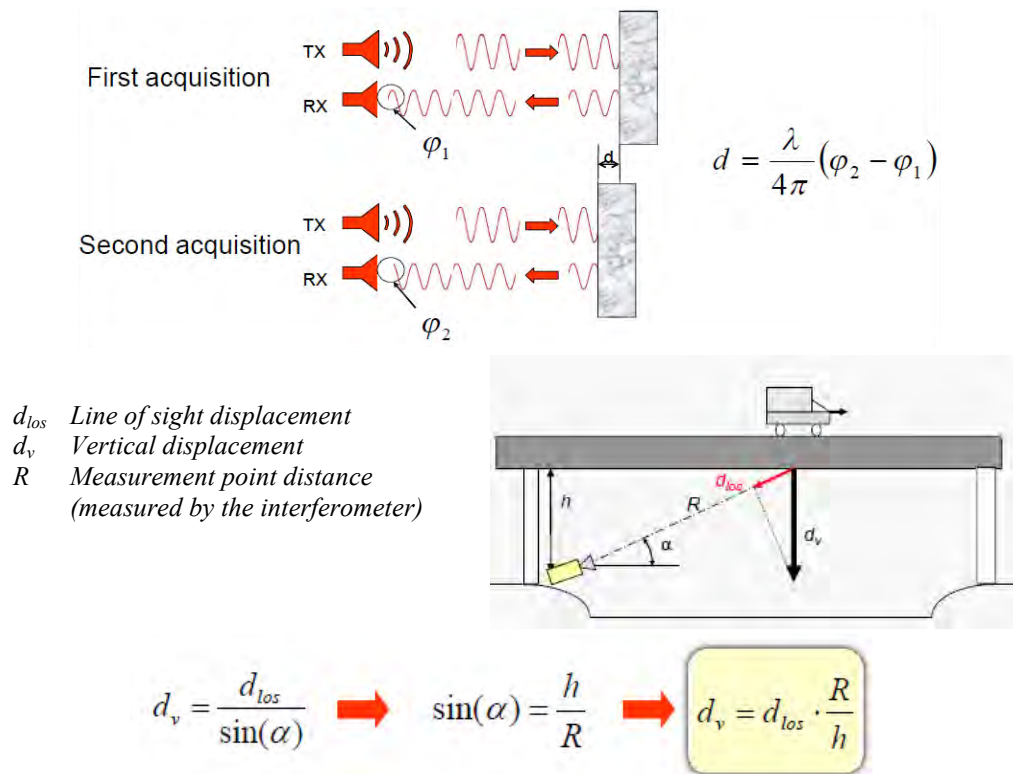


Figure 3.10 Remote radar interferometric monitoring of structural movements and deformation [29]

3.2.3 Advantages and drawbacks compared to conventional techniques

The main advantages of the microwave interferometer are:

- remote sensing at large distances (up to 1 km) with no need for equipment to be installed on the monitored structure;
- measurement precision of up to 0,01 mm;
- real-time simultaneous deformation mapping;
- simultaneous static and dynamic monitoring;
- structural vibration sampling up to 100 Hz;
- 24/7 operation, regardless of weather conditions;
- delivery of direct displacement measurements, not derived quantities;
- remote operation, surmounting accessibility difficulties and obviating any need to modify the service conditions of the structure.

The primary drawback, however, is the high initial cost of such a system.

4 DETECTION AND EVALUATION OF FATIGUE DAMAGE

4.1 Overview

Fatigue deterioration is a mechanical process consisting of a structural change of the base material caused by the action of alternate stress. In engineering structures, fatigue is induced by actions and loads varying with time and/or space and/or by random vibrations. Thus fatigue can be originated by natural events, like waves, wind and so on, or by loads deriving from the normal use of the structure itself, as it happens in bridges, under traffic loads [1].

Among other infrastructures, bridges are exposed to fatigue, under the action of trucks or trains crossing them. Thus, as has been mentioned in Chapter 4 of HB1 [1], fatigue assessment and evaluation of residual fatigue life is a key topic in verification of existing infrastructures, also in view of designing repair interventions of fatigue damaged details and planning of future maintenance and inspection programmes.

Traditionally, two types of fatigue models have been used for the description of fatigue failures caused by fluctuating actions:

- $S-N$ model based on experiments;
- fracture mechanics model;

both summarized in Chapter 4 of HB1 [1].

Fatigue deterioration is a process conditioned by the amplitude and the total number of stress increments the studied material will be subjected to. Variations of stresses in roadway bridges of medium length spans are mainly due to continuous traffic action. On the other hand, the internal forces caused by traffic action lead to different stresses within the section as a function of sectional stiffness [30]. Thus, fatigue depends on the nature of the varying actions and loads, and additionally on structural details, classified according to the relevant $S-N$ curves for a given material [31].

As for new structures, fatigue loads can be given in terms of load spectrum, expressing the load variation or the number of recurrences of each load level during the design life of the structure; load spectrum can be expressed by means of an appropriate function, graph, histogram or table, deduced from recorded data or by comparison with similar structures. Whenever, as it happens for bridges, the actual load spectrum results too complicated for direct use in fatigue checks, it can be replaced by some conventional load spectrum, aimed to reproduce the fatigue damage induced by the real one. Nevertheless, the definition of load spectra for bridges requires careful consideration of fatigue assessment methodology, to assure that conventional spectra and real spectra involve the same effects [31].

Studies have shown that fatigue evaluation is highly site-specific. From a roadway bridge fatigue effect point of view the important parameters are the frequency and magnitude of axle loads and the spacing between them in time as they cross a bridge [32]. To investigate fatigue of bridges loaded with heavy trucks, it is convenient to use the load spectra obtained by weigh-in-motion (WIM) measurements [33]. WIM results can be used to calculate statistical stress parameters for the studied bridge.

4.2 Weigh-in-motion measurements

The ability to weigh vehicles as they travel at speed on highways has become known as Weigh-in-Motion (WIM) technology. By using a WIM system, virtually a 100% sample of traffic data for statistical purposes can be obtained. The information can be transmitted immediately in real time, or at some future time, to locations remote from the WIM site via conventional communications networks [34].

A WIM test attempts to gather truck traffic data, which includes axle weight, axle spacing, total vehicle weight, vehicle velocity, multiple truck presence on the bridge, and average daily truck traffic (ADTT). These parameters are obtained while the car or truck is moving, which allows to inspect much more vehicles at the same time than with a static weighing method [35].

Basically two types of WIM systems can be distinguished: systems that are mounted on the road surface and systems that are mounted underneath a bridge to provide a signal that allows classifying vehicles. A common WIM system of the former type is based on wheel scales that are integrated into the road surface. These systems can be easily calibrated by means of static methods and allow to determine directly the axle load. Even though wheel scales provide

reasonable accuracy for lower vehicle velocities, these systems are rarely employed nowadays since maintenance is costly and the traffic has to be interrupted during service actions [35].

Another commonly used WIM systems mounted on the road surface are load sensors based on strip lines. Thin wires with a cross section of a few mm^2 to cm^2 are installed in the road surface. The pressure-, force-, and drag influence is measured while a vehicle passes the test section. An integrating method is required since only a small part of the tire affects the measurement section. Even though the accuracy for the strip line system is typically lower than for the wheel scales due to the integrating measurement method, installation is significantly easier.

For systems mounted underneath a bridge (also called Bridge-WIM systems or B-WIM systems), the elongation underneath the bridge is measured, typically by means of strain gauges or inductive displacement sensors. Furthermore, these systems usually include axle detectors (tape switches or infrared sensors) and data acquisition and processing system. Bridge WIM systems have the advantage that maintenance and calibration does not affect the traffic at all [35].

The WIM stations should be regularly calibrated and verified. Nevertheless, due to the dynamic nature of moving loads, low percentages of erroneous results can arise during everyday use. Therefore some filtering of the data is required.

Fatigue assessment of bridges requires the collection of actual dynamic stress time histories of various bridge members and components. Following the collection of time histories by the WIM system, data must be processed into a usable form. Commonly occurring load histories in fatigue analysis often are categorized as either narrowband or wideband processes. Narrowband processes are characterized by an approximately constant period (fig 3.11a) while wideband processes are characterized by higher frequency small excursions superimposed on a lower, variable frequency process (fig 3.11b) [36].

According to [31], the powerful methods of stochastic process theory, often used in defining fatigue load spectra in other engineering structures, cannot be applied to highway bridges, as the loading is both random and dynamic and the induced stress histories are wideband in nature. So, that implies that the link between action and effect cannot be expressed by simple formulae, while further difficulties arise when vehicle interactions become significant.

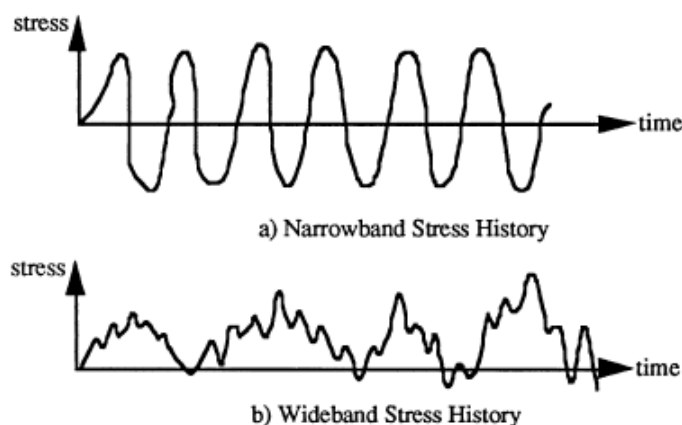


Figure 3.11 Examples of narrowband (a) and wideband (b) stress histories [36]

Stress histories that are wideband in nature do not allow for simple cycle counting. The cycles are irregular with variable frequencies and amplitudes. Several cycle-counting methods are available for the case of wideband and nonstationary processes, each successful to a degree in predicting the fatigue life of a structure. The rainflow method [37] is preferred due to the identification of stress ranges within the variable amplitude and frequency stress histogram and

that it allows the application of Miner's rule [38] in order to assess the fatigue life of a structure subject to complex loading. The rainflow method counts the number, n , of cycles in each predetermined stress range, S_i , for a given stress history.

The results obtained from WIM measurements can be presented as traditional histograms or cumulative distributions functions (CDFs). Fig. 3.12 (left) [33] shows an example of CDFs of strains obtained using the WIM data from a 10-girders steel bridge and represented on the normal probability paper. The equivalent stresses, σ_{eq} , needed to find the number of cycles to failure from the $S-N$ relationship can be calculated on the basis of Miner's rule [38] and his assumption that the damage in material is accumulating in a linear way according to the applied number of load cycles. The equivalent stress values for the load spectra given in fig. 3.12 (left) are shown in fig. 3.12 (right) [33].

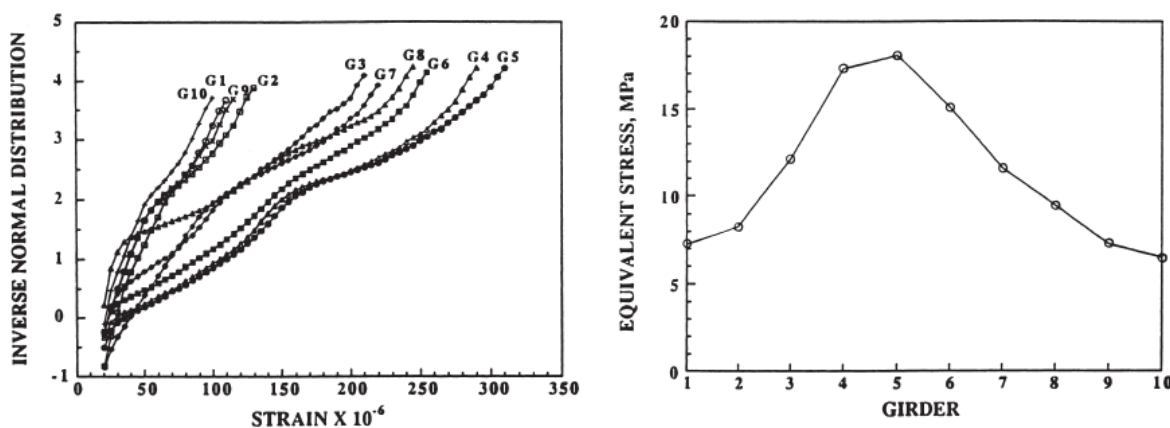


Figure 3.12 CDFs of strain (left) and the corresponding equivalent stresses (right), obtained from WIM measurements in a 10-girder steel bridge (taken from [33])

The obtained fatigue cycle information from WIM measurements is local to the area of the WIM station and should be used only for assessing bridges within that network of the same traffic volume [32].

5 FINAL REMARKS

In this chapter, operational methods for the determination of model parameters for deterioration processes such as corrosion, sulfate attack and alkali-aggregate reaction have been briefly described. The use of microwave interferometry for remote monitoring and control of aging infrastructures is also described. Weigh-in-motion technology for determining the fatigue load parameters for the assessment of roadway bridges is presented. The following conclusions can be drawn:

- The assessment of corrosion-deteriorated infrastructures involve the determination of parameters such as corrosion rate, electrical resistivity and potential. Environmental parameters such as temperature, moisture content, chloride content and depth of carbonation front, should also be determined.
- The parameters normally used to determine sulfate concrete damage include expansion, loss of compressive or tensile strength, wear rating, loss of mass, surface hardness, variation of dynamic modulus of elasticity, and volume instability. Due to the complicated mechanisms involved in sulfate attack, no simple parameter can be used to evaluate sulfate-related damage in all conditions. Hence, it is advisable to use a combination of the mentioned parameters for evaluating the degradation of concrete.

- A detailed field survey is normally the first stage for identifying the possible presence of AAR in concrete elements, and the extent of deterioration. The most commonly reported field symptoms of AAR are deformations and displacements, cracking and the presence of gel. Visual survey is generally complemented by laboratory testing on cores extracted from the studied elements to confirm the presence of AAR and assess the current condition of concrete. The parameters for the assessment of AAR damaged concrete normally include expansion, and variation of the compressive and the tensile strength, and of the dynamic modulus of elasticity.
- Fatigue deterioration is a process conditioned by the amplitude and the total number of stress cycles a given fatigue detail will be subjected to. Variations of stresses in roadway bridges are mainly due to continuous traffic action.
- Fatigue assessment of bridges requires the collection of actual dynamic stress time histories. WIM systems can be used for the collection of these stress histories in roadway bridges. Following WIM measurements, obtained data must be processed into a usable form.

REFERENCES

- [1] Holicky M., Diamantidis D. et al. (2014), *Methods for the risk assessment and risk-based management of aging infrastructure*, Lifelong Learning Programme, Czech Technical University in Prague, Klokner Institute, ISBN: 978-80-01-05611-0.
- [2] CONTECVET (2001), *A validated user's manual for assessing the residual service life of concrete structures*, EC Innovation Program IN30902I, IETCC-CSIC, Geocisa, Madrid.
- [3] Andrade, C. (2012), "Corrosion Data Interpretation in Concrete Structures", In: Andrade C. and Gulikers J. (eds.) *Advances in Modelling Concrete Service Life: Proceedings of the 4th International RILEM PhD Workshop, Madrid, Spain, November 19, 2010*, RILEM Bookseries, Vol. 3, pp. 1-10, ISBN 978-94-007-2702-1.
- [4] Andrade C., D'Andréa R., Castillo A., Castellote M. (2009), "The use of electrical resistivity as NDT method for specification the durability of reinforced concrete", In: *NDTCE'09, Non-Destructive Testing in Civil Engineering*, Nantes, France, June 30th – July 3rd, 2009.
- [5] Wenner F. (1915), "A Method of Measuring Earth Resistivity", *U.S National Bureau of Standards*, Paper 258, Bull. 12(4), pp 469–478.
- [6] Andrade C., Alons, C., Gulikers, J., Polder R., Cigna R., Vennesland O., Salta M., Raharinaivo A., Elsener, B. (2004) "Rilem TC 154-EMC Recommendations, Test methods for on-site corrosion rate measurement of steel reinforcement in concrete by means of the polarization resistance method", *Materials and Structures*, Vol. 37.
- [7] Feliú S., González J. A., Feliú S. jr., Andrade, C. (1990), "Confinement of the Electrical Signal or in-situ Measurement of Polarization Resistance in Reinforced Concrete", *ACI Materials Journal*, Vol. 87.
- [8] Tixier R. and Mobasher B. (2003), "Modelling of Damage in Cement-Based Materials Subjected to External Sulfate attack. II: Comparison with experiments", *ASCE Journal of Materials in Civil Engineering*, Vol. 15, No. 4, , pp. 314-322.
- [9] Skalny J., Marchand J. and Odler I. (2002), *Sulfate Attack on Concrete*, Spon Press, London, New York, ISBN 0-419-24550-2.
- [10] Santhanam M., Cohen M. D. and Olek J. (2001), "Sulfate Attack Research – Whither now?", *Cement and Concrete Research*, Vol. 31, pp. 845-851.
- [11] ASTM C452/C452M-10 (2010), *Standard Test Method for Potential Expansion of Portland-Cement Mortars Exposed to Sulfate*, ASTM International, West Conshohocken, PA, USA.

- [12] ASTM C1012/C1012M-13 (2013), *Standard Test Method for Length Change of Hydraulic-Cement Mortars Exposed to a Sulfate Solution*, ASTM International, West Conshohocken, PA, USA.
- [13] Santhanam M. (2007), “Sulphate Attack from an Engineering Perspective”, In: De Belie N. (ed.) *Proc. of RILEM Workshop on Performance of Cement-based Materials in Aggressive Aqueous Environments Characterization, Modelling, Test Methods and Engineering Aspects*, September 2007, Ghent, Belgium.
- [14] Neville A. (2004), “The confused world of sulfate attack on concrete”, *Cement and Concrete Research*, Vol. 34 pp. 1275–1296.
- [15] Xu A., Shayan A. and Baburamani P. (1998), *Test methods for sulfate resistance of concrete and mechanism of sulfate attack - state of the art review*, ARRB Transport Research Ltd Review Report 5, Vermont South, Australia, ISBN: 0-86910-772-0.
- [16] Croce P., Holicky M. et al., (2013), *Operational Methods for the Assessment of Existing Structures*, Lifelong Learning Programme, Pisa, ISBN: 978-88-8250-135-8.
- [17] Santhanam M. (2001), *Studies on sulfate attack: mechanisms, test methods, and modeling*, Ph. D. Thesis, Purdue University, West Lafayette, USA.
- [18] Nazarian S. and Stokoe K. H. (1984), “Nondestructive testing of pavement using surface techniques”, *Transportation Research Record*, Vol. 993, pp. 67-79.
- [19] Menendez E. (2011), “Aplicación de Técnicas Instrumentales al Diagnóstico y Monitorización de Hormigón Alterado por Reacciones Expansivas Internas”, En: Andrade C., Menéndez E., Lima L. y Luchtemberg C. (eds.), *Avances en Seguridad y Durabilidad – Ciclo de vida de las Estructuras – Auscultación y Diagnóstico de Estructuras Deterioradas*, Madrid, ISBN: 978-84-694-1597-9.
- [20] Swamy R. N. (1989), “Structural Implications of Alkali Silica Reaction,” *Proc. Of 8th International Conference on Alkali-Aggregate Reaction*, Kyoto, Japan, Elsevier Applied Science Ltd., London, United Kingdom.
- [21] Fournier B. and Bérubé M. A. (2000), “Alkali-aggregate reaction in concrete: a review of basic concepts and engineering implications”, *Canadian Journal of Civil Engineers*, Volume 27, pp. 167 –191.
- [22] Ben Haha M. (2006), *Mechanical effects of alkali silica reaction in concrete studied by SEM-image analysis*, Ph. D. Thesis, EPFL, Lausanne, Switzerland.
- [23] Jones A. E. K. and Clark L. A. (1994), “The practicalities and theory of using crack width summation to estimate ASR expansion”, *Proceedings of the Institution of Civil Engineers - Structures and Buildings*, Vol. 104, Issue 2, May, pp. 183 – 192.
- [24] DURACRETE (1998), *Probabilistic Performance Based Durability Design of Concrete Structures – Modelling of Degradation*, The European Union – Brite EuRam III, Contract BRPR-CT95-0132, Project BE95-1347, Document BE95-1347/R4-5.
- [25] Jones A. E. K. and Clark L. A. (1998), “The effects of ASR on the properties of the concrete and the implications for assessment”, *Engineering Structures*, Vol. 20, Issue 9, pp. 785 – 791.
- [26] Rivard P. and Saint-Pierre F. (2009), “Assessing alkali-silica reaction damage to concrete with non-destructive methods: From the lab to the field”, *Construction and Building Materials*, Vol. 23, pp. 902 – 909.
- [27] Li H. N, Li, D. S. and Song, G. B. (2004) “Recent applications of fiber optic sensors to health monitoring in civil engineering”, *Engineering Structures*, Vol. 26, pp. 1647-1657.
- [28] Gentile C. (2009) “Radar-based measurement of deflections on bridges and large structures: advantages, limitations and possible applications”, In: *Proceedings of IV ECCOMAS Thematic Conference on Smart Structures and Materials (SMART’09)*, 13-15 July, Porto, Portugal.
- [29] Olson Instruments Inc. *Infrastructure imaging for assessment, monitoring and repair - The IBIS-S radar system*, Wheat Ridge, Colorado, USA <http://www.OlsonEngineering.com>.

- [30] Crespo-Minguillón C. (1996), *A Reliability Based Methodology to Define the Limit State of Decompression in Prestressed Concrete Bridges*, Ph. D. Thesis, Universidad Politécnica de Cataluña, Barcelona, Spain.
- [31] Croce P. (2001), “Background to fatigue load models for Eurocode 1: Part 2 Traffic Loads”, *Progress in Structural Engineering and Materials*, Vol. 3, pp. 333-345.
- [32] Treacy M. and Brühwiler E. (2012), “Fatigue loading estimation for road bridges using long term WIM monitoring”, In: Bérenguer, Grall and Guedes Soares (eds.), *Advances in Safety, Reliability and Risk Management*, Taylor & Francis Group, London, pp. 1870-1875, ISBN 978-0-415-68379-1.
- [33] Szerszen M. M., Nowak, A. S. and Laman, J. A. (1999) “Fatigue reliability of steel bridges”, *Journal of Constructional Steel Research*, Vol. 52, pp. 83-92.
- [34] Miao T. J. and Chan T. H. T. (2002), “Bridge live load models from WIM data”, *Engineering Structures*, Vol. 24, pp. 1071-1084.
- [35] Lechner B., Lieschnegg M., Mariani O., Pircher M. and Fuchs A. (2010) “A Wavelet-Based Bridge Weigh-in-Motion System”, *International Journal on Smart Sensing and Intelligent Systems*, Vol. 3, No. 4, pp. 573-591.
- [36] Nowak, A. S. and Kim, S. (2000), “Weigh-in-Motion Measurement of Trucks on Bridges”, In: Wai-Fah Chen and Lian Duan (eds.) *Bridge Engineering Handbook*, Boca Raton: CRC Press.
- [37] Matsuishi M. and Endo, T. (1968) “Fatigue of metals subjected to varying stress”, Proceedings of the *Japan Society of Mechanical Engineering*, Fukuoka, Japan, March.
- [38] Miner M. A. (1945), “Cumulative damage in fatigue”, *ASME Journal of Applied Mechanics*, Vol. 12, n° 3, September.

CHAPTER 4: STRUCTURAL FAILURE AND ASSESSMENT OF A DEPARTMENT STORE

Milan HOLICKÝ

Klokner Institute of the Czech Technical University in Prague, Czech Republic

Summary

After few years in service of the department store serious performance defects of cladding, interior partitions, and other secondary elements had been observed. A detailed analysis has shown that the serviceability failure of the second storey was primarily caused in design by lack of consideration of deflections from permanent load and shrinkage [3], [4]. Presented theoretical model of public perception, which is a substantial extension of the previous study [4], takes into account uncertainty and vagueness in perceiving observed defects as well as effects of possible consequences. It appears that the developed theoretical model can well explain the wide differences between the public perception and the expert assessment of its structural condition.

1 INTRODUCTION

The load bearing structure of a recently built department store in Prague consists of the flat (double ribbed) reinforced concrete slabs supported directly on columns located within span distances 12×12 m. Slabs above the first and second storey cantilever out by 3 m beyond the edge columns. After few years in service serious performance defects of cladding, interior partitions, and other secondary elements had been observed [1,2].

Incidentally at the same time another department store of the same user collapsed. This was perhaps partly the reason why all the performance defects of the new building had been carefully recorded and publicly reported, although the collapsed department store was a steel structure and its failure occurred due to well-recognised causes. Unfavourable engineering climate (psychological aspects) seems to have played a significant role in the subsequent assessment of structural damage. The observed defects were often exaggerated and interpreted as structural condition indicating insufficient safety against collapse, not just serviceability defects. Consequently, after less than 10 years in service, the second storey of the two-floor building was completely closed and the damaged non-bearing components were reconstructed.

2 DESCRIPTION OF THE STRUCTURE

The plan view dimensions of the building are 78×53 m. The load-bearing structure consists of reinforced concrete double ribbed slabs of the total thickness 0.45 m supported directly by columns of the cross section 0.5×0.5 m or 0.7×0.7 m located within span distances 12×12 m (see Figure 1). The slabs are provided by in-depth heads, 1.65×1.65 m (at the edge columns) and 3.35×3.35 m (at the interior columns), where the coffer ceiling is replaced by solid slab. In the remaining part of the slab, the ribs of the cross section 0.18×0.38 m support a thin plate (of the thickness 0.07 m and interior spans 0.8×0.8 m). Equivalent thickness of a solid slab having the same rigidity would be 0.34 m only, which indicates that the stiffness of the slab is very low. Moreover, slabs above the first and second storey cantilever out beyond edge columns by 3 m.



Figure 1 Internal view of the structure

Design loads of the slab above the ground floor considered in the original analysis consist of a permanent part 7.0 kN/m^2 and a variable part 4.0 kN/m^2 , corresponding values for the slab above the first floor are 7.2 kN/m^2 and 1.5 kN/m^2 . However, the actual permanent load of this slab is due to actual roof and ceiling greater and could be as high as 10 kN/m^2 . Nevertheless, the ultimate strength of the slab is sufficient, and no strengthening of the load bearing structure was needed.

Non-bearing elements of the second storey, which were affected by deformations of bearing structures consist of façade cladding, interior partition walls and interior built-in components like glass walls and shelf stands. Cladding of the building consists of large glass windows, brick walls and window pillars, located within regular distances of 2.4 m. The window pillars, reinforced by steel ties anchored into floor and ceiling, were built in the bearing slabs without any movement joints. Similarly all interior masonry partition walls, reinforced by rolled steel elements of I- and U-section were constructed without any separation from roof slab. Expansion joints were not used in any interior built-in components. All of these non-bearing structures were designed without consideration of differential deflection of both floor and ceiling slabs due to their different stiffness and loading.

3 PERFORMANCE DEFECTS

After few years in service serious performance problems concerning cladding as well as interior non-bearing structures have been observed and analysed [3,4]. The most alarming were perhaps the defects appearing in the non-bearing structures: cracks of partition walls (see Figure 2 and 3).

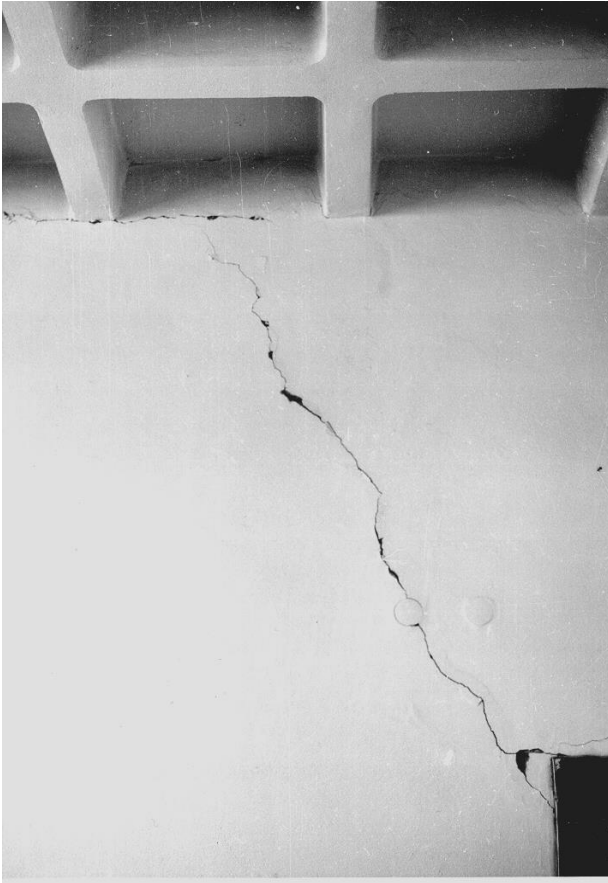


Figure 2 Partition wall

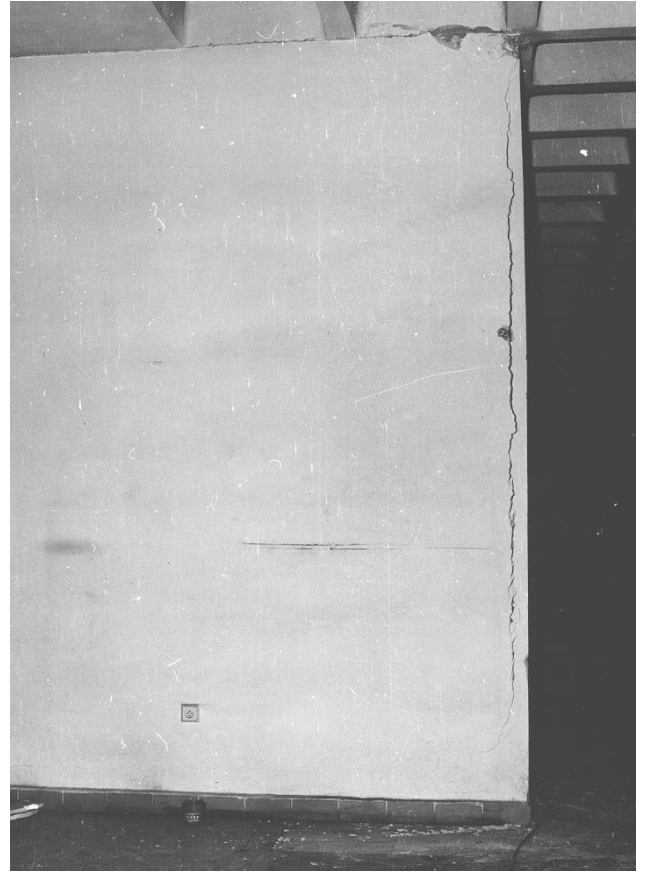


Figure 3 Partition wall



Figure 4 Façade corner



Figure 5 Façade wall

Tensile cracks of the window pillars and cladding elements were particularly noticeable near the exterior corners of the building (see Figure 4 and 5). Also, the deformed doorframes and a buckled shelf stand were visible and impressive. There were also sporadic shear cracks in the slab ribs close to the hidden column heads; however, they were mostly near construction joints. These cracks, which were of smaller importance, were the only detected defects of the load bearing structure.

4 ASSESSMENT

All of the defects of non-bearing structures in the first floor are caused by differential deflections of the floor slab (above the ground floor) and of the roof slab, primarily due to permanent load and shrinkage. As mentioned above the permanent load of the more flexible roof is by 3 kN/m² greater than that of the slightly less flexible floor slab. This could lead to considerable differences in the midspan deflection (shortening up to 30 mm) as well as cantilever deflection (extension up to 5 mm, at exterior corner up to 10 mm). Also shrinkage may lead to similar mutual differences in slab deflections; midspan shortening and cantilever extension may reach 5 mm (extension at exterior corners may be 10 mm).

Deformations due to temporary load and temperature are of smaller importance and may cause a maximum midspan extension 6 mm and shortening 1 mm, cantilever extension or shortening less than 1 mm. The observed deformation effects correlate well with theoretical results. Unfortunately, no calculation of structural deformations had been made in the original design. This was partly due to inadequate provisions of the contemporary standards.

Another construction fault mentioned above concerns the permanent load of the roof slab. Due to the actual self-weight of the ceiling and roof (sloped concrete layers) the permanent load of the slab is by 30 % greater than that assumed in design calculation. However, this discrepancy arises from the neglect of some load components in the design calculation. Also the actual permanent load of the slab above the ground floor may be slightly greater than that considered in design.

Even though the deformation effects would be considerably lower if the actual load equalled the assumed load, many of the serviceability defects would have appeared anyway. This concerns, above all, the cracks in the cladding elements, particularly at the exterior corners of two-way cantilevered slabs. Most of the observed defects were primarily due to lack of consideration of deflection in the design and due to inaccurate determination of the design load. Construction errors, however, considerably added to deformation effects.

5 REPAIR

Although there were almost no defects apparent on the load bearing structure (except sporadic shear cracks in ribs), it was decided to close the first floor and to reconstruct damaged interior partitions and other non-bearing structural components as well as the cladding components. Interior partitions including steel elements have been separated from the ceiling and new movement joints have been covered by panel strip. New ties located near window pillars have mutually tied up the cantilevered slabs. These measures were proposed by the designer, even though an additional analysis shows that the expected deformations due to temporary load and temperature (as mentioned above) are limited, and in some cases could be admitted without any modification of the non-load-bearing structures.

6 PUBLIC PERCEPTION

Public perception (recently discussed in [5]) played an important role in the assessment and final decision concerning the building. The new department store became soon a building closely watched by a large number of users and local authorities. For more, at the same time another department store suffered from construction faults and this was partly the reason why all the performance deficiencies have been carefully recorded (similar experience is described in [5,6]). This unfavourable engineering climate seems to enhance the intensity of public perception. The observed defects were often exaggerated and regarded as indicators of insufficient structural safety. Widespread public perception of defects and discrepancies in expert assessments was reported in newspapers and finally resulted in a strong public demand for strengthening of the building.

7 THEORETICAL MODEL OF PUBLIC PERCEPTION

Evaluation of public as well as expert assessments has indicated that there is no distinct point in any commonly used performance indicator x (e.g. deflection, crack width) that would uniquely separate acceptable and unacceptable structures. Rather there seemed to be a transition region $\langle a, b \rangle$ in which the structure gradually becomes unserviceable and the degree of caused damage $\nu(x)$ increases [4,7]. A conceivable model for $\nu(x)$ is indicated in Figure 6 as a trilinear function. Note that the values of $\nu(x)$ are within the conventional interval from 0 to 1. There is no damage below a certain lower limit value a , and full damage above the upper limit b .

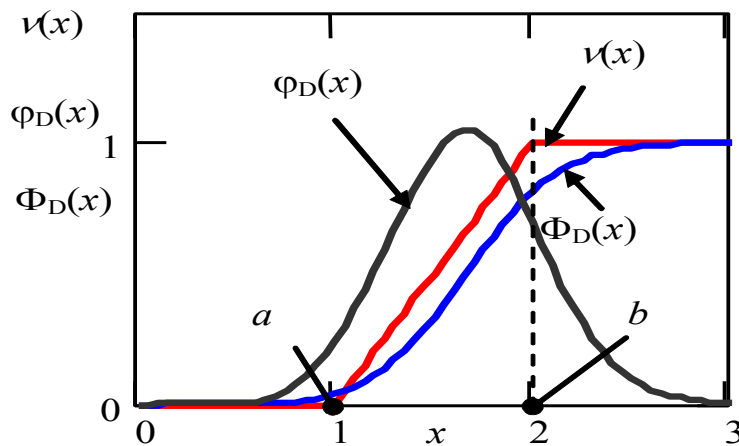


Figure 6. Perception model

Obviously, at any damage level $\nu(x)$ there may be a perception scatter expressed by the distribution function $\Phi_p(x, \mu_p, \sigma_p)$, for which lognormal distribution having the mean $\mu_p = x$ and standard deviation $\sigma_p = s \times a$, where s is a relative measure of scatter related to the lower bound a , is accepted here. Taking into account all levels $\nu(x)$, the cumulative damage $\Phi_D(x)$ is [4,7]

$$\Phi_D(x) = K \int_a^b \nu(\xi) \Phi_p(x, \xi, \sigma_p) d\xi \quad (1)$$

where K is the normalising factor to normalise $\Phi_D(x)$ into the interval from 0 to 1 and ξ is the integration variable. The cumulative damage $\Phi_D(x)$ and a corresponding density function $\phi_D(x)$, shown in Figure 6 for $a = 1$, $b = 2$ and $s = 0.3$, can be considered as generalised probabilistic models (involving economic aspects). The cumulative damage $\Phi_D(x)$ can be used to specify in a rational way the required serviceability constraints [2,3].

Further, considering an appropriate load effect E (e.g. deflection, crack width) having the mean μ_E and an assumed coefficient of variation $w_E (=0.2)$ the expected perception level $\pi(\mu_E)$ can be defined as

$$\pi(\Delta, \sigma_P, \mu_E) = \int_{-\infty}^{+\infty} \varphi_E(x) \Phi_D(x) dx \quad (2)$$

Here $\varphi_E(x)$ is the probability density function of E . Gamma distribution having the mean μ_E is assumed. The mean μ_E equal to the lower limit of the transition region a , $\mu_E = a$, and the standard deviation $\sigma_E = 0.2\mu_E$ (the coefficient of variation 0.2) is assumed in the example shown in Figure 7, where the expected perception level $\pi(\Delta, \sigma_P, \mu_E)$ is indicated as a function of the ratio $\Delta = (b-a)/a$ for selected σ_P . Figure 8 shows $\pi(\Delta, \sigma_P, \mu_E)$ versus μ_E .

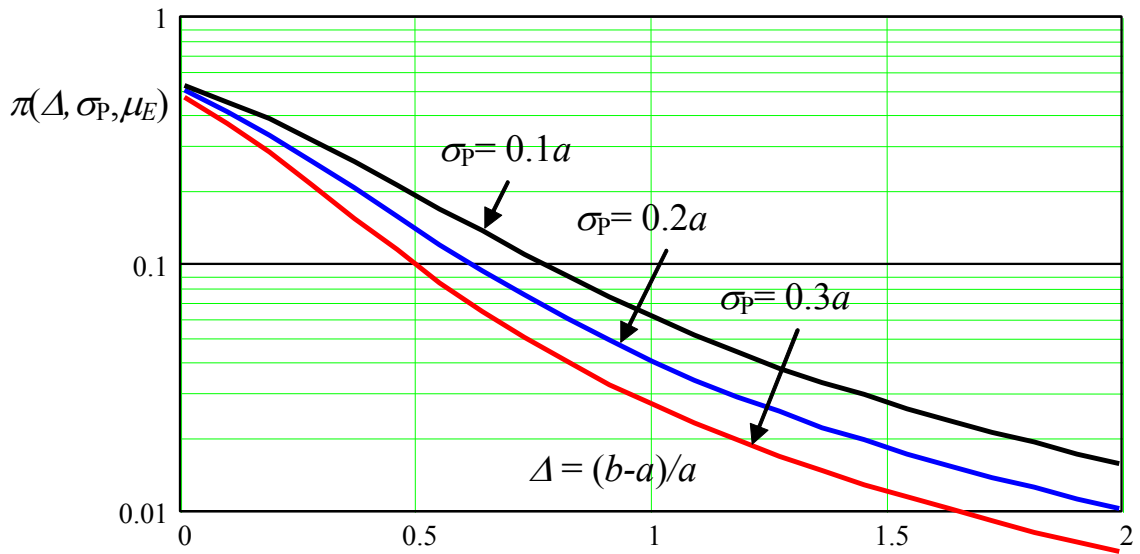


Figure 7 Perception level $\pi(\Delta, \sigma_P, \mu_E)$ for $\mu_E = a$

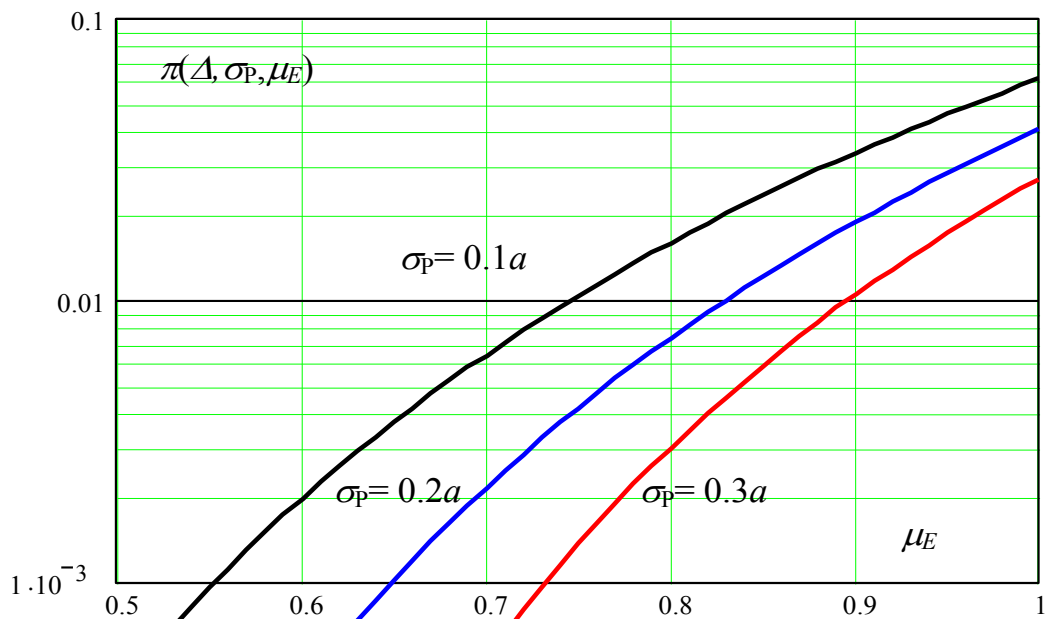


Figure 8 Perception level $\pi(\Delta, \sigma_P, \mu_E)$ for $\Delta = 1$

It follows from Figure 7 and 8 that the expected damage (perception) level $\pi(\Delta, \sigma_p, \mu_E)$ is strongly dependent on both the ratio $\Delta = (b-a)/a$ and the mean μ_E , which may further depend on the sensitivity or experience of the observer. This finding explains the observed differences in public perception and discrepancies in expert assessments.

8 EFFECTS OF EXPECTED CONSEQUENCES

In addition to psychological aspects an assessment of a structure may be affected also by the expected economic (and other) consequences. Both these factors may be considered explicitly or implicitly only. On the one hand consideration of expected consequences may lead to a rational specification of structural constraints, on the other hand it may significantly affect the assessment of the structure.

Assume that the optimum mean μ_E of the load effect E would correspond to the minimum of the total cost C_{tot} . Assuming a given coefficient of variation w_E , the optimum mean μ_E of the load effect E (the most suitable value assessed by an expert) may be obtained from the minimum of the total expected cost of a structure. Consider the total cost C_{tot} as a sum

$$C_{tot} = C_0 + C_m/\mu_E + \pi(\Delta, \sigma_p, \mu_E) C_f \tag{3}$$

where C_0 denotes the initial cost independent of μ_E , and C_m/μ_E is an additional cost affected by modification of the mean μ_E , where C_m is a relevant marginal cost. Finally the multiple $\pi(\Delta, \sigma_p, \mu_E) C_f$ describes the expected cost due to structural failure. Obviously the minimum C_{tot} will occur when the partial cost

$$C_{part} = 1/\mu_E + \pi(\Delta, \sigma_p, \mu_E) C_f/C_m \tag{4}$$

is the minimum, where $C_{part} = (C_{tot} - C_0)/ C_f$. Figure 9 shows the partial cost C_{part} for the following parameters: $(b-a)/a=1$, $\sigma_p=0.3a$, $\sigma_E=0.2\mu_E$.

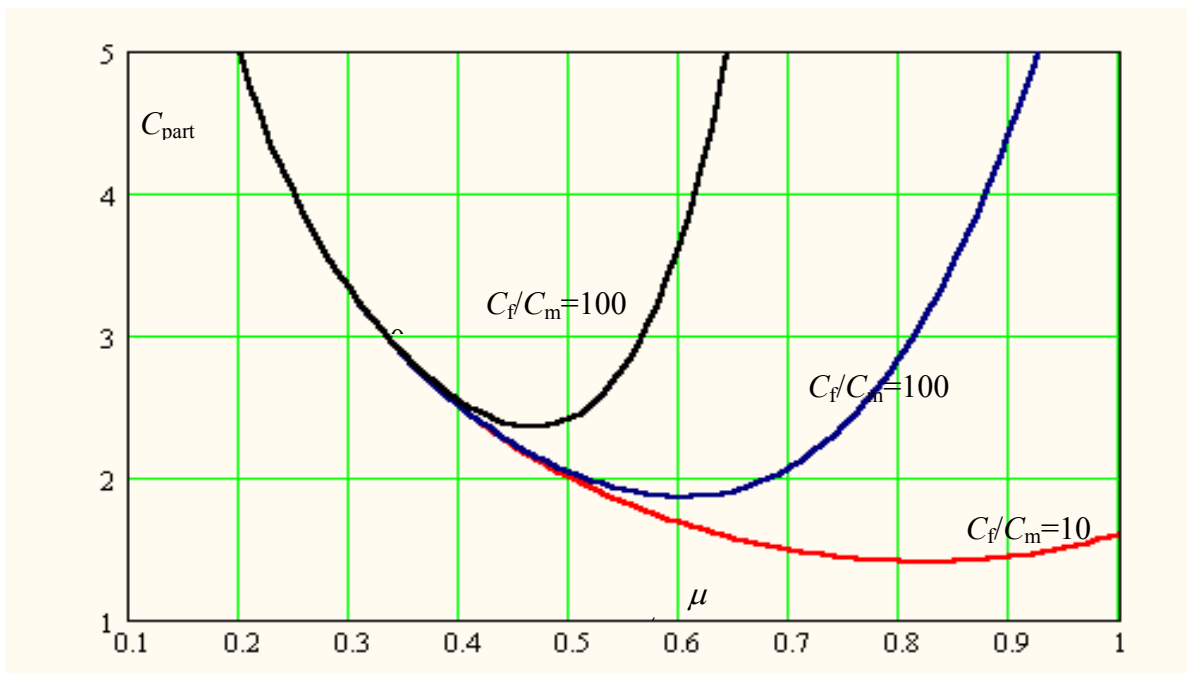


Figure 9 The partial cost C_{part} versus μ_E/a for $\Delta = (b-a)/a=1$, $\sigma_p=0.3a$, $\sigma_E=0.2\mu_E$

It follows from Figure 9 that the optimum mean μ_E may be expected from $0.5a$ to $0.8a$. However, for extremely high cost of failure C_f greater than $1000 C_m$ the optimum mean will be lower than $0.5a$. Obviously, depending on the assumed cost ratio C_f/C_m the optimum (the most suitable) mean μ_E of the load effect E may considerably vary. A further analysis is certainly needed in order to take into account various parameters and expected consequences, including life safety.

9 CONCLUSIONS

1. The serviceability failure of the department store was primarily caused by lack of consideration in design of deflection due to permanent load, shrinkage, variable loads including thermal actions.
2. The construction faults (additional permanent load and imperfect anchoring of ties) increased the unfavourable deformations of the structure.
3. The current engineering climate (psychological aspects) and the expected consequences seem to play an important role in the public perception of performance deficiencies, in the subsequent structural assessment and in the decisions made by the public authorities.
4. There is no distinct value that would uniquely distinguish acceptable and unacceptable structural conditions.
5. The disturbing variance in public perception and in expert assessment of the observed defects may be well explained using proposed theoretical model for public perception.
6. There seems to be an optimum value of the performance indicator that would lead to the minimum total cost and may be considered by an expert as most suitable.
7. The effects of vagueness in structural requirements and of the possible unfavourable consequences, including jeopardy of life, on the judgement of experts requires a more detailed investigation..

REFERENCES

- [1] Holický M., Serviceability problems of department store - Case Study, Symposium on serviceability of buildings, NRC Canada, 1988, pp. 166-171.
- [2] Holický M., Fuzzy concept of serviceability limit states. Symposium on serviceability of buildings, NRC Canada, 1988, pp. 19-25.
- [3] Holický M., Fuzzy probabilistic optimisation of building performance, Automation in Construction, 8/1999pp 437-443.
- [4] Holický M., Performance Deficiency of a Department store - Case Study. IABSE International Conference on Safety, Risk and Reliability - Trends in Engineering, Malta, March 2001, pp 321-326.
- [5] Lewis R., The public perception of risk. RSA Journal, November 1995, pp. 52-63.
- [6] Steward M.G. and Melchers R.E., Probabilistic risk assessment of engineering systems. Chapman & Hall, London, 1997.

LIST OF SYMBOLS

a	lower bound of the transition region
b	upper bound of the transition region
s	relative measure of the perception scatter σ_P/a
x	performance indicator
w_E	coefficient of variation of the load effect E
C_0	initial cost
C_f	malfunction cost
C_m	marginal cost
C_{part}	partial cost
C_{tot}	total cost
E	load effect
K	normalising factor
μ_E	mean of the load effect E
μ_P	mean of the perception level
σ_P	standard deviation of the perception level
$v(x)$	damage level
$\varphi_D(x)$	probability density of the damage
$\varphi_E(x)$	probability density function of E
$\pi(\Delta, \sigma_P, \mu_E)$	perception level
ξ	generic point of the performance indicator x
Δ	transition region ratio $(b-a)/a$
$\Phi_P(x, \mu_P, \sigma_P)$	distribution function of the perception level
$\Phi_D(x)$	distribution function of the damage level

CHAPTER 5: ASSESSMENT OF A CORROSION-DAMAGED REINFORCED CONCRETE STRUCTURE

Peter Tanner¹, Miguel Prieto¹, Carlos Lara¹

¹Eduardo Torroja Institute for Construction Science, IETcc-CSIC, Madrid, Spain

Summary

The building under consideration is situated in the Northwest of Spain and is exposed to a severe marine environment. The existing structure has been in disuse for more than 20 years and is affected by heavy corrosion damages. Formerly used for industrial purposes, the building is to be transformed into a cultural centre for public use.

Reliability verification is required for the structural members to be maintained on the occasion of the building transformation. To this end, the future service conditions and period are to be taken into account. In a first step, site specific information about resistance parameters such as material properties and geometry is obtained from different members of the same building. The assessment based on this information leads to the conclusion that most beams do not meet the safety requirements for the future conditions. Therefore, substitution of the existing floor is proposed, connecting the new concrete slab to the existing beams by means of shear connectors for the purpose of strengthening. Structural reliability is to be verified for this new situation. This second step of the assessment is based on improved information on the existing structure, mainly about material properties and geometry, determined directly for the most critical members, particularly beams.

1 INTRODUCTION

The assessment of an existing structure to resolve its adequacy for present and future use involves different sorts of issues than encountered when designing new structures. The differences are circumscribed essentially to the nature of the available information. In existing structures, deteriorated or otherwise, the level of accuracy of the models used for such assessments can be increased by acquiring more data. However, the updating of information if not carefully planned may result ineffective.

This case study deals with the assessment of the structural reliability of a reinforced concrete (RC) structure of an industrial building from the 1940's located in the Northwest of Spain. After exposure to a severe marine environment during 70 years, and having been in disuse for more than 20 years, it should be transformed into a public building for cultural events. Beams and columns were affected by corrosion due to faulty workmanship as a result of using unwashed sea sand for concrete, in combination with the influence of the marine environment. The existing building in its state before this transformation is represented in Figure 1.

Due to architectural requirements partial demolition of the structure was performed although the transformed building will integrate most of the existing beams and columns. Therefore, firstly the damaged concrete cover of the beams is to be removed and corroded bars are to be cleaned. Finally beams are patch repaired. Reliability verification is required for the structural members to be integrated into the structure of transformed building. To this end, the future service conditions and period are to be taken into account. A rendering of the final condition of the building, which at present is not yet finished, can be seen in Figure 2.



Figure 1 Existing industrial building before the transformation and one of the beams affected by corrosion



Figure 2 Final condition of the building (rendering from Diaz and Diaz Architects)

2 ASSESSMENT PROCEDURE

The assessment of the structural safety is carried out applying a staged procedure. Figure 3 shows the concept of this procedure and its relation to the collection of site data by inspection, material- and field testing.

In this case study, the partial factor method is used for the assessment with site specific data, applying the verification criteria for existing structures defined in the current Spanish Technical Building Code [1] and summarized in section 3. In the first stage, site information for material properties and geometry is obtained from a limited number of members of the same building. This data is used to deduce site specific characteristic values for load and resistance variables and the corresponding partial factors. For purpose of example, in this chapter updating is illustrated for material strength variables only. In the assessment based on that information it is concluded that most beams do not meet the safety requirements for the future conditions.

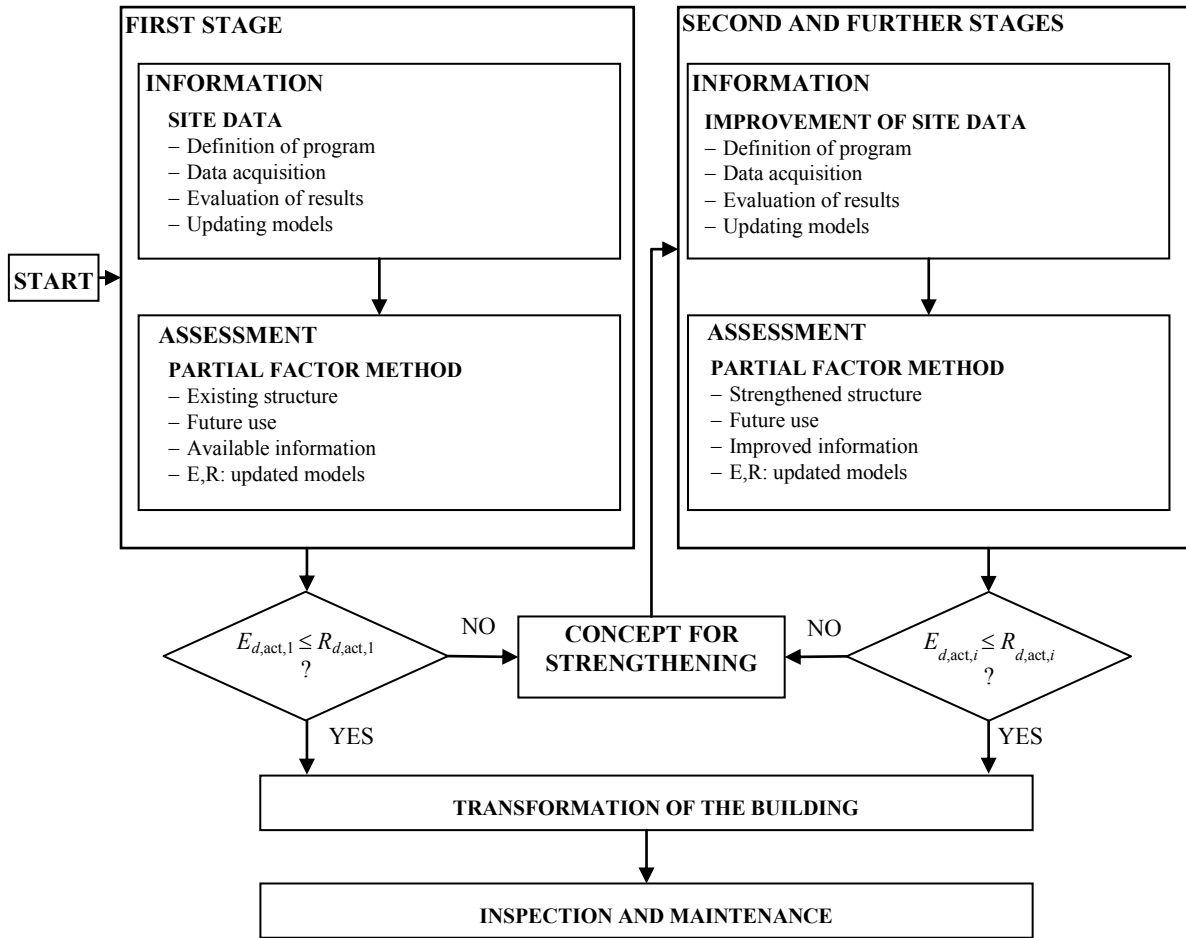


Figure 3 Staged procedure used in this case study

Therefore, an intervention on the structure is to be adopted. Substitution of the deteriorated existing floor is proposed, connecting the new concrete slab to the existing beams by means of post installed rebars for the purpose of strengthening (Section 5). Structural reliability is to be verified for this new situation. In this second stage of the assessment, an additional data acquisition program is put into practice to obtain improved information about the existing beams for further updating of the characteristic values of the resistance variables and the associated partial factors. If in this stage of the evaluation safety is not verified a different concept for strengthening of the structure is to be adopted.

3 BASIS OF EXAMINATION

3.1 Partial factor format for assessment

As described in [2], a cross-section, structural member or connection, is deemed to be structurally safe for its remaining service life if the following criterion holds in all significant hazard scenarios:

$$E_{d,act} = R_{d,act} \quad (1)$$

For persistent and transient situations, the examination values for the action effects, $E_{d,act}$, can be determined as follows:

$$E_{d,act} = \gamma_{Sd,act} \cdot E \left\{ \sum_{j \geq 1} \gamma_{g,j,act} \cdot G_{k,j,act}; \gamma_{p,act} \cdot P_{k,act}; \gamma_{q,1,act} \cdot Q_{k,1,act}; \sum_{i > 1} \gamma_{q,i,act} \cdot \psi_{0,i} \cdot Q_{k,i,act} \right\}. \quad (2)$$

The symbols $G_{k,j,act}$, $P_{k,act}$, $Q_{k,1,act}$ and $Q_{k,i,act}$ represent, respectively, the updated characteristic values for the permanent, prestressing, leading and accompanying variable actions; and $\gamma_{f,act}$ represents the updated partial factors through which possible unfavourable deviations in the action values from the updated characteristic values are introduced in the model. With updated partial factor $\gamma_{Sd,act}$, the model makes allowance for the uncertainties associated with the action effect models and the simplified representation of actions. The partial factor format adopted to establish examination values for action effects differs from standard code rules for structural design such as laid down in the Eurocodes [3]. However, this format is more accurate for assessment purposes as explained below. Due to the change of use of the building, in this case study the examination values for the action effects are not updated.

The examination value for ultimate resistance, $R_{d,act}$, is determined by using updated characteristic values for material or product properties, $X_{k,i,act}$, and the updated design values for geometric data, $a_{d,act}$, according to the definition in the Eurocodes [3]:

$$R_{d,act} = \frac{1}{\gamma_{Rd,act}} R \left\{ \eta_{i,act} \frac{X_{k,i,act}}{\gamma_{m,i,act}}; a_{d,act} \right\} \quad i \geq 1 \quad (3)$$

The partial factor for resistance is divided into the updated partial factors for material or product properties, $\gamma_{m,i,act}$, and an updated partial factor associated with resistance model uncertainties, $\gamma_{Rd,act}$. In reinforced concrete structures, for instance, different updated partial factors associated with resistance model uncertainties (described in detail in [4]) are defined for bending moments, $\gamma_{Rd,M,act}$, tensile forces in the web, $\gamma_{Rd,Vs,act}$, diagonal compression forces in the web, $\gamma_{Rd,Vc,act}$, and axial compression forces, $\gamma_{Rd,N,act}$. The criteria applicable to action effects also apply to the respective resistances: the partial factor format adopted to calculate the examination value for ultimate resistance is a more accurate approach to assessment than the usual code formats used for design purposes [3]. While updating partial factors for action effects and resistance variables is relatively a straightforward process, updating partial factors associated with action effects and resistance model uncertainties is the opposite case. Therefore normally prior values of partial factors for action effects and resistance model uncertainties are commonly used.

3.2 Load bearing capacity of corrosion-damaged structures

3.2.1 General

Corrosion of reinforcement bars is generally considered as the most unfavourable deterioration mechanism of RC structures. The main effects of corrosion include:

- Reduction in steel cross-section,
- Embrittlement and decreasing ductility of steel,
- Stress concentrations due to geometric discontinuities induced by non-uniform corrosion, particularly due to pitting corrosion caused by chloride ingress,
- Cracking and spalling of concrete cover,
- Bond deterioration.

As a result of these effects, and depending on the degree of deterioration, corrosion of reinforcement bars may affect both, serviceability and ultimate limit states.

3.2.2 Resistance models

Resistance models given in EN 1992-1-1 [5] and fib Model code 2010 [6] (hereafter “MC2010”) for bending and shear, respectively, are adapted for the assessment of corrosion-damaged structures. In depth details are given in previous publications [7, 8]. The assumptions described in Chapter 3 of Handbook 1 of this Leonardo da Vinci Project [9], are summarized below:

- The remaining cross-section of steel is considered while mechanical properties of corroded steel are insignificantly affected by embrittlement or stress concentrations due to the uniform corrosion. This can be normally assumed for ductile materials.
- The expansion of corrosion products may yield cracking of the concrete subjected to compression; this is described by reducing the concrete compressive strength to $k_{cp}f_c$. When the concrete is sufficiently confined, the reduction factor k_{cp} is equal to $1.0\eta_{fc}$. The brittleness factor $\eta_{fc} = (30/f_c)^{1/3}$ accounts for the more brittle behaviour of concrete with higher strength [10]. Concrete cover cracks due to bar corrosion in a compression zone are usually parallel to the bars. Therefore, $k_{cp} = 0.75\eta_{fc}$ is considered consistently with the reduction factor in MC 2010 [6] for struts with cracks parallel to the direction of the compression. Note that the reduction affects the concrete cover only and its relative importance might decrease with an increasing height of cross-section. This approach is approximate and the reduction of concrete compressive strength due to cracking of concrete in compression should be further investigated.
- Upper and lower limit for the resistance is established following [11]. The reduced compressive strength $k_{cp}f_c$ is used to assess the upper limit. For the lower limit, concrete spalling as a result of the expansion of the corrosion products is assumed and the concrete cover in the compressive zone of the cross-section is disregarded.

4 FIRST STAGE OF THE EVALUATION

4.1 Information

In the first stage of the evaluation, site information for material properties and geometry is obtained from members of the same building. The concrete and reinforcing steel mechanical properties are summarized in Tables 1 and 2, respectively. The symbols f_{cm} , σ_{fc} and V_{fc} represent, respectively, the mean concrete compressive strength according to the tests, the standard deviation and the coefficient of variation. The symbols f_{ym} and V_{fy} represent, respectively, the mean value and the coefficient of variation of the yield strength of reinforcing steel. The symbols f_{tm} and V_{ft} , represent, respectively, the mean value and the coefficient of variation of the tensile strength of reinforcing steel.

4.2 Updating of material strength

4.2.1 General

The assessment of the existing RC structure entailed updating the characteristic values and the distribution function parameters for the yield strength of the reinforcing steel and the compressive strength of concrete. A “Bayesian prediction method with vague prior distributions” for updating the material properties was performed in the first stage for both materials according to publications [3, 12, 13] with the material properties available from a series of tests performed on specimens extracted from the structure under investigation (Tables 1 and 2). The assessment of the existing corrosion damaged building structure is simplified here for the intention is not to discuss case-specific details, but to illustrate the application of the staged procedure and the

effect of improving the accuracy of information. Hence, in this case study, geometry regarding the remaining steel cross-section is assumed to be updated and prior probabilistic model parameters are adopted from [4].

Table 1 Concrete mechanical properties

Source	Number of tests	f_{cm} [N/mm ²]	σ_{fc} [N/mm ²]	V_{fc}
Site data	6	27.3	9.7	0.36

Table 2 Reinforcing steel mechanical properties

Source	Diameter [mm]	Number of tests	f_{ym} [N/mm ²]	V_{fy}	f_{tm} [N/mm ²]	V_{ft}
Site data	10	3	390	0.06	452	0.02
	12	3	358	0.03	405	0.08
	20	3	219	0.05	350	0.07

The beam cross-section is defined in Figure 4. The represented figures correspond to the mean values measured on different beams from the same structure.

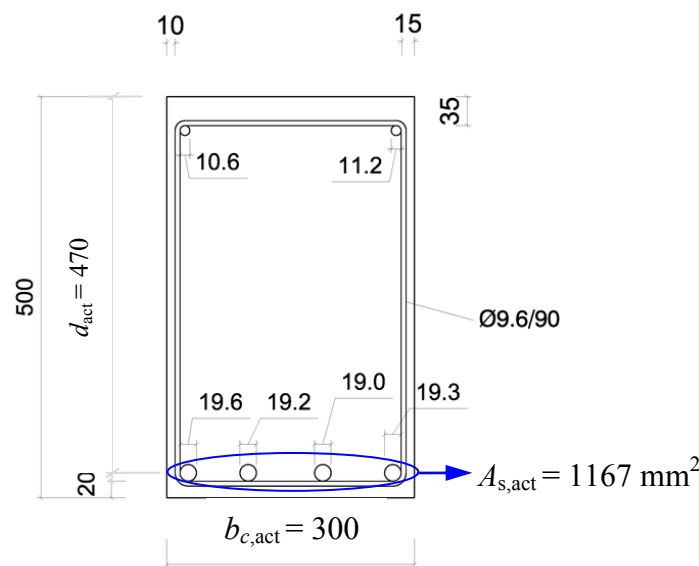


Figure 4 Geometry of beam cross-section according to on site measurements

4.2.2 Concrete

For concrete, the prior probabilistic model was assumed to be log-normally distributed with a known coefficient of variation, $V_X = 0.25$. The estimated coefficient of variation for concrete strength is derived from the Spanish reinforced concrete code [14] that most likely was in force when the building structure was designed.

If a variable X is log-normally distributed, it can be considered as a particular case of a normal distribution Y . Consequently if

$$X \approx LN(\mu, \sigma^2) \quad (4)$$

the methodology described in [13] can be applied, taking into account the transformation:

$$Y = \ln(X) \approx N(\mu, \sigma^2) \quad (5)$$

Therefore, the posterior predictive distribution function of the concrete compressive strength is found to be also log-normally distributed [13] and is given by

$$Y = \ln X \equiv N\left(x \mid m_1, \frac{n_1 + 1}{n_1} \sigma_x^2\right) \quad (6)$$

According to [12], if V_x is known from prior knowledge

$$\sigma_{\ln X} = \sqrt{\ln(1 + V_x^2)} = \sqrt{\ln(1 + 0.25^2)} \approx 0.25 \quad (7)$$

Pursuant to [12, 13], prior information on distribution parameters can be characterized by four estimators: n_0 (prior sample size), m_0 (prior logarithmic sample mean), w_0 (prior logarithmic sample standard deviation), c_0 (prior number of degrees of freedom for w_0). Further to the available prior information and with the assumptions of known standard deviation and vague prior information, the values for the prior distribution estimators in the first stage are equal to zero and $w_0 = \sigma_{\ln X}$.

From the findings of the data acquisition campaign of the building site, the parameter values obtained from the concrete sample are as follows:

- Sample size, $n = 6$;
- Logarithmic sample mean, $\sigma_{\ln X} = 3.24$;
- Logarithmic sample standard deviation, $s_{\ln X} = 0.41$.

The vague prior information is combined with the results of n concrete tests from the site investigation to obtain the posterior estimators. The expressions for the updated values of the logarithmic mean, $\mu_{\ln X, \text{act}}$, the logarithmic standard deviation, $\sigma_{\ln X, \text{act}}$, and the characteristic values were:

$$\mu_{\ln X, \text{act}, 1} = m_1 = \frac{n_0 m_0 + n \mu_{\ln X}}{n_1} \quad (8)$$

$$\sigma_{\ln X, \text{act}, 1} = \sqrt{(n_1 + 1)/n_1} \sigma_{\ln X} \quad (9)$$

$$X_{k, \text{act}, 1} = \exp(\mu_{\ln X, \text{act}, 1} - T_{c1} \sigma_{\ln X, \text{act}, 1}) \quad (10)$$

According to the literature [12, 13] if $\sigma_{\ln X}$ is known, then $c_1 = \infty$ and T_{c1} is equal to $u_{0.05}$, the 0.05 fractile of the standard normal distribution. The updated characteristic value of the compressive strength of concrete and the updated distribution parameters are summarized in Table 3.

Table 3 Updated concrete compressive strength and distribution parameters corresponding to the first stage

$f_{ck, \text{act}, 1}$ [N/mm ²]	$V_{fc, \text{act}, 1}$	$S_{fc, \text{act}, 1}$ *
16.55	0.27	1.55

*: Bias coefficient (ratio between mean and representative (characteristic) value of the basic variable)

4.2.3 Reinforcing steel

For the reinforcing steel, the updating procedure for the yield strength is performed for the bar diameters of 10, 12 and 20 mm. As in the case of concrete, the prior probabilistic model was assumed to be log-normally distributed with a known coefficient of variation, $V_X = 0.10$. This coefficient of variation was estimated from the former code [14].

Expressions (4) to (10) are also applicable for the reinforcing steel yield strength. Likewise, the posterior predictive distribution function of yield strength of the reinforcing steel is found to be log-normally distributed.

The logarithmic standard deviation for each of the bar diameters considered is equal to $\sigma_{\ln X} = 0.10$. The values for the prior distribution estimators in the first step with the assumptions of known standard deviation and vague prior information are equal to zero and $w_0 = \sigma_{\ln X}$. From the findings of the data acquisition campaign, the parameter values obtained for each of the bar diameter samples are given in the following table.

Table 4 Parameter values for each of the bar diameter samples at the first stage of evaluation

	Bar diameter		
	10 mm	12 mm	20 mm
Sample size (n)	3	3	3
Logarithmic sample mean ($m_{\ln X}$)	5.96	5.88	5.39
Logarithmic sample standard deviation ($s_{\ln X}$)	0.06	0.03	0.05

The vague prior information is combined with the results of n tests of each bar diameter sample from the site investigation to obtain the posterior estimators. The updated characteristic value of the yield strength of reinforcing steel and the updated distribution parameters for each of the bar diameters considered are summarized in Table 5.

Table 5 Updated reinforcing steel yield strength and distribution parameters corresponding to the first stage

Bar diameter [mm]	$f_{yk,act,1}$	$V_{fys,act,1}$	$S_{fys,act,1}$
10	322.1	0.12	1.21
12	296.1	0.12	1.21
20	181	0.12	1.21

4.2.4 Updating of partial factors

The parameters of concrete and steel strength obtained in sections 4.2.2 and 4.2.3, respectively, are used to update the partial factors for the concrete compressive strength, $\gamma_{c,act}$, and the reinforcing steel strength, $\gamma_{s,act}$. In practice, the procedure is based on diagrams developed for these purposes [15] or, alternatively, the respective analytical expressions.

Since, in this case study, for the resistance to bending moments and tensile forces in the web, respectively, reinforcement yield strength is the dominant resistance variable and the area of the reinforcement bar cross-section non-dominant, the following equation can be used for updating the corresponding partial factor:

$$\gamma_{s,act} = \frac{1}{S_{f_{ys,act}} S_{A_{s,act}}} e^{\alpha_{F_{ys}} \beta \sqrt{V_{f_{ys,act}}^2 + V_{A_{s,act}}^2}} \geq 1.0 \quad (11)$$

According to international standards such as [3] and [12], a sensitivity factor of $\alpha_{F_{ys}} = 0.8$ is to be adopted for dominant strength variables. Applying the target reliability index for a 50 year reference period, updated values for the coefficients of variation for the reinforcing yield strength associated with the different bar diameters and for the corresponding bias coefficients from Table 5, as well as the prior coefficient of variation and the prior bias coefficient for the cross-sectional area of the reinforcing steel (in this case assumed, for the sake of simplicity, as the prior probabilistic model from [4]), yielded the same updated partial factor for the different bar diameters, $\gamma_{s,act,1} = 1.18$.

Since reinforcement yield strength is in this case the dominant resistance variable, concrete strength is a non-dominant resistance variable and therefore a sensitivity factor of $\alpha_{F_{ys}} = 0.32$ is adopted. The following equation can be used for updating the partial factor for the concrete compressive strength:

$$\gamma_{c,act} = \frac{1}{S_{f_{c,act}}} e^{\alpha_{f_c} \beta V_{f_{c,act}}} \geq 1.0 \quad (12)$$

According to the available information, the updated partial factor for concrete strength in the first stage of the assessment is: $\gamma_{c,act,1} = 1.0$.

The updated partial factors for reinforcing steel strength as well as for concrete compressive strength are not directly comparable to the value of the partial factor adopted in international design codes [5]. For comparison, these partial factors are to be multiplied by the partial factors associated with the resistance model uncertainties, according to the format adopted for assessment (section 3.1).

4.3 Structural analysis and verification

Analysis and verification are conducted in keeping with the basic principles laid down in the current Spanish Technical Building Code [1] and in EN 1992-1-1 [5], as well as with the additional principles introduced in the preceding sections referring to the updating of resistance variables by using site-specific data. The safety assessment of the structure is described below.

In the first stage of the assessment, the structural system analysed consists of a series of simply supported beams with 6 m span length. The separation between these beams, which support the existing floor, is 5 m. No shear connection exists between the existing beams and floor.

The building will be a cultural centre thus belonging to the consequence category CC3 with potentially high consequences, in terms of loss of human life, in case of failure. After the transformation of the building, the permanent load will be equal to $g_k = 7 \text{ kN/m}^2$ (including self weight of the existing floor, partition walls, etc.). According to EN 1991-1-1 [16] the characteristic value for the imposed load in congregation areas is $q_k = 5 \text{ kN/m}^2$.

The load bearing capacity of the corrosion-damaged, patch repaired beams is established according to the specifications from section 3.2. The force transfer between concrete and steel is guaranteed due to the positive influence of the lateral pressure in the area of the support. As a consequence, premature bond failure can be excluded. Therefore, only the examination values for bending and shear resistance are to be investigated. As a result, the beam structural safety is

not verified for the remaining service period under the new use conditions since requirement (1) is fulfilled for shear resistance but not for bending resistance:

$$M_{Ed,act} = M_{Ed} = 246.4 \text{ kN} \cdot \text{m} \geq M_{Rd,act,1} = 71.8 \text{ kN} \cdot \text{m} \quad \text{Not fulfilled}$$

$$V_{Rd,act,1} = 174.3 \text{ kN} \geq V_{Ed,act} = V_{Ed} = 164.3 \text{ kN} \quad \text{Fulfilled}$$

For illustration purposes, the updated examination value for bending resistance is obtained from equation (13). Where available (Figure 4; Tables 3 and 5), updated characteristic values are used for the different variables, as well as updated partial factors (section 4.2.4). Otherwise, default values are taken from the literature [2, 15]. In order to establish the effective concrete strength, the reduction factor k_{cp} is used (section 3.2.2). Since structural members are patch repaired (section 1) by using mortars with mechanical, as well as chemical, properties which need to be compatible with those of the original concrete, the same value $k_{cp} = 1.0$ can be assumed for both, the confined existing concrete and the cover material:

$$M_{Rd,act} = \frac{1}{\gamma_{Rd,M,act}} \cdot \left(\frac{A_{s,act} \cdot f_{yk,act}}{\gamma_{s,act}} \cdot d_{act} - 0.5 \cdot \left(\frac{A_{s,act} \cdot f_{yk,act}}{\gamma_{s,act}} \right)^2 \cdot \frac{\gamma_{c,act}}{\eta_{fc,act} \cdot k_{cp} \cdot f_{ck,act}} \cdot \frac{1}{b_{c,act}} \right) \quad (13)$$

$$= \frac{1}{1.125} \cdot \left(\frac{1167 \cdot 181}{1.18} \cdot 470 - 0.5 \cdot \left(\frac{1167 \cdot 181}{1.18} \right)^2 \cdot \frac{1.0}{1.0 \cdot 1.0 \cdot 16.55} \cdot \frac{1}{300} \right) = 71.8 \text{ kN} \cdot \text{m}$$

Uncertainties associated with the bending resistance model provided in EN 1992-1-1, adapted for corrosion damaged beams as described in section 3.2.2, can be estimated by the following statistical parameters: $\mu_\theta \approx 1.0$; $V_\theta \approx 0.1$. According to a previous publication [17], the corresponding updated partial factor is estimated at $\gamma_{Rd,M,act} = 1.125$.

4.4 Recommendations

As the structural safety is not verified in the first stage of the assessment, strengthening is necessary (Figure 3). The intervention proposed consists in demolishing the existing concrete slab, connecting the new one to the existing beams. To this end, post installed reinforcement bars are used for shear connection and structural reliability is to be verified for this new, slab on top of existing beam-composite system (Figure 5). Also an additional data acquisition programme is performed for obtaining improved information about the existing beams to further update the resistance models.

5 SECOND STAGE OF THE EVALUATION

5.1 Improved information

In this second stage of the evaluation, additional information about the material properties is obtained from one of the existing beams. The new information on the mechanical properties of the reinforcing steel and the concrete is summarized in Tables 6 and 7.

Table 6 Concrete mechanical properties

Reference	Number of tests	f_{cm} [N/mm ²]	σ_{fc} [N/mm ²]	V_{fc}
Critical Beam	4	25.85	2.42	0.09

Table 7 Steel mechanical properties

Reference	Diameter [mm]	Number of tests	f_{ym} [N/mm ²]	V_{fy}	f_{tm} [N/mm ²]	V_{ft}
Critical Beam	10	3	390	0.04	468	0.01
	12	4	514	0.05	609	0.09
	20	4	307	0.01	451	0.01

The cross-section according to the proposed intervention in the final building is shown in Figure 5, being b_{eff} the effective flange width, which may be established by applying the rules from the Eurocode [5]. Further to the demolition of the existing concrete slab, a new concrete slab of 0.25 m height is proposed that will be supported by the existing beams to which it will be connected with post installed rebars. As in the existing structure, the span is of 6 m and the separation between beams of 5 m. Concrete strength class C30/37 is chosen for the new slab, whereas the concrete cover is 0.03 m. The shear connection is designed with a view to avoid premature longitudinal shear failure or longitudinal splitting. Class C [5] bars are used for the reinforcement of the slab. The contribution of the longitudinal bottom reinforcement ($\phi 12$ at 0.2 m) to the bending resistance of the new cross-section is taken into account.

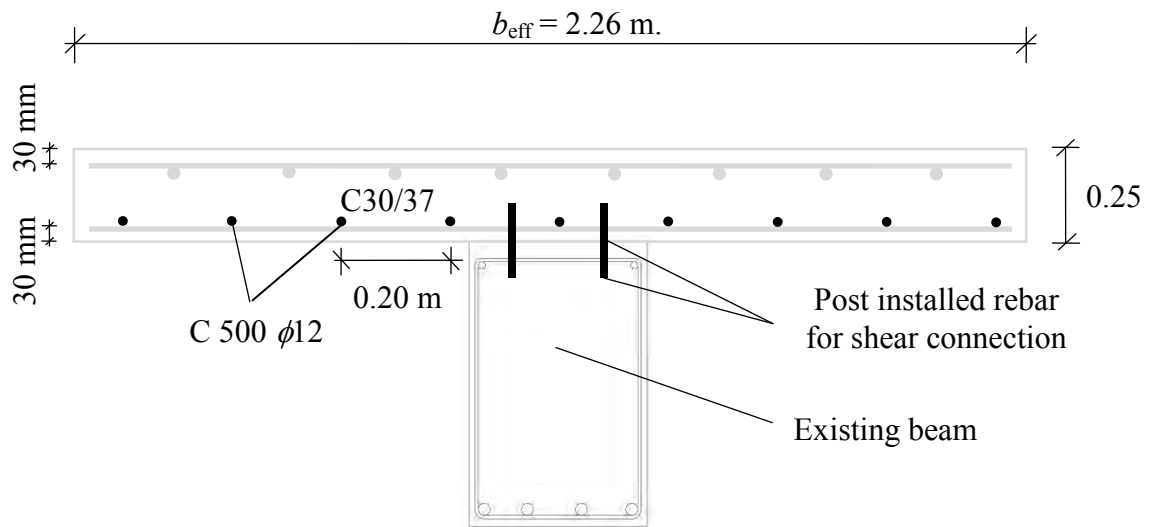


Figure 5 Cross-section according to the proposed intervention: new concrete slab connected to the existing beam

5.2 Updating of material strength

5.2.1 General

In the second stage, the updated material properties of the first stage are used as prior information and updated with the material properties obtained from the existing critical beam. Although geometry also is updated, for sake of simplicity only the updating of material strength is explicitly shown in this contribution.

5.2.2 Concrete

According to [12, 13], prior information on distribution parameters from section 4.2.2 is characterized by $n_0 = 6$, $w_0 = \sigma_{\ln X, act, 1} = 0.27$ and $m_0 = \mu_{\ln X, act, 1} = 3.24$. From the findings of the data acquisition program of the existing beam, the following parameter values are obtained:

- Sample size, $n = 4$;
- Logarithmic sample mean, $m_{\ln X} = 3.25$;
- Logarithmic sample standard deviation, $s_{\ln X} = 0.09$.

With $n_1 = n_0 + n = 10$ and pursuant to equations (8), (9) and (10), in the second stage the updated characteristic value of the compressive strength of concrete and the updated distribution parameters are summarized in Table 8.

Table 8 Updated concrete compressive strength and distribution parameters corresponding to the second stage

$f_{ck, act, 2}$ [N/mm ²]	$V_{fc, act, 2}$	$S_{fc, act, 2}$ *
16.24	0.28	1.58

*S: Bias coefficient (ratio between mean and representative (characteristic) value of the basic variable)

5.2.3 Reinforcing steel

In the same way as for concrete, for reinforcing steel prior information is assumed from the first stage of the evaluation procedure. According to [12, 13], prior information on distribution parameters for the different bar diameter is provided in Table 9.

Table 9 Parameter values for each of the bar diameter samples in the second stage

	Bar diameter		
	10 mm	12 mm	20 mm
Prior sample size (n_0)	3	3	3
Prior logarithmic sample mean (m_0)	5.96	5.88	5.39
Prior logarithmic sample standard deviation (w_0)	0.12	0.12	0.12

From the findings of the data acquisition program of the existing critical beam, the parameter values obtained for each of the bar diameter samples are given in Table 10.

With $n_1 = n_0 + n = 7$ for bar diameters of 12 mm and 20 mm and $n_1 = 6$ in the case of 10 mm diameter bars and pursuant to equations (8), (9) and (10), in the second stage the updated characteristic values of the yield strength of reinforcing steel and the updated distribution parameters for each bar diameter are summarized in Table 11.

In comparison with the characteristic values for the yield strength in the first stage, the data acquisition in the second stage leads to an increase of the order of 20% for bar diameters of 12 mm and 20 mm. In the case of 10 mm diameter bars, the characteristic steel yield strength is virtually the same as in the first stage.

Table 10 Parameter values for each of the bar diameter samples in the second stage

	Bar diameter		
	10 mm	12 mm	20 mm
Sample size (n)	3	4	4
Logarithmic sample mean ($m_{\ln X}$)	5.97	6.24	5.73
Logarithmic sample standard deviation ($s_{\ln X}$)	0.04	0.05	0.01

Table 11 Updated reinforcing steel corresponding to the second stage

Bar diameter [mm]	$f_{yk,act,2}$	$V_{fys,act,2}$	$S_{fys,act,2}$
10	317.4	0.12	1.23
12	359.2	0.12	1.19
20	216.8	0.12	1.22

5.2.4 Updating of partial factors

The updated partial factors for yield the reinforcing steel strength in the second stage are obtained using equation (11) and the values from Table 11. The results are summarized in Table 12.

Table 12 Updated partial factors for the reinforcing steel strength according to the information available in the second stage

	Bar diameter [mm]		
	10	12	20
$\gamma_{s,act,2}$	1.20	1.19	1.19

The updated partial factor for the concrete of the existing beam in the second stage is obtained by using equation (12) and the values from Table 8, leading to a value of $\gamma_{c,act,2} = 1.0$.

5.3 Structural analysis and verification

As structural safety criteria are not fulfilled in the first stage, a new structural system is proposed (Figure 5). Principles for the analysis and verification are similar as in the first stage, considering the slab on top of the existing beam-composite system and the updated characteristic values of the material properties for the existing members as well as the corresponding partial factors. Likewise, as stated in the first stage of the assessment, force transfer between concrete and steel is considered to be fulfilled. As mentioned in section 5.1, the shear connection is designed so as to avoid its premature failure.

The examination value for shear resistance in the second stage is determined considering only the capacity of the existing beam. The examination value of the positive bending resistance,

on the other hand, is established for the strengthened system according to Figure 5. The structural safety requirements are fulfilled for both failure mechanisms:

$$M_{Rd,act,2} = 300.6 \text{ kN} \cdot \text{m} \geq M_{Ed,act} = M_{Ed} = 246.4 \text{ kN} \cdot \text{m}$$

$$V_{Rd,act,2} = 169.3 \text{ kN} \geq V_{Ed,act} = V_{Ed} = 164.3 \text{ kN}$$

6 CONCLUDING REMARKS

In the present case study, the procedures and tools developed to accommodate site data by updating the representative load and resistance variables as well as the associated partial factors [2, 4, 15] are used for a rational decision-making on the reliability of the existing industrial building that will undergo a transformation into a cultural centre for future use. The partial factor format used is equivalent to the format normally applied in the design of new structures.

The evaluation procedure is divided into two stages. In the first stage, except patch repair of the corrosion damaged members, no structural intervention is assumed and information about material properties obtained from different members of the same building is updated with a Bayesian method using vague prior distributions. Also the partial factors for the reinforcing steel strength and concrete compressive strength are updated. In this stage a comparison of the examination values of action effects to the examination values for shear and bending resistance of the beams revealed that the structural safety requirements for the future conditions are not met. Therefore, a structural intervention is proposed substituting the existing floor by a new concrete slab connected to the existing beams with post installed rebars. In this second stage an additional data acquisition programme is performed to obtain information from one of the existing beams which is particularly critical from a structural reliability point of view. For verification, information about material properties from the first stage is updated with additional data and also the partial factors for reinforcing steel strength and concrete compressive strength are further updated. Finally, according to the proposed intervention, structural safety requirements are fulfilled for the future service period after the transformation of the building.

REFERENCES

- [1] CTE DB-SE, *Código Técnico de la Edificación. Documento Básico: Seguridad Estructural*, Ministerio de Vivienda, Madrid, 2006.
- [2] Tanner P., Lara C. and Prieto M., “Analysis of the present condition and deterioration in the main dome over La Laguna cathedral”, *37th IABSE Symposium Madrid 2014 – Engineering for Progress, Nature and People*, ISBN 978-3-85748-135-2.
- [3] EN 1990 *Eurocode – Basis of Structural design*, European Committee for Standardization, CEN, Brussels, 2002.
- [4] Tanner P., Lara C., and Hingorani R., “Seguridad estructural. Una lucha con incertidumbres” (Structural safety. A struggle with uncertainties - in Spanish), *Hormigón y Acero*, No. 245, Madrid, 2007, ISSN 0439-5689, pp. 59-78.
- [5] EN 1992-1-1 *Eurocode 2 – Design of concrete structures – General rules and rules for buildings*, European Committee for Standardization, CEN, Brussels, 2004.+
- [6] fib, *fib Model Code for concrete structures 2010*, International Federation of Structural Concrete (fib), Lausanne, 2013.
- [7] Prieto M., *Estudio de la adherencia de armaduras corroídas y su influencia en la capacidad resistente de elementos de hormigón armado (Study of bond with corroded steel and its influence in the resistance of reinforced concrete elements - in Spanish)*, Ph.D. Thesis, Universidad Politécnica de Madrid (UPM), Madrid, 2014, pp. 344.

- [8] Prieto M., Tanner P., Lara C., “Modelos de campos de tensiones para la evaluación de estructuras de hormigón armado corroídas (Stress field models for the assessment of corrosion-damaged reinforced concrete structures - in Spanish)”. Jornadas Internacionales conmemorativas del 80 aniversario del Ietcc, Noviembre 12-14, 2014, Madrid, Spain. ISBN: 978-8-4729-2382-9.
- [9] Lara C. and Tanner P., “Chapter 3: Degradation modelling”, *Methods for the risk assessment and risk management of aging infrastructure*, pp. 41-79, Milan Holický & Dimitris Diamantidis (eds), Prague, 2014, ISBN: 978-80-01-05611-0.
- [10] Muttoni A., Schwartz J., Thürlimann B., *Design of Concrete Structures with Stress Fields*, Birkhäuser, Basel, 1997, ISBN: 3-7643-5491-7, pp.143.
- [11] CONTECVET, *A validated user’s manual for assessing the residual service life of concrete structures*, EC Innovation Program IN30902I, 2001.
- [12] ISO 2394:1998 (E), *General principles on reliability for structures*, International Organization of Standardization, ISO, Geneva, Switzerland, 1998, pp. 73.
- [13] Lara C., Tanner P. y López Agüí J. C. “Metodología para la combinación de información en la evaluación de estructuras existentes (Methodology for the combination of information in the assessment of existing structures - in Spanish)”, *Cemento Hormigón*, No. 928, 2009, pp. 42-52, ISSN 0008-8919.
- [14] INSTITUTO TÉCNICO DE LA CONSTRUCCIÓN Y DEL CEMENTO, *Instrucción especial para estructuras de hormigón armado. Instrucción H.A. 57*, Madrid, 1957.
- [15] Tanner P., Lara C., and Prieto, M., “Semi-probabilistic models for the assessment of existing concrete structures”, In Faber, Köhler and Nishijima (eds), *Applications of Statistics and Probability in Civil Engineering*, Taylor & Francis Group, London, 2011.
- [16] EN 1991-1-1, *Eurocode 1 – Actions on structures – General actions. Densities, self-weight, imposed loads for buildings*, European Committee for Standardization, CEN, Brussels, 2002.
- [17] Sýkora M, Holický M, Prieto M, Tanner P. *Uncertainties in resistance models for sound and corrosion-damaged RC structures according to EN 1992-1-1*; In: *Materials and Structures* (article in press). DOI: 10.1617/s11527-014-0409-1.

CHAPTER 6: SILOS - A CASE STUDY

Pietro Croce¹, Maria Luisa Beconcini¹, Martina Muzzi¹, Elisa Rosso¹

¹Department of Civil and Industrial Engineering – Structural Division – Univ. of Pisa, Italy

Summary

Silos are warehouses equipped for receiving and unloading incoherent materials, usually cereals. The shape is determined by their function, so they are generally composed by slender cylinders, adjacent to each other, and with the bottom provided with inclined surface and a central hole, aimed to unload materials on the trucks below.

In several European countries, mostly in the Mediterranean area, many of these buildings date from the post-war period, so that they need accurate studies in order to determine their reliability and, eventually, to design interventions for their rehabilitation.

In the present chapter the studies conducted on a r.c. silo in central Italy is presented; the properties of materials, the theoretic basis of design and the techniques typical of the time have been accurately retrieved and employed for assessing the actual state of the structure.

1 INTRODUCTION

The silos are particular constructions used to store loose materials and granular products, such as cereals, in large quantities; with both a function of storage in the industrial production cycle, and as warehouses regulating the disposal of substances. They usually are composed of adjacent elements, called cells, which have a cylindrical shape with flared bottom; the overall configuration is strictly related to the activities undertaken inside, which are usually highly automated.

In the past, they were built with masonry structure; later on, the introduction of modern materials, steel and reinforced concrete, contributed sensibly to the development of new structural and architectural typologies. Between the two world wars, there was a wide diffusion of reinforced concrete silos for storing and refining cereals, especially in Italy, Germany, France, Libya and France, and, later, in Spain.

At present, some of these buildings, particularly well conserved, may be considered as part of the industrial heritage, that is worth preserving because of their historical importance and because they often represent a sort of landmark in our territories.

In what follows, the case-study of a reinforced concrete silo, dating back about a century ago, is presented. As well as many other reinforced concrete structures built during the 20th century, it needs maintenance works, renovations and repair of damages caused by degradation or accidental events, in order to preserve its aspect and its structural reliability. Before proceeding at the design of the preservation works, specific studies must be performed in order to know the actual conformation of the structural elements. Since the materials and the basis of design for r.c. structures in use at the time of construction are quite different from those in use today, an accurate recognition of the geometry of structural elements is needed; afterwards, on the basis of the design approaches and the characteristics of the materials commonly used at the time, the reinforcing of the structural elements can be obtained through a simulated project. Afterwards the actual characteristics of the materials must be acquired, so that the effective safety level can be assessed and, if the case, specific preservation works designed, on the basis of codes and methods currently in use.

As recommended in [5], the study has been setup following the standardized procedure of the ISO 13822 [1], which is aimed to the evaluation of the actual reliability of a structure, through a preliminary assessment and, if necessary, a detailed assessment, organized in accordance with the step-by-step procedure outlined in the flow chart shown in figure 1.

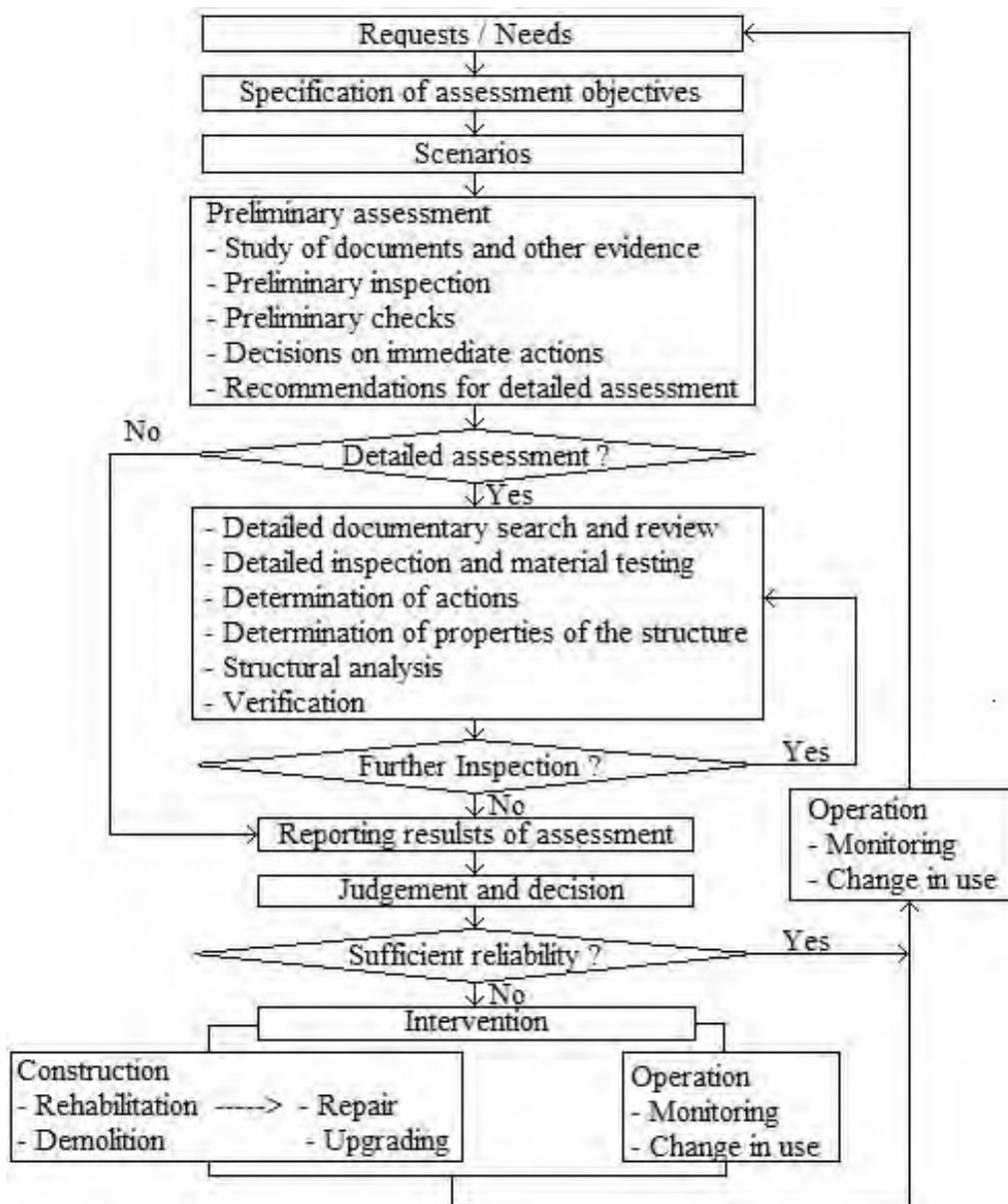


Figure 1 Flow chart of the ISO 13822

2 THE AGRICULTURAL CONSORTIUM SILO IN GROSSETO

The silo of the Agricultural Consortium of Grosseto (Tuscany, Italy) (figs. 2, 3), is one of the first reinforced concrete silos built in Tuscany (1933); it is still in use to amass and store cereals coming from the surroundings and from foreign countries, and it is considered a particular example of reinforced concrete monumental structures.

It is located near the town centre, just outside the ancient walls dating from the Medicean period and it was built very close to the railroad, so as to speed up the operations of loading and unloading, and it is part of a wider system of warehouses where goods were refined and then sold (figs. 4 and 5).



Figure 2 Main façade of the silo



Figure 3 Side view of the silo of the Agricultural Consortium of Grosseto



Figure 4 Localization of the silo

The silo was the first tall building of the town, with the essential and monumental shapes, typical of the rationalist and government architecture of the period. It was designed by the *Foundations and Construction Society* of Milan and was built, like many others in Italy and in the colonies, during the so called *wheat battle* promoted by the Italian fascist regime in the '30s, in order to control the price of cereals and to solve the food problem of the country.



Figure 5 Plan of the silo

3 PRELIMINARY ASSESSMENT

3.1 Study of the available documentation.

In the historical archive of Grosseto, only the original architectural design was found (fig. 6), which does not contain information about the structural configuration, the foundations, the properties of the materials, the quantity of reinforcing bars, and so on.

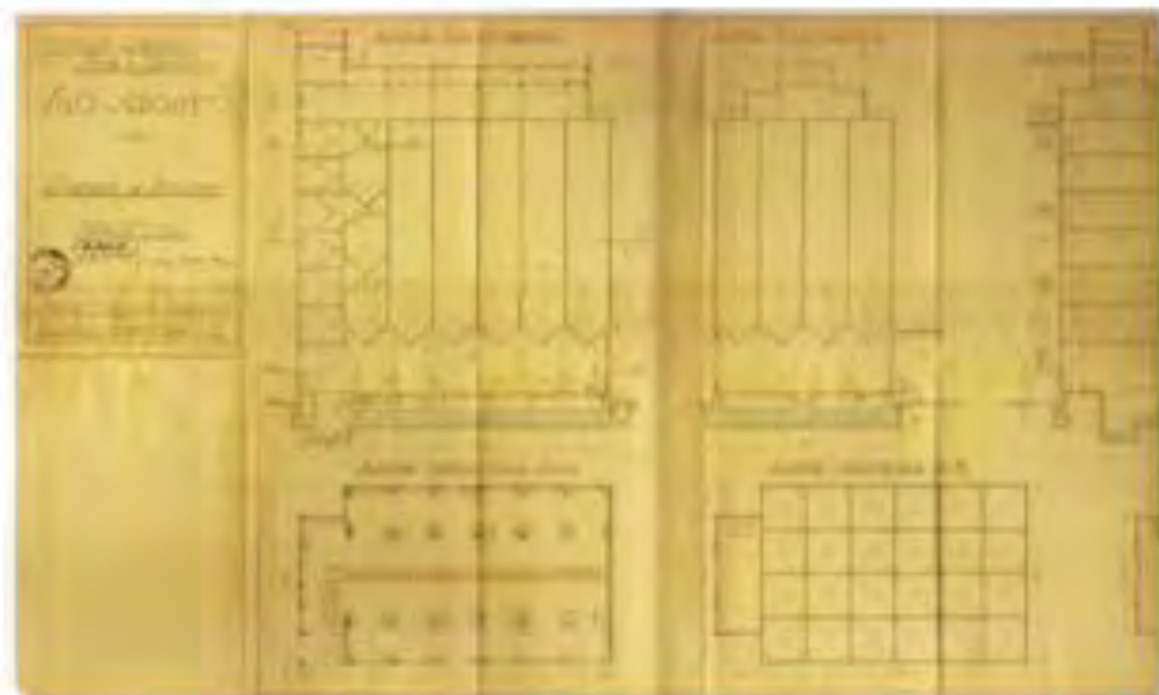


Figure 6 Original architectural drawings

Generally, silos have different dimensions, depending on the kind of goods stored, but the shape and the working principles are similar: usually, goods are put on horizontal conveyors at the ground floor and then sucked, by means of vertical conveyors to the top of the structure, in the so-called drying gallery; from here, cereals are deposited in the vertical cells.

As revealed by the architectural maps, the silo is divided in two different parts: the first one, bigger than the other, is composed of vertical cells, in which cereals are stored; the latter, called '*torretta*' (small tower), contains the staircase through which it is possible to go to the top of the building, to enter into the cells and the machinery for refining goods (figs. 7 and 8).

The first part of the silo consists of 32 vertical cells: twenty of them, adjacent to each other, are $3.80 \times 3.80 \times 18$ m; the remaining twelve lay on three levels and are $3.80 \times 3.80 \times 6$ m. At the ground floor there is the operating room, where are located the hoppers, truncated cone shaped. At the top of the building, there is the drying gallery.

The ground floor is characterized by a *pilotis* scheme, with rectangular columns. The cross section of the central columns is larger than that of external and corner ones, according to simplified design principles, mainly governed by compression stresses. The rectangular cells are composed by reinforced concrete walls, 17 cm thick.

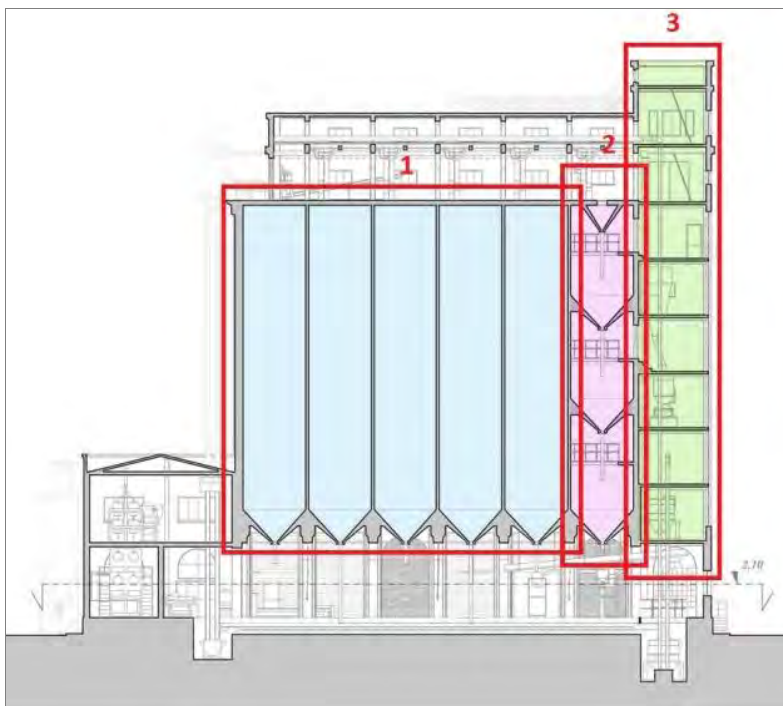


Figure 7 Longitudinal section of the silo

Legend:

- (1) Vertical Cells
 $3.80 \times 3.80 \times 18.00$ m;
- (2) Vertical Cells
 $3.80 \times 3.80 \times 6.00$ m;
- (3) '*Torretta*'.

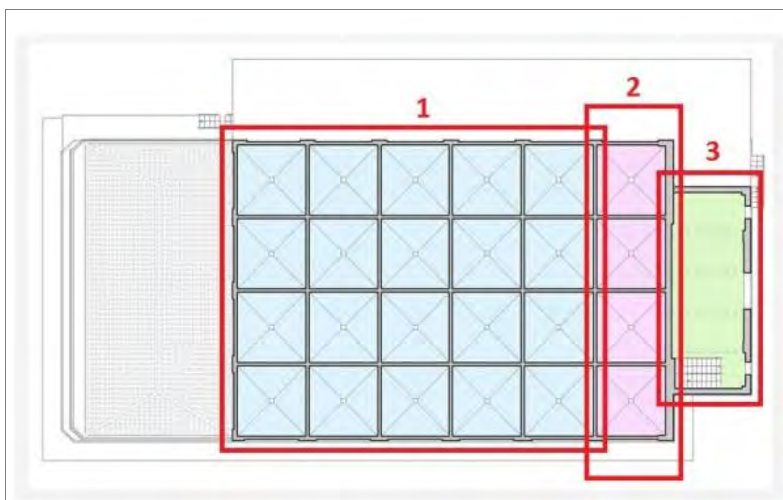


Figure 8 Plan view of the silo's cells

Legend:

- (1) Vertical Cells
 $3.80 \times 3.80 \times 18.00$ m;
- (2) Vertical Cells
 $3.80 \times 3.80 \times 6.00$ m;
- (3) '*Torretta*'.

3.2 Decision on immediate actions

From the information collected so far, it is possible to evaluate the forces acting on the structural elements of the silo.

The next operations to perform in view of assessing the actual safety level, are:

- a survey of the current state of decay of the building and of the structural materials;
- the survey of the crack patterns;
- the so-called *simulated design*, aimed to reconstruct the most probable arrangements of the rebars in the different sections of the structural elements;
- the structural analysis based on the current static model and the state of materials.

4 DETAILED ASSESSMENT

4.1 Detailed documentary search and review

The fundamental design rules for r.c. structures in the 19ths were collected in some technical texts [14], [17], [18] and handbooks [20], in which it is also possible to find the characteristics of the most employed materials.

Loose materials which are stored in the silos apply pressure on the walls of the cells [14]. The values of the pressure could be calculated following the *theory of earth pressure*, which assumptions are met since we have homogeneous materials, but, in the case of the silos, the cross section is small in comparison to its height, so it is demonstrated that pressures are smaller than those calculated following the Rankine theory for earth pressure and they tend to a limit value below a certain depth.

Janssen [10] and Koenen [11] faced the study of the horizontal and vertical pressures in a silo; their results are still valid and the values of certain coefficients have been obtained from experiences.

Knowing the main dimensional parameters of the silo and the kind of material stored in it, it is possible to calculate the horizontal and vertical pressures, through which the stress patterns in structural elements and in the walls of the cells can be determined [17], [18].

4.2 Detailed visual inspection

The first step to investigate the actual state of the silo is a visual survey, that can be subdivided in three sub-steps: dimensional survey, materials survey and decay survey.

The dimensional survey (Fig. 9, 13, 17) has been carried out by means of the polygonal measurements, in order to minimize errors.

As a result, the main resistant elements have been identified, and their dimensions measured, so that it has been possible to understand the silo's static scheme:

- the ground floor works as a *pilotis* floor, composed by a set of pillars, with different cross sections, and beams;
- the cells, composed by a continuous system of r.c. walls;
- the drying gallery and the “torretta” are sustained by frames with pillars and beams.

All the different parts are connected to each other, to form a unique structure.

The building materials have been identified and indicated on a map by different colors (fig. 10, 14, 18). The structural elements and the walls are all made of reinforced concrete, covered with a thick layer of plaster.

The survey allowed to identify the main decay and deterioration phenomena (fig. 11, 15, 19); the results are summarized and classified in a specific table (table 1) and in a photo gallery (fig. 12, 16, 20). Globally, the building appears in a good state of maintenance. The phenomena

observed are those typical of ageing reinforced concrete structures, but are not related to instability or overstress, since no crack pattern has been observed.

It had been also possible to identify, in a pillar of the ground floor, a smooth longitudinal rebar, 30 mm in diameter, and a 16 mm diameter stirrup.

Some relevant examples of the survey are shown below: for each one, the geometrical and material data are represented on maps and a photo gallery showing the main decay phenomena.

Table 1 Degradation types and causes

CLASSES	DEGRADATION	MAIN CAUSES	TAG
A LOSS OF PLASTER	Total loss of plaster	Atmospheric agents Thermal and hygrometric variations Moisture action	A1
	Partial loss of plaster	Lack of maintenance Action of rising moisture	A2
B MOISTURE ACTION	Moisture action	Thermal and hygrometric variations Action of rising moisture	B
C PATINA	Biological patina	Wind and rain Action of rising moisture	C1
	Efflorescence	Water infiltration Salt crystallization	C2
	Stain	Thermal and hygrometric variations Moisture action	C3
D	Plaster reintegration with cement mortar or other materials	Anthropogenic causes	D
E	Lack of elements	Lack of maintenance Anthropogenic causes Action of rising moisture	E
F	Not Cross Cracks	Atmospheric agents Thermal and hygrometric variations Moisture action	F
G	Overgrown plants	Favorable hydrothermal and sunshine conditions	G
H	Differential degradation	Lack of maintenance Anthropogenic causes Action of rising moisture	H
I	Corrosion of steel rebars	Carbonation action Chlorides action	I

4.2.1 Ground Floor

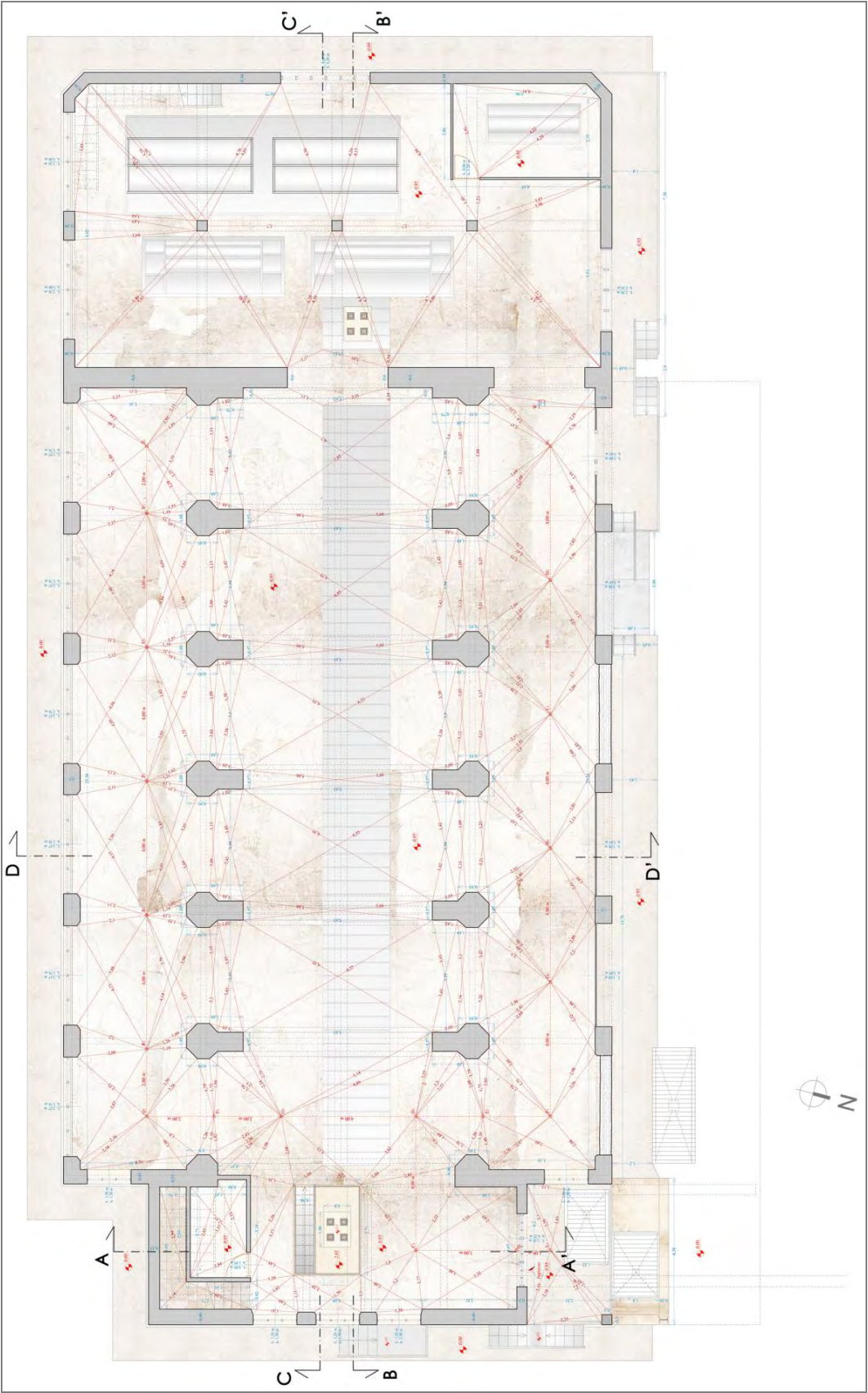


Figure 9 Example of dimensional survey: ground floor map



Figure 10 Example of the building materials survey: ground floor map

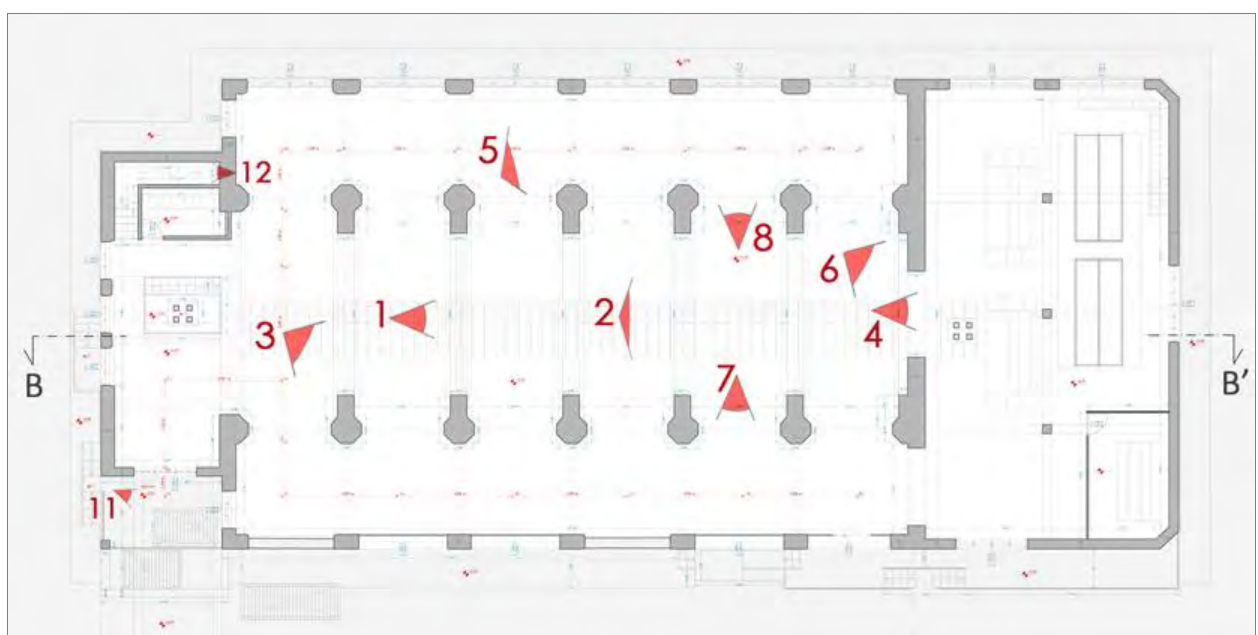


Figure 11 Example of the decay survey: ground floor map

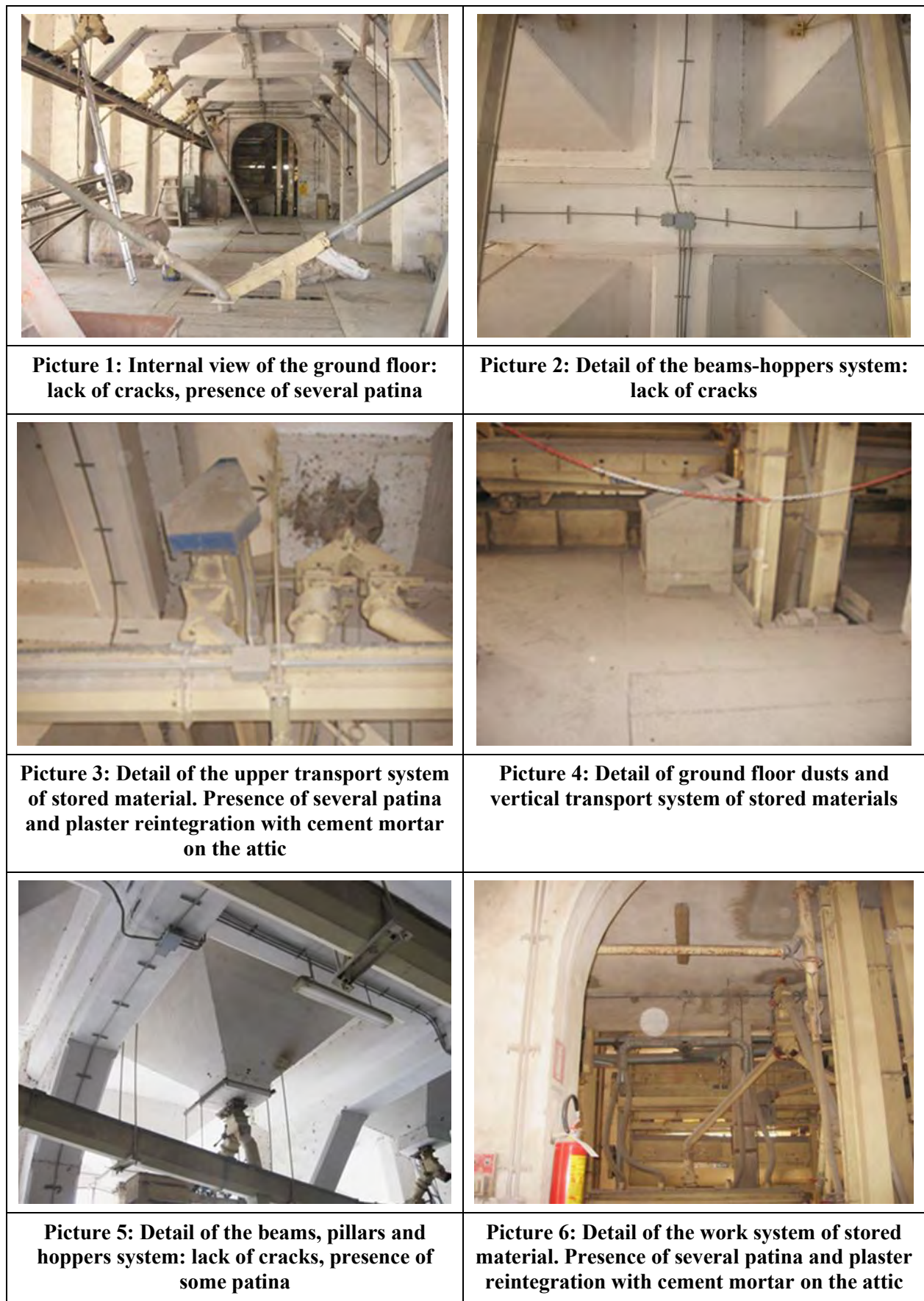


Figure 12 Photo gallery: ground floor (with reference to fig. 11)



Picture 7: Detail of the flooring. Presence of several patina and cracks



Picture 8: Detail of the flooring. Presence of several patina and relevant not cross cracks

Figure 12 (continuation) Photo gallery: ground floor (with reference to fig. 11)

4.2.2 Longitudinal Section BB'

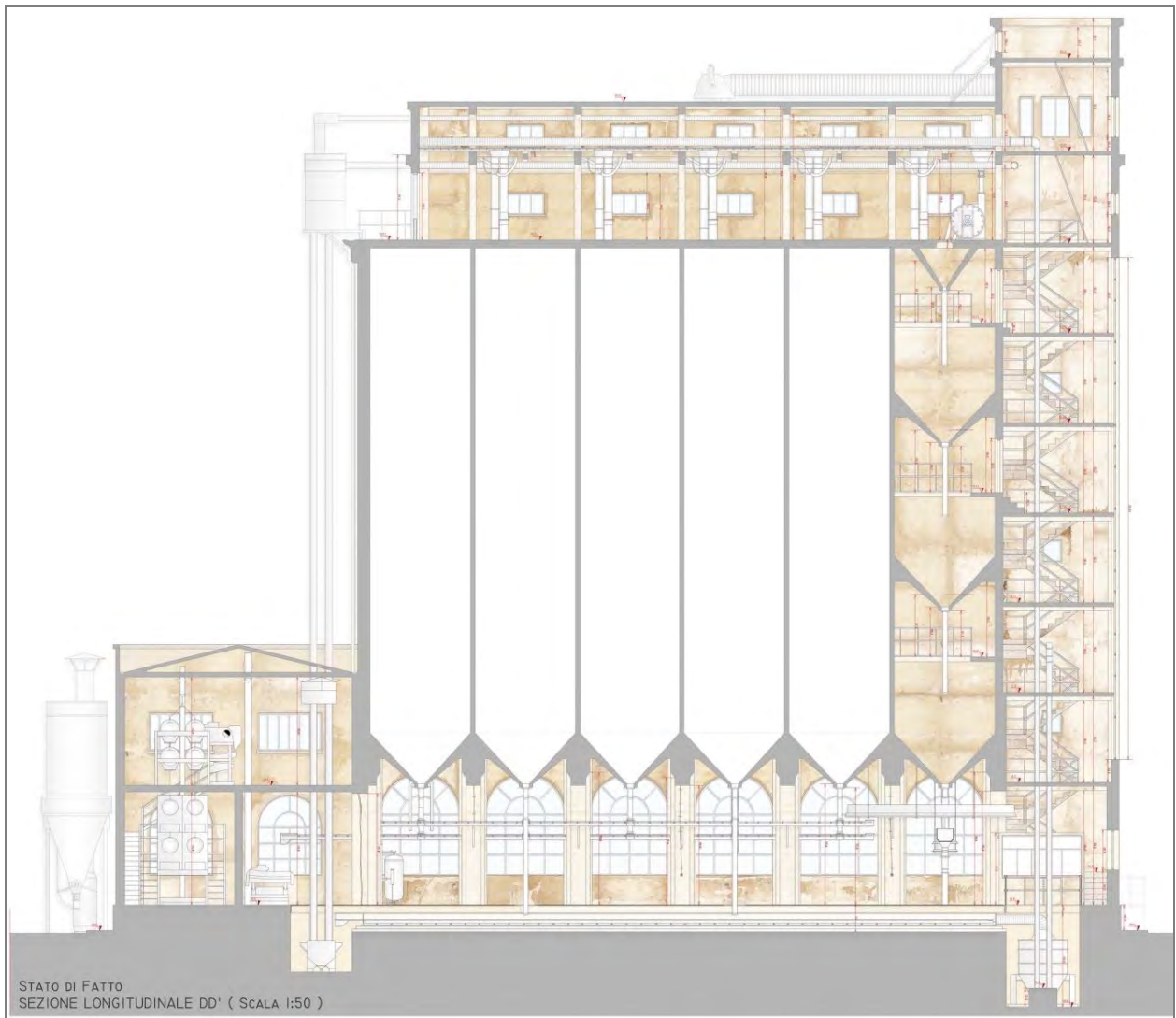


Figure 13 Example of dimensional survey: longitudinal section BB'



Figure 14 Example of building materials survey: longitudinal section BB'

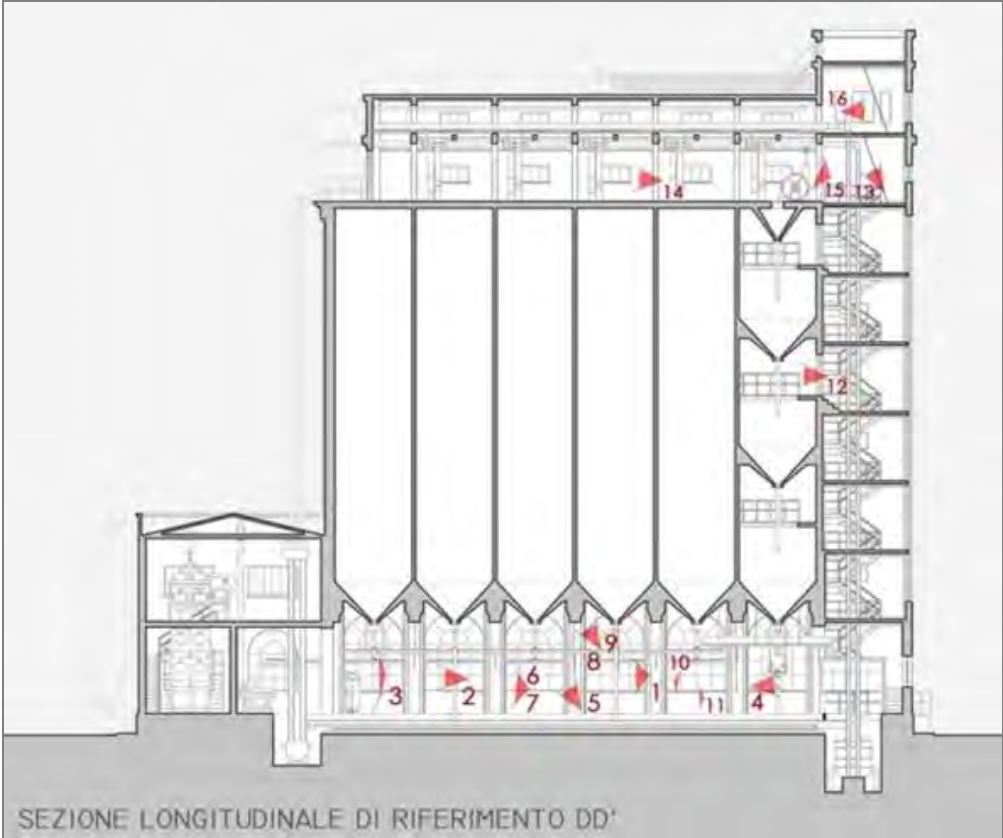


Figure 15 Example of decay survey: longitudinal section BB'



Figure 16 Photo gallery: longitudinal section BB' (with reference to Fig. 15)

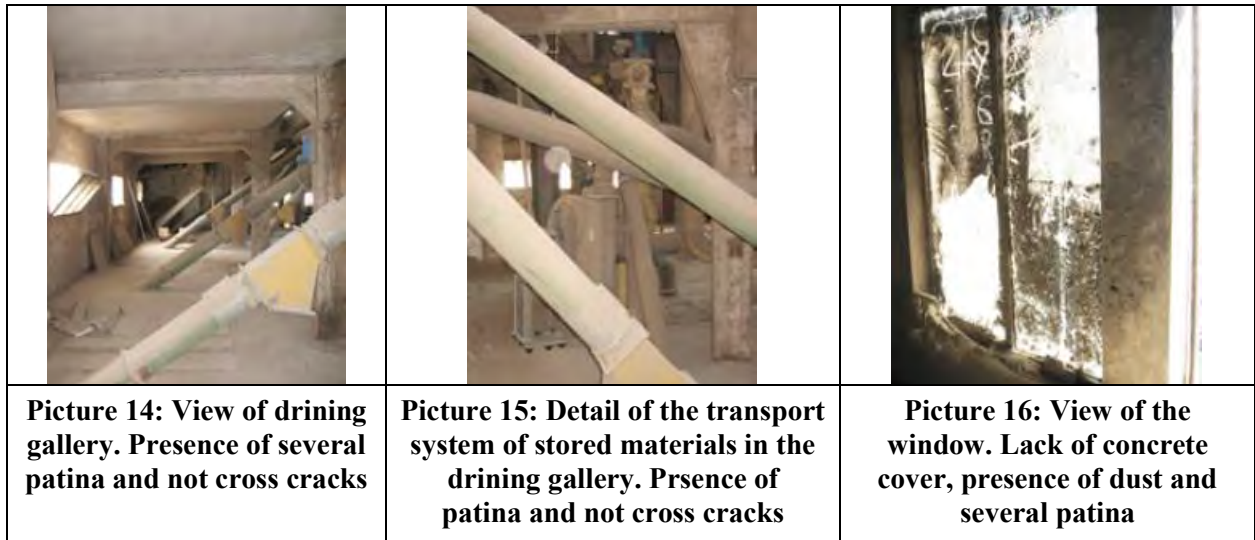


Figure 16 (continuation) Photo gallery: longitudinal section BB' (with reference to Fig. 15)

4.2.3 The main façade survey

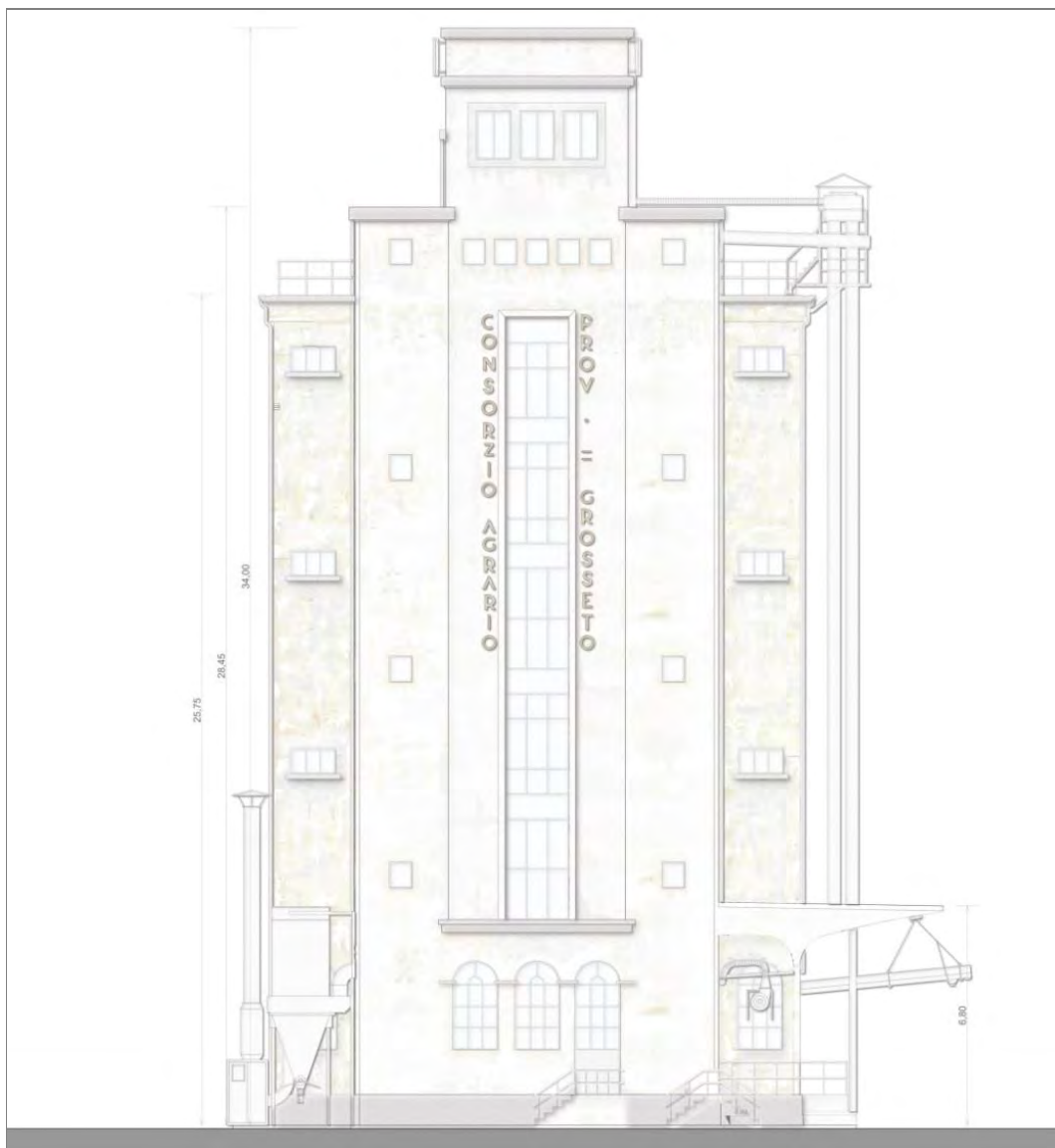


Figure 17 Example of dimensional survey: the main façade

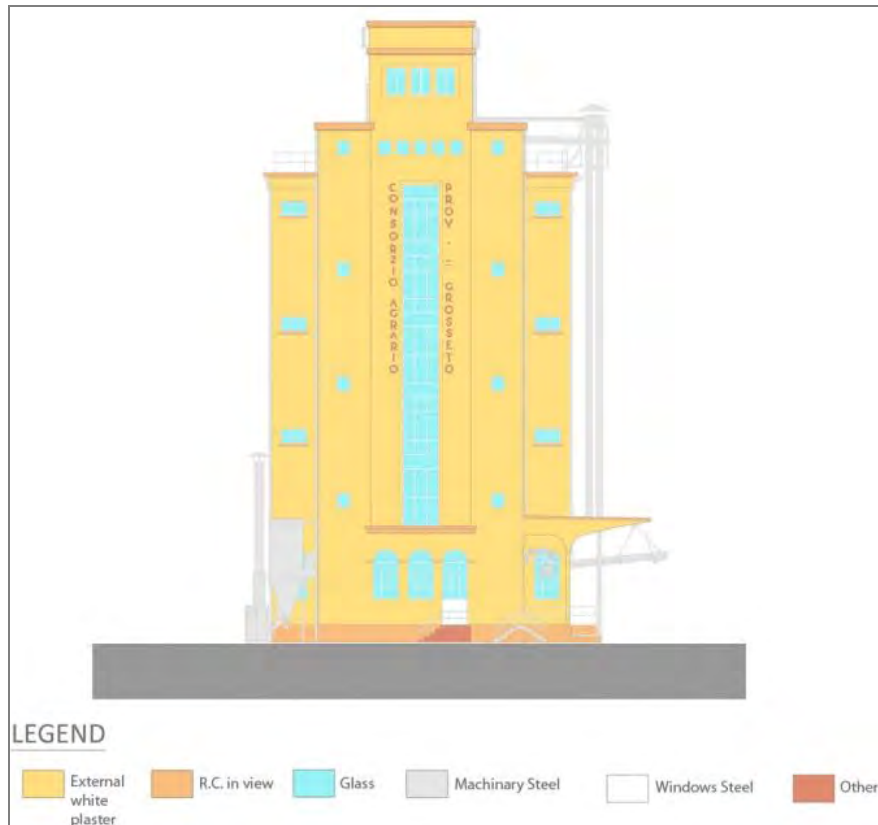


Figure 18 Example of building materials survey: the main façade

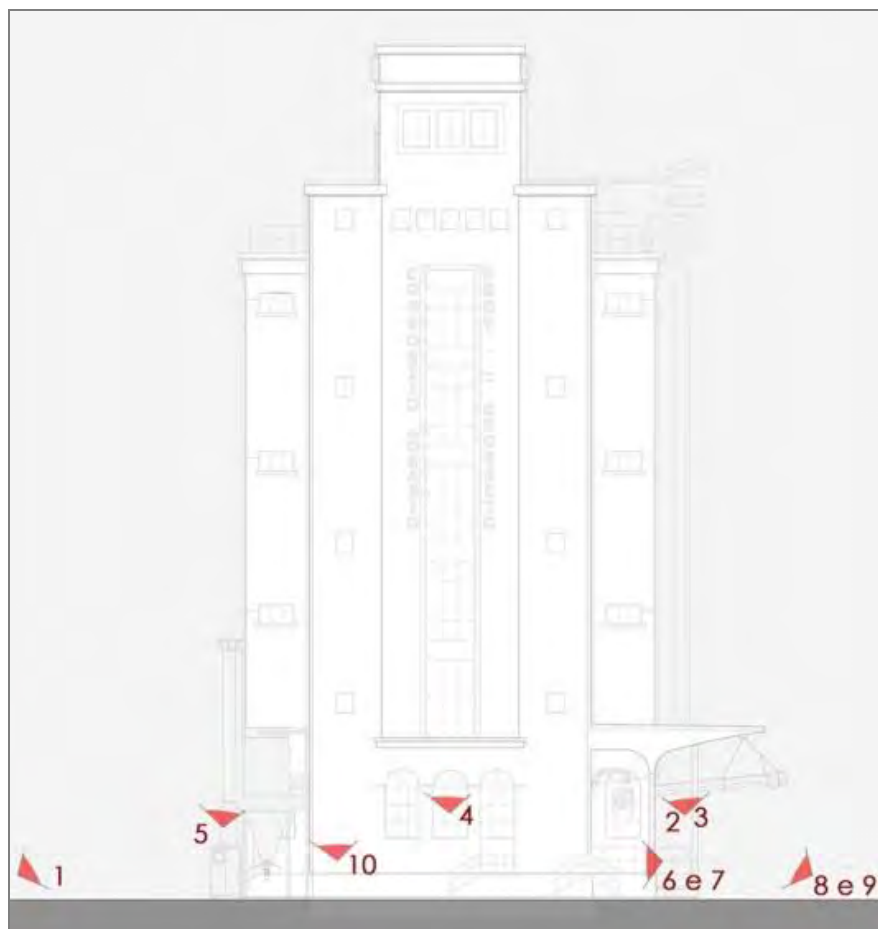


Figure 19 Example of decay survey: the main façade

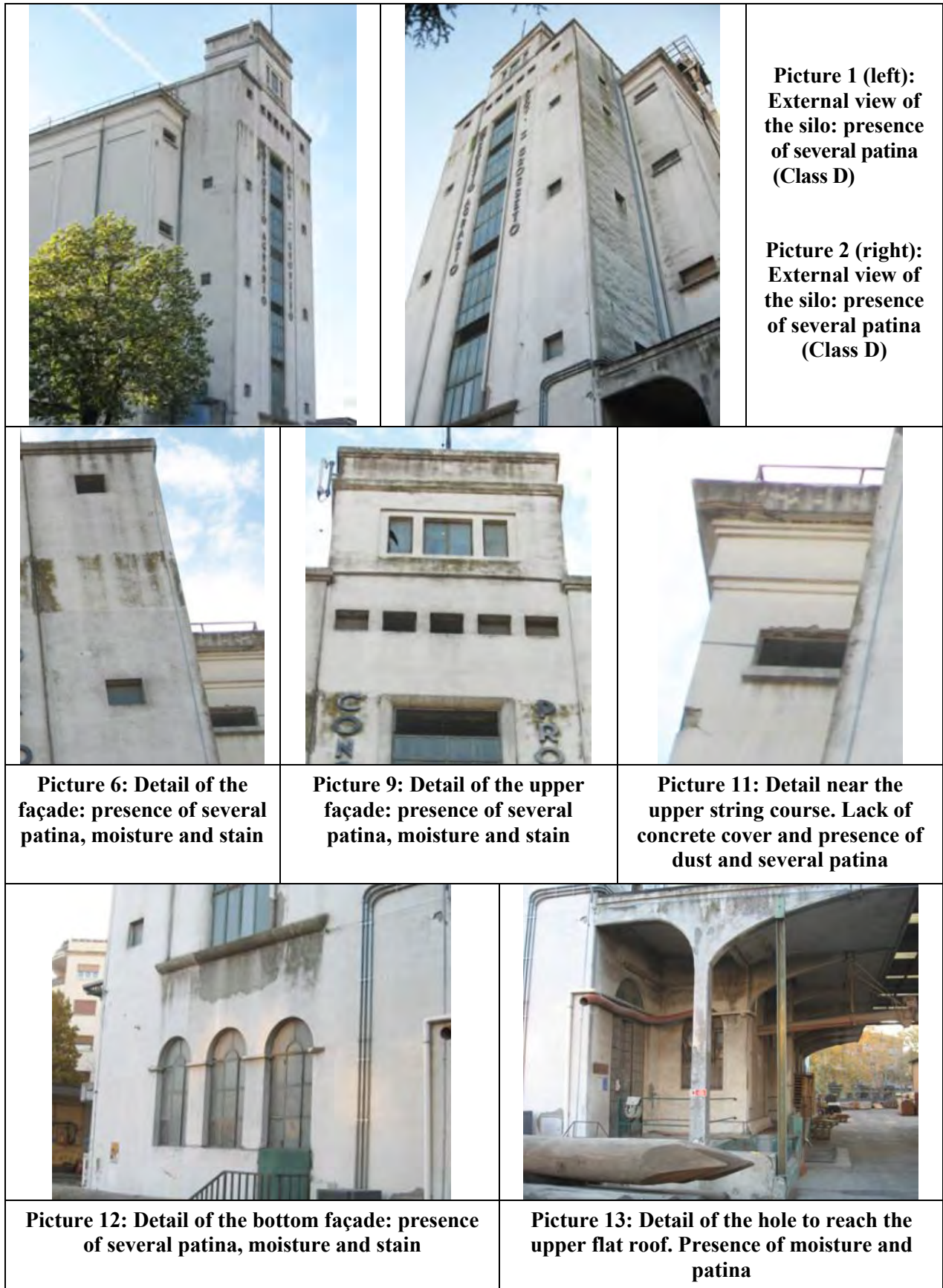


Figure 20 Photo gallery: the main façade (with reference to Fig. 19)

As it is clear from the images above, the main degradation phenomena are constituted by patina (class C) on the internal, external and flat surfaces of the silo, probably due to the perishable stored materials which accelerate the biological attack, and even to negligence. Other decay phenomena frequently detected are not-cross cracks, that often have determined partial loss of plaster, and in some cases, deterioration of the concrete cover, and even the corrosion of steel rebars. In some structural elements the plaster was refurbished with cement mortar.

In conclusion, the decay phenomena analysis shows no symptom of activation of failure mechanisms: cracks are limited to the plaster and do not affect the r.c. element. All the phenomena are primarily caused by lack of maintenance during the years.

4.3 Structural analysis

The structural analyses has been performed with reference to the stability of the r.c. walls of the cells, taking into account the characteristics of materials, concrete and steel, accordingly to what found in the literature of the building time. So the probable quantity of reinforcing bars in the walls has been evaluated. Before proceeding to eventual interventions, in situ tests to determine the real quality of concrete and steel and the number and diameters of the rebars should be performed. The information obtained from the detailed analyses will be useful for limiting the extension and invasiveness of the tests.

4.3.1 Determination of actions

The main actions which affect the structure of the silo are induced by the materials stored in the cells: the pressure exerted by the stored materials can be evaluated following the *Janssen theory*, and the subsequent stresses accordingly to the *Ritter theory of plane frames*.

It is assumed that for a cell the following characteristics remain constant:

- A = area of the inner section of the cell;
- l = length of the inner perimeter of the cell;
- φ = angle of internal friction of the stored material (assumed incoherent);
- γ = specific weight of the material;
- δ = angle of friction between the material and the containing wall.

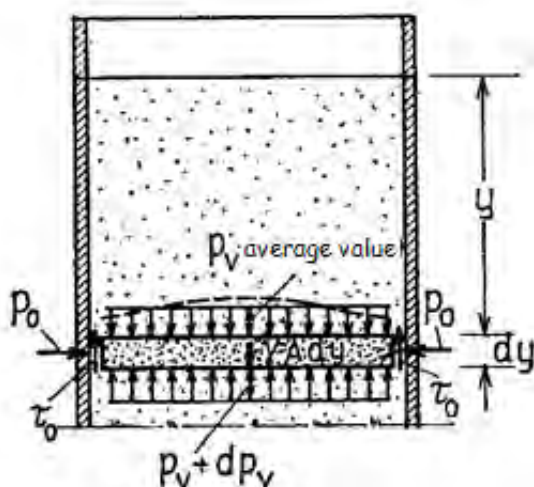


Figure 21a Horizontal and vertical pressures on a horizontal section of a cell, according to the Janssen theory

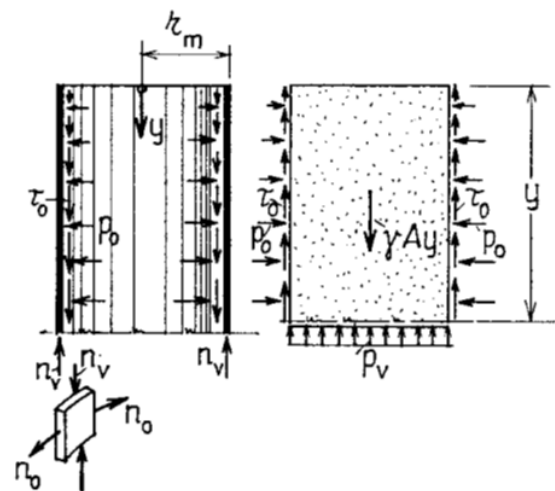


Figure 21b Pressures and actions in a general silo section

Janssen theory assumes that in a generic horizontal section of the cell the vertical pressure is uniformly distributed (Fig. 21a), so that the equilibrium equation in the vertical direction for a layer of material whose thickness is infinitesimal can be written:

$$- dp_v \cdot A - \tau_o l \cdot dy + \gamma A \cdot dy = 0 \quad (1)$$

where:

- p_v : vertical pressure;
- p_o : horizontal pressure;
- τ_o : shear stress on the boundary.

Stated that:

$$\frac{p_o}{p_v} = \lambda \qquad \frac{\tau_o}{p_o} = tg\delta = f \qquad \frac{\tau_o}{p_v} = \lambda \cdot f \quad (2)$$

equation (1) can be rewritten:

$$\frac{dp_v}{dy} + \frac{\lambda \cdot f \cdot l}{A} \cdot p_v - \gamma = 0 \quad (3)$$

Supposing that λ, f, γ maintain constant through y , and setting:

$$\text{the characteristic depth } y_0 = \frac{A}{\lambda \cdot f \cdot l} \quad \text{and} \quad 1 - e^{-y/y_0} = \psi(y) \quad (4)$$

the solution of (3) is:

$$p_v = \gamma \cdot y_0 \cdot \psi(y) \quad (5)$$

$$p_o = p_v \cdot \lambda = \gamma \cdot y_0 \cdot \lambda \cdot \psi(y) = \frac{\gamma \cdot A}{f \cdot l} \cdot \psi(y) \quad (6)$$

Experimental studies have confirmed that λ and f are practically constant with the depth, y , and that the pressure p_v is almost uniform in each horizontal section. On the other hand, the experiences show that the values of the pressures, for a given filling level, are sensibly different when the material is at rest from when it is moving (unloading operation); specifically, p_v is greater at rest while p_o is greater at the unloading.

For the p_v it is important to know not only the maximum value but also the minimum, which corresponds to the maximum load hanging on the wall due to the friction (Fig. 21b). The vertical normal stress, n_v , in the wall is equal to the difference between the weight of the material above the generic height y and the reaction $p_v A$ of the material below (l_m is the length of the medium line between the outer and the inner contour):

$$n_{v \max} = (\gamma \cdot y - p_{v, \min}) \cdot A : l_m \quad (7)$$

In order to evaluate the level of pressure on the silo's walls, it's important to take into account the behaviour of the material stored inside. In particular, the situation changes according to the characteristics of material (granular or powdered material) and to the two different conditions, static or dynamic, when the outfalls are close or open.

Indeed, the coefficients λ , f , and δ depend on the characteristics of material (angle of friction), on the roughness of the walls and on the condition (static or dynamic). In Annex A the values adopted for the case study, a silo containing cereals, are given, as derived from the manuals of the time [14].

The trend of the pressures along the height of the cell is defined by the equations (5) and (6); using the specific coefficients for the dynamic and static condition we have two different functions for each case (horizontal pressure and vertical pressure).

In the dynamic condition, the horizontal pressures, along the height of the cell, are higher than in the static condition; but in the vicinity of the outlet hole the pressure is smaller than that resulting from equation (6). To take account of that, it is correct to assume for the dynamic pressure:

- the value of the static pressure at the bottom of the cell
- the value of the dynamic pressure at a height h_f from the bottom
- and a linear variation between the two values from the bottom to h_f .

The height h_f is the lower of the following two values:

$$h_{f'} = 2d \qquad h_{f''} = \frac{H}{3} \qquad (8, 9)$$

where:

d = is the diameter of the maximum circle inscribed in the cell;

H = is the total height of the cell.

In figs. 22, 23, the diagrams of p_v and p_o for the single cell of the case study, both in the static and in the dynamic condition. In Annex A the evaluation of the pressures is illustrated.

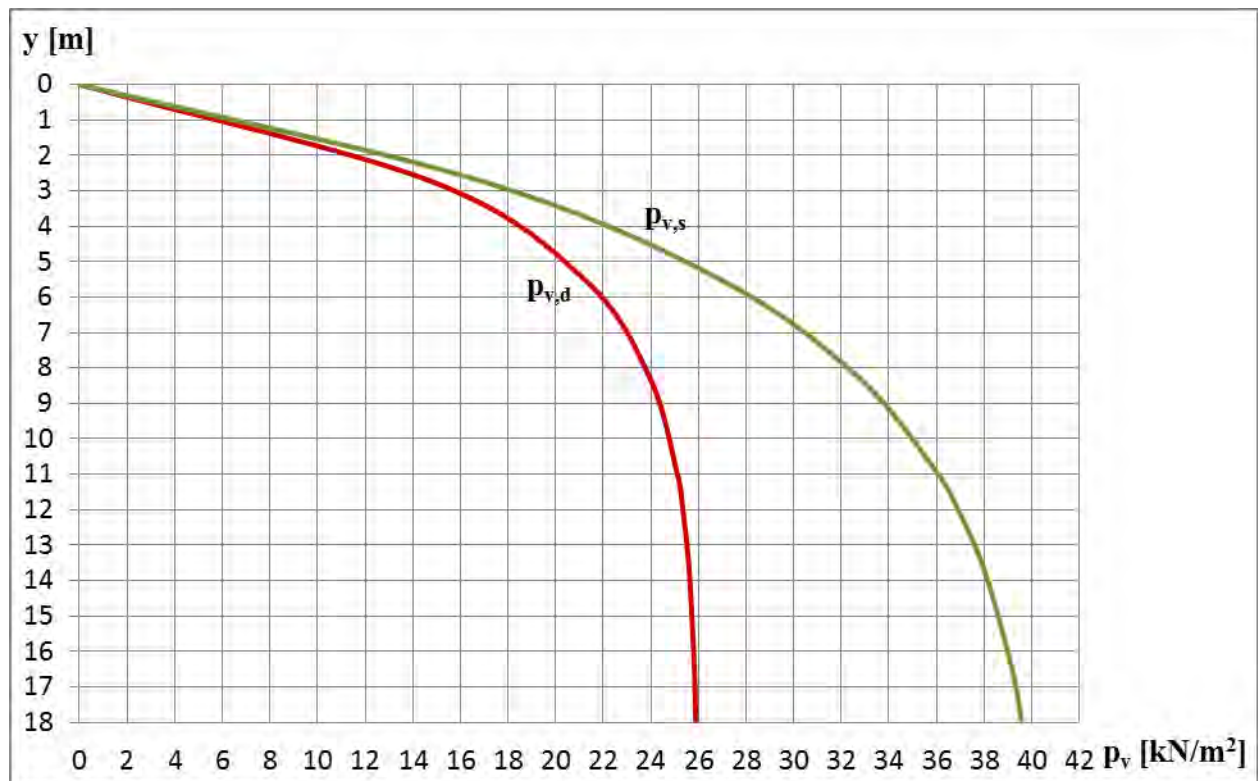


Figure 22 Actual vertical pressure diagram along the height of the cell

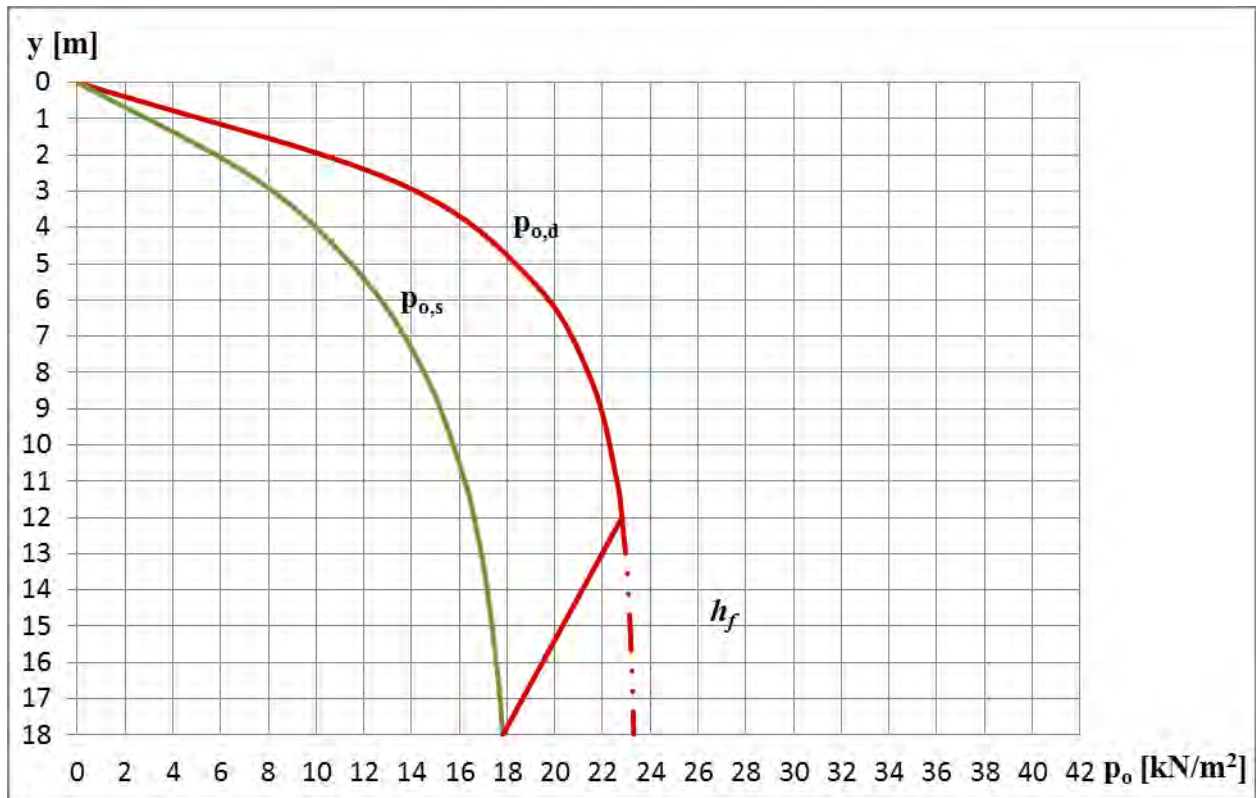


Figure 23 Actual horizontal pressure diagram along the height of the cell

4.3.2 Stresses evaluation

In a group of cells, all full, only the external walls of the perimeter are subjected to bending, while the internal ones are subjected only to tension. The loading conditions which generate the maximum bending moments are:

- chessboard load (fig. 24) to which correspond the maximum moments at the centreline;
- load in the cells of a row (fig. 25) which gives the maximum negative moments.

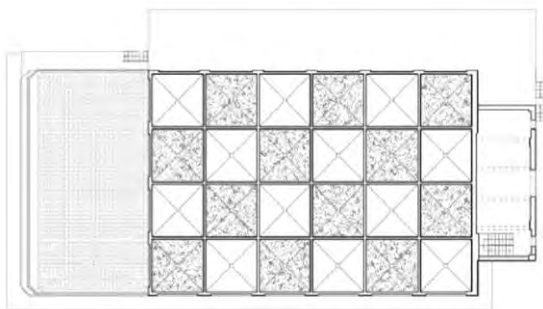


Fig. 24: Chessboard load.

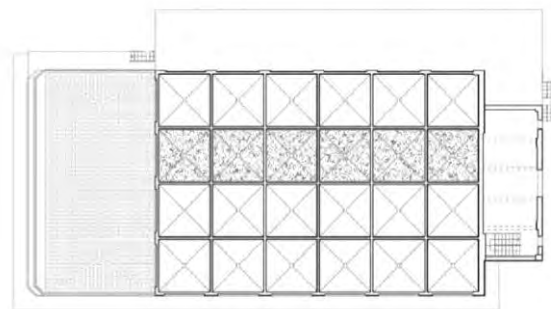


Fig. 25: Load in the cells of a row.

In a finite group of cells, the stresses may be evaluated considering a horizontal slice of the cells with unitary height, as a frame in the horizontal plane.

Given that no modern structural modelling was available at the time of building, the values of the bending moment are calculated following the Ritter theory. For the loading condition of fig. 24, the loaded cell is considered isolated from the others and it is calculated as a close frame loaded by the internal pressure, orthogonal to the walls (fig. 26).

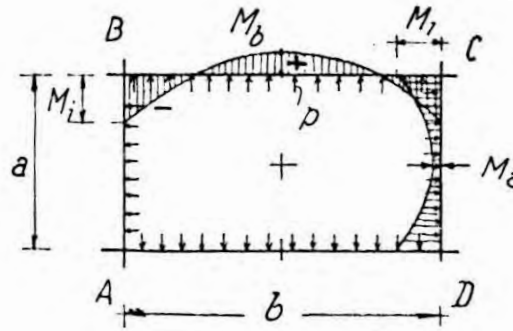


Figure 26 Cell calculated as a close frame loaded by the internal pressure, orthogonal to the walls

For square cells (side a) of constant thickness, the values of the bending moments at the joints, M_j , and in the centreline, M_m , are:

$$M_j = -\frac{p_o}{12} \cdot a^2 \qquad M_m = \frac{p_o}{24} \cdot a^2 \qquad (10, 11)$$

The walls of an internal cell are subjected not only to flexure, but also to tension. In the chessboard load condition, it occurs the maximum bending moment in the walls, but not the maximum tension. In this case the tension is:

$$N = p_o \cdot \frac{a}{2} \qquad (12)$$

while, if the cell adjacent on the side b (see fig. 25) is full, the tension is:

$$N = p_o \cdot a \qquad (13)$$

When all the cells are full, in the internal walls acts only the maximum tension and there is no bending moment.

With chessboard load, in the outside walls of the external cells both the tension and the bending moment are maximum.

4.4 Determination of properties of the structure.

Once the maximum stresses have been calculated as described above, the evaluation of the amount of rebars is done accordingly to the Italian standards valid at the time (R.D.L. 07/06/1928 n. 1431) and to proven texts of that period [17], [18].

The verification method is the allowable strength; the modular ratio is taken $m=10$ and the rebars are supposed to be symmetrically distributed.

The calculations are shown in Annex A.

5 CONCLUSIONS

The assessment of a historical silo has been discussed, with particular emphasis on simulation of original design, carried out on the basis of the relevant literature and codes available when the silo was built, demonstrating that this procedure is a valuable help in understanding the structural scheme and the detailing of the building.

REFERENCES

- [1] ISO 13822 (2001) Basis for design of structures - Assessment of existing structures. ISO, Geneva, Switzerland.
- [2] EN1992 – 1-1, Eurocode 2 – Design of concrete structures. Part 1-1: General rules and rules for buildings, CEN, Brussels 2006.
- [3] Chapperon R., Silo e magazzini per ammassi granari., Istituto delle edizioni accademiche, Udine, 1936.
- [4] Crispolti E., Mazzanti A., Quattrocchi L., Arte in Maremma nella prima metà del Novecento, Silvana Editore, Grosseto 2005.
- [5] Croce P., Holický M. eds. (2013) Operational methods for the assessment of existing structures.
http://www.leonardo.cvut.cz/download/march2014/Operational_Methods_for_the_Assessment_of_Existing_Structures.pdf
- [6] Dalla Negra R., Nuzzo M., L'architetto restaura: guida al laboratorio di restauro architettonico, Spring Edizioni, Caserta 2008.
- [7] Diamantidis D., Holický M. eds. (2012) Innovative methods for the assessment of existing structures. CTU in Prague, Klokner Institute, Prague.
http://www.leonardo.cvut.cz/download/Innovative_Methods_for_the_Assessment_of_Existing_Structures.pdf
- [8] Docci M., Maestri D., Manuale di rilevamento architettonico e urbano, Laterza, Bari 2009.
- [9] Ientile R., Tempestività di intervento e autenticità, in La conservazione del calcestruzzo armato nell'architettura moderna e contemporanea: monumenti a confronto, in Quaderni di Ananke n.2, pag.51, Milano 2010.
- [10] Janssen, H.A., Versuche uber Getreidedruck in Silozellen, VDI Zeitschrift, 1895.
- [11] Koenen, Berechnung des Seiten u. Bodendruckes in Silozellen, Centralblatt der Bauverwaltung, 1896.
- [12] Mariani F., Depositi, magazzini e sili, Bazzi editore, Milano, 1940.
- [13] Nelvi R., Signorelli B., Avvento ed evoluzione del calcestruzzo armato in Italia: il sistema Hennebique, AITEC, Milano 1990.
- [14] Pozzati P., Teoria e tecnica delle strutture. Volume I. Preliminari e fondamenti. Ed. UTET, Torino, 1972.
- [15] Readelli E., Come intervenire senza sostituire, in La conservazione del calcestruzzo armato nell'architettura moderna e contemporanea: monumenti a confronto, in Quaderni di Ananke n.2, pag.70, Milano 2010.
- [16] Ritter, Armiert. Beton, 1913.
- [17] Santarella L., Il cemento armato. Volume II. Le applicazioni alle costruzioni civili ed industriali., Ed. n° 14, 1975.
- [18] Santarella L., Il cemento armato. Volume I. La tecnica e la statica., Ed. n° 19, 1975.
- [19] Zevi B., Storia dell'architettura Moderna, Torino 1950.
- [20] Manuale dell'ingegnere, Colombo G., 80a Edizione, Hoepli, 1971.

CHAPTER 4 - ANNEX A

CALCULATION OF PRESSURES AND STRESSES IN THE SILO

A.1 DATA

h	= 18,00 m	(maximum height of vertical cells)
a	= 3,80 m	(length of the inner side of a cell)
s	= 0,17 m	(thickness of the walls of the cell)
A	= 14,44 m ²	(area of the inner section of a cell)
l	= 15,20 m ²	(length of the inner perimeter of a cell)
φ	= 30°	(friction angle of the stored material, wheat)
γ	= 8,00 kN/m ³	(specific weight of the material, wheat)

All these characteristics are supposed to be constant.

As mentioned in §4.3.1, the coefficients λ , f , and δ depend on the characteristics of the stored material, on the roughness of the walls and on the condition, static or dynamic, i.e. material at rest or unloading.

For the two conditions, the values of such coefficients as derived from the manuals of the time [14], are shown in Table A.1, where:

δ_s	is the friction angle between the stored material and the wall in the static condition
δ_d	is the friction angle between the stored material and the wall in the dynamic condition
$f_s = \text{tg}\delta_s$	is the friction coefficient in the static condition
$f_d = \text{tg}\delta_d$	is the friction coefficient in the dynamic condition

Table A.1 Values of coefficients λ , f , and δ for a silo containing wheat.

STATIC CONDITION				DYNAMIC CONDITION		
φ	δ_s	f_s	λ_s	δ_d	f_d	λ_d
30°	0,75 φ	0,41	0,45	0,60 φ	0,32	0,9

A.2 EVALUATION OF THE PRESSURES

a) Evaluation of the *Characteristic Depth*

a.1) Evaluation of the *Characteristic Depth*, $y_{0,s}$ in the static regime:

$$y_{0,s} = \frac{A}{\lambda_s \cdot f_s \cdot l} = \frac{14,44}{0,45 \cdot 0,41 \cdot 15,20} = 5,10\text{m} \quad (\text{A1})$$

a.2) Evaluation of the *Characteristic Depth*, $y_{0,d}$ in the dynamic regime (unloading phase):

$$y_{0,d} = \frac{A}{\lambda_d \cdot f_d \cdot l} = \frac{14,44}{0,90 \cdot 0,32 \cdot 15,20} = 3,25\text{ m} \quad (\text{A2})$$

b) **Evaluation of the *Horizontal Pressures***

b.1) The *Minimum Horizontal Pressure*, $p_o(y)$, occurs when the material is at rest and it depends on the characteristic depth in static regime, $y_{0,s}$. It can be derived evaluating p_o , which depends on y , as:

$$p_{o,s} = \frac{\gamma \cdot A}{f_s \cdot l} \cdot \psi(y_i) = \frac{8,00 \cdot 14,44}{0,41 \cdot 15,20} \cdot \psi(y_i) = 18,35 \frac{\text{kN}}{\text{m}^2} \cdot \psi(y_i) \quad (\text{A3})$$

where:

$$\psi(y) = 1 - e^{-\frac{y}{y_0}} \quad (\text{A4})$$

The distance h_f is:

$$h_f = \frac{H}{3} = \frac{18,00}{3} = 6,00\text{m} \quad (\text{A5})$$

b.2) The *Maximum Horizontal Pressure*, $p_o(y)$, occurs during the unloading phase, therefore the *Horizontal Pressure Diagram* is calculated in dynamic condition and it depends on the characteristic depth in dynamic regime, $y_{0,d}$. It can be derived evaluating p_o , which depends on y , as:

$$p_{o,d} = \frac{\gamma \cdot A}{f_d \cdot l} \cdot \psi(y_i) = \frac{8,00 \cdot 14,44}{0,32 \cdot 15,20} \cdot \psi(y_i) = 23,39 \frac{\text{kN}}{\text{m}^2} \cdot \psi(y_i) \quad (\text{A6})$$

where:

$$\psi(y) = 1 - e^{-\frac{y}{y_0}} \quad (\text{A7})$$

Using the equations (A1) through (A7) and the Table A.1, the values of the horizontal pressure along the height of the cell are evaluated (see Fig. 23 in §4.3.1).

Table A.2 Horizontal pressures

	Section 1	Section 2	Section 3	Section 4	Section 5	Section 6	Section 7	Section 8	Section 9
y_i (m)	0.00	2.74	5.48	8.22	10.96	12.00	13.71	16.45	18.00
ψ_s	0.00	0.42	0.66	0.80	0.88	0.91	0.93	0.96	0.97
$p_{o,s}$ (kN/m ²)	0.00	7.63	12.09	14.69	16.21	16.61	17.10	17.62	17.81
$p_{o,d}^*$ (kN/m ²)	0.00	13.33	19.06	21.53	22.59	22.81	21.38*	9.10*	7.81*

* reduced values from a height of 6 metres from the bottom.

c) **Evaluation of the *Vertical Pressures***

c.1) The *Maximum Vertical Pressure*, $p_v(y)$, occurs when the material is at rest and it depends on the characteristic depth in the static regime, $y_{0,s}$. It can be derived evaluating p_v , which depends on y , as:

$$p_{v,s} = \gamma \cdot y_{0,s} \cdot \psi(y_i) = 8,00 \cdot 5,10 \cdot \psi(y_i) = 40,80 \frac{\text{kN}}{\text{m}^2} \cdot \psi(y_i) \quad (\text{A8})$$

c.2) The *Minimum Vertical Pressure*, $p_v(y)$, occurs when the material is at rest and it depends on the characteristic depth in dynamic regime, $y_{0,d}$. It can be derived evaluating p_o , which depends on y , as:

$$p_{v,d} = \gamma \cdot y_{0,d} \cdot \psi(y_i) = 8,00 \cdot 3,25 \cdot \psi(y_i) = 26,00 \frac{\text{kN}}{\text{m}^2} \cdot \psi(y_i) \quad (\text{A9})$$

Using the equations (A1), (A2), (A8), (A9) and the Table A.1, the values of the vertical pressure along the height of the cell are evaluated (see Fig. 22 in §4.3.1).

Table A.3 Vertical pressures

	Section 1	Section 2	Section 3	Section 4	Section 5	Section 6	Section 7	Section 8	Section 9
y_i (m)	0.00	2.74	5.48	8.22	10.96	12.00	13.71	16.45	18.00
ψ_d	0.00	0.57	0.81	0.92	0.97	0.98	0.99	0.99	1.00
$p_{v,s}$ (kN/m ²)	0.00	16.96	26.86	32.65	36.03	36.90	38.01	39.16	39.58
$p_{v,d}$ (kN/m ²)	0.00	14.81	21.18	23.92	25.10	25.34	25.61	25.83	25.89

d) Evaluation of the maximum vertical normal stress, n_v

Using the equation (7) §4.3.1 the values of the maximum vertical normal stress are calculated. They depend on the dynamic condition and are connected to the minimum values of the vertical pressure, $p_{v,d}$.

Table A.4 Vertical normal stresses

	Section 1	Section 2	Section 3	Section 4	Section 5	Section 6	Section 7	Section 8	Section 9
y_i (m)	0.00	2.74	5.48	8.22	10.96	12.00	13.71	16.45	18.00
ψ_d	0.00	0.57	0.81	0.92	0.97	0.98	0.99	0.99	1.00
$p_{v,d}$ (kN/m ²)	0.00	14.81	21.18	23.92	25.10	25.34	25.61	25.83	25.89
$n_{v,max}$ (kN/m)	0.00	6.76	21.53	39.75	59.45	67.12	79.87	100.49	112.21

A.3 EVALUATION OF STRESSES

The walls of the cells, being subjected to bending moment in both directions, are reinforced with two symmetrical series of horizontal rebars disposed in the vicinity of the surfaces, according to the diagram of pressures which increase from the top to the bottom. Usually the diameter of the horizontal rebars remains constant and the mutual distance in the vertical direction varies. Usually the reinforcing bars are maintained constant for the whole perimeter of the wall, therefore the sections where the stress is highest are considered. Indeed the sections to consider are those in the vicinity of the joints subject to the maximum bending moment, according to equation (10) §4.3.2, for the horizontal pressures in dynamic regime, $p_{o,d}$.

The stresses are evaluated for a slice high 100 cm of the internal walls or the external walls, and for the two situations: chessboard load and load in the cells of a row.

a) Internal wallsa.1) *chessboard load:*

$$M_1 = \frac{p_{o,d}}{12} \cdot a^2 \qquad N_1 = \frac{p_{o,d} \cdot a}{2} \qquad (\text{A10, A11})$$

a.2) *load in the cells of a row:*

$$M_2 = 0 \qquad N_2 = p_{o,d} \cdot a \qquad (\text{A12, A13})$$

b) External wallsb.1) *chessboard load:*

$$M_1 = \frac{p_{o,d}}{12} \cdot a^2 \qquad N_1 = \frac{p_{o,d} \cdot a}{2} \qquad (\text{A14, A15})$$

For the design of rectangular sections in bending and axial force, following the verification method of the allowable strength which was in use at the time of the construction, it is possible to use tables which allow, once set a percentage of reinforcement, μ , to obtain coefficients to be used in the calculation of the stresses, σ_c and σ_s . Such coefficients, η_1 , η_2 , depend on the percentage of reinforcement, μ , on the modular ratio, m , and on the ratio β between the eccentricity, e , and the thickness of the section; also, there are different tables to be used in the case of simple or symmetrical reinforcement, and in the case of bending+compression or bending+tension.

For the case study, we have set:

- symmetric rebars
- $\mu = 2\%$;
- $m=10$.

Both for internal and external walls, in the chessboard load condition, the eccentricity, e , in the various sections is constant:

$$e = \frac{M}{N} = \frac{a}{6} = 0,63\text{m} \qquad (\text{A16})$$

The corresponding coefficient β is:

$$\beta = \frac{e}{s} = 3,73 \qquad (\text{A17})$$

Once defined the values of β and μ , it is possible to find, through Table A.5 (derived from [18]), the coefficients, η_1 and η_2 , for the evaluation of the concrete and steel stresses, σ_c and σ_s .

$$\sigma_c = \frac{2 \cdot N}{s \cdot a} \cdot \eta_1 \qquad \sigma_s = \sigma_c \cdot \eta_2 \qquad (\text{A18, A19})$$

The values of the stresses for the case study are shown in tables A.6 and A.7.

Table A.5 Coefficients for the calculation of stress in r.c. sections (derived from [18])

Tensoflessione - Armatura simmetrica $F_f = F'_f$.

$$\underline{2 F_f = \mu a b; \quad m = 10}$$

α	$\mu = 0,010$		$\mu = 0,015$		$\mu = 0,020$		η_2	η_3
	β	η_1	β	η_1	β	η_1		
0,290					∞	∞	22,66	8,17
0,280					11,654	29,17	23,82	8,11
0,270					5,753	14,14	25,06	8,04
0,265			∞	∞			25,74	8,00
0,260					3,801	9,15	26,42	7,96
0,255			10,270	30,11			27,14	7,92
0,250			6,883	20,00	2,828	6,67	27,88	7,88
0,240			4,127	11,76	2,246	5,17	29,45	7,79
0,232	∞	∞					30,82	7,72
0,230			2,932	8,19	1,858	4,17	31,17	7,70
0,220	7,980	28,95	2,266	6,18	1,583	3,46	33,05	7,59
0,210	4,242	15,11	1,841	4,90	1,376	2,92	35,10	7,48
0,200	2,867	10,00	1,547	4,00	1,217	2,50	37,35	7,35
0,180	1,717	5,70	1,168	2,83	0,986	1,88	42,61	7,06
0,160	1,213	3,77	0,935	2,09	0,828	1,45	49,19	6,69
0,140	0,933	2,67	0,780	1,58	0,715	1,13	57,64	6,21
0,120	0,757	1,95	0,669	1,20	0,630	0,87	68,92	5,58
0,100	0,638	1,43	0,588	0,91	0,564	0,67	84,70	4,70
0,075	0,538	0,95	0,514	0,62	0,503	0,46	116,27	2,93
0,050	0,471	0,57	0,462	0,38	0,458	0,28	179,40	-0,60
0,000	0,400	0,00	0,400	0,00	0,400	0,00	∞	$-\infty$

Table A.6 Values of stresses in the chessboard load condition

	Section 1	Section 2	Section 3	Section 4	Section 5	Section 6	Section 7	Section 8	Section 9
y_i (m)	0.00	2.74	5.48	8.22	10.96	12.00	13.71	16.45	18.00
$p_{o,d}$ (kN/m ²)	0.00	13.33	19.06	21.53	22.59	22.81	21.38	9.10	7.81
M_1 (kN*m)	0.00	16.04	22.94	25.90	27.18	27.45	25.73	22.99	21.43
N_1 (kN)	0.00	25.32	36.22	40.90	42.92	43.34	40.63	36.29	33.84
η_1	8.96	8.96	8.96	8.96	8.96	8.96	8.96	8.96	8.96
η_2	26.53	26.53	26.53	26.53	26.53	26.53	26.53	26.53	26.53
σ_{cl} (N/mm ²)	0.00	2.67	3.82	4.31	4.52	4.57	4.28	3.82	3.57
σ_{sl} (N/mm ²)	0.00	70.80	101.26	114.37	120.01	121.17	113.61	101.48	94.63

Table A.7 Values of stresses in the situation of load in the cells of a row

	Section 1	Section 2	Section 3	Section 4	Section 5	Section 6	Section 7	Section 8	Section 9
y_i (m)	0.00	2.74	5.48	8.22	10.96	12.00	13.71	16.45	18.00
$p_{o,d}$ (kN/m ²)	0.00	13.33	19.06	21.53	22.59	22.81	21.38	9.10	7.81
M_2 (kN*m)	0.00	0.00	0.00	0.00	0.00	0.00	0.00	0.00	0.00
N_2 (kN)	0.00	50.64	72.43	81.81	85.84	86.67	81.26	72.59	67.68
σ_{s_2} (N/mm ²)	0.00	14.89	21.30	24.06	25.25	25.49	23.90	21.35	19.91

CHAPTER 7: PIPELINES AND WATER SUPPLY

Selcuk Toprak¹, A. Cem Koc¹, Engin Nacaroglu¹, Mehmet Inel¹, Sevket Murat Senel¹

¹Pamukkale University, Denizli, Turkey

Summary

Water supply system of a city must be evaluated continuously for the quality of service and performance by considering the existing and expected conditions and future hazards. “Maintenance only when problem occurs” concept is being replaced by the “preventive maintenance” and “proactive management” concepts especially in the last decades. These relatively new concepts require more robust and comprehensive evaluation of the system but produce more effective and reliable water supply. Presented case study from Denizli, Turkey here shows a practical example in this direction.

1 INTRODUCTION

It is important to put in the most proper pipeline from the start as replacing or retrofitting the pipelines later requires substantial investment. Sufficient considerations should be given regarding the pipe materials and joints from the life expectancy and hazards points of view. However, most of the pipelines in Europe are the existing ones and new placements are rather limited. Buried pipes of distribution systems are worn in the length of time because of the temperature, soil moisture, corrosion and other aging effects [1, 2]. For example, aging of pipes in a water distribution system may have three main results. First, aging of pipe material causes a decrease in the strength of pipe. Then pipe breaks are increased at the high pressure areas of the system. Second, aging of a pipe increases the friction coefficient of the pipe so the energy loss in that pipe rises. Then more pumping cost occurs and sometimes a gravity working system needs pumping. Finally, aging of pipes affect the water quality in the system and may cause discolored water. Aging of a pipe is unavoidable but this process may be delayed by some precautions. Cathodic protection for steel pipes, lining and coating for steel and ductile iron pipes are some anti-aging techniques. In the design phase of a water distribution system, analyzing the temperature changes in the area, pressure values of the system, chemical components of the soil and ground water helps for the selection of long life pipe material and suitable burial depth of pipes.

Most public water utilities use the concept of “maintenance only when a breakdown occurs”. However, in recent years “preventive maintenance” and “proactive management” concept is getting more attraction. The logic behind preventive maintenance (PM) is that it costs far less to regularly schedule downtime and maintenance than it does to operate the network until breakdown at which repair or replacement is imperative. The primary goal of PM is thus to prevent the failure of components of the network before they actually occur by using advanced methods of statistical and risk analysis. The consequences of “maintenance on the run” are unreliable service, customer dissatisfaction, and significant water losses of valuable resources due to leakage or pipe rupture. To take full advantage of this, the utilities must have an accurate topological image of the network, the age and type of materials used in its various branches and past maintenance records.

This chapter presents a case study regarding evaluation of existing water distribution systems and proposed solutions against hazards. The case study is from Denizli City, Turkey. It shows how IWA/AWWA water balance methodology was used to decide the replacement

program in the old part of the city and how seismic improvements incorporated into the pipe replacement and asset management program.

2 DENIZLI WATER SUPPLY SYSTEM

2.1 Introduction to Water Supply System of Denizli

Denizli Municipality provides water to the City of Denizli from various springs (e.g., Gökpınar, Derindere, and Kozlupınar) and deep wells. The water from these sources being collected in water storage tanks, treated and released to the distribution system. Due to the topography of the area, the water distribution system primarily relies on gravity flow. The GIS database of the water supply system and its details are provided in Toprak and Taskin [3]. But for convenience, Figure 1 [4] shows the details of the water distribution system in Denizli City and, Figure 2 [3] the composition, relative lengths and pipe diameters as of 2007. It can be seen that the total length of pipeline is about 1745 km with some 95% of the transmission and connection lines made of steel. The main and distribution lines are asbestos cement (AC -54%), polyvinyl chloride (PVC – 44%) and cast iron (CI – 2%). The diameter of the distribution lines is between 65 and 200 mm whereas the main lines are between 100 and 600 mm in diameter. The CI pipelines are the oldest in the system and primarily serve the more well-established parts of Denizli which include important local business districts with a high population density.

The first water network of Denizli Municipality was built in 1952 and was improved later in 1958. In this network, cast iron pipes between diameters of 60-200 mm were used. Construction of drinking water system, which covers major part of the center settlement was completed between 1975 and 1981 by Bank of Provinces. In this network, asbestos cement pipes (AC) between diameters of 80-500 mm were used. With the “greater City” law enacted in 2009, the smaller nearby municipalities merged with Denizli Municipality. In 2014, with the establishment of the metropolitan municipality, all the province water works became the responsibility of DESKİ which was also founded in 2014.

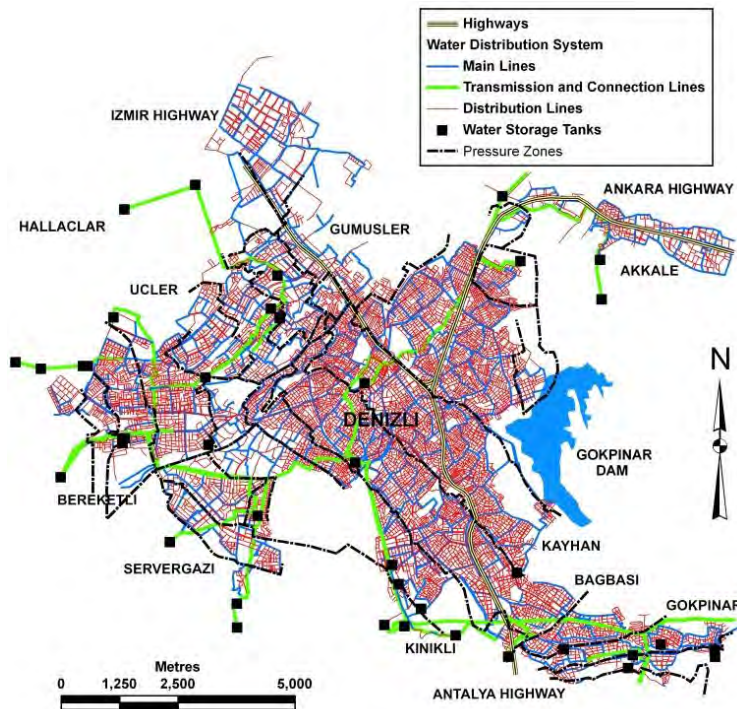
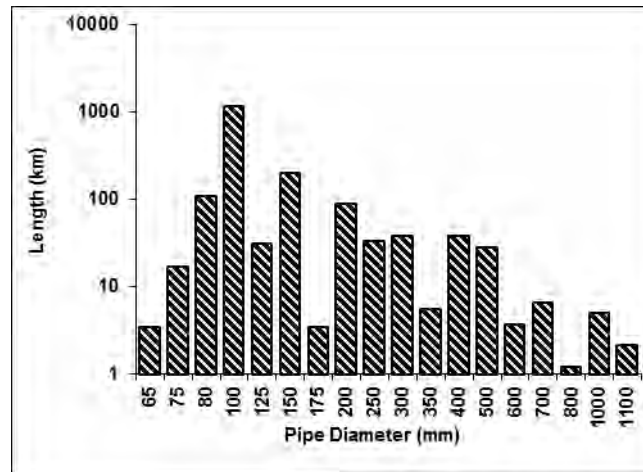
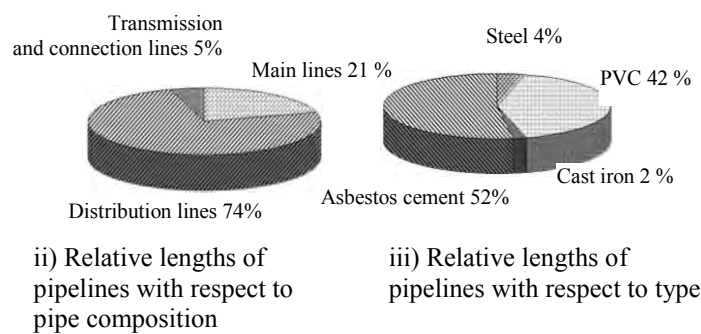


Figure 1 GIS Map of Denizli City water supply system [4]



i) Length of pipelines with respect to pipe diameter



ii) Relative lengths of pipelines with respect to pipe composition

iii) Relative lengths of pipelines with respect to type

Figure 2 Composition of pipelines in the Denizli City water supply system (after [4])

2.2 Assessment of the Water Distribution System

In addition to the natural hazards, one of the important reason for the assessment of water supply system is the water loss in the system. Water loss or non-revenue water (NRW) represents inefficiency in water delivery and measurement operations in transmission and distribution networks and, for some systems, can amount to a sizeable proportion of total water production [5]. The Water Losses for a whole system or for a partial system are calculated as the difference of Systems Input Volume and Authorised Consumption. The Water Losses consist of Real and Apparent Losses:

- Real Losses are physical losses of leaks, bursts and overflows from the pressurized system, up to the point of metering on the service connections.
- Apparent Losses consist of all types of meter inaccuracies (input, output, and customer meters) and unauthorised consumption (e.g., theft and illegal use). Also termed as commercial losses.

Water loss occurs on all the systems, it is only the volume that varies and it reflects the ability of a utility to manage its network. To understand the reasons why, how and where water is being lost managers have to carry out an appraisal of the physical characteristics of the network and the current operational practice. In many instances the problem of water loss is caused by poor infrastructure, bad management practice, network characteristics, operational practices, technologies, skills and social and cultural influences. A high level of real or physical loss reduces the amount of precious water reaching customers, increases the operating costs of

the utility and makes capital investments in new resource schemes larger. A high level of apparent or commercial losses reduces the principal revenue stream to the utility.

The starting point for any water utility is to make an assessment of how much, where and why water is being lost from their network or part of their network i.e. between its point of entry into the transmission and distribution system (often a water treatment plant) and the customer's meter. The amount of water loss can be determined by conducting a water audit and this process contains two elements:

- A review or appraisal of network operating practices.
- The quantification of the amount of water that is being lost from the network.

2.3 Reviewing Network Operational Practices

In order to fully understand why water is being lost from a network a review of the distribution network and how it is being operated should be undertaken. The review will answer questions relating to the condition of the infrastructure, behaviour of the system and how well it is being managed.

The review should assess:

- Regional characteristics, local factors and components of water loss
- Current methods used for operating and managing the distribution system
- The level of technology for monitoring and detecting leakage
- Staff numbers, skills and capabilities
- The utility's current data and methodology for estimating current level of loss

The appraisal should also include interviews with senior managers to gain views on the current management culture, financial and political constraints of the utility. There should also be discussions with key staff involved with the day to day operation of the system, especially with regard to:

Information about the system e.g. population served, length of mains, topography, typical demand and source management

- Condition of the system including frequency of bursts
- Estimates of current level of leakage
- Customer metering policies
- Billing data
- Economic information i.e. the cost of producing water
- Current method of leakage control and repair policy practiced by the utility

2.3.1 Quantifying Water Loss

The second component of an audit is the estimation of the amount of water that is being lost from the network. There are three methods for estimating the level of losses in a system:

- The establishment of a water balance.
- Night flow analysis (bottom up leakage assessment)
- Component analysis.

The calculation of water balance is the most common method of assessing losses. It must be emphasized that before embarking upon the development and introduction of a water loss strategy it is vitally important to know the starting position.

3 WATER BALANCE AND REPLACEMENT PROGRAM

3.1 The Water Balance

The amount of water loss from a system can be determined by constructing a water balance. This is based on the measurement or estimation as to the amount of water produced (taking account of any water imported and/o exported), consumed and lost. In its simplest form the water balance is:

$$\text{Losses} = \text{Distribution System Input} - \text{Consumption}$$

The calculation of a water balance is very important because:

- It is the basis of assessing the level of water loss for any utility.
- A first time calculation reveals the availability and reliability of data and level of understanding.
- Mechanism for benchmarking.
- Provides a first step towards improvement.
- Understanding a water balance is essential for prioritizing actions and investments.

Ten years ago there was a diversity of definitions and formats for the calculation of water loss. In the late 1990's the IWA recognized the need to have a workable water audit structure with common terminology and as a result its Water Loss Task Force developed a standard water balance. This standard water balance has now been accepted with or without some minor modifications and used worldwide.

Table 1 The IWA standard water balance

	Authorized Consumption	Billed Authorized Consumption	Billed Metered Consumption Billed Unmetered Consumption	Revenue Water
	Water Losses	Unbilled Authorized Consumption	Unbilled metered Consumption Unbilled Unmetered Consumption	Non-Revenue Water
Apparent (Commercial) Losses		Unauthorized Consumption Metering Inaccuracies		
System Input Volume		Real (Physical) Losses	Leakage on Transmission and/or Distribution Mains Leakage and Overflows at Utility's Storage Tanks Leakage on Service Connections up to Customer Metering	

In year 2003, Denizli Municipality evaluated the water balance of Denizli City-Turkey. The water balance was prepared as part of a project supported by the World Bank according to the IWA/AWWA methodology [6]. Table 2 [7] presents the results, according to which there existed about 43 % non-revenue water. Physical losses amounted up to 36 %.

Table 2 Year 2003 water balance of Denizli City-Turkey [7]

			Billed Metered Consumption	
			13.636.509 m ³ /year (57,18%)	Revenue Water
				13,637,252 m ³ /year (57,18%)
			Billed Unmetered Consumption	
			-0 m ³ /year (0,00%)	
	Authorized Consumption			
	14.815.114 m ³ /year (62,12%)			
			Unbilled Metered Consumption	
			1.078.605 m ³ /year (4,52%)	
			Unbilled Unmetered Consumption	
			100.000 m ³ /year (0,42%)	
Water supplied to network system				
23.849.688 m ³ /year (100%)				
			Unauthorized Consumption	Non-revenue
			3.095 m ³ /year (0,02%)	10,212,436 m ³ /year (42,82%)
			Commercial Losses	
			438.320 m ³ /year (1,84%)	
	Water Losses			
	9.034.574 m ³ /year (37,88%)			
			Metering Inaccuracies and Date Handling Errors	
			435.225 m ³ /year(1,82%)	
			Physical Losses	
			8.596.254 m ³ /year (36,04%)	

3.2 Replacement Program

Because of these relatively high physical losses, water quality issues and excessive repair costs, Denizli Municipality decided to start a comprehensive replacement program and speed up the pipe replacement efforts. Assessments indicated that replacement of small segments of the system was not an option because of the scale of the problems. Pipeline repair logs and

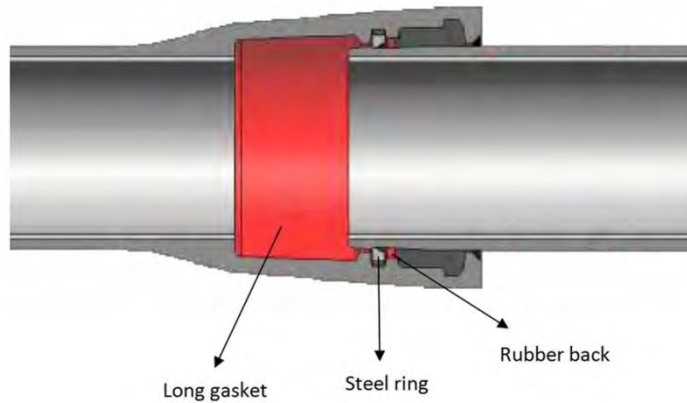
complaints from the customers pointed especially to the pipelines located in the central part of the city. A comprehensive evaluation of the system following the elements of a distribution integrity management program (DIMP) plan showed that any replacement should have started from the central part of the city. Here are the seven elements of a DIMP plan and how they may relate to a replacement program [8]:

- 1) Knowledge: Operators must develop an understanding of their distribution systems and identify pipeline characteristics and materials which may include Cast iron, Bare Steel, PVC, AC and other high risk pipe materials.
- 2) Identify Threats: Operators must identify threats that affect or could potentially affect their distribution pipeline.
- 3) Evaluate and Rank Risks: Operators must evaluate the risks to their pipeline and the relative importance of each threat.
- 4) Measures to Address Risks: Operators must determine and implement measures to reduce the risks from failure of their pipeline. These measures must include an effective leak management program which may identify higher leak incidence rates.
- 5) Measure Performance: Operators must develop and monitor performance measures to evaluate the effectiveness of their integrity management program.
- 6) Periodic Evaluation And Improvement: Operators must reevaluate risks and threats on their entire pipeline at least every five years and consider the relevance of threats in one location to other areas of their systems.
- 7) Report Results: Operators must report annually the number of leaks eliminated or repaired. One method of eliminating leaks is to replace leaking pipe.

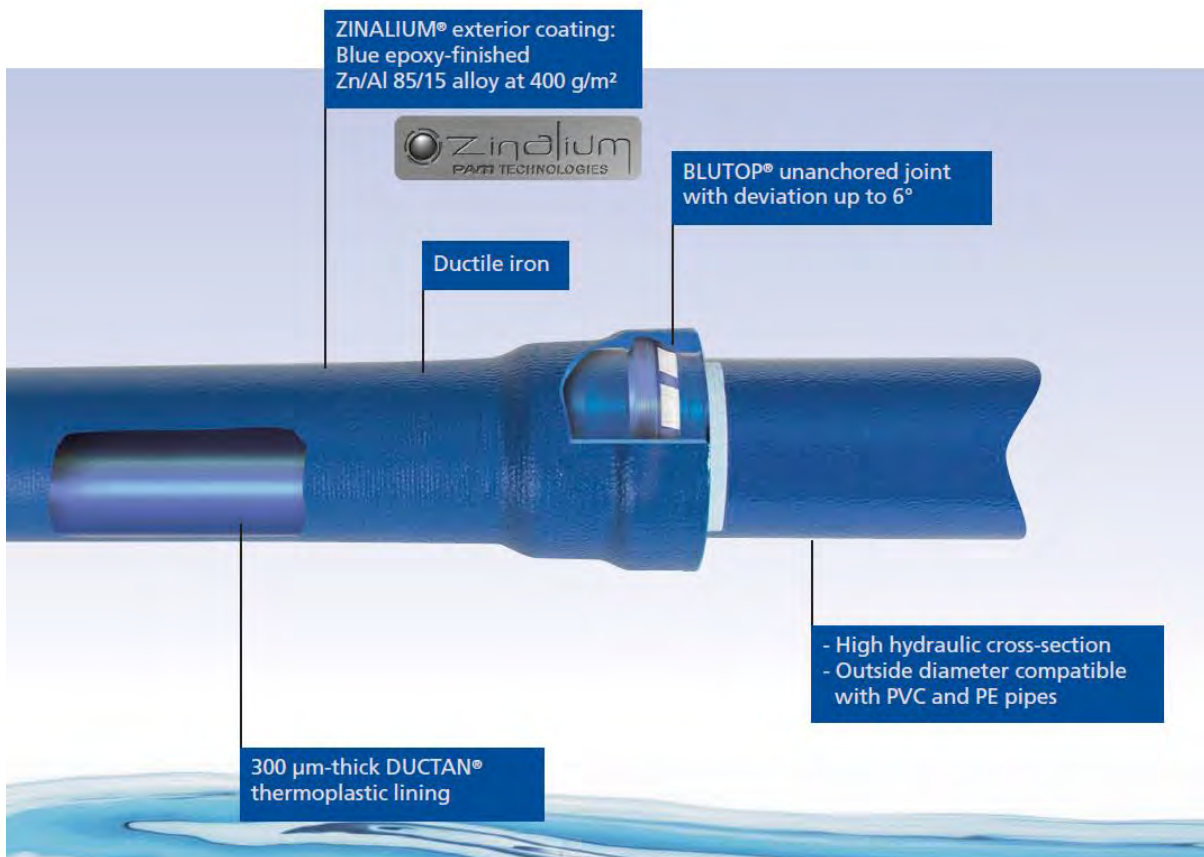
The replacements program started in 2008. Ductile iron was selected as the pipe material. The replacement program is still continuing but in the first few years pipelines primarily in the liquefaction prone areas [4] were renewed. Contractors obtained ductile iron pipes and their fittings mainly from two sources. One of them is the Samsun Makina Sanayi Inc. from Turkey and the other is the Saint-Gobain Group from France (Figure 4a and 4b, respectively). Samsun Makina Sanayi Inc. produces special earthquake resistant type connections in order to avoid the deformation of the socket and pipe end. The socket parts of those pipes are manufactured with “long standard-type sockets”, which has a longer design length than the standard manufactured pipes’ sockets and inside the socket standard-type gasket is used together with the rubber backed steel ring, which prevents the pipe displacing from the socket. The groove opened to the end of the pipe prevents the pipe from displacing by attaching the steel ring. According to the Samsun Makina Inc. earthquake resistant type connection conforms the values mentioned in ISO 16134: 2006 (E) Table 2 [9].

- Expansion/Contraction performance: Class S-1 \pm % 1 of L (L is the length of pipe usually 6 meters)
- Slip-out resistance: Class A \geq 3D kN (D is the nominal diameter of pipe),
- Joint deflection angle: M-2 \pm 7.50 to < 150.

BLUTOP is the patented name of the Saint-Gobain PAM Group ductile iron pipes which are designed to withstand a particularly high angular deviation of 6°. The enhanced jointing depth also decreases the risk of pipe dislocation. As a result, BLUTOP® offers excellent performance in soil subject to ground movements [10].



a) Samsun Makina Sanayi Inc. earthquake resistant type connection



b) The Saint-Gobain PAM BLUTOP® jointing

Figure 4 Seismic joints used in Denizli, Turkey water pipelines replacement program [2]

4 CONCLUSIONS AND RECOMMENDATIONS

It is the best to take into account properly the seismic and other hazard considerations in the design phase of a water distribution system. If there is no seismic code available in the country for water distribution systems, the existing guidelines from other countries should be utilized [16, 17, 18, 19]. Sufficient considerations should be given regarding the pipe materials, joints and soil-pipe interaction from the life expectancy and hazards points of view.

For a comprehensive and continuous assessment of water supply systems, the utilities must have an accurate topological image of the network, the age and type of materials used in its

various branches and past maintenance records. This type of information is also necessary for distribution integrity management program (DIMP) plan of the water supply system. The past maintenance records can be used to assess the system like the one used by Toprak, et al. [20] for seismic hazards.

Continuous service of lifeline systems such as drinking water and natural gas pipeline systems or getting their functionality quickly back right after an earthquake is very important and crucial for urban societies. Some earthquake resistant design and technologies proved to be working in recent earthquakes. This provides a motivation to increase international exchange and cooperation on earthquake resistant technologies.

Another observation is that pipeline monitoring and mitigation studies are important to reduce the pipeline damage risk from seismic and other hazards. To increase the applicability and sustainability, seismic improvements should be incorporated into the pipe replacement and asset management programs [2]. The best and sustainable maintenance programs are the ones which consider the regular maintenance problems together with possible hazard problems.

REFERENCES

- [1] Toprak S., Koç A. C., Güngör M., Kaya M., Stathaki A. (2012) Application of a training project in Turkey on preventive maintenance of water utility networks against earthquakes, Paper No. 5673, 15th World Conference on Earthquake Engineering (15WCEE), September 24-28, 2012, Lisbon, Portugal.
- [2] Toprak S., Nacaroglu E., Koç A. C. (2015) Seismic response of underground lifeline systems, Perspectives on European Earthquake Engineering and Seismology Vol. 2, Ansal, A. (Ed.).
- [3] Toprak S. and Taşkin F. (2007) Estimation of earthquake damage to buried pipelines caused by ground shaking, Natural Hazards, Springer. The Netherlands, 40, 1-24.
- [4] Toprak S., Taşkin F., Koç A. C. (2009) Prediction of earthquake damage to urban water distribution systems: A case study for Denizli, Turkey, *The Bulletin of Engineering Geology and the Environment*, 68:499-510.
- [5] Pilcher R., Dizdar A., Dilsiz C., Toprak S., Angelis E. D., Angelis K. D., Koç A. C., Dikbaş F., Fırat M., Bacanlı U. G. (2009) How to prevent water losses?, Eflatun Publishing House Ankara, Turkey.
- [6] Denizli City Water Works (2005), Denizli Municipality, Denizli.
- [7] Toprak S., Koc A. C., Gungor M., Kaya M., Stathaki A., Sofotasios D., Tsakiris G., Vangelis H., De Angelis E., Iacovou G., Charalambous B. (2011) Su dağıtım borularının doğal afetlere karşı koruyucu bakımı: PM4WAT projesi uygulaması, Bildiri No. 181, Yedinci Ulusal Deprem Mühendisliği Konferansı, 30 Mayıs 2011-3 Haziran, İstanbul.
- [8] Goodman, L. and Burnie, G. (2011) Guidelines for successful LDC pipe replacement Programs, January 2011 Vol. 238 No. 1
- [9] Samsun Makina (2014), ductile iron pipe fittings catalogue, http://www.samsunmakina.com.tr/_en/_docs/tech_docs.html
- [10] Saint Gobain (2014), BLUTOP pipe and fittings catalogue, http://www.saint-gobain-pam.co.uk/assets/docs/ws/Blutop_Brochure.pdf
- [11] Lund L. (1995), "Water Systems", TCLEE Monograph No. 8, A. J. Schiff, Ed., ASCE, NewYork, NY, Aug., pp. 96-131.
- [12] Toprak S. (1998), Earthquake effects on buried lifeline systems, Ph.D. thesis, Cornell University, Ithaca, NY.
- [13] O'Rourke T. D., and Toprak S. (1995) Case history of pipeline response to ground deformation at Balboa Blvd., 1994 Northridge earthquake, Proceedings, Sixth U.S. - Japan Workshop on Earthquake Disaster Prevention for Lifeline Systems, Osaka, Japan, July, pp. 3-20.

- [14] Eguchi, R. T., and Chung R. M. (1995) Performance of lifelines during the January 17, 1994 Northridge earthquake, TCLEE Monograph No.6, M. J. O'Rourke, Ed., ASCE, New York, NY, pp. 120-127.
- [15] Labay J. (2010) <http://www.waterworld.com/articles/print/volume-25/issue-8/departments/automation-technology/geospatial-software-helps-la-water-system-go-digital.html>
- [16] Toprak S., ve Yoshizaki K. (2003) Boru hatlarına deprem yüklerinin etkisi, 5. Ulusal Deprem Mühendisliği Kongresi, CDROM Bildiri No: 25, 26-30 Mayıs 2003, İstanbul.
- [17] Japan Water Works Association (JWWA, 1997) Seismic Design and Construction Guidelines for Water Supply Facilities.
- [18] American Lifelines Alliance (ALA, 2005) Seismic Guidelines for Water Pipelines, prepared by ASCE, FEMA and NIBS.
- [19] ISO 16134:2006 (2006), Earthquake- and subsidence-resistant design of ductile iron pipelines.
- [20] Toprak, S., E. Nacaroglu, O. A. Cetin, and A. C. Koc (2009) Pipeline damage assessment using cluster analysis, TCLEE 2009: Lifeline Earthquake Engineering in a Multihazard Environment Proceedings of the 2009 ASCE Technical Council on Lifeline Earthquake Engineering Conference ASCE Conf. Proc. 357, 78 (2009), Alex K. K. Tang P.E., Stu Werner P.E., Editors, June 28–July 1, 2009, Oakland, California, DOI:10.1061/41050(357)78.

CHAPTER 8: WATER TANKS – A CASE STUDY

Raffaello Bartelletti¹, Maria Luisa Beconcini¹, Pietro Croce¹, Paolo Formichi¹

¹Department of Civil and Industrial Engineering – Structural Division – Univ. of Pisa, Italy

Summary

The proper functioning of pipelines and water supply systems involves relevant social and economic aspects, so that their maintenance in the optimal conditions is of primary importance. Considering the financial commitment related, it is necessary that interventions are carefully planned and optimally designed, which can be reached only after accurate surveys and investigations. In the present chapter an example is presented concerning the static and dynamic assessment of a hanging water tank, built with r.c. structure, around 1960.

1 INTRODUCTION

Pipelines and water supply systems, in general, are particularly significant, because of their diffusion and of the economic and societal consequences of their faults, malfunctioning or failure.

It must be highlighted that for these particular infrastructures the indirect cost of severe out of service condition can be comparable or even higher than the direct costs related to failure of the system, as frequently happens in network infrastructures.

For the above mentioned reasons, reliability analyses play an important role not only in planning the maintenance operations, the improvement or extension of the network, to take into account the increases or changes in demand, but also in adopting decision to dismantle or rebuild the network itself.

Given the great commitment that results, it is necessary that interventions are optimally designed, so as to make best use of economic resources, and to safeguard the architectural and functional characteristics of the constructions.

An optimal design involves a thorough knowledge of the current state of the building, which is reached through historical investigation, surveys of the typological and geometrical characteristics, characterization of the materials and of the state of deterioration, as well as through experimental tests that provide objective information on the response of the building to impressed actions.

On the basis of the results of surveys and investigations, reliable numerical models can be implemented, through which it is possible to evaluate the response of structures to the design actions and assess the effectiveness of strengthening interventions.

In order to consolidate the practice to carry out a thorough investigation prior to work out the structural project, reliable and, at the same time, economic testing methods must be available, as described in HB1 and in other chapter of the present one, but it is also necessary that designers are aware of the potential and limitations of each method, in order to competently choose among the various possibilities offered by the market.

The methods of investigation based on the observation of the dynamic properties, although are very effective tools to know the overall behavior of a structure, constitute a field little used in current practice, sometime for the lack of knowledge on the subject, sometime for the small number of laboratories equipped to perform such tests, sometime for the cost which is often quite high, but in many cases the dynamic tests [1] represent an almost irreplaceable method in testing the structural response under dynamic actions.

In particular, the results of such tests, similarly to those of the static load tests, provide information about the stiffness of the structures, and allow to calibrate the numerical models in order to estimate the safety in terms of strength.

In the present chapter an example is presented concerning the static and dynamic assessment of a hanging water tank, built around 1960 and located in Pontedera (Italy).

The aim of the numerical and experimental studies carried out is to allow a refined check of the structural reliability of the structure also in view of planning of future maintenance and rehabilitation works, after 50 years of service.

These needs are more stringent considering that, since in recent years the frequent seismic events to which Italy is prone increased the awareness that prevention policy is the only way to limit damages from earthquakes, in the most recent Italian building Codes the extension of Country areas subject to seismic hazard increased considerably. At the same time particular attention has been devoted toward planning interventions aiming to improve the seismic resistance of existing buildings and infrastructures.

It must be stressed that the tank was built over fifty years ago in an area not classified seismic at the time, for which, on the occasion of interventions to counteract the degradation of materials, it is necessary to proceed even to seismic retrofitting.

In the study, particular attention has been devoted to planning and execution of a specific experimental campaign aiming to investigate the mechanical properties of the materials and to check the experimental dynamic response of the structure to horizontal actions. Among the outcomes of the investigations, particularly relevant was the dynamic identification, that allowed to define a structural model, refined enough, on which to perform structural verifications, also checking the effect of the implementing the seismic retrofitting measures.

2 DESCRIPTION OF THE STRUCTURE

The structure under investigation is a reinforced concrete hanging water tank, whose capacity is about 400 m³ (fig. 1).

The tank is supported by a set of eight inclined columns, arranged at the vertices of an octagon, along the radial axes.

The eight columns, which are connected by three reinforced concrete rings, lying in horizontal planes, and located at different heights, are crowned at the top by a ring of larger size, which is also the connection between the two parts, the central spherical cap and the peripheral truncated cone, that form the bottom of the tank.

The tank is cylindrical, with an average diameter of 9.00 m and a height of 7.50 m about; the total height of the structure from the ground level is more than 29 m (see fig. 2).

The documentation available at the beginning of experimental activities consisted of a schematic drawing in which they were shown the morphology of the structure and the overall dimensions. From these sketches it appeared that the foundation was made of a r.c. circular plate with a diameter of 11.00 m; while there was no indication of the depth of the foundation itself.

Therefore, first of all it was carried out a geometric survey, followed by reinforcement's survey and not destructive tests for the concrete's characterization, in such a way that, using the inferred parameters, it was possible to arrive to a finite element model of the structure, able to furnish more sound estimate of its static behaviour and its dynamic characteristics.

Through in situ measurements, it was very easy to determine the size of the vertical structure of support, columns and connecting rings, as well as the main dimensions of the tank.

Through the examination of the areas in which the concrete cover was damaged and using a *Covermeter*, it has been surveyed the arrangement and the diameter of the reinforcing bars.



Figure 1 The tank under study

The reinforcement of the columns was formed, for the whole height, by 8 plain bars, 18 mm diameter; the overlapping joints of rebars were located at mid-height between the rings, while the stirrups are 6 mm plain bars at about 20 cm spacing. In the connecting rings, it was possible to detect only the reinforcement of the lower face, which was consisted of 4 longitudinal bars $\text{Ø}18$ and 6 mm stirrups, spaced 22-24 cm (see fig. 3).

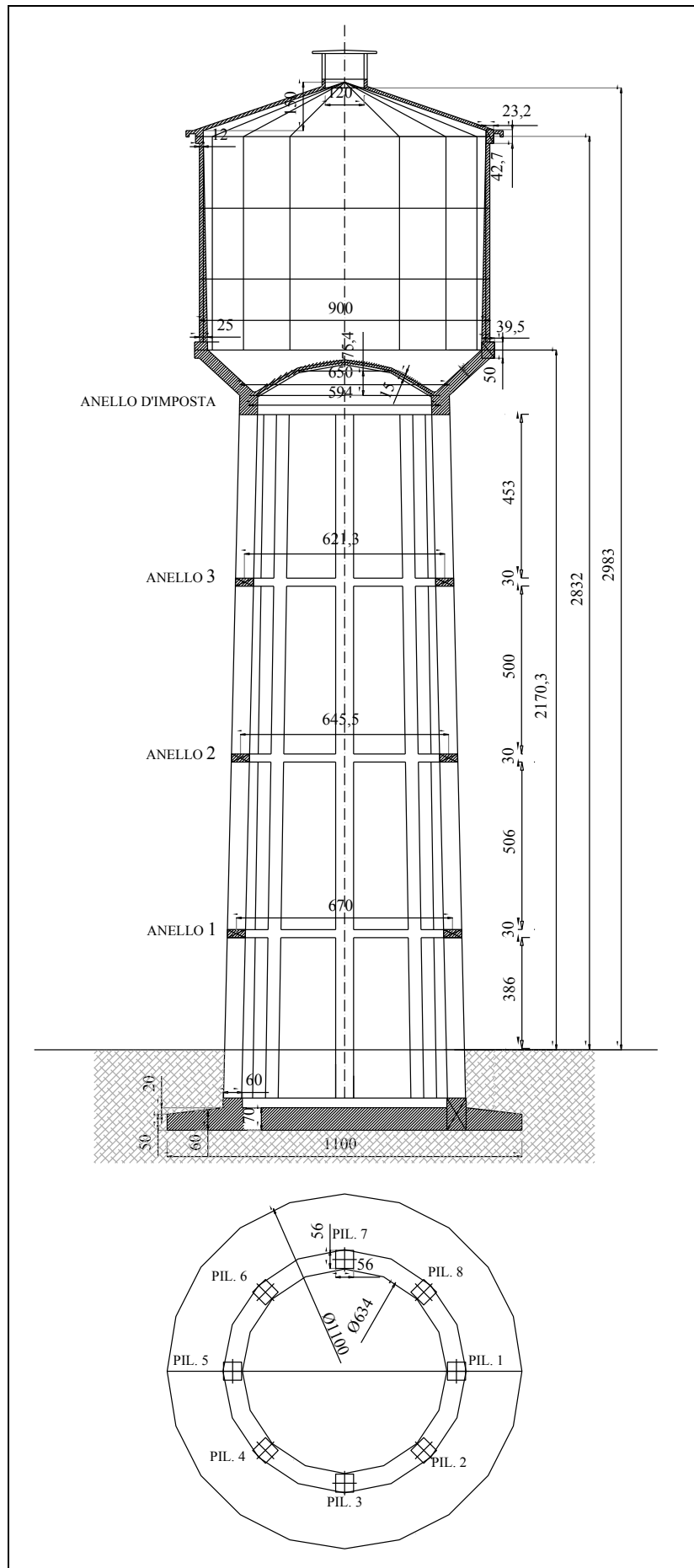


Figure 2 Sketch of the r.c. tank structure

The concrete is deteriorated in many parts of the outer surface, as a result of the expulsion of the concrete cover, caused by the corrosion of the outer reinforcing bars.

In order to estimate the mechanical characteristics of concrete, measures of the rebound index and of the ultrasonic velocity were performed.

The results of measurements were processed according to the method described in [2], giving an average value of the cubic strength of concrete approximately 60 N/mm^2 , with a confidence interval of $\pm 15 \text{ N/mm}^2$.

In addition, lots of experimental studies regarding static and dynamic tests, in two different conditions of full and empty tank were executed, as described in the following.

The results of these tests have permitted to refine the structure's model, obtaining in this way a better model to describe the actual situation, necessary to carry out safety tests and to start designing strengthening intervention.

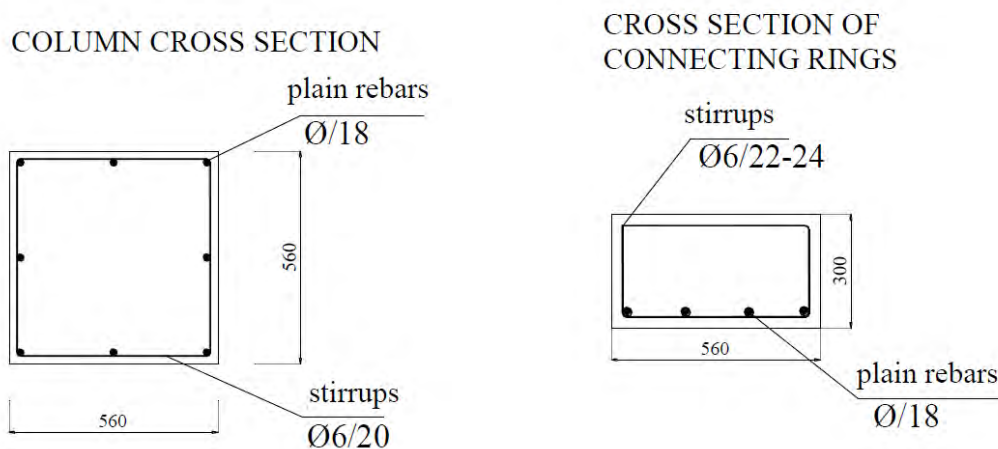


Figure 3 Details of structural elements

3 THE EXPERIMENTAL TEST CAMPAIGN

In order to determine the horizontal stiffness, the dynamic behaviour and in particular the natural frequencies and the mode shapes of the structure, an ad hoc experimental campaign was planned.

The four tests were performed considering two extreme tank filling conditions: empty tank (3 tests), without water inside, and full tank (one test), with the tank completely filled with water.

In both cases the test sequence consisted in applying increasing load to the structure by means of an inclined cable put under tension by a mobile crane (fig. 4), until occurrence of the brittle failure of a calibrated bar interposed in the cable (figs. 5, 6 and 7), in such a way that the sudden release of the cable tension induced the free vibration of the tank.

During the tests the loads was measured with a load cell (fig. 6).

The breaking loads of the calibrated bars measured in the four tests are reported in table

1.

Table 1 Breaking loads of the calibrated bars

<i>full tank</i>	<i>empty tank</i>		
test 1P	test 1V	test 2V	test 3V
85.27 kN	29.49 kN	61.31 kN	94.23 kN

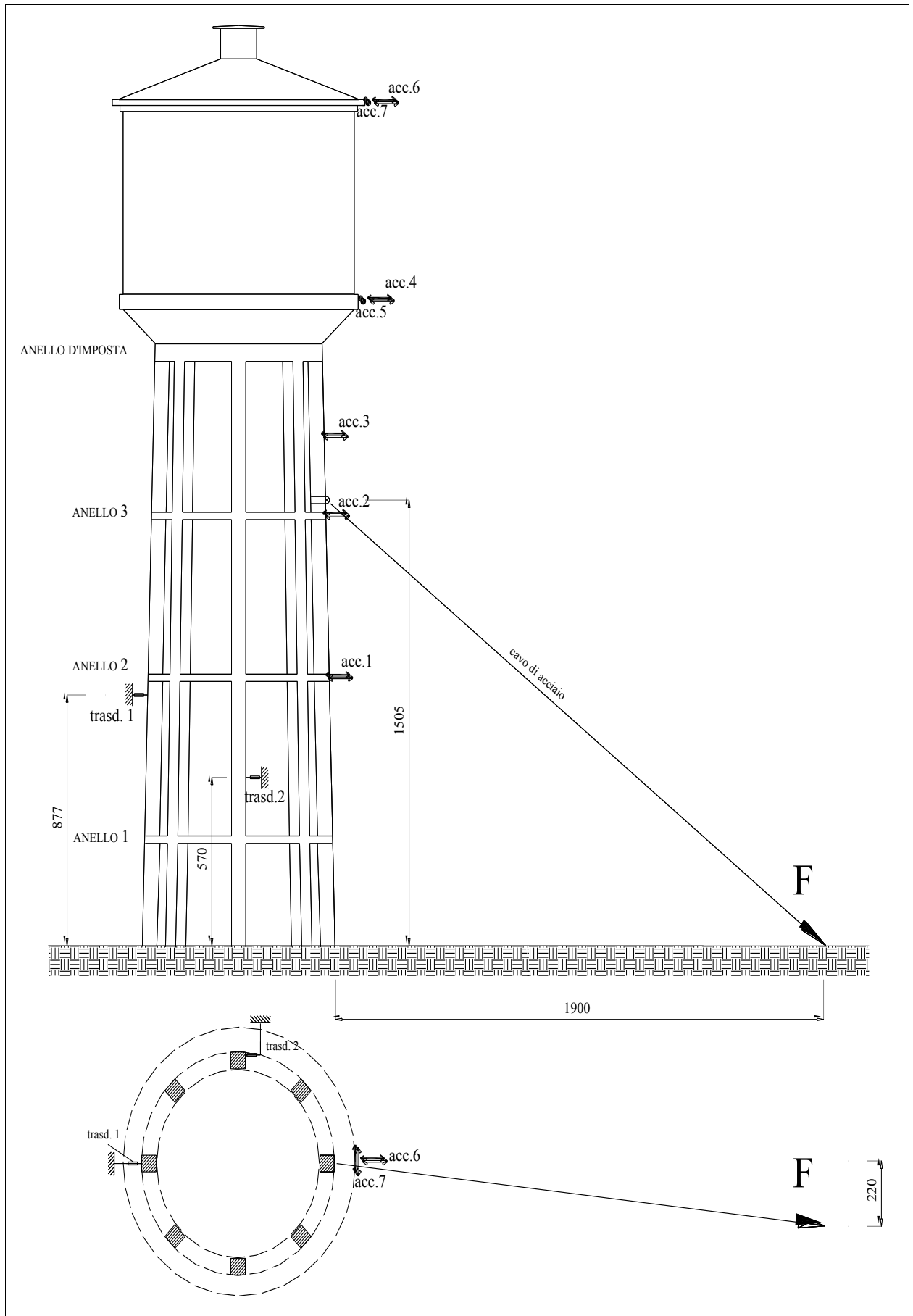


Figure 4 Sketch of the test



Figure 5 Cable attachment on the structure



Figure 6 Load cell and calibrated bar



Figure 7 Detail of the calibrated bar (before and after breaking)

The tank tower was equipped with displacement transducers and accelerometers allowing to record the corresponding time histories.

The force-displacement diagrams recorded during the tests showed a roughly linear progression (see an example in fig. 8).

The signals provided by the accelerometer placed in the direction of the force, in the four tests, were processed by Fourier analysis; in figures 9 and 10 are illustrated, by way of example, the results of the processing of the signals provided by the accelerometer 6 in the test with full tank and in the three tests with the empty tank, respectively.

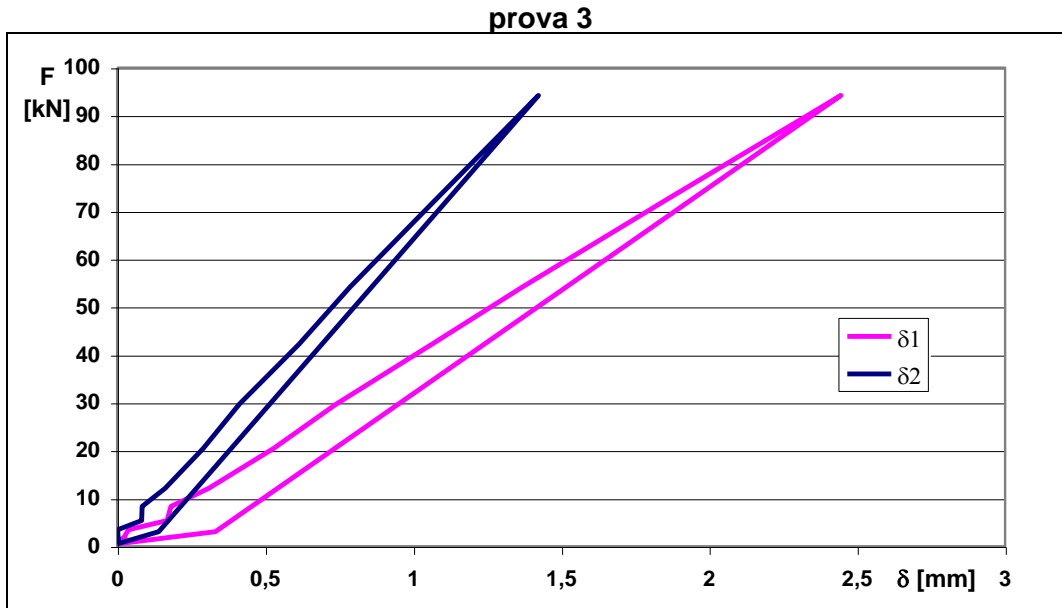


Figure 8 Force-displacement diagram - test 3V

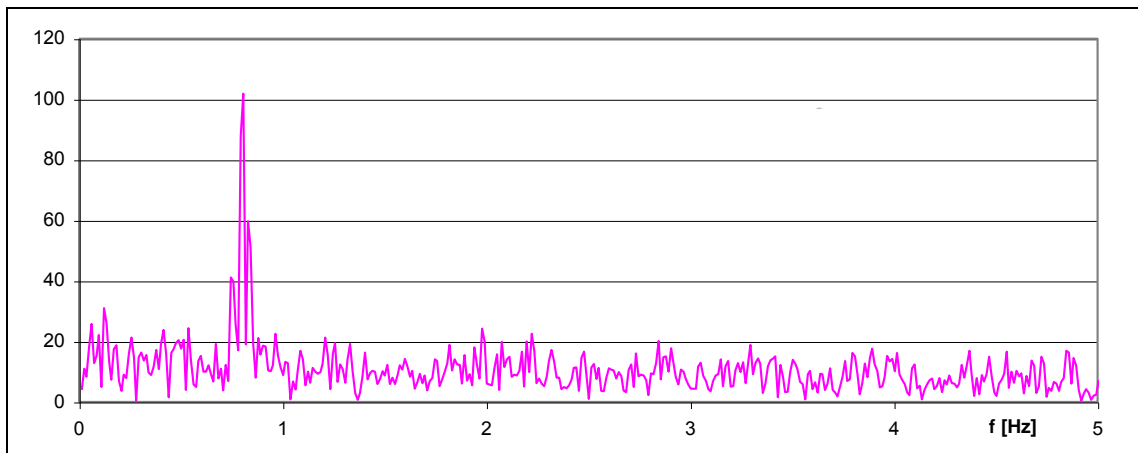


Figure 9 FFT diagrams obtained from accelerometer nr 6 in test 1 P (full tank)

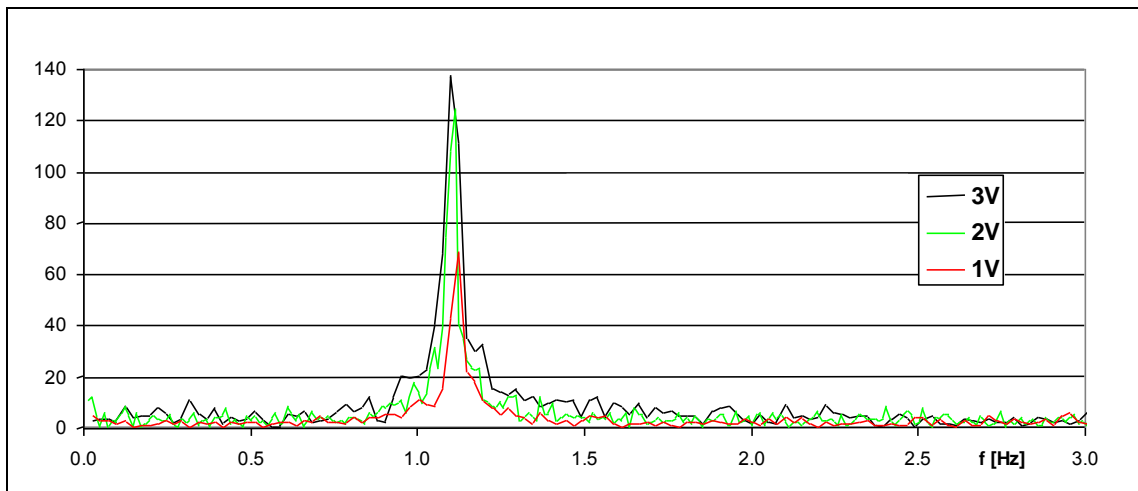


Figure 10 FFT diagrams obtained from accelerometer nr. 6 in test 1 V, 2 V and 3 V (empty tank)

It must be highlighted that in all tests, the accelerations in the direction orthogonal to the applied force resulted practically zero.

With the exception of the accelerometer nr. 1, which presented a signal in which the background noise was comparable with the recorded vibration amplitude, all the accelerometers gave similar results:

- in test 1P, the only carried out in the full tank condition, the maximum amplification was recorded at frequency 0.80 Hz;
- in tests 1V, 2V, 3V, made in empty tank condition, with initial amplitudes of the deformation gradually increasing, the maximum amplifications resulted very similar, at frequency of 1.11 Hz around;
- the ratios between maximum amplitudes provided by the five accelerometers resulted very similar.

These values of frequencies were assumed as the natural frequencies in the direction of initial displacement. In both situations, full and empty tank conditions, modal shapes were assumed proportional to the corresponding values of the FFT amplitude relative to the signals of the different accelerometers.

From the analysis of the signals of the instruments in the time domain, it was also possible to obtain, by applying the method of the logarithmic decrement, sufficiently approximate values of the damping coefficient ξ .

The results of the processing described above are reported in Table 2, where for each test are indicated, relatively to the first mode of vibration, the natural frequency f , the value of the damping coefficient ξ , the values of the modal coordinates in correspondence of the points of application of the instruments, related to the value corresponding to the instrument placed higher (accelerometer nr. 6).

Table 2 Characteristics of the vibrations detected by the tests

	f [Hz]	ξ [%]	$a2$	$a3$	$a4$	$a5$	$a6$
<i>test 1P</i>	0.80	5.5	---	0.92	1.10	0.97	1.00
<i>test 1V</i>	1.12	1.1	0.50	0.78	0.87	0.96	1.00
<i>test 2V</i>	1.11	1.1	0.52	0.81	0.91	0.99	1.00
<i>test 3V</i>	1.10	1.5	0.48	0.79	0.87	0.95	1.00

4 STRUCTURAL MODELLING

The modeling of the structure, using the finite element program SAP2000, was conducted in two successive phases: in a first phase, prior to testing, the values of the main variables that characterize the model have been set on the base of a priori knowledge, in order to roughly foresee the behavior under test loads; the second step, performed after the static and dynamic tests, was aimed at the calibration of the above variables in order to calibrate the numerical model, in order to reproduce at the best fit the actual static and dynamic behaviour of the structure under the test conditions.

On the model so identified it was then possible to perform the appropriate safety verifications.

In both phases, the analysis were performed considering:

- linear elastic constitutive laws for the structural materials;
- negligible second-order effects arising from geometric nonlinearity of the structure;
- stiffness of r.c. columns and rings in no crack condition;
- membrane and bending behaviour and no crack condition for the shell elements used to model cylindrical wall of tank, lower dome and tank cover modelled;
- foundation slab dimensions derived from the available design documents;
- Winkler spring model for the soil.

Of course, the mechanical and geometrical characteristics of the structure whose knowledge was uncertain, represented the parameters to be identified, namely:

- Young modulus of concrete;
- depth of the foundation slab with respect to the ground level;
- soil-structure constraint, that is the stiffness of the elastic springs between the foundation slab and the ground.

4.1 Actions modelling

The effects of the water inside the tank were evaluated with reference to static and dynamic loading conditions.

In dynamic conditions the action of water has been modeled taking into account the effects that the convective and the impulsive components of the motion of the liquid exert on the walls, and the influence that this phenomenon has on the natural frequencies of the whole structure [3], [4].

According to the above mentioned approach, the total mass of the water inside the tank has been divided into two parts: the impulsive mass and the convective mass. The impulsive mass of the water represents the fraction of the total mass that moves with synchronous motion with respect to the walls of the tank; the convective mass represents the remaining amount of water that moves independently from the tank walls.

The two masses can be modeled in a simplified way as concentrated masses, applied in two points, whose heights with respect to the bottom of the tank are suitably assigned.

The impulsive mass is considered rigidly connected to the walls of the tank, while the convective mass is considered connected by springs, with elastic constant assigned in function of the characteristics of the liquid and the size of the tank.

The values of the masses, of the heights to which place them, the stiffness of the springs, have been obtained as a function of the size of the tank through the formulas contained in Eurocode 8 Part 4 [5].

Assuming $R = 4.50$ m, the radius of the tank, and $H = 5.04$ m, the maximum height of fill within the container, it results

- $m_i = 244.000$ kg, the impulsive mass, placed at height $h_i = 3,30$ m from the tank bottom;
- $m_c = 135.000$ kg the convective mass, placed at height $h_c = 3,60$ m from the tank bottom.

The stiffness of the springs which constrain the convective mass to the wall was determined according to the expression

$$K_{c1} = \omega_{c1}^2 m_{c1} \quad (1)$$

Where ω_{c1} and m_{c1} are the frequency and participating mass of the water in the tank in the first oscillating mode - sloshing. In the present case, given the size of the tank and the maximum height of the water inside, the elastic constant may be obtained: $K_{c1} = 619$ kN/m.

The constraint was modeled by 16 springs, each with an elastic constant equal to 76.6 kN/m, arranged radially so as to connect the mass concentrated in the center with the lateral surface of the tank.

4.2 FEM model identification

As just said, the data obtained from static and dynamic tests have allowed to identify the most uncertain model parameters.

From the comparison between the results of modeling, obtained by varying the above parameters, with the experimental results, it is obtained the model that best approximates the behavior of the structure, both in terms of displacements under horizontal loads, both in terms of frequencies of the first mode of vibration in empty and full conditions.

In the identified model, the elastic modulus of the concrete was put equal to 58.000 N/mm² and columns were supposed clamped at a depth of -1.00 m from the ground level.

With such model, the static analysis was conducted for a horizontal load equal to the maximum value reached in the test 3V: the results, in terms of displacements of the points of application of the transducers are shown in Table 3 and put in comparison with the experimental results.

Table 3 Results of static load test

	F_x [kN]	δ_1 [mm]	δ_2 [mm]
<i>experimental</i>	73,09	2,44	1,42
<i>FEM</i>		2,52	1,47

The dynamic analysis was conducted under the conditions of empty and full tank. The results obtained, in terms of frequencies and amplitudes of the first mode of vibration at the points of application of the accelerometers, are shown in Table 4, and compared with the corresponding results obtained experimentally in tests 1P and 2V.

Table 4 Results of dynamic tests

		f [Hz]	$a1$	$a2$	$a3$	$a4$	$a6$
<i>full tank</i>	<i>experimental</i>	0.80	---	0.92	1.10	0.97	1.00
	<i>FEM</i>	0.83	0.50	0.83	0.95	1.01	1.00
<i>empty tank</i>	<i>experimental</i>	1.11	0.52	0.81	0.91	0.99	1.00
	<i>FEM</i>	1.12	0.52	0.85	0.93	1.01	1.00

Considering the small discrepancies between the experimental results and the theoretical ones and the results obtained for the parameters to be identified, which appear reasonable and, regarding the dynamic elastic modulus of the concrete, in good agreement with the excellent quality observed with the non-destructive testing.

Finally, the identified model was fit enough to evaluate the response of the structure, both static and dynamic.

4.3 Discussion about experimental and numerical values

The preliminary simplified numerical model was based on the geometry of the structure, as detected, adopting reasonable a priori values for uncertain parameters:

- elastic modulus of concrete $E = 30.000$ N/mm²;
- depth of foundation slab above the ground level = - 2,0 m;
- Winkler modulus for the soil foundation $k = 2$ daN/cm³.

On the base of experimental tests, the values of these parameters were refined as:

- elastic modulus of concrete $E = 58.000 \text{ N/mm}^2$;
- depth of foundation slab above the ground level = - 1,0 m;
- Winkler modulus for the soil foundation $k = \infty$.

In order to estimate the influence of different modeling on the evaluation of the stresses in the structural elements, we proceeded to a comparison of stresses in the most severe load condition for the columns and the connecting rings.

Table 5 shows the values of maximum stresses for the pillars and the rings, which are obtained from the dynamic analysis, in the seismic condition in full tank condition.

Table 5 Comparison of stress values obtained from the two models

	FEM element number	Position	Calibrated model			Preliminar model		
			N [kN]	M13 [kNm]	T13 [kN]	N [kN]	M13 [kNm]	T13 [kN]
Full tank - Seismic analysis	1	Base of column nr. 1	-434	185,7	26,7	-585,5	90,6	25,6
			-1326	-183,1	-27,8	-1180,7	-158,4	-10,9
	4	Top of column nr. 1	-525	67,5	39,4	-579,6	73,9	7,8
			-948	-176,2	-26,7	-874	-126,3	-18,9
	17	Base of column nr. 5	-430,8	185,7	27,4	-581,2	90,5	25,7
			-1329	-184,5	-27,6	-1176	-158,5	-10,9
	20	Top of column nr. 5	-502	123,7	14,2	-575	74,3	7,9
			-954	-174,12	-25,4	-869	-125,9	-19,9
	34	Ring nr. 1	-5,47	-100,6	-71,8	-5,9	-57,7	-50,5
47	Ring nr. 2	-0,7	-130,6	-107,8	3,94	-98	-82	
55	Ring nr. 3	-10,5	-109,2	-64,2	-11,9	-84,7	-74	

In the table the column "a priori model" shows the values of the internal forces obtained from the analysis of the preliminary model, calibrated on the geometry of the structure and the assumptions above about materials and constraints; the column "calibrated model" shows the internal forces obtained using the values derived from the experiments.

The final model is much more stiff than the preliminary one, due to the higher value of the elastic modulus of the concrete detected with non-destructive tests, and to the very high Winkler modulus of the soil under the columns, emerging from the results of dynamic tests, probably due to some kind of soil consolidation during the years.

As a consequence of the greater stiffness of the model is observed that, in general, the bending moments which engage the elements of the identified model are greater than the corresponding values obtained by the preliminary model. Then carrying out the verification of the same sections with reference to various stresses obtained, were found significant differences in the degree of stress of the materials, so as to show the same sections verified for the stresses of the preliminary model and not verified for the stresses obtained from the identified model.

5 CONCLUSIONS

In the framework of the assessment of the static and seismic behavior of a r.c. hanging tank, an experimental campaign has been performed consisting in

- non-destructive examination of the members. aiming to qualify the structural materials and the assessment of their state of deterioration;
- static and dynamic load tests for the dynamic identification of the structural behavior
- calibration of a FE model, using the output of dynamic identification analysis;
- structural assessment according the current structural code in seismic areas in Italy.

The investigations, in particular the static and dynamic tests, were performed using instruments of current use, at acceptable costs and time, so allowing to obtain relevant information about the characteristics of materials and the behavior of the structure.

The structural model identified, in fact, made it possible to assess in a more reliable way the level of safety of the structure also in view to predict the effects of the retrofitting interventions.

In particular, the experimental results obtained can be used, together with the results of similar tests, to assess the strengthened structure and subsequently, during the time, as a tool permanent monitoring of the static conditions of the structure.

REFERENCES

- [1] Ewins, D.J., "Modal testing: Theory and practice", John Wiley & Son, New York, 1984.
- [2] Beconcini M.L., Formichi P., "Resistenza del calcestruzzo, misure sclerometriche e di velocità di propagazione degli ultrasuoni in strutture esistenti: risultati di una campagna di indagini", 10° Congr. Naz. AIPnD, Ravenna, 2003.
- [3] Housner G. W., "Dynamic pressures on accelerated fluid containers", BSSA, vol. 47, 1957.
- [4] Davidovici V., Haddadi A., "Calcul pratique de réservoirs en zone sismique", A.I.T.B.T.P., n. 409, 1982.
- [5] EN 1998-4: Eurocode 8: Earthquake resistant design of structures, Part 4: Tanks, Silos and Pipelines, 2005.

CHAPTER 9: AQUEDUCTS – A CASE STUDY

Pietro Croce¹, Maria Luisa Beconcini¹, Martina Muzzi¹, Elisa Rosso¹, Francesca Marsili¹

¹Department of Civil and Industrial Engineering – Structural Division – Univ. of Pisa, Italy

Summary

The Medicean Aqueduct of Pisa (Tuscany, Italy), is a relevant historical infrastructure built at the end of the XVI century, composed of 954 masonry arches over a total length of 6 km. Many of the arches are affected with several decay phenomena, which occurred during the years. These have changed the original static arrangement, so that several arches are collapsed or degraded.

In view of the conservation of this relevant infrastructure, in the present study the procedure provided by the ISO 13822 for the assessment of existing masonry structures is applied; such procedure is a useful tool for the survey of the current state of the building and the resistance of the materials. In particular the present case study shows the importance of the careful observation of the deterioration phenomena for the comprehension of the causes and the possible evolution of the damage mechanisms.

1 INTRODUCTION

The masonry is one of the oldest building materials, so there are many examples of masonry buildings and infrastructures belonging to the artistic and cultural European heritage.

In view of the preservation of their historical, artistic, social and economic values, the assessment of existing masonry structures is an important engineering task in our era, which requires the application of sophisticated analysis methods, based on national building codes and on International Standards, such as ISO 2394, ISO 13822 and ISO 12491, recently developed. In particular, the ISO 13822 provides an useful procedure for the evaluation of existing structures, indicating a method to inquire into the current state of the case study and the resistance of its materials.

The ISO 13822 explains why current standards for structural design are not sufficient for the reliability assessment of existing structures and for the design of their repairs or upgrading. As the ISO 13822 flow chart illustrates, this procedure is characterized by the appraisal of the structures actual reliability, which is reached through a preliminary assessment and, when necessary, by a detailed assessment.

The aim of this research, that has especially been developed in the framework of Leonardo da Vinci Project, is to demonstrate the practical application of the ISO 13822 for the assessment of a relevant historical infrastructure: the Medicean Aqueduct of Pisa (Tuscany, Italy), an arched masonry structure, built at the end of the XVI century.



Figure 1 Panoramic view of the Medicean Aqueduct

The Medicean Aqueduct of Pisa is a case study suitable for the purpose, because many of the arches are affected with several decay phenomena, which occurred during the years, due to ordinary and extraordinary causes. These have changed the original static arrangement, so that several arches are collapsed or degraded.

The goal of this study is to understand how these causes induced the alteration of the original static model. Since the masonry behaves according to a set of specific macro-elements, namely of rigid-bodies, the structural analysis mainly concerns the identification of these macro-elements and the related failure mechanisms activated by specific actions, such as the settlement of foundation or earthquakes.

The structure has been studied with various types of analysis. Since the various aspects of the structural behaviour are captured by different methods, comprehensive answers are obtained only through a combined approach.

The study is organized in accordance with a step-by-step procedure, such as the flow chart of the ISO 13822 (Chapter 6, figure 1) suggests: in the first step the preliminary assessment was performed, considering the available documentation and results from inspection and check; the following step concerns a more detailed appraisal, in which the structural analysis is carried out.

2 PRELIMINARY ASSESSMENT

The purpose of the Preliminary Assessment is a first evaluation of the structural condition using simple methods, such as:

- study of the available documentation;
- preliminary inspection;
- preliminary checks;
- decision on immediate actions;
- recommendations for detailed assessment.

In some case, the outcomes of this first stage could be sufficient to describe by themselves the state of the building and even to arrive to make a diagnosis of the actual damage, but in other cases the conclusion will ask for additional studies and investigations, in order to achieve a more precise and reliable knowledge. Obviously, severe and/or evident crack patterns generally requires deeper investigations.

2.1 Study of available documentation. A brief history

Due to the relevance of this construction, an extensive and important documentation has been found, not only in the State archive in Pisa, but also in the extensive literature about it. Nevertheless, it was also possible to collect some additional interesting information through a local no-profit association '*Salviamo l'Acquedotto Mediceo*' (*Save the Medicean Aqueduct*), specifically devoted to the preservation of the Medicean Aqueduct.

The study of the aforementioned documentation and the comparison of pictures and maps associated to different periods, allowed to deduce the evolution of the Aqueduct during its life, recreating its historical and architectural evolution.

The Medicean Aqueduct is an infrastructure built in 1613 by the Granduke of Tuscany Ferdinando I de' Medici, in order to convey fresh and clean water from Asciano, a small village in the neighbouring of Pisa, to the centre of the town.

This work is constituted by an elevated pipeline, sustained by 954 masonry arches, such as the Roman aqueducts, carrying the water by gravity, and covers a total length of 6 km.

The construction of the aqueduct was framed in a plan of actions originally developed by the Granduke Cosimo I de' Medici - Granduke of Tuscany from 1519 to 1571 - to improve the

hygienic conditions in the town of Pisa. This plan was mainly focused on an hydraulic reorganization of the territory, aimed to guarantee the development and maintenance of strategic communication networks and to recover wetlands, so as to turn them into florid agricultural lands. Further on, this plan allowed the urban renovation of the town by the construction of the Cavalieri Palace and the Medicean Arsenal.

In the original conception, the Medicean Aqueduct was intended to carry water by gravity through an underground pipeline connecting the Spring Valley, near Asciano, to the Pisa town centre, but the difficulties encountered during the excavation as well as the conspicuous water infiltrations, soon persuaded to abandon this design scheme in favour of a more reliable and safe Roman Aqueduct scheme, consisting in an elevated pipeline running on the straight extrados of masonry arches.

The semi-circular masonry arches, spanning generally about 5 meters, are in brick masonry and are sustained by pillars, whose height decreases from the spring to the town.



Figure 2 View of the Medicean Aqueduct, in 1600, during the erection



Figure 3 Historical picture of the Aqueduct

Except the semi-circular arches, the other parts of the structure were built using mixed masonry composed by layers of cut stones intercalated, to regularize the structure, by thin layers of bricks. Finally, to stabilize the construction, transversal buttresses were built every eleven arches.

The water transfer system was composed of three different works: the water collecting and filtering system with the big cistern, the elevated pipeline and the urban distribution networks.

The springing water, duly purified and filtered, was transferred in a big cistern, “*Il cisternone*”, (fig. 4) where it became cleaner since the sediments could deposit. Finally water reached a cabin, from where it was conveyed in the pipeline.



Figure 4 “*Il Cisternone*”, a big cistern for collecting water, in Asciano

The aqueduct, composed by the arches carrying the elevated pipeline, was realized in two different phases: the first one from 1588 to 1594 and the last one from 1610 to 1613. In the first step, the aqueduct was quite completed, so that in 1595 it began to work. During this phase, in the upstream section near to Asciano, several pillars foundations were realized with a system of wooden piles, according to the Vitruvian scheme, due to the swampy ground and the layout of the aqueduct. Finally, in the last section of the aqueduct, the urban distribution network of the water was composed by an underground pipe that conveyed water to the fountains, some of which still in use.

During its construction, the aqueduct began to lean, as a result of the upstream marshland and of design errors, probably in consequence of the undersizing of the foundations, so that already in 1610, few years after its completion, the first rehabilitation works were necessary. Moreover, water was stagnating in the conduit and could not get to Pisa. As a consequence, the upper part of the pipeline was rebuilt in “cotto” and covered with sheets of stone.

Today, the elevated pipe is disused, because of the advanced state of decay: the collapse of several arches and the impending failure of some others.

From upstream to downstream, there is a difference in height of 5.2 meters. The maximum altitude of the pipeline is 7 m above the ground, the total span of each arch is 7 m, the clear span is 5.3 m, and the thickness is 1.2 m about. The dimensions of most of the arches are similar, due to the use of a single timber temporary structure during the construction.

The aqueduct course changes direction in several points (fig. 5.a). Probably the changes in direction aimed also to realize some kind of expansion joints between the various sections of the aqueduct itself, so as to reduce temperature effects. The arches have an *original numbering*, in ascending order from the town centre to upstream, reported in a suitable sign (see, for example, fig. 5.b).

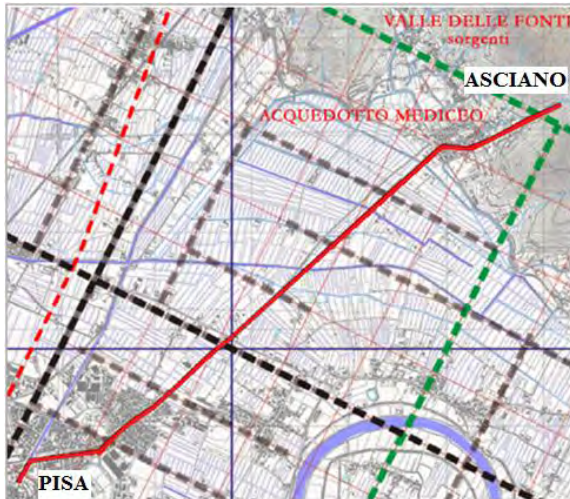


Figure 5.a Aqueduct's layout

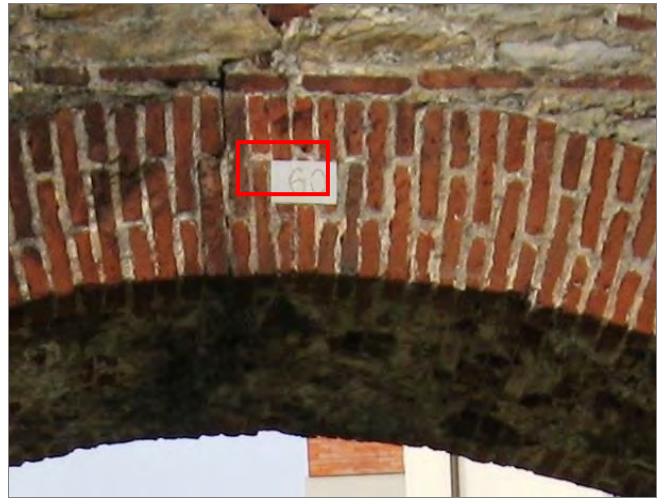


Figure 5.b Original arch sign of the arch nr. 60

The conduit is no longer been used since World War II; a pressurized pipeline has been built underground, following the path of the arches, that allows water to reach the ancient fountains in the city centre (see figs. 6, 7).

2.2 Preliminary inspection

It is useful to analyse separately the phenomena concerned to each structural element, namely:

- the clay pipeline;



Figures 6, 7 Original fountains in Pisa centre: Piazza delle Gondole and Piazza dell'Arcivescovado

- the arches;
- the pillars;
- the buttresses;
- the bases and foundations.

As said, the clay pipeline (fig. 8), with a semi-elliptical section, runs over the arches, covered by a sheet of stone (fig. 9) with protecting function. Nowadays, in the most degraded sections, the sheets of stone are no more in place.



Figure 8 Arch nr. 58, where the core structure and the clay pipeline are visible



Figure 9 The sheet of stone that covers pipeline

As noted, the arches are mainly semi-circular (fig. 10), but in the vicinity of the centre of the town, there are some elliptical arches (fig. 11). There are also some splayed arches (fig. 12): probably this anomaly is an attempt to adjust the arch to the path of the river channels that centuries ago flowed under the aqueduct.

The arches are constituted by brick masonry, 0.45 m thick; the core of the wall is made of stones of irregular shape and size; only some rows of bricks extend throughout the depth of the wall, with regularizing and containing function.

The pillars are of different types, both in size and materials (figs. 13, 14 and 15): stone masonry, mixed masonry, brick masonry, etc. The pillars have a rectangular section, usually 1.8 m long and 1.2 m thick. The pillars of the upstream part of the aqueduct, which support the highest arches, have a larger base, in order to distribute the greater weight on a wider area.



Figure 10 Semi-circular arch (arch nr. 98)



Figure 11 Elliptical arch (nr. 28)



Figure 12 Splayed arch(nr. 29)



Figure 13 Pillar between arches nr.131 and nr. 132



Figure 14 Pillar between arches nr.837 and 838



Figure 15 Pillar between arches nr. 815 and nr.816

The buttresses, which were originally inserted every 11 arches, on both sides of the pillar, in order to contrast the out of plane overturning, differ in size and materials: those located upstream are made of bricks, while the others are made of stones, with the same wall texture of the pillars (figures 16 and 17). The buttresses have a height slightly lower than the pillars, variable according to the corresponding arch; the sloping is about 15 degrees.



Figure 16 Buttress between arches nr. 89-90



Figure 17 Buttress between arches nr. 199-200

The foundation soil of the aqueduct has very poor characteristics, similarly to other sites in and around Pisa. The first information about the foundations have been derived from the

existing literature. Upstream the soil is marshy, so that pile foundations were employed, made of pine logs.

According to the practice of construction, typical of that area and time, we assumed that timber piles have variable length from 6 to 10 m (fig. 18). Approaching the centre of the town, the soil becomes more resistant, therefore the pillars have no pile foundation but a large base which gradually becomes wider (figures 19 and 20).

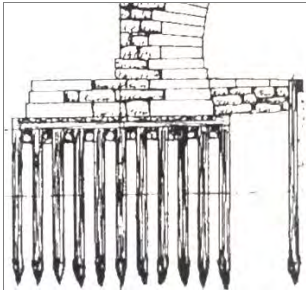


Figure 18 Example of foundation piles, according to the precepts of Vitruvius



Figure 19 Large base under the pillar, between arches nr. 502-503



Figure 20 Base under the pillar, between arches n°410-411

2.3 Preliminary checks

In this phase a visual inspection of the structure has been conducted, in order to judge its current condition; special attention has been paid to the critical parts.

Over the years, the aqueduct has been subjected to several modifications due to planning mistakes, changes in water demand and difficulties in the maintenance operations. In particular, some earthquakes caused the collapse of some arches: some of these were rebuilt according to a layout different from the original one; others were shored up to avoid their collapse; in some cases, buttresses were built or rebuilt to reinforce the arcade. Obviously, all these changes had the effect of modify the structural setting of the aqueduct.

Nowadays, the observation of the work shows that it is in very critical condition: some arches are collapsed (fig. 21), other are damaged by vehicles impacts (fig. 22); many of them present various decay phenomena: the most evident are cross cracks and organic patinas, such as moisture stains or efflorescence. Over the years some elements, more probably those made almost exclusively in bricks, have been completely or partially rebuilt (figs. 23, 24).



Figure 21 Arch nr. 99, collapsed



Figure 22 Arch n°162, damaged by vehicles impact



Figure 23 Arch nr. 49, rebuilt in bricks



Figure 24 Pillar of arch nr. 130, rebuilt in bricks

The most degraded arches are in the upstream portion of the aqueduct: many of them have been filled with mixed masonry (fig. 25), often different in quality from the original one. The arches that showed an imminent crisis have been provisionally supported by steel or timber scaffoldings (figs. 26, 27 and 28) in the last 30 years.



Figure 25 Some of the stopped up arches, from nr. 685 to nr. 694



Figure 26 Arches nr. 394 and 395, provisionally supported



Figure 27 Arch nr. 870



Figure 28 Arch nr. 890

2.4 Decision on immediate actions and recommendations for detailed assessment

By the preliminary inspection it has been possible to observe that there are types of cracks located in a recurrent way in specific elements, the formation of which can be attributed to the activation of typical arch mechanisms.

In addition, it must be noted that, during the years, poor maintenance was made over the Aqueduct, so that some arches collapsed, while, in other cases, the interventions were mainly devoted to temporarily tackle the most dangerous situations.

Conclusions of the Preliminary Assessment can be summarized as follows:

- the decay occurs with total or partial collapses of arch and with various types of cracks;
- the cracks are probably related to progress of the failure mechanisms;
- several arches in the town centre are unsafe or collapsed, because of vehicle impacts;
- the most damaged arches are those located in the upstream part, which have an evident out of plane inclination;
- the main cause of deterioration is probably the settlement of foundations.

These preliminary results indicate that, for the most critical parts of the structure of the Medicean Aqueduct so identified, further and more detailed inspections are necessary to investigate the real causes of the main decay phenomena, in particular cracks and out of plane rotation of the structure.

Beside the actual damage survey, the evaluation of the original static model of the structure, the knowledge of the actions as well as the evaluation of material properties are key activities to understand the structural behaviour and to arrive to diagnose the actual failure mechanisms and/or crack patterns.

3 DETAILED ASSESSMENT

The detection of the phenomena that led to the damages and the identification of the main causes of observed faults and defects is the first essential step for each safety assessment and for any decision to be taken on possible consolidation of the structure.

Causes of the most relevant degradation phenomena that can be observed in masonry structures can be different, i.e.:

- a) degradation due to the passing of time: deterioration of the material due to endogenous effects (ageing mortar, with progressive decrease in binding capacity; moisture action; plants overgrown) or to exogenous ones (traffic induced vibrations);
- b) the masonry expansion and contraction due to temperature and moisture variation;
- c) the freeze-thaw cycles on the porous walls, which involve swelling and cracking of the masonry; the degradation due to the acid rain; the air pollution effects; the presence of water in the soil which can seep into underground masonry and which can be captured by walls through capillary action;
- d) subsidence, landslide and viscosity, caused by the different soil nature, that involved settlements of foundation;
- e) action of accidental natural forces, such as earthquakes and flooding or by vehicle impacts;
- f) alteration of the original structural scheme through human interventions, such as the insertion of some brick buttresses, the injection of cement mortar inside some cracks, demolition of some arches to help the transit of vehicles on the roads.

Table 1 Typical causes of the most relevant decay phenomena in masonry structures

Variable and environmental actions:	Accidental actions:
a Age dependent effects	e Earthquakes and floods
b Thermal and hygrometric variations	
c Freeze-thaw cycles and atmospheric agents	f Human actions (alteration, impacts, etc.)
d Ground motions	

To better address the subsequent investigations, it is useful to recall that the masonry arch is conceived in such a way to be mainly subject to compression: this is obtained when the arch shape (the arch axis) follows the line of thrust (“*the antifunicular of permanent loads*”).

Over the centuries, many theories have been developed about the typical failure mechanisms of the arch under vertical loads; among them, particularly relevant are: the theory due to De La Hire and Belidor, that considers the sliding of the central part of the arch, and the one due to Mascheroni, which considers the flexural failure mechanism.

In the De La Hire and Belidor’s arch sliding mechanism (fig. 29), the central part of the arch is considered to behave like a wedge, sliding between smooth frictionless surfaces. In the model, the failure occurs when the central body slides down, while the pillars rotate outwards.

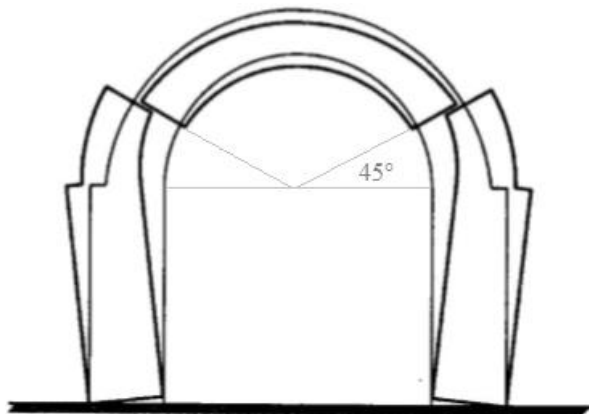


Figure 29 De La Hire and Belidor’s sliding mechanism of the arch

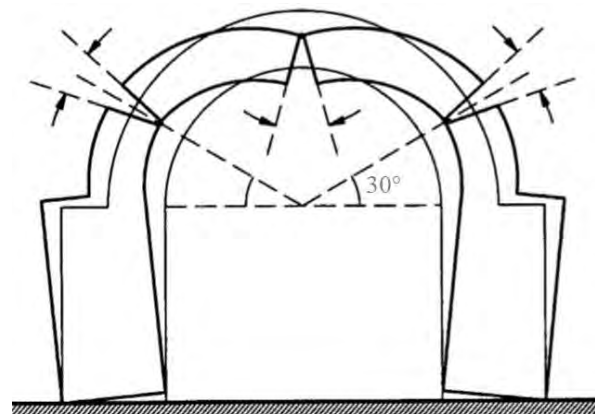


Figure 30 Mascheroni’s flexural failure mechanism of the arch

In Mascheroni’s flexural failure mechanism (fig. 30), the collapse occurs due to the formation of hinges, one at the crown on the extrados and two at the haunches on the intrados, and the rigid rotation of the pillars.

3.1 Detailed documentary search and review of accidental actions

Over the years the aqueduct has been subjected to some accidental events, which altered its structural behaviour.

Probably, the most relevant documented events are two important earthquakes that occurred in the area, probably affecting the stability of the arches. The first one occurred in 1846 with epicenter in Orciano Pisano (fig. 31), of Magnitude 5.6; the second one in 1920, epicenter in Garfagnana (fig. 32), of Magnitude 6.5.



Figure 31 Earthquake with epicenter in Orciano Pisano (5.6 M)



Figure 32 Earthquake with epicenter in Garfagnana (6.5 M)

3.2 Detailed inspection

A careful judgment of the structural condition can be made through specific inspections. Typically, also in ISO 13822, the assessment is a cyclic process. In order to gain a better knowledge of the actual structural condition (particularly in case of damaged structures) and to verify information required for determination of the characteristics and representative values of all basic variables, the first inspection must be often supplemented by subsequent investigation.

The investigation procedure aims to identify:

- the actual state of the structure as well as the crack pattern;
- types, characteristics and mechanical properties of structural materials and soils;
- actions acting on the structure, including environmental effects and accidental actions.

3.2.1 Deteriorations and cracks classification

As seen during the preliminary inspection, the Medicean Aqueduct is subjected to damage that can manifest as deterioration, crack patterns and even partial collapse of arches, depending on the severity of the causes. The careful recording of the decay phenomena during the *in situ* investigations, is the basis for a precise diagnosis of deterioration causes. Therefore, the main deterioration phenomena have been classified, according to the type and the position (see table 2).

Cracks located in the mortar joints are the outcome of tensile stress patterns in masonry elements. Those which are extended on the whole depth of the wall section are identified as *cross cracks*, the others are identified as *not cross cracks*. In addition, both can be further classified according to their position on the masonry wall.

Cross cracks (class A) may be located in the voussoir of the arch, typically at the crown (A2) or at the haunches (A1), and are linked with the opening of hinges, following the Mascheroni's classical failure mode. Other *cross cracks* can be located in the backfill of the arch, following horizontal (A3) or vertical paths (A4); in other cases, they are associated with a

relative displacement in the mortar joint plane (class G). *Not cross cracks* (class B) are often not visible on the intrados; they are classified in analogy to those of class A, with reference to the position and the direction (B1-B2-B3-B4). It is quite frequent to observe the detachment of the arch from the backfill (class E) and/or deterioration phenomena of some masonry elements (class F). Other types of damage are caused by settlement of foundations (class C), which occur with out of plane rotation (C1) or with vertical displacement of the pillar and horizontal cracks in the backfill of the arch (C2). Sometimes, the simultaneous presence of cross cracks and settlement can cause the displacement of a voussoir along the mortar joint (class G). During the years, the concurrence of several cracks in the same arch could activate failure mechanisms (class D), involving the partial collapse of the arch elements -arch crown, masonry backfill, buttress- (D1), or even the collapse of the whole arch (D2).

The considered classes, listed in tab.2, are illustrated by representative pictures in figs. 33 to 39.

Table 2 Types of deterioration

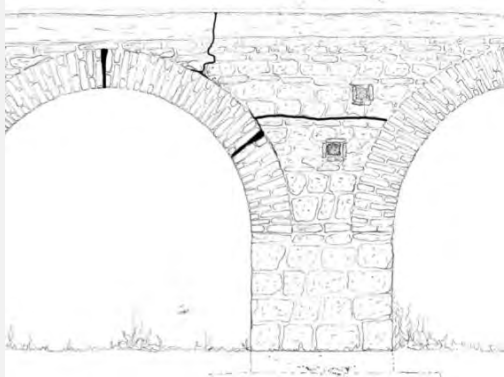
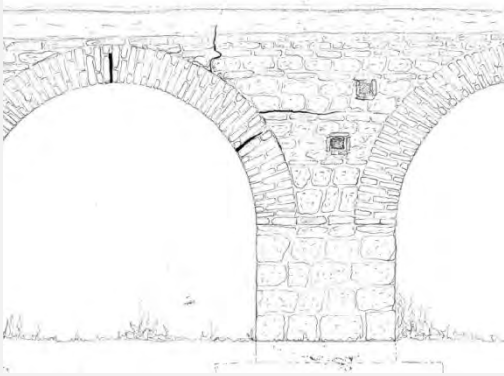
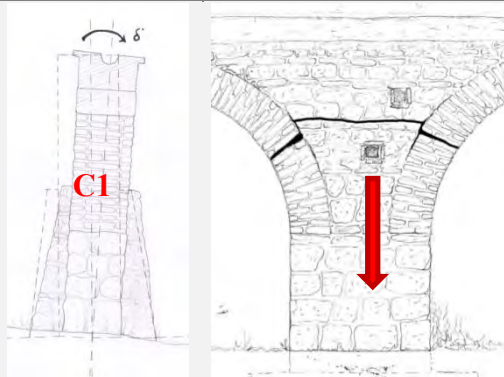
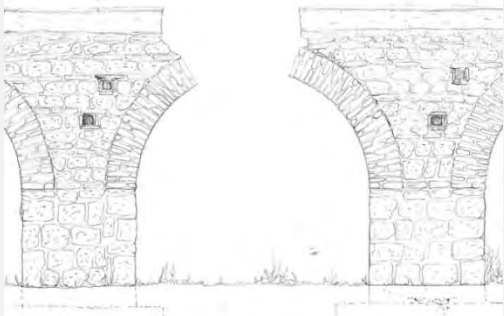
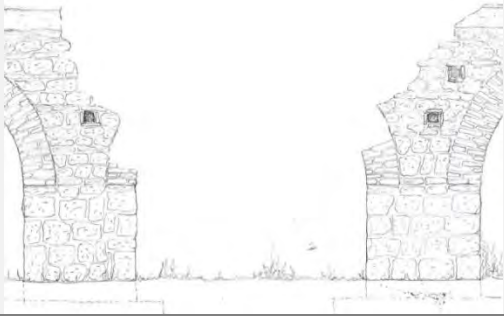
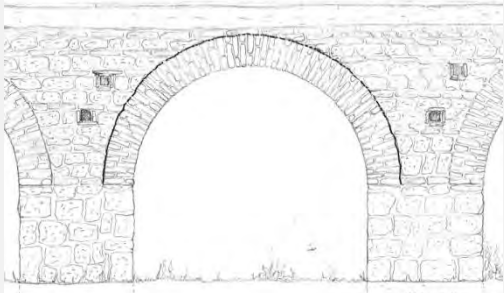
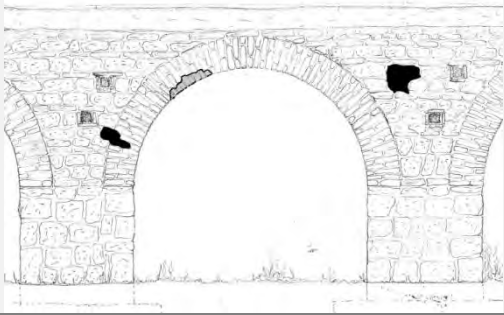
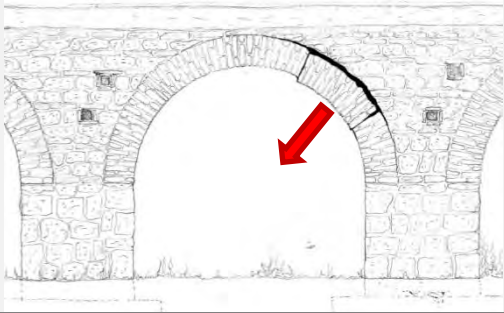
CLASS	GRAPHIC SCHEMES	DESCRIPTION	TAG
(A) CROSS CRACKS		Cracks at the haunch, visible on the arch's bricks and extended through the whole depth	A1
		Cracks at the crown, visible on the arch's bricks and extended through the whole depth	A2
		Horizontal cracks visible on the masonry wall (backfill) and extended through the whole depth	A3
		Vertical or oblique cracks, visible on the masonry wall (backfill) and extended through the whole depth	A4
(B) NOT CROSS CRACKS		Cracks on the voussoir, visible on the arch's bricks but not extended through the whole depth	B1
		Cracks at the crown, visible on the arch's bricks but not extended through the whole depth	B2
		Horizontal cracks, visible on the masonry wall (backfill) but not extended through the whole depth	B3
		Vertical or oblique cracks, visible on the masonry wall (backfill) but not extended through the whole depth	B4
(C) SETTLEMENTS		Settlement of foundation that involves an out of plane rotation of the pillar's foot	C1
		Vertical settlement of foundation	C2

Table 2 Types of deterioration (continuation)

(D) COLLAPSE		Partial collapse of arch elements (arch, masonry backfill or buttress)	D1
		Total collapse of an arch.	D2
(E) DETACHMENT		Detachment between the arch and the masonry backfill.	E
(F) DETERIORATION		Deterioration of masonry elements.	F
(G) RELATIVE DISPLACEMENT		Relative displacement along the mortar joint plane.	G

A1: crack in the haunch, visible on the arch's bricks and extended through the whole depth



Arch n. 21 – Side A

Extrados crack detail and intrados crack detail



A2: crack in the crown, visible on the arch's bricks and extended through the whole depth



Arch n. 62 – Side A

Extrados crack detail and intrados crack detail



A3: horizontal crack in the masonry wall (backfill)



Arches n. 8, 9 – Side A

Horizontal crack in the backfill

A4: vertical crack in the masonry wall (backfill)



Arch n. 145 – Side B

Vertical cracks in the backfill and in the arch crown

Figure 33 Examples of cross cracks

B1: crack visible on the arch's bricks, placed in the haunch



Arch n. 251 – Side B

Intrados crack detail

B2: crack in the crown, visible on the arch's bricks



Arch n. 211 – Side B

Intrados crack detail

B3: horizontal crack, visible on the masonry wall



Arch n. 17 – Side A

Horizontal crack on the backfill, close to buttress

B4: oblique crack, visible on the masonry wall



Arches n. 101, 102 – Side A

Oblique crack on the backfill and pillar

Figure 34 Examples of not cross cracks

C1: settlement of foundation that involves the out of plane rotation of the pillar



Arch n. 144 – Section
Out of plane rotation (9°) of a pillar between buttresses

C2: vertical settlement of foundation



Arch n. 16, 17 – Side A
Vertical settlement appearing by a crack in the backfill, extended to arch's brick

Figure 35 Examples of settlements of foundations

D1: partial collapse of arch/masonry wall (backfill)



Arch n. 395 – Side A
Partial collapse of arch

D2: total collapse of arch



Arch n. 100 – Side B
Total collapse of the arch

Figure 36 Examples of collapses

E: detachment between the arch and the masonry wall



Arch n. 113 – Side B
Detachment between the arch's bricks and the backfill.



Arch n. 137 – Side A
Detachment of some brick elements from the arch

Figure 37 Examples of detachments

F: deterioration of some masonry elements



Arch n. 163 – Side A
Deterioration of arch's bricks at the extrados and intrados, caused by lorry impact



Arch n. 163 – Side A
Deterioration at the intrados of the arch and deterioration of the façade of the arch

Figure 38 Examples of deterioration of some masonry elements

G: displacement of a voussoir along the mortar joint plan



Arch n. 101 – Side A
Relative displacement in the mortar joint plane



Arch n. 22 – Side A
Relative displacement in the mortar joint plane

Figure 39 Examples of relative displacement along the mortar joint plane

3.2.2 The survey of the Medicean Aqueduct

In order to store the results of the survey, the whole Aqueduct has been subdivided in 9 sections (fig. 40); the original numbering of individual arches, ascending from the town centre towards upstream, has been maintained. The survey has been carried out filling the specific *arch survey form* shown in fig. 41, one for each side, A and B, of every arch. All the collected data, both geometric and related to deterioration, have been collected in summary tables (eg tables 4, 5).

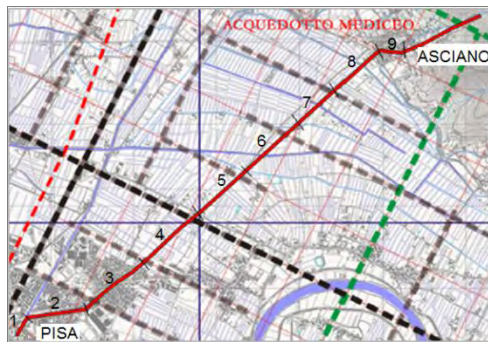


Figure 40 Aqueduct layout divided into 9 sections

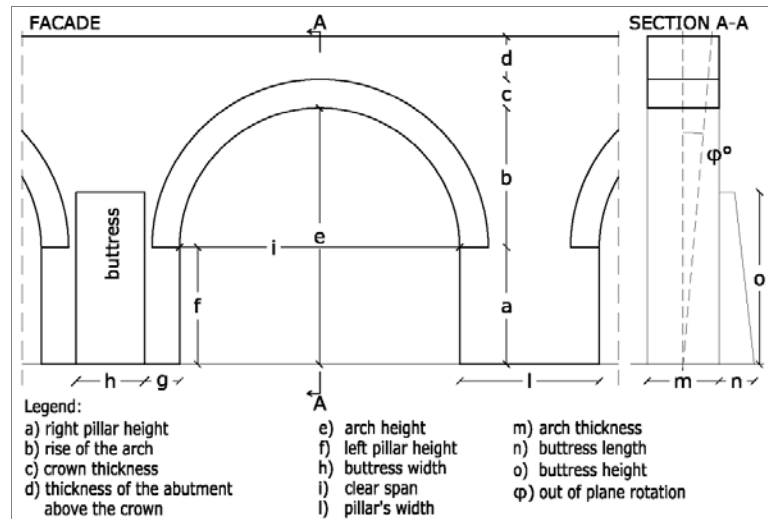


Figure 41 Arch survey form

The investigation of existing crack patterns shows that often several damage phenomena occur simultaneously. For example, the presence of horizontal cracks on a pillar (A3 or B3), on both sides of the arch, is probably associated to vertical settlements of foundation (C2). In this condition, the settlement of one pillar could result in the detachment of the pillar itself from the remaining part, so determining the formation of a new natural arch, spanning between the pillars adjacent to that subject to the settlement, so allowing a new equilibrium configuration, as shown below (fig. 54). The survey on the structure shows that, in some section of the Aqueduct, there are some pillars with an out of plane rotation from 5 to 9 degrees about: for this reason, the following study was carried out also taking account a rotated starting configuration of the structure.

The Medicean Aqueduct also suffers from other decay phenomena such as plants overgrown, that can determine the splitting of stones, moisture and salt efflorescence, which, creeping in the masonry pores, can crumble the materials. If not promptly stopped, these actions can contribute to damage the structure.

4 STRUCTURAL ANALYSIS

A series of structural analyses were conducted on a representative sample of the aqueduct, composed of the 11 arches, placed between two consecutive buttresses.

At first, the studies were conducted on the model of the structure in its original geometry, i.e. in the undamaged state. A preliminary sensitivity analysis was devoted to define the stress patterns under gravitational loads, also accounting for the effects of vertical settlements of foundations and out of plane rotations of the pillars foot. The effects of seismic actions have been investigated, in order to find out the most probable causes of the damages pattern (Global analyses).

Afterwards, in order to identify the failure mechanisms acting on the structure, the effects of seismic actions were investigated on models which describe the actual deformed configuration of the arcades (Local analyses).

In any case, the considered seismic actions are those acting transversely to the mean plane of the aqueduct.

4.1 The case study

For the purposes of the present study, the structural analysis focused on a significant part of the construction, affected by almost all types of decay identified in the classification described above. The sample under investigation consists of eleven arches, placed between two consecutive buttresses, numbered from 90 to 100 (figs. 42, 43), in the section n. 2, next to the town centre of Pisa (fig. 40).

In the following, the product of the survey is illustrated for a relevant portion of the examined sample, corresponding to the three arches numbered 98, 99 and 100 (fig. 44). The cracks, identified by codes accordingly to the classification described above, are highlighted and labelled in different colours. The dimensional data and the crack patterns detected during the survey and previously classified, are summarized in tables 4 and 5. Some other decay phenomena, such as plants overgrown and efflorescence, are evident, but in this case they do not seem to have played a primary role in damaging the structure. For this reason, mainly primary causes have been investigated in assessing the reliability of the structure.



Figure 42 The modelled arches – side A



Figure 43 The modelled arches – side B – side B



Figure 44 Crack pattern of arches n. 98, 99 and 100 – side B

Table 4 Geometric data of arches n. 98, 99 and 100

ARCH	SECTION	GEOMETRIC DATA (m)													
		a	b	c	d	e	f	g	h	i	l	m	n	o	δ
98 A	2	1,99	2,35	0,45	0,45	4,34	2,01	1,80	/	5,32	1,80	1,18	/	/	0°
98 B	2	2,01	2,35	0,45	0,45	4,34	1,99	1,80	/	5,32	1,80	1,18	/	/	0°
99 A	2	COLLAPSED ARCH													
99 B	2														
100 A	2	2,01	2,31	0,45	0,43	4,32	2,05	0,30	1,18	5,30	1,80	1,18	1,07	4,01	0°
100 B	2	2,05	2,31	0,45	0,43	4,32	2,01	1,80	/	5,30	0,30	1,18	1,07	4,01	0°

Table 5 Damages of arches n. 98, 99 and 100

ARCH	SECTION	CROSS CRACK				NOT CROSS CRACK				SETTLEMENT		COLLAPSE		DETACHMENT	DETERIORATION	RELATIVE DISPLACEMENT
		A1	A2	A3	A4	B1	B2	B3	B4	C1	C2	D1	D2	E1	F1	
98 A	2	X	X	X							X			X	X	
98 B	2	X	X			X		X			X			X		
99 A	2											X				
99 B	2											X				
100 A	2	X		X		X								X		X
100 B	2	X			X				X				X	X	X	X

4.2 Characteristics of the models: properties of materials and soil

Since it was not possible to perform direct tests on materials, the mechanical properties were derived from the existing literature related to similar structures, built in the same period and in the same area of the aqueduct.

Almost the whole structure is still composed by the original materials: the masonry of full bricks and lime mortar for the arch crowns, and the mixed masonry in cut stone blocks in all the other parts of the structure. Originally, the employed materials should be of good quality, since they are still in fairly good condition after more than 400 years; so, in the tables contained in the Italian Code [5] (see Annex A), we have referred to good quality materials; in order to take into account the decay due to the age, between the limit values indicated in the table, we have chosen the minimum for the resistances and the medium for the elastic modulus.

The values of the mechanical properties assumed in the analyses are shown in table 6.

Table 6 Mechanical properties of structural materials adopted in the analyses

Type of masonry	Compressive strength f_m [N/mm ²]	Shear strength f_{v0} [N/mm ²]	Elastic modulus [N/mm ²]		Shear modulus G [N/mm ²]	Specific weight W [kN/m ³]
			uncracked condition E	cracked condition E_{cr}		
Cut stone masonry	2,6	0,056	1740	870	580	21
Full brick masonry and lime mortar	2,4	0,060	1500	750	500	18

Unfortunately, direct survey of the existing foundation system is not available, as well as soil testing.

Historical documents testify that, at the construction time, there was a palustrine area at the foot of the mountain. Moreover, in that period, the ground level at the construction site was lower than that of the surrounding plain.

Geological evidences show that the “green” area in Figure 45.a mainly consists of a recent soft alluvial clay layer (2 to 4 m in thickness) overlaying stiffness fan deposit of cobbles. The variable thickness of the shallower soft layer (increasing from upstream to downstream) may be responsible of the observed differential settlements.

The “yellow” areas in Figure 45 mainly consist of outcropping recent silty – sandy alluvial deposits. On the other hand, the “blue” areas mainly consist of clay or peat clay.

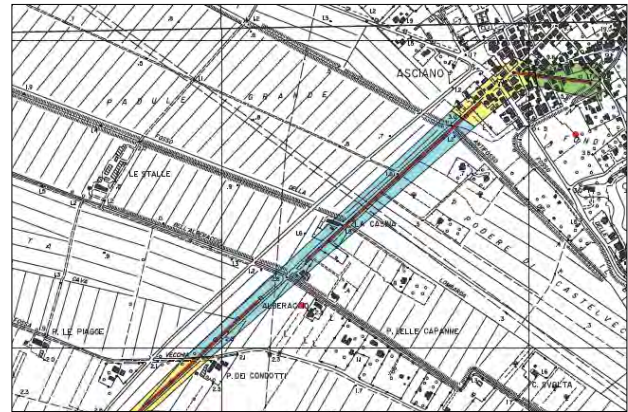


Figure 45.a Geographical framework–upstream



Figure 45.b Geographical framework–intermediate section

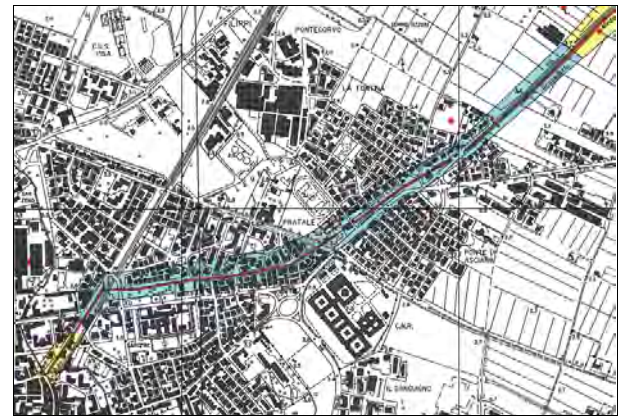


Figure 45.c Geographical framework – downstream section

This area exhibits a shallower layer of vegetable soil of about 0.8 m in thickness overlaying alluvial deposits 3 to 5 m thick with a compressive strength of 200 kPa. A very soft and compressible deposit of clay to peat–clay extends below the alluvial soils. High stratigraphic horizontal heterogeneity of the shallower layers has been observed near the rivers.

4.3 Evaluation of actions

In addition to self-weight, the actions which have been taken into account are:

- vertical settlement of foundation (fig. 46.a), equal to 10, 20, 30 or 40 mm;
- out of plane rotation of a pillar’s foot (fig. 46.b), equal to 1°, 2°, 3° or 4°;
- seismic actions, in terms of response spectrum of the horizontal component of the ground acceleration, evaluated according to the Italian Code [4] (Annex B) for the Service Limit State and the Ultimate Limit State (figs. 47, 48), and of response spectrum of the horizontal displacement for the ULS (fig. 49).

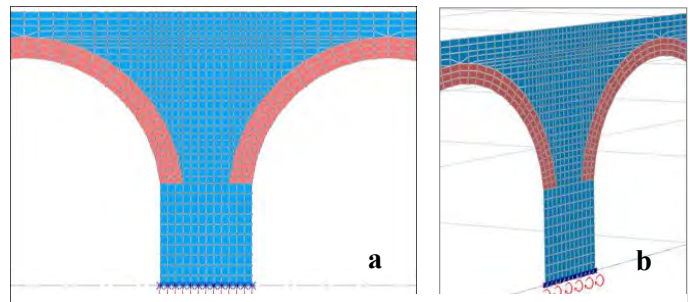


Figure 46.a Vertical settlement of foundation

Figure 46.b Out of plane rotation of pillar’s foot

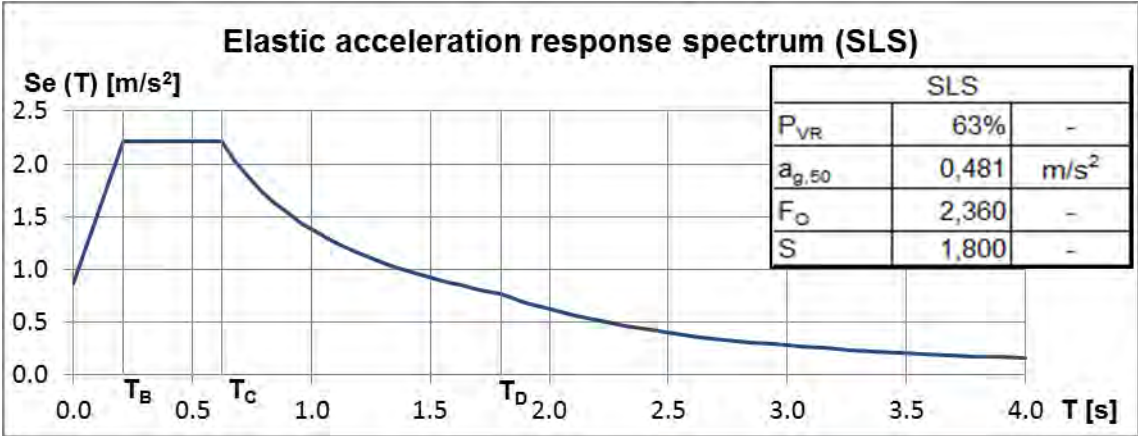


Figure 47 Elastic response spectrum of the horizontal component of the acceleration at SLS

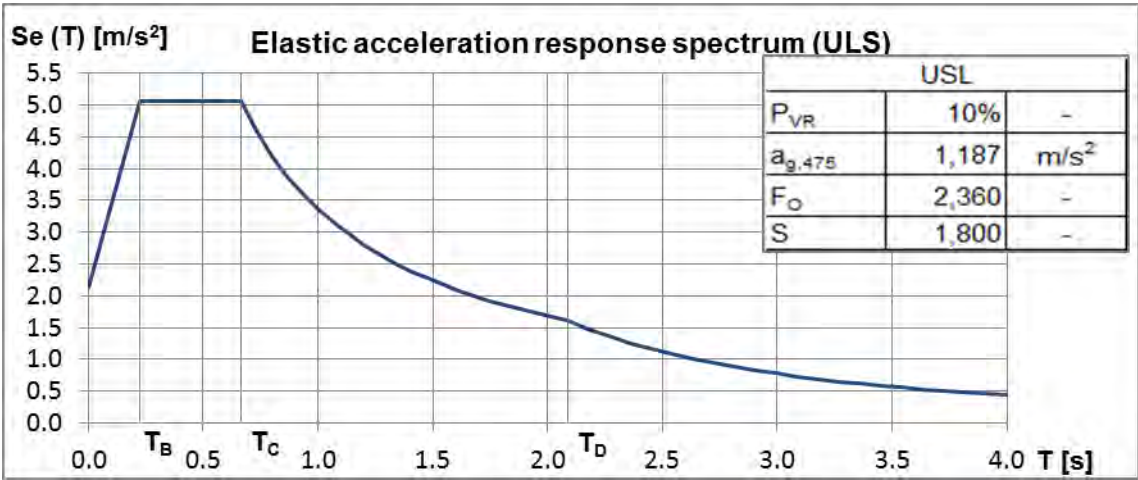


Figure 48 Elastic response spectrum of the horizontal component of the acceleration at ULS

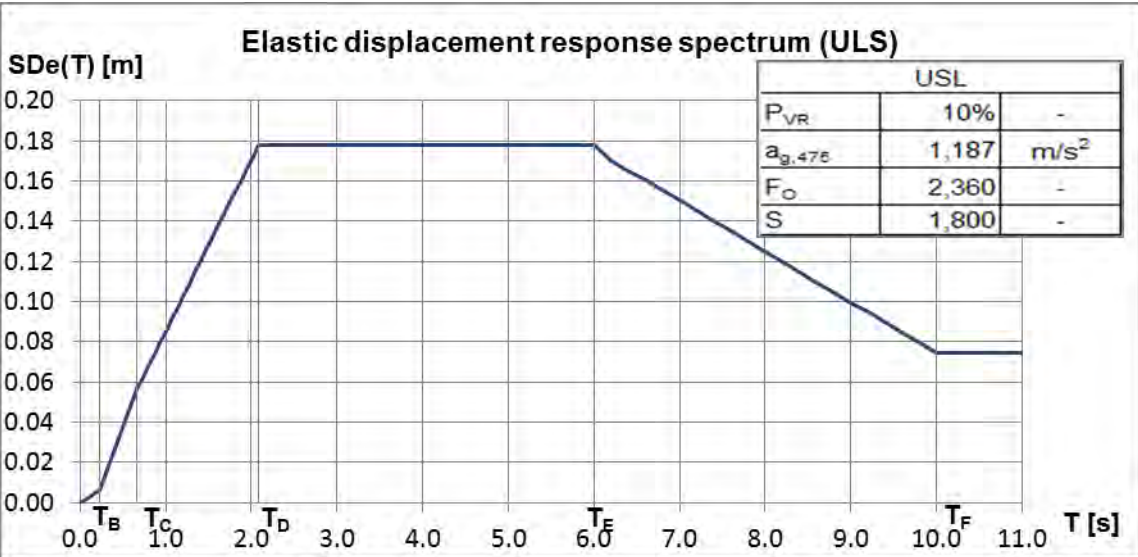


Figure 49. Elastic response spectrum of the horizontal component of the displacement at ULS

4.4 Global analyses

4.4.1 Implemented model

The static and dynamic behaviour of the eleven arches has been numerically studied with a refined *Finite Element Analysis*, performed using the SAP2000 software.

The global finite element model, consisting of about 10299 nodes and 9780 shell elements, is very accurate and it simulates carefully all the details of the modelled arches and buttresses, as well as the soil-foundation interaction. As shown in Figure 50, the model was built with SHELL elements with appropriate thickness; the arches were modelled in the X-Z plane, whereas the buttresses in the orthogonal plane Y-Z.

In order to simulate the soil-structure interaction according to the Winkler model, soil was modelled by a bed of springs with appropriate stiffness. The spring stiffness for vertical movement was defined considering the soil characteristics outlined above. The stiffness to the out-of-plane rotation due to the pillar's thickness was modelled by rotational springs, whose stiffness was evaluated by means of a partial model including a single pillar realized with SOLID elements. In this model, the pillar's foot has vertical springs of equal stiffness; the rotational spring's stiffness is evaluated as the ratio between the moment applied at the top of the pillar and the corresponding rotation.

The stiffness values, assigned to the springs at the foot of the pillars, are shown in table 7.

Table 7 Stiffness assigned to the springs at the foot of the pillars

Spring stiffness for vertical movement	$k_z = 20\,000 \text{ kN/m}^3$
Spring stiffness for the out-of-plane rotation	$k_\theta = 2824 \text{ kN}\cdot\text{m/rad/m}$

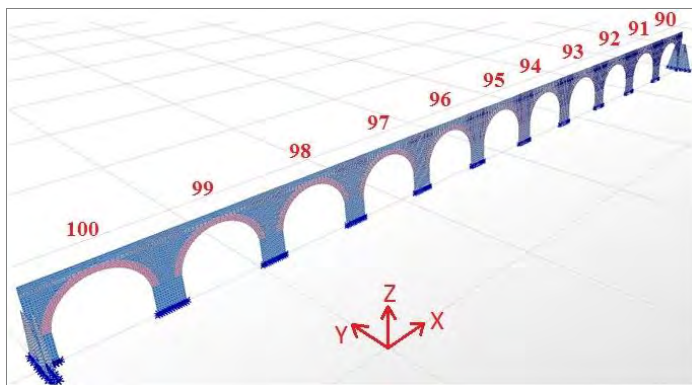


Figure 50.a The finite element model of the eleven arches (shell elements): 3D view

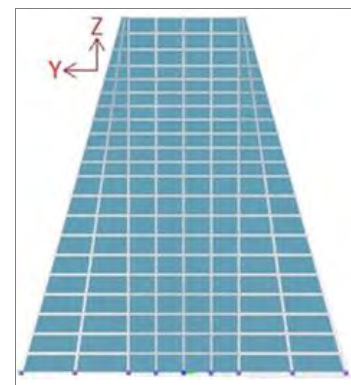


Figure 50.b Finite element model of the buttresses (shell elements) – (Y-Z plane)

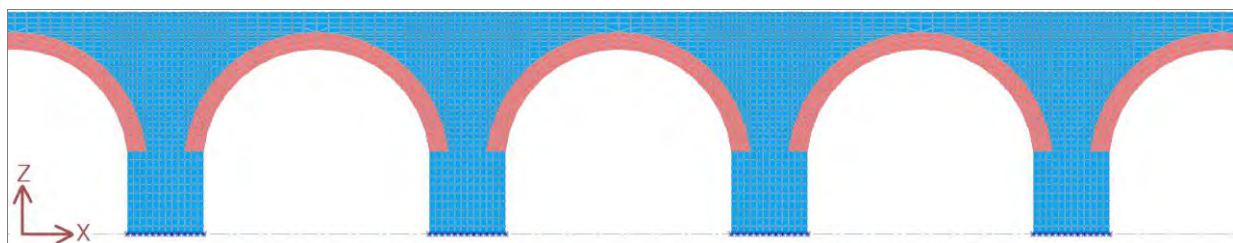


Figure 50.c Finite element mesh of the arches (shell elements) – (X-Z plane)

4.4.2 Static analysis

The static analysis for the self-weight load condition was performed on the global model described above, in the un-cracked situation (elastic modulus = E , see table 6). The results in terms of stresses are shown in fig. 51.

On the same model, vertical settlement of foundation and out of plane rotation of the pillar's foot were imposed alternately on different pillars, to evaluate how the level of stress evolves, on varying of assigned actions: the vertical settlement was applied with an increase of 10 mm at a time, from 0 mm to 40 mm, and the out of plane rotation was applied with an increase of 1° at a time, from 0° to 4° . In fig. 52 the level of stress associated to self-weight and a vertical settlement of 30 mm is shown; in fig. 53, it is shown the level of stress associated to self-weight and an out-of-plane rotation of 4° applied to the pillar's foot.

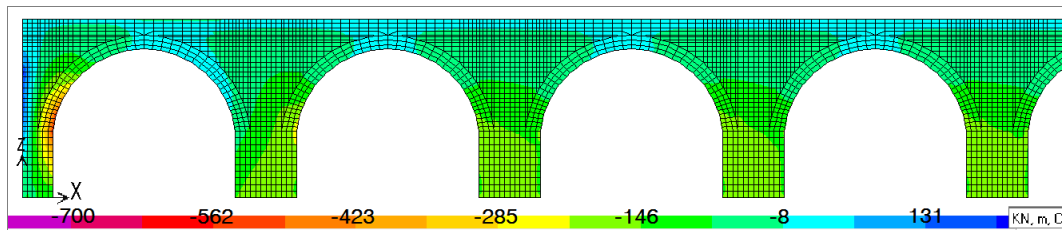


Figure 51 Level of stress, on the shells positive face, along Z direction, in self-weight condition (values expressed in kN/m^2)

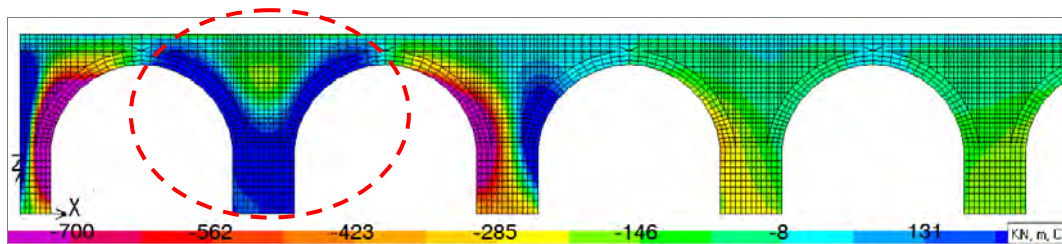


Figure 52 Level of stress, on the shells positive face, along Z direction, self-weight + vertical settlement of 30 mm applied at the foot of the highlighted pillar (values expressed in kN/m^2)

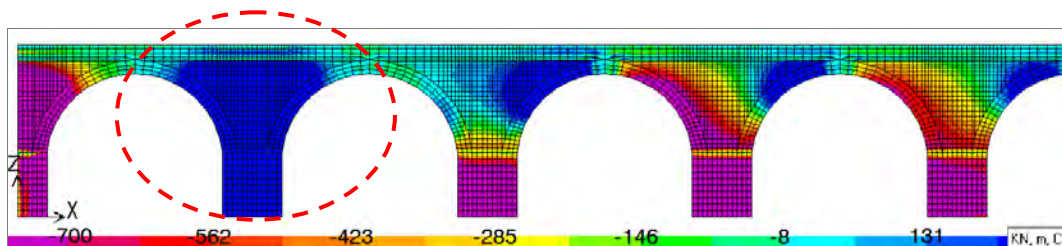


Figure 53 Level of stress, on the shells positive face, along Z direction, self-weight + out-of-plane rotation of 4° applied at the foot of the highlighted pillar (values expressed in kN/m^2)

The figures above show that, while in the self-weight load condition all the structural elements are in compression, when settlement of the pillar foot occurs, tensile stresses appear in that pillar, which values are compatible with the opening of cracks. The distribution of tensile stresses matches with the frequently detected crack pattern, with horizontal cracks on pillars and vertical cracks in the key section of arches, so that we can state that the settlement of foundations is the probable cause of many of the detected crack patterns.

The pattern of stress shown in fig. 52, suggests that, when settlement of foundation occurs, a horizontal cross crack forms in the pillar, and a new mechanism may establish, formed by an arch which includes the two pillars adjacent to the one affected by settlement (fig. 54).

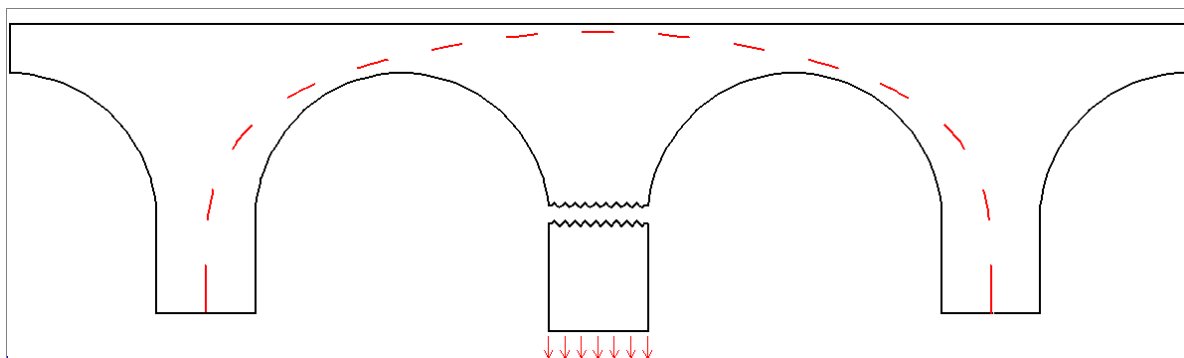


Figure 54 Probable formation of a new mechanism due to the vertical settlement of a pillar

4.4.3 Dynamic analysis

On the global model, both in case of uncracked and cracked conditions, the dynamic modal analysis was performed, obtaining the natural frequencies and the mode shapes of the structure. In figures 55, 56, 57 the first three mode shapes are shown.

The main results can be summarized as follows:

- the first three modes of vibration are in the transversal direction; the corresponding periods are:
 - $T_1 = 1,18 \text{ s}$, $T_2 = 0,88 \text{ s}$, $T_3 = 0,64 \text{ s}$, for uncracked condition (elastic modulus = E);
 - $T_1 = 1,67 \text{ s}$, $T_2 = 1,24 \text{ s}$, $T_3 = 0,91 \text{ s}$, for cracked condition (elastic modulus = E_{cr});
- the participating mass of the first mode of vibration is 78%;
- the first 9 modes of vibration mobilize the mass mainly in the out-of-plane direction;
- 115 modes of vibration are required to reach 95% of participating mass in the transversal direction.



Figure 55 The first mode shape of the structure



Figure 56 The second mode shape of the structure



Figure 57 The third mode shape of the structure

4.4.4 Seismic analysis

The verifications for the seismic design situation were performed for the SLS and the ULS in the bottom section of the pillars, where the seismic action is most relevant. The models were those described above, namely that for the uncracked condition (elastic modulus = E) for SLS verifications, and that for the cracked condition (elastic modulus = E_{cr}) for ULS.

For the two limit states, the return periods of the seismic action, according to the Italian Standard [4], are:

- $T_{R,SLS} = 50 \text{ years}$;
- $T_{R,ULS} = 475 \text{ years}$.

The analyses were conducted considering the response spectra shown in figs. 47, 48.

The SLS verification consists in checking the formation of cracks; so the SLS requirement is fulfilled when, in the most stressed sections, the eccentricity of normal force is less than the radius of the inertia central core. The analysis reveals that none of the examined sections satisfies the verification: this means that earthquakes expected with a return period of 50 years probably produce flexural cracking at the bottom of pillars.

The ULS verifications consists in checking the resistance conditions, that is the values of out of plane shear and bending moment do not exceed the design shear strength and bending moment capacity of the section (Annex C). The characteristic values of the strength of the materials are assumed equal to the mean values, shown in table 6.

The analysis shows that the pillars located in the central position are the most stressed; anyway, for the ULS, none of the examined sections of the pillars foot satisfies the above mentioned verifications.

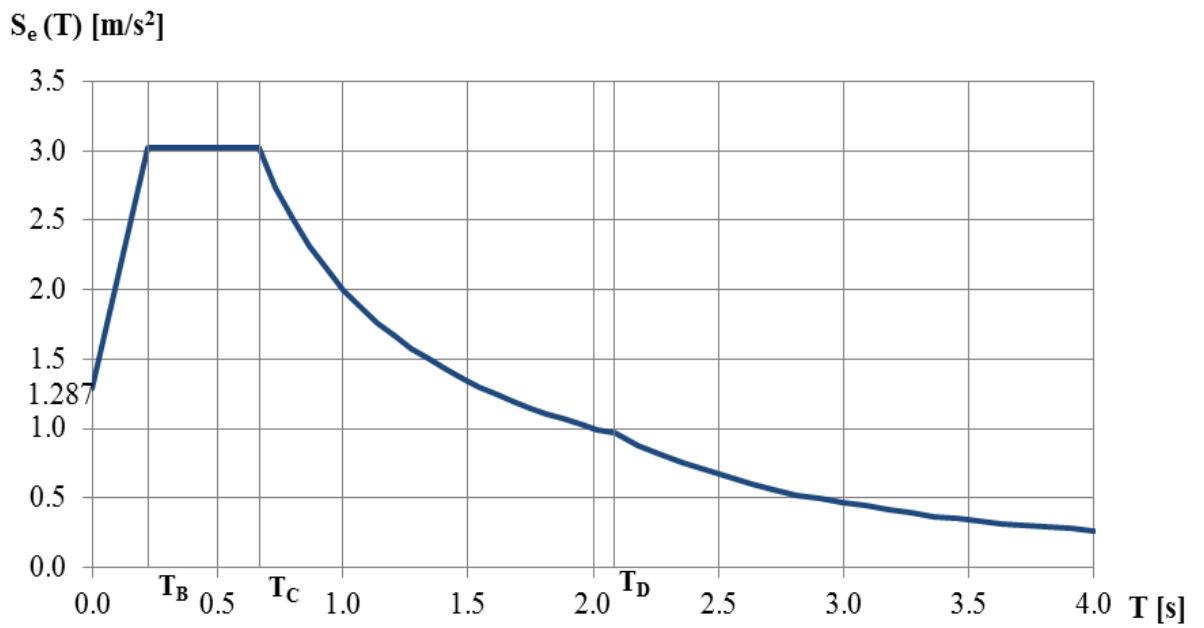


Figure 58 Reduced acceleration response spectrum

Repeating the analysis for reduced acceleration spectra, we found that the verifications were strictly satisfied for the response spectrum shown in fig. 58, corresponding, for the area of interest, to a return period of 140 years. Using such spectrum, a measure of the seismic vulnerability of the structure may be obtained.

The vulnerability index, I_v , may be defined as the ratio between the capacity of the structure and the demand. The capacity of the structure may be expressed by the peak ground acceleration, $a_{g,C}$, in the spectrum compatible with the resistance of the structure, obtained as described above (fig. 58); while the demand is represented by the peak ground acceleration, $a_{g,D}$, in the Standard response spectrum for $T_{R,ULS}$ (fig. 48). So we have:

$$I_{v,a} = \frac{a_{g,C}}{a_{g,D}} \quad (1)$$

For the case study, the vulnerability index is:

$$I_{v,a} = \frac{a_{g,C}}{a_{g,D}} = \frac{1,287}{2,137} = 0,60 \quad (2)$$

4.4.5 Soil-structure interaction and second order effects

The seismic analyses performed with the FEM as described above considers only the elastic behaviour of the structure and of the soil interacting with it, and the verifications apply only to the structure above ground.

In order to take into account the behavior up to failure of the soil interacting with the structure and the second order effects produced by the out-of-plane rotation of the pillars, a specific analysis has been conducted on a limited portion of the examined sample.

The considered portion consists of the central pillar and the two semi-arches on the two sides, isolated from the rest of the arcades; this model does not take into account the stabilizing effect of the buttresses, which is really negligible for the central portions of the sample.

The studied element is considered as a deformable body, connected with its foundation and interacting with soil, in the sense that its base can move vertically and rotate, following the deformation of the underlying soil.

The geometric characteristics of the system are illustrated in fig. 59. The element and the foundation are subdivided in layers, whose mechanical properties are those indicated in table 6 and illustrated in fig. 60; the soil interacting with the element is modelled by layers of elasto-plastic material, 50 cm thick and with horizontal dimensions increasing with depth; the mechanical characteristics of the layers change with the depth, as indicated in fig. 61, taking properly into account the over-consolidation effect.

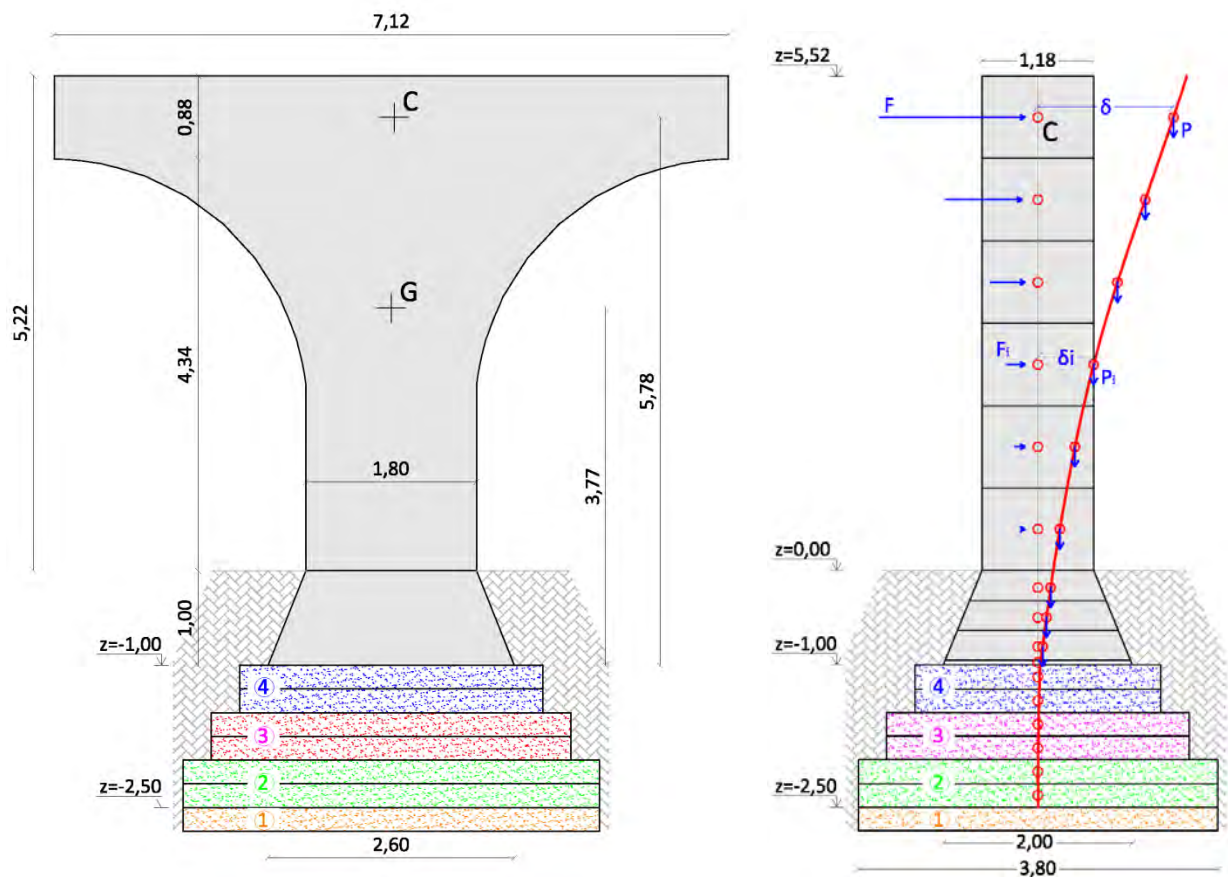


Figure 59 The system element+foundation+soil, modelled as a series of overlapped layers

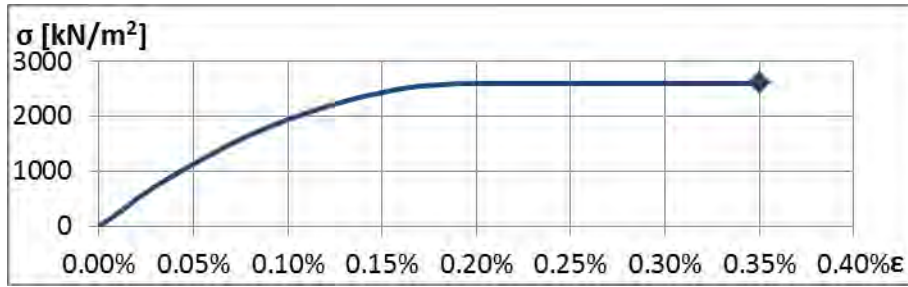


Figure 60 Stress-deformation diagram for masonry

Each layer of the element is subjected to the corresponding self-weight and to a lateral force, F_i , simulating the seismic action; lateral forces are equal to the product of the mass of the layer for its height related to the extrados of the foundation, and for the acceleration of soil, a .

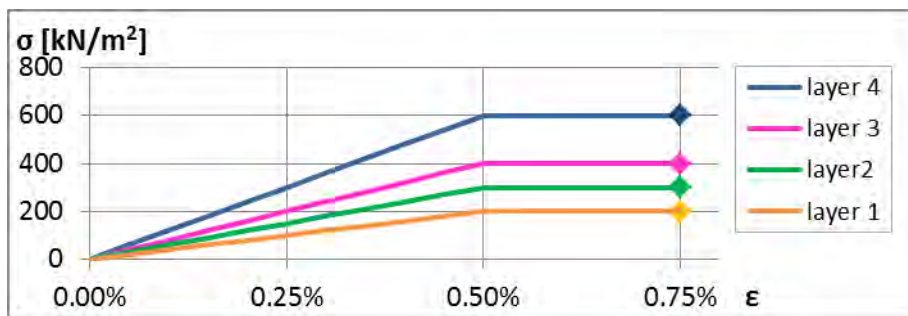


Figure 61 Stress-deformation diagrams for the 4 layers of soil at different depths

The acceleration a is increased by steps; for each step the deformed configuration is evaluated as described in Annex E, taking into account the second order effects too. The procedure stops when in one of the layers the resisting moment is reached.

The result of the procedure is the capacity curve of the system, illustrated in fig. 62, in terms of a , spectral acceleration, and d , displacement of the control point, C.

The failure occurs at the base of the pillar for $a = 1,17 \text{ m/s}^2$. In correspondence, the vulnerability index may be calculated:

$$I_{v,a} = \frac{a_{g,C}}{a_{g,D}} = \frac{1,170}{2,137} = 0,55$$

It can be noted that the seismic vulnerability evaluated taking into account the behaviour of the soil and the second order effect is slightly lower than that in the hypothesis of linear behaviour.

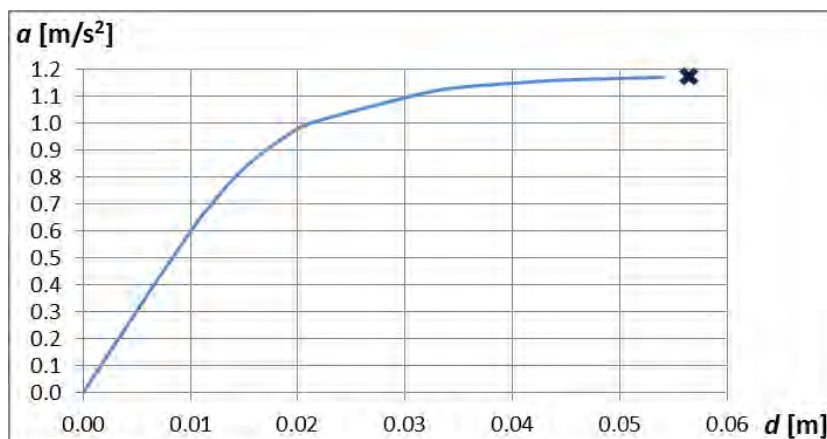


Figure 62 Capacity curve

4.5 Local analyses

The seismic analyses have shown that seismic events with a return period corresponding to the SLS cause the cracking of the sections at the bases of the pillars, and events with a return period of only 140 years induce tensions higher than the flexural strength of those sections.

In structures subjected to seismic actions, in particular masonry structures, the fact that in some sections the strength is exceeded does not imply that the structure or some elements collapse. In many structures, with ductile behaviour, the actions are redistributed among the different elements, and the entire structure may withstand actions much higher. Such structures are usually verified taking into account the post-elastic behaviour, or by means of non-linear analyses or adopting the design spectra, reduced with respect to the response spectra by the behaviour factor, q .

Masonry structural elements do not have a real ductility; however, in complex masonry structures, after the elastic phase, different mechanisms may take place, through which the structure may withstand actions much higher.

In the case study, subjected to seismic actions orthogonal to the main plane, a portion of the structure, separated from the others by the cracks formed for various reasons, may begin to oscillate (activation of the mechanism) and, for stronger actions, overturn (collapse).

This kind of crisis cannot be predicted by the elastic analysis of the structure in the original geometry; in these cases, it is appropriate to recognize the mechanisms that probably establish and evaluate the behaviour of each of them under increasing lateral forces through the so-called kinematic analysis.

The kinematic analysis is based on the kinematic theorem of the limit analysis method: this type of analysis, as well as its main field of application, is fully described in "Annex D".

The first step of the analysis consists in the identification of the conditions which may produce the activation of the local damage or the collapse mechanism. In the structure under examination the probable mechanisms that have been identified take place from the formation of vertical cracks at the key of two arches. There are two extreme situations:

- 1) the cracks form in the arches next to the buttresses (fig. 63.a),
- 2) the cracks form in the arches next to an intermediate pillar (fig. 63.b).



Figure 63.a Mechanism with cracks in the arches next to the buttresses



Figure 63.b Mechanism with cracks in the arches next to an intermediate pillar

In both cases, the macro-element consists of one pillar and the two adjacent semi-arches (highlighted in red in fig. 63.a and fig. 63.b), separate, because of cracks, from the rest of the structure and from the foundation. The characteristics of the macro-element are described in fig. 64.

In situation 1), the central macro-element, which is in the worst situation, is not affected by the stabilizing effect exerted by the buttresses; so, it is subjected to the self-weight and to lateral forces simulating the seismic actions.

In situation 2), a sort of arch effect may develop in the horizontal plane, as illustrated in fig. 63.b, by which the side portions of the arcade transmit stabilizing forces to the macro-element, in correspondence of the arches. So the macro-element is now subjected also to stabilizing horizontal forces, which intensity depends on the out-of-plane position of the arch itself.

The two situations are examined below, for the macro-element modelled as a rigid body rotating around a cylindrical hinge placed at the edge of the pillar's base.

The following cases have been examined:

- case A) macro-element in situation 1), i.e. isolated, subjected to the self-weight and to lateral forces simulating the seismic actions, rotating as a rigid body around a cylindrical hinge placed at the edge of the pillar's base; also the cases of macro-element initially rotated by 5° or 9° have been studied;
- case B) evaluation of the stabilizing forces acting in situation 2);
- case C) macro-element in situation 2), subjected to the self-weight, to lateral forces simulating the seismic actions and to the stabilizing actions (from case B), rotating as a rigid body around a cylindrical hinge placed at the edge of the pillar's base.

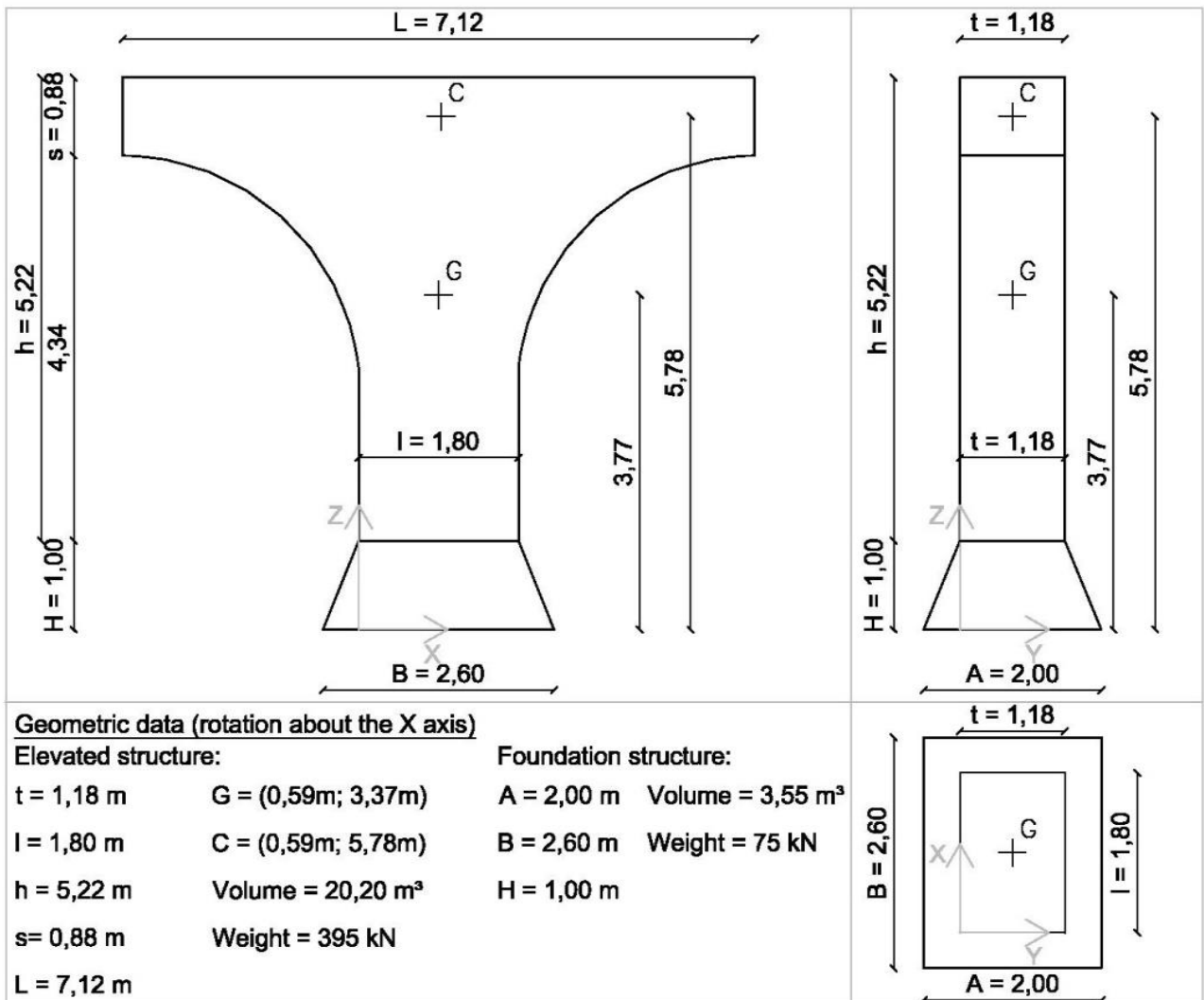


Figure 64 Kinematic Analysis – geometric properties of the macro-element

4.5.1 Case A)

The macro-element is considered as a single degree of freedom rigid body (fig. 65); the seismic actions are modelled as horizontal forces equal to the gravity forces amplified by a kinematic multiplier α . The linear kinematic analysis (see Annex D, §D.3) has been performed to evaluate the kinematic multiplier, α_0 , corresponding to the activation of the mechanism. Afterwards, by means of the non-linear kinematic analysis (see Annex D, §D.4), the displacement capacity of the structure has been determined. Finally, the capacity curves of the structure (see Annex D, §D.5) have been determined and the safety verifications conducted both for the SLS and the ULS (see Annex D, §D.6).

The results of the analysis are shown in table 8 and table 9.

In the tables the symbols indicate:

- φ is the initial rotation of the macro-element
- α_0 is the kinematic multiplier corresponding to the activation of the mechanism
- M^* is the participating mass
- a_0^* is the spectral acceleration corresponding to the activation of the mechanism
- $a_{g,SLS}$ is the acceleration demand related to SLS
- $a_{g,ULS}$ is the acceleration demand related to ULS
- θ_{max} is the rotation corresponding to $\alpha=0$, i.e. to the overturning
- d_0 is the displacement of the control point corresponding to $\alpha=0$
- d_0^* is the spectral displacement corresponding to $\alpha=0$
- d_u^* is the displacement capacity at the ULS
- d_s^*, a_s^*, T_s are the parameters for the calculation of $S_{De}(T_s)$ (see Annex D, §D.6)
- $S_{De}(T_s)$ is the displacement demand at the ULS

In fig. 66, for the element in the three initial conditions, 0° , 5° , 9° , are shown the a^* - d^* curves, the points representing d_u^* , the limit lines representing $a_{g,SLS}$ and $a_{g,ULS}$, and the limit lines representing $S_{De}(T_s)$. It appears clearly that, for the macroelement in the vertical position, the mechanism does not activate for earthquakes corresponding to SLS, for earthquakes corresponding to ULS, the mechanism activates but the element does not collapse; for elements initially inclined 5° the mechanism activates also for earthquakes corresponding to SLS but it does not collapse for ULS earthquakes, while the collapse occurs for macro-elements initially inclined by 9° .

In the case of element initially vertical the index of vulnerability is bigger than 1,00.

Table 8 Results of verifications of the activation of the mechanism

	CAPACITY			DEMAND	VERIFICATION	DEMAND	VERIFICATION
	α_0	M^* [kg]	a_0^* [m/s ²]	SLS $a_{g,SLS}$ [m/s ²]	SLS $a_0^* > a_{g,SLS}$	ULS $a_{g,ULS}$ [m/s ²]	ULS $a_0^* > a_{g,ULS}$
0°	0,174		1,702	0,865	YES	2,137	NO
5°	0,085	43	0,831	0,865	NO	2,137	NO
9°	0,015		0,145	0,865	NO	2,137	NO

Table 9 Results of verifications of collapse

CAPACITY			DEMAND					VERIFICATION
φ	d_0^* [m]	θ_{max} [°]	d_u^* [m]	d_s^* [m]	a_s^* [m/s ²]	T_s [s]	$S_{De}(T_s)$ [m]	ULS
0°	0,839		0,336	0,134	1,430	1,925	0,164	YES
5°	0,427	10°	0,171	0,068	0,698	1,964	0,167	YES
9°	0,086		0,034	0,014	0,121	2,110	0,177	NO

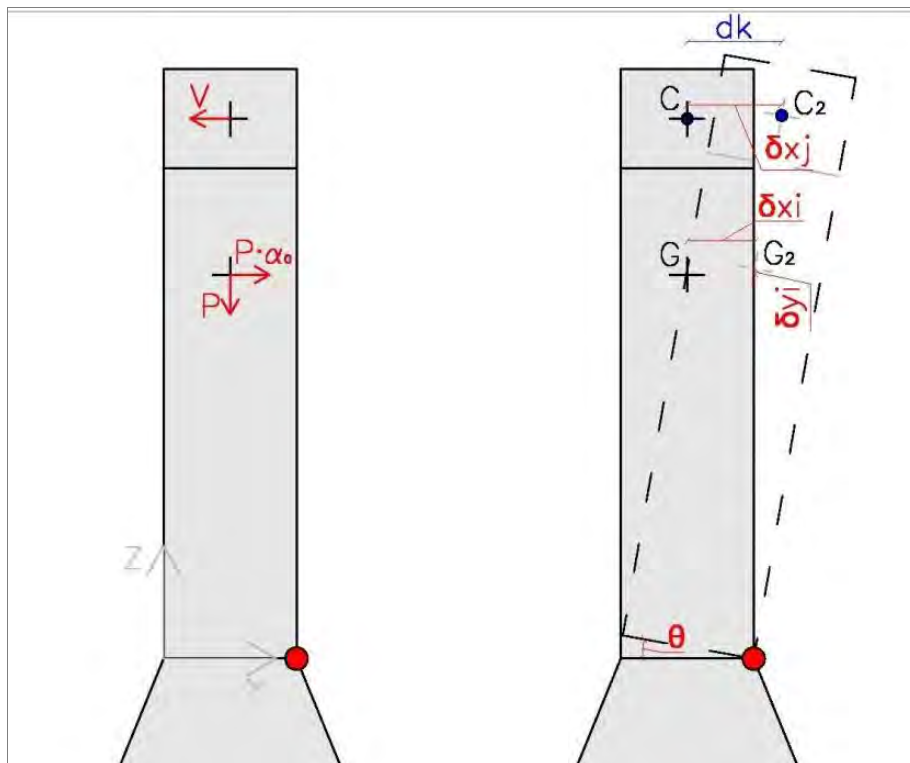


Figure 65 Macro-element as a single degree of freedom body

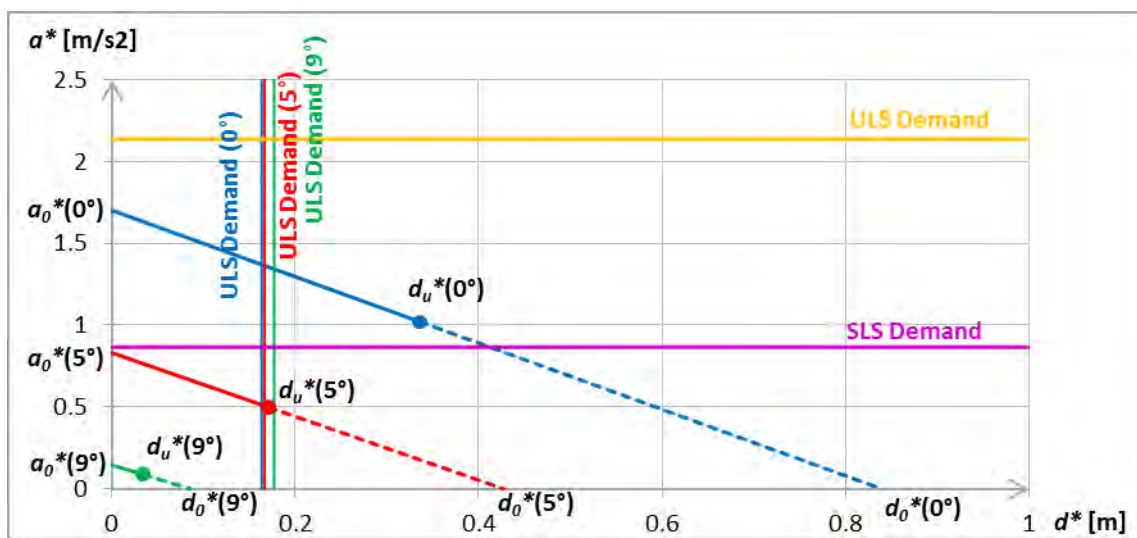


Figure 66 a^* - d^* capacity curves ($\varphi=0^\circ, 5^\circ, 9^\circ$) compared with demand values

4.5.2 Case B): evaluation of the stabilizing forces

In situation 2), shown in fig. 63.b, the out-of-plane rotation of the studied macro-element induces horizontal compressive forces in the upper part of the macro-element itself and in the adjacent ones, due to their geometry, essentially the thickness/length ratio, which is quite high. So, a sort of arch effect may develop in the horizontal plane (fig. F.1 – Annex F), by which the side portions of the arcade transmit stabilizing forces to the macro-element, which intensity depends on the out-of-plane position of the macro-element itself.

The magnitude of the horizontal forces, V , which act on the studied macro-element in opposition to the seismic forces, is a function of the transversal displacement, δ , of the macro-element; it may be evaluated following the procedure described in Annex F. The result for the case under examination is shown in the diagram of fig. 67.

It can be noticed that initially the force V increases from 0 to a maximum, because the tension in the compressed bands increases; after that, the tension no longer increases, while the forces N and H are more and more aligned, so that V decreases up to 0.

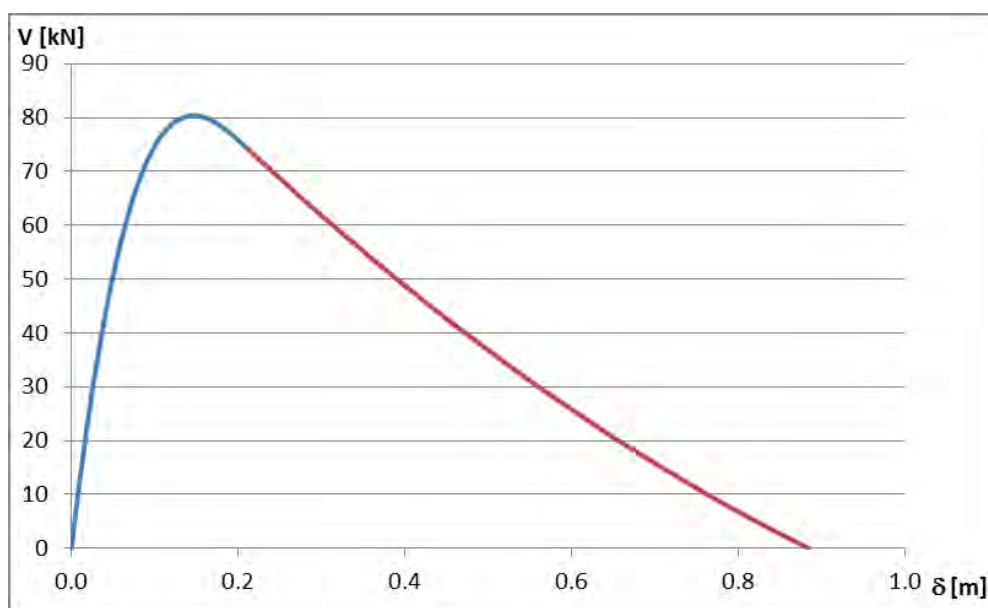


Figure 67 Diagram of V as a function of δ

4.5.3 Case C)

The macro-element is considered as a single degree of freedom rigid body mechanism (fig. 65); the seismic actions are modelled as horizontal forces equal to the gravity forces amplified by a kinematic multiplier α . In this case the horizontal forces, V , act on the studied macro-element in opposition to the seismic forces.

The linear kinematic analysis (see Annex D, §D.3) has been performed to evaluate the kinematic multiplier, α_0 , corresponding to the activation of the mechanism. Afterwards, by means of the non-linear kinematic analysis (see Annex D, §D.4), the displacement capacity of the structure has been determined. Finally, the capacity curves of the structure (see Annex D, §D.5) have been determined and the safety verifications conducted both for the SLS and the ULS (see Annex D, §D.6). The results of the analysis are shown in table 10 and table 11.

In fig. 68, for the element in the three initial conditions, 0° , 5° , 9° , are shown the a^* - d^* curves, the points representing d_u^* , the limit lines representing $a_{g,SLS}$ and $a_{g,ULS}$, and the limit lines representing $S_{De}(T_s)$.

It appears clearly that, for the macro-element in the vertical position, the mechanism does activate for earthquakes corresponding to ULS but the element is much more stable than in the

case A) since the acceleration must still increase to induce greater displacements. Also in this case the vulnerability index is greater than 1,00.

For the element initially inclined 5° the situation is sensibly safer than in case A), with vulnerability index greater than 1,00. Only the element inclined 9° is still vulnerable, and this is logic, considering that even in absence of lateral forces it is at the point of overturning (10°).

Table 10 Results of verifications of the activation of the mechanism

φ	CAPACITY			DEMAND	VERIFICATION	DEMAND	VERIFICATION
	α_0	M^* [kg]	a_0^* [m/s ²]	SLS $a_{g,SLS}$ [m/s ²]	SLS $a_0^* > a_{g,SLS}$	ULS $a_{g,ULS}$ [m/s ²]	ULS $a_0^* > a_{g,ULS}$
0°	0,174		1,702	0,865	YES	2,137	NO
5°	0,392	43,276	3,845	0,865	YES	2,137	YES
9°	0,084		0,825	0,865	NO	2,137	NO

Table 11 Results of verifications of collapse

φ	CAPACITY			DEMAND				VERIFICATION
	d_0^* [m]	θ_{max} [°]	d_u^* [m]	d_s^* [m]	a_s^* [m/s ²]	T_s [s]	$S_{De}(T_s)$ [m]	ULS $d_u^* > S_{De}$
0°	0,889		0,356	0,142	1,430	1,982	0,168	YES
5°	0,471	10,6	0,188	0,075	3,230	0,959	0,081	YES
9°	0,134		0,054	0,021	0,693	1,106	0,094	NO

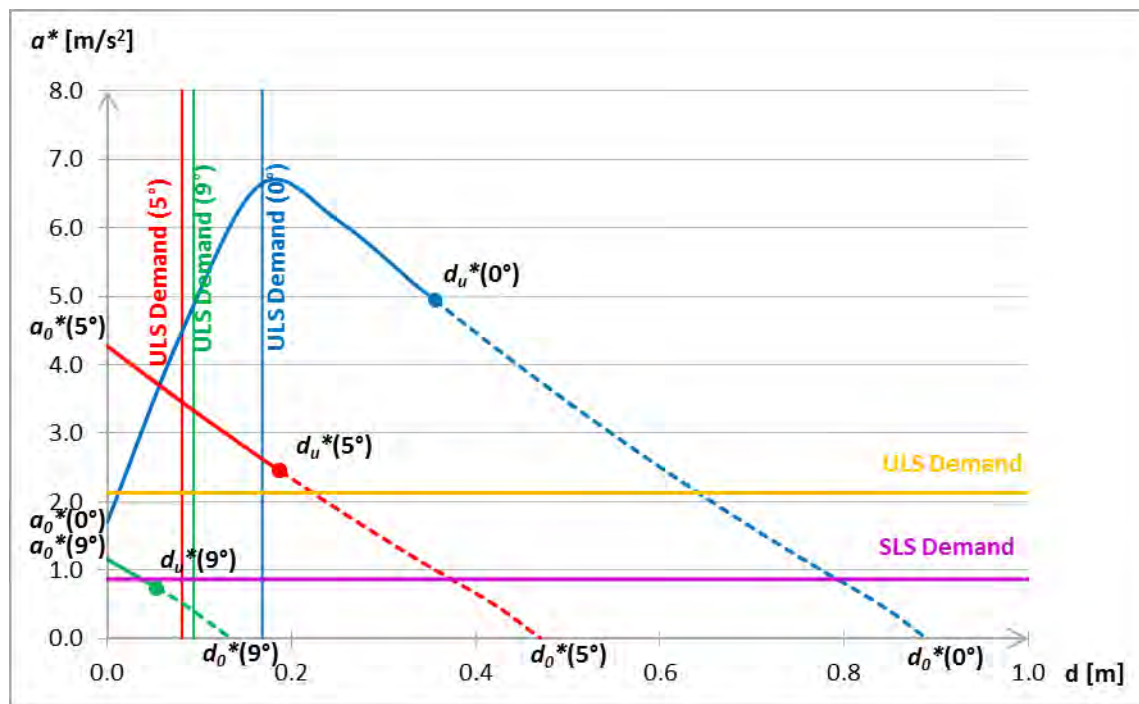


Figure 68 a^* - d^* capacity curves ($\varphi=0^\circ, 5^\circ, 9^\circ$) compared with demand values

5 CONCLUSIONS

The Medicean Aqueduct is an infrastructure which strongly characterizes the territory of the town of Pisa (Tuscany, Italy), for its historical and architectural value.

The Aqueduct was built at the end of the XVI century and just from the beginning it had structural problems, caused by design and construction defects, so that changes and consolidation have been implemented through time. Despite all, the construction is still standing, and, although not working and deteriorated, it is an important monument that must be preserved.

Every consolidation design must be preceded by an accurate analysis, both historical and structural, so that the intervention will be well calibrated for the specific situation.

For the Aqueduct, the procedure outlined by the ISO 13822 has been followed: on the basis of an accurate assessment of the geometry, the materials and the decay, refined models have been implemented in order to justify the main cracks, rotations and collapse observed.

Afterwards, seismic analyses have been conducted, both on global and local models, also taking into account the interaction with soil and the second order effects; the vulnerability of the structure has been obtained and also indications useful for the design of consolidation works.

The methodology followed in the present work has proved to be a useful tool for the study of historical constructions, in view of their conservation.

REFERENCES

- [1] ISO 12491 “Statistical methods for quality control of building materials and components”, 1st edition, 1997.
- [2] ISO 2394 “General principles on reliability for structures”, 1998.
- [3] ISO 13822 “Basis for design of structures - Assessment of existing structures”, 2001. ISO, Geneva, Switzerland.
- [4] *D.M. 14 gennaio 2008* Norme Tecniche per le Costruzioni, Italian Standard.
- [5] *Circ. n° 617, 02 febbraio 2009*, Italian Standard.
- [6] EN 1998-1 (2004): Eurocode 8: Design of structures for earthquake resistance – Part 1: General rules, seismic actions and rules for buildings [Authority: The European Union Per Regulation 305/2011, Directive 98/34/EC, Directive 2004/18/EC].
- [7] EN 1996-1-1 (2006): Eurocode 6: Design of masonry structures - Part 1-1: General rules for reinforced and unreinforced masonry structures.
- [8] Croce P., Holický M. eds. (2013) “Operational methods for the assessment of existing structures”.
http://www.leonardo.cvut.cz/download/march2014/Operational_Methods_for_the_Assessment_of_Existing_Structures.pdf
- [9] Desideri A., Russo G., Viggiani C., *Rivista Italiana di Geotecnica* (n°1 1997), “La stabilità di torri su terreno deformabile”.
- [10] Diamantidis D., Holický M. eds. (2012) “Innovative methods for the assessment of existing structures”. CTU in Prague, Klokner Institute, Prague.
http://www.leonardo.cvut.cz/download/Innovative_Methods_for_the%20Assesstement_of_Existing_Structures.pdf
- [11] Gasperini M., Associazione “Salviamo l’Acquedotto Mediceo” di Pisa (2010), “Progetto preliminare di recupero, valorizzazione e riqualificazione ambientale dell’Acquedotto Mediceo di Pisa e delle sue aree contermini”.
- [12] Giannessi O. (1967), “Si deve salvare l’Acquedotto Mediceo?”, Extracted from the n°9-10 Year III della “Rassegna periodica di informazione del Comune di Pisa”, Tipografia Comunale, Pisa.
- [13] Giuffrè A. (2003), “La meccanica nell’architettura: La Statica”.
- [14] Heyman J. (1997), “The Stone Skeleton: Structural Engineering of Masonry Architecture”.

- [15] Holický M., Návarová V. eds. (2013) “Basics for assessment of existing structures”.
http://www.leonardo.cvut.cz/download/march2014/Basics_Assessment_Existing_Structures_CB.pdf
- [16] Letizia M. G. e Quercioli C. (2007), “Chiare, fresche et dolci acque, C'era una volta l'Acquedotto Mediceo... e le fontane di Pisa”, Musetti Libri, Pisa.
- [17] Zamperini E. (2010), Notes of the Course of Recupero e Conservazione degli edifici, “L'arco in muratura”.

CHAPTER 9 - ANNEX A

MECHANICAL PROPERTIES OF STRUCTURAL MATERIALS

For the different kinds of masonry most often found in structures, the Italian Standard [5], in Table C8A.2.1 shown below (Tab. A.1), provides a range of the reference values for the mechanical parameters.

In the tables the symbols indicate:

- f_m is the average compressive strength of masonry;
- τ_0 is the average shear strength of masonry in absence of compression;
- E is the average value of the modulus of elasticity;
- G is the average value of the shear modulus;
- w is the average specific weight of the masonry.

Table A.1 Reference values of the mechanical parameters and the specific weight - Tab. C8A.2.1 of Italian Standard [5]

Type of masonry:	f_m [kN/m ²]	τ_0 [kN/m ²]	E [N/mm ²]	G [N/mm ²]	w [kN/m ³]
Masonry in disorganized cut stones	1000	20	690	230	19
	1800	32	1050	350	
Masonry with rough-hewed stones, thin skin and internal core	2000	35	1020	340	20
	3000	51	1440	480	
Cut stone masonry	2600	56	1500	500	21
	3800	74	1980	660	
Masonry in pieces of soft stone	1400	28	900	300	16
	2400	42	1260	420	
Masonry in rough-hewed pieces of igneous rock	6000	90	2400	780	22
	8000	120	3200	940	
Full brick and lime mortar	2400	60	1200	400	18
	4000	92	1800	600	
Half-full brick and lime mortar	5000	240	3500	875	15
	8000	320	5600	1400	
Half-full clay block	4000	300	3600	1080	12
	6000	400	5400	1620	
Half-full clay block, with vertical dry mortar joint	3000	100	2700	810	11
	4000	130	3600	1080	
Masonry in concrete block or expanded clay	1500	95	1200	300	12
	2000	125	1600	400	
Masonry in concrete half-full block	3000	180	2400	600	14
	4400	240	3520	880	

For the two types of masonry found in the Aqueduct, the reference values highlighted in the above table have been considered.

The compressive and shear strength have been assumed equal to the minimum values, the elastic and the shear modulus in the uncracked condition equal to the mean values; the elastic modulus in the cracked condition is equal to half the value of modulus for the uncracked condition.

CHAPTER 9 - ANNEX B
ELASTIC RESPONSE SPECTRA

In Italian Standard [4], as well as in Eurocode EN1998-1 [6], the elastic response spectrum of the horizontal component of the acceleration is given by:

$$\begin{aligned}
 0 \leq T < T_B & \quad S_e(T) = a_g \cdot S \cdot \eta \cdot F_o \cdot \left[\frac{T}{T_B} + \frac{1}{\eta \cdot F_o} \left(1 - \frac{T}{T_B} \right) \right] \\
 T_B \leq T < T_C & \quad S_e(T) = a_g \cdot S \cdot \eta \cdot F_o \\
 T_C \leq T < T_D & \quad S_e(T) = a_g \cdot S \cdot \eta \cdot F_o \cdot \left(\frac{T_C}{T} \right) \\
 T_D \leq T & \quad S_e(T) = a_g \cdot S \cdot \eta \cdot F_o \cdot \left(\frac{T_C \cdot T_D}{T^2} \right)
 \end{aligned} \tag{B1}$$

where $S = S_s \cdot S_T \geq 1.0$ depends on soil category and on topography, while T_B , T_C and T_D , expressed in s, are the values of the fundamental period corresponding to the starting points of the constant acceleration branch, of the constant velocity branch and of the constant displacement branch of the elastic response spectrum, respectively. F_o is the factor of the maximum amplification, which in Eurocode is set equal to 2,5 and in Italian Standard assumes different values ($\geq 2,2$) depending on the site.

In eqs. (B1) the coefficient η takes into account the effects of damping coefficient ξ , expressed in percent. The general expression for η is

$$\eta = \sqrt{\frac{10}{5 + \xi}} \geq 0,55 \tag{B2}$$

usually set equal to 1,00.

The elastic response spectrum of the horizontal component of the displacement is defined as:

$$\begin{aligned}
 0 \leq T \leq T_E & \quad S_{De}(T) = S_e(T) \cdot \left(\frac{T}{2\pi} \right)^2 \\
 T_E < T \leq T_F & \quad S_{De}(T) = 0,025 \cdot a_g \cdot S \cdot T_C \cdot T_D \cdot \left[F_o \cdot \eta + (1 - F_o \cdot \eta) \cdot \frac{T - T_E}{T_F - T_E} \right] \\
 T > T_F & \quad S_{De}(T) = 0,025 \cdot a_g \cdot S \cdot T_C \cdot T_D
 \end{aligned} \tag{B3}$$

T_E varies from 4,5s to 6,0s, depending on soil category, and T_F is equal to 10,0s.

CHAPTER 9 - ANNEX C

SEISMIC VERIFICATIONS

The seismic verifications were performed according to Italian Standard [4]. As far as ULS, out of plane failure in shear or bending was checked, while for SLS cracking check has been performed.

Out of Plane Shear Verification (ULS)

At the ULS, the design value of the shear load applied to the masonry wall, V_{Ed} , shall be less than or equal to the design value of the shear resistance of the wall, V_{Rd} :

$$V_{Ed} \leq V_{Rd} \quad (C1)$$

The design value of the shear resistance is given by:

$$V_{Rd} \leq f_{vd} t l_c \quad (C2)$$

with:

$$f_{vd} = f_{vk} / \gamma_M \quad \text{and} \quad f_{vk} = f_{vk0} + 0,4 \sigma_0 \quad (C3)$$

- f_{vd} is the design value of the shear strength of the masonry;
- f_{vk0} , f_{vk} are the characteristic shear strength respectively in absence or in presence of compression stress related to the vertical loads acting on the control section;
- σ_0 is the compression stress related to the vertical loads acting on the control section;
- t is the thickness of the wall;
- l_c is the length of the compressed part of the wall.

Out of Plane Bending Moment Verification (ULS)

At the ULS, the design value of the moment applied to the masonry wall, M_{Ed} , shall be less than or equal to the design value of the moment of resistance of the wall, M_{Rd} , such that:

$$M_{Ed} \leq M_{Rd} \quad (C4)$$

The design value of the lateral moment of resistance of a masonry wall, M_{Rd} , is given by:

$$M_{Rd} = (l \cdot t^2 \cdot \sigma_0 / 2) \cdot (1 - \sigma_0 / 0,85 \cdot f_d) \quad (C5)$$

where:

- l is the length of the wall;
- t is the thickness of the wall;
- σ_0 is the compression stress related to the vertical loads and to the complete section;
- f_d is the design compressive strength of the masonry.

Out of Plane Crack Check (SLS)

Cracking of reinforced masonry walls is prevented when the eccentricity of loads is less than the radius of the central core of inertia. For a rectangular section, in which t is the thickness of the wall, the eccentricity of loads is given by:

$$e = \frac{M_{Ed}}{M_{Rd}} \leq \frac{t}{6} \quad (C6)$$

CHAPTER 9 - ANNEX D

KINEMATIC ANALYSIS

D.1 INTRODUCTION

The modes of damage caused by seismic actions in masonry buildings depend essentially on their structural organization: in case of lacking of efficient connections between the components of the building (walls and floors), the masonry structure does not show a clear global behaviour but rather it is frequent the occurrence of partial collapses, generally corresponding to the loss of equilibrium of portions of the structure, the so called “macro-elements”.

In these circumstances, a global model does not comply with the actual seismic behaviour of the structure, and the seismic assessment must consider also local collapse mechanisms, which are generally less resistant and less ductile than those involving the response of the whole building. The first step of the analysis concerns the identification of the mechanisms that can be activated; for each of them, the kinematic analysis may be performed, aimed to evaluate the seismic actions that activate the mechanism (SLS) and the ones that cause the collapse of the macro-element (ULS).

A masonry wall, subject to earthquake, may exhibit different damage mechanisms, conventionally classified into two basic failure mode categories, depending on the direction of the horizontal forces relatively to the mean plane of the wall:

- 1st failure mode category: the mechanism is activated by seismic forces acting orthogonally to the wall plane, which cause the overturning of a portion or the entire wall (figs. D.1, D.2);
- 2nd failure mode category: the mechanism is activated by seismic forces acting parallel to the wall plane, which usually induce diagonal shear cracks (fig. D.3).

Considering that in case of the aged structures, the mechanisms of the 1st failure mode category take place early during an earthquake, their study is very important, also in view of the design of interventions for improvement and/or seismic retrofitting. The analysis must be performed on a limited number of mechanisms, which are identified as probable to occur, considering the characteristics of the building and/or the crack patterns, eventually induced by an earthquake.



Figure D.1 Overturned tympanum and cracks indicating incipient overturning of the building facade



Figure D.2 Out of plane overturned wall



Figure D.3 Diagonal shear cracks in a masonry wall

D.2 TYPES OF ANALYSIS AND BASIC ASSUMPTIONS

Local mechanisms which may occur in the masonry walls can be studied by means of the kinematic analysis, which allows to determine the variation of the horizontal action that the structure is able to withstand as the mechanism develops. The kinematic analysis is based on the kinematic theorem of the limit analysis method. According to the kinematic approach, the application of virtual works theorem allows to estimate the load multiplier corresponding to the activation of the local mechanisms (damage limit state) and to the collapse (ultimate limit state).

Generally, two different kind of analysis are foreseen:

- Linear kinematic analysis, leading to the definition of the load multiplier, or the peak ground acceleration (PGA), activating the local mechanism;
- Non-linear kinematic analysis, leading to the definition of the local displacement corresponding to the local collapse.

For each significant local failure mode identified, the following procedure should be applied:

- *transformation of a part of the building in a mechanism (kinematic chain)*, through the identification of rigid bodies, delimited by the fracture planes and able to rotate or slide relative to one another according the damage and collapse mechanisms;
- *assessment of the α_o loads multiplier* corresponding to the mechanism activation (damage limit state);
- *assessment of the evolution of horizontal loads multiplier α* until the annulment of the horizontal seismic force, as a function of the increase of the displacement d_k of a suitable control point of the kinematic chain, point that is usually chosen close to the center of gravity of the considered part;
- *transformation of the curve so obtained in a capacity curve*, expressing the relationship between the spectral acceleration a^* and the spectral displacement d^* , and evaluation of the ultimate displacement, corresponding to failure (ultimate limit state);
- *safety assessment*, by controlling the compatibility of displacements and/or strengths required by the analysis with those offered by the structure.

The method applied is essentially based on the Heyman model [14], that is on the following assumptions:

- masonry tensile strength equal to zero;
- lack of sliding between the blocks;
- infinite masonry compressive strength.

However, in many cases, in order to arrive to a more realistic simulation of the actual behaviour, it is appropriate to improve the model taking under consideration, at least in an approximate form:

- the sliding between the blocks, considering the friction presence;
- the connections, also of limited strength, between the masonry walls;
- the presence of metal chains;
- the limited masonry compressive strength, considering the hinges set back with respect to the edge of the section;
- the presence of disconnected wall facades.

D.3 LINEAR KINEMATIC ANALYSIS

The linear kinematic analysis consists in the evaluation of the α_0 load multiplier that determines the local damage mechanism activation and it is mainly used to assess serviceability limit states (SLS).

Each macro-element is considered as a kinematic chain, composed of rigid blocks, connected by hinges (fig. D.3).

The following systems of forces must be taken into account:

- a system of vertical forces W_i and P_j , being W_i the weight of i -th masonry block, applied in its centroid, and P_j the vertical loads transmitted to the blocks by floors, roofs, vaults and other masonry elements not considered in the structural model;
- a system of horizontal forces, proportional through α to the vertical loads carried by each block, provided that they are not effectively transmitted to other parts of the building;
- internal horizontal forces Q_k transmitted by structural elements, like the thrusts of arches, domes and vaults;
- horizontal component of stabilizing external forces F_h , such as those transmitted by metal chains or FRP tie, or stabilizing internal forces, like those offered by the connections with adjacent walls.

The kinematic multiplier can be evaluated using the Virtual Work Theorem.

Assigned a virtual rotation θ_i to the i -th masonry block, the virtual displacements δ associated with it can be easily determined as a function of the geometry of the structure.

The multiplier α_0 is obtained by applying the Principle of Virtual Work, in terms of displacements, equalling the total work performed by the external and internal forces applied to the system at the act of virtual motion:

$$\alpha_0 \left(\sum_i W_i \delta_{xi} + \sum_j P_j \delta_{xj} \right) + \sum_k Q_k \delta_{xk} - \sum_i W_i \delta_{yi} - \sum_j P_j \delta_{yj} - \sum_n F_h \delta_{xn} = L_{fi} \quad (D1)$$

where δ_x are the virtual displacements of the horizontal forces, δ_y are the virtual displacements of the vertical forces and L_{fi} the virtual works of other internal forces.

D.4 NON-LINEAR KINEMATIC ANALYSIS

The non-linear kinematic analysis is devoted to investigate the displacement capacity of the structure when the collapse occurs through the considered mechanism.

The horizontal load multiplier α can be calculated not only on the initial configuration, as described above for linear analysis, but also on the macro-element displaced configurations: in this way, the evolution of the mechanism can be exhaustively defined, through a relationship $\alpha = \alpha(d_k)$ linking the load multiplier α with the displacement d_k of a control point of the macro-element, as explained in C8A.4 of Italian Standard [5]. The analysis will be terminated when the load multiplier becomes zero; the correspondent displacement of the control point $d_{k,0}$ is representative of the collapse situation.

The relationship $\alpha = \alpha(d_k)$ can be obtained analytically, graphically or numerically, applying the Virtual Work Theorem in the deformed configurations, and considering the effect of the displacements on the load configuration.

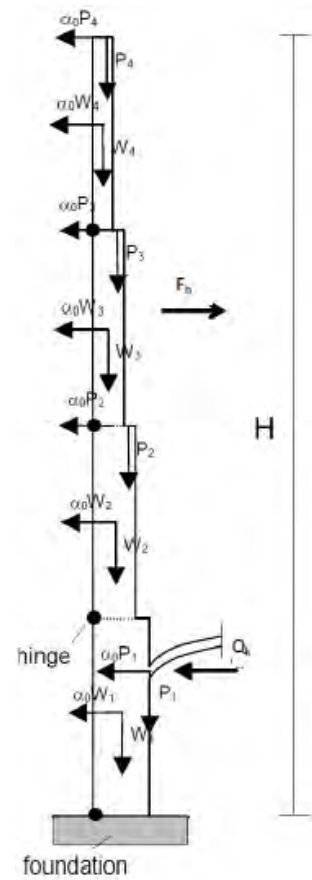


Figure D.4 Kinematic analysis of a macro-element

If the forces (weight forces, external or internal force) are not depending on the displacement, the $\alpha=\alpha(d_k)$ curve can be approximated by a straight line expressed by:

$$\alpha = \alpha_0 \left(1 - \frac{d_k}{d_{k,0}} \right) \quad (D2)$$

where: α and d_k are the load multiplier and the corresponding displacement in a generic displaced configuration; α_0 can be derived from linear kinematic analysis and $d_{k,0}$ from non-linear analysis in correspondence of $\alpha=0$.

D.5 CAPACITY CURVE

From the relationship $\alpha = \alpha(d_k)$ may be derived the capacity curve of the equivalent simple oscillator, in terms of acceleration a^* and displacement d^* .

The participating mass M^* can be estimated considering the virtual displacements of the points of the macro-elements as a simplified representation of its fundamental mode shape, so that it results:

$$M^* = \frac{\left(\sum_i W_i \delta_{xi} + \sum_j P_j \delta_{xj} \right)^2}{g \left(\sum_i W_i \delta_{xi}^2 + \sum_j P_j \delta_{xj}^2 \right)} \quad (D3)$$

where the sums are extended to all the applied weights W_i and vertical loads P_j associated with the macro-element under examination.

From (D1) and (D2), it can be determined the spectral acceleration a^* :

$$a^* = \frac{\alpha \left(\sum_i W_i + \sum_j P_j \right)}{M^*} \quad (D4)$$

In particular, introducing α_0 , we can obtain the spectral acceleration a_0^* which can be seen as the acceleration to be applied to the participating mass M^* to obtain the horizontal inertia forces activating the mechanism. In other words, a_0^* is the maximum spectral acceleration to which the macro-element can resist before the mechanism activation.

The spectral displacement d^* of the equivalent oscillator may be evaluated as the weighted average of the displacements of the points where the weights are applied. Approximately, we can define d^* on the base of the virtual displacements in the initial configuration:

$$d^* = d_k \frac{\sum_i W_i \delta_{xi}^2 + \sum_j P_j \delta_{xj}^2}{\delta_{x,k} \left(\sum_i W_i \delta_{xi} + \sum_j P_j \delta_{xj} \right)} \quad (D5)$$

where $\delta_{x,k}$ is the virtual horizontal displacement of the control point and the other symbols have been defined above.

When the curve may be approximated by a straight line, the capacity curve assumes the following expression:

$$a^* = a_0^* \left(1 - \frac{d^*}{d_0^*} \right) \quad (D6)$$

where d_0^* is the spectral displacement corresponding to $d_{k,0}$.

The resistance and the displacement capacity related to the SLS and ULS are derived from the capacity curve, at the following points:

- SLS: spectral acceleration a_0^* , corresponding to the activation of the mechanism;
- ULS: spectral displacement d_u^* , equal to the smaller between:
 - the 40% of d_0^*
 - the displacement corresponding to local situation inconsistent with the stability of the construction elements (i.e. fall of the beams).

D.6 SAFETY VERIFICATIONS

Serviceability Limit State

The safety verification SLS is satisfied when spectral acceleration corresponding to the activation of the mechanism, a_0^* , is higher than the acceleration demand.

In case of verifying an element placed directly on the ground, the acceleration demand is the peak ground acceleration, i.e. the spectral acceleration for $T=0$:

$$a_0^* \geq a_g(P_{VR}) \cdot S \quad (D7)$$

where:

a_g is the peak ground acceleration of the site for the given probability of exceeding, P_{VR} [4]

S is the subsoil coefficient [4].

In the case that the local mechanism affects a portion of the building situated at a certain height, the amplification of the acceleration must be taken into account, so:

$$a_0^* \geq S_e(T_1) \cdot \psi(Z) \cdot \gamma \quad (D8)$$

where:

$S_e(T_1)$ is the value of the elastic response spectrum corresponding to the fundamental period T_1 of the entire structure in the direction of the mechanism, $\psi(Z)$ is the amplitude of the mode shape, normalized with respect to the maximum mode shape amplitude, at the height Z of the constraints between the blocks involved in the mechanism and the rest of the structure, γ is the corresponding modal mass participation factor.

Ultimate Limit State

The safety verification of the local mechanism in the Ultimate Limit State consists of comparing the capacity spectral displacement d_u^* , as defined above, with the displacement demand obtained from the displacement spectrum for the secant period T_s :

$$T_s = 2\pi \sqrt{\frac{d_s^*}{a_s^*}} \quad (D9)$$

where:

$$d_s^* = 0,4 \cdot d_u^* \quad (D10)$$

a_s^* is the acceleration corresponding to d_s^* in the capacity curve.

When assessing an element placed directly on the ground, the check is satisfied when:

$$d_u^* \geq S_{De}(T_s) \quad (D11)$$

where $S_{De}(T_s)$ is the displacement elastic response spectrum.

In the case that the local mechanism affects a portion of the building situated at a certain height, the displacement elastic spectrum at the height of the portion involved in the mechanism must be considered; approximately:

$$d_u^* \geq S_{De}(T_1) \cdot \psi(Z) \cdot \gamma \cdot \frac{\left(\frac{T_s}{T_1}\right)^2}{\sqrt{\left(1 - \frac{T_s}{T_1}\right)^2 + 0,02 \frac{T_s}{T_1}}} \quad (D12)$$

CHAPTER 9 - ANNEX E

EVALUATION OF SOIL-STRUCTURE INTERACTION AND SECOND ORDER EFFECTS

The out-of-plane capacity curve of the studied system (masonry element and foundation + interacting soil) was studied taking into account the mechanical characteristics of the masonry and of four different layers of soil, and the second order effects due to bending induced by self weight acting eccentrically as a consequence of the horizontal displacements of the layers.

The method applied is the iterative method of *Finite Differences*.

The studied system was previously subdivided in several layers, each characterized by its own cross section, mechanical properties and compression force, N . For each layer, the moment-curvature diagram was calculated.

E.1 MOMENT-CURVATURE DIAGRAMS

The relationship between moment and curvature has been evaluated by a step-by-step procedure, in the following hypotheses:

- the principle of conservation of plane sections is valid;
- the materials are no-tension;
- the behaviour of the materials is elastic-perfectly plastic;
- the value of normal force, N , is constant for each layer.

For each value of the curvature of the section, χ , the vertical deformation of the centroid of the section, $\varepsilon_G^{(1)}$, is arbitrarily fixed; by this way, the neutral axis, and, by means of the constitutive law, the stress diagram and the resultant force, $N^{(1)}$, are determined. If the value of $N^{(1)}$ is not sufficiently close to the value of N really acting on the section, the procedure is repeated, changing appropriately the tentative value of ε_G , according to the *Newton-Raphson* algorithm.

When the requested approximation is reached, the value of $N^{(i)}$ satisfies the translational equilibrium; the corresponding value of the eccentricity allows to calculate M , i.e. the value corresponding to χ in the moment-curvature diagram. The procedure is repeated for a discrete series of values of χ ; so the diagram is built by segments.

For the case under examination, the curves to be determined are sixteen, one for each layer, taking into account the dimensions and vertical load acting on each of them. fig. E.1 shows the diagram found for the layer at the base of the pillar.

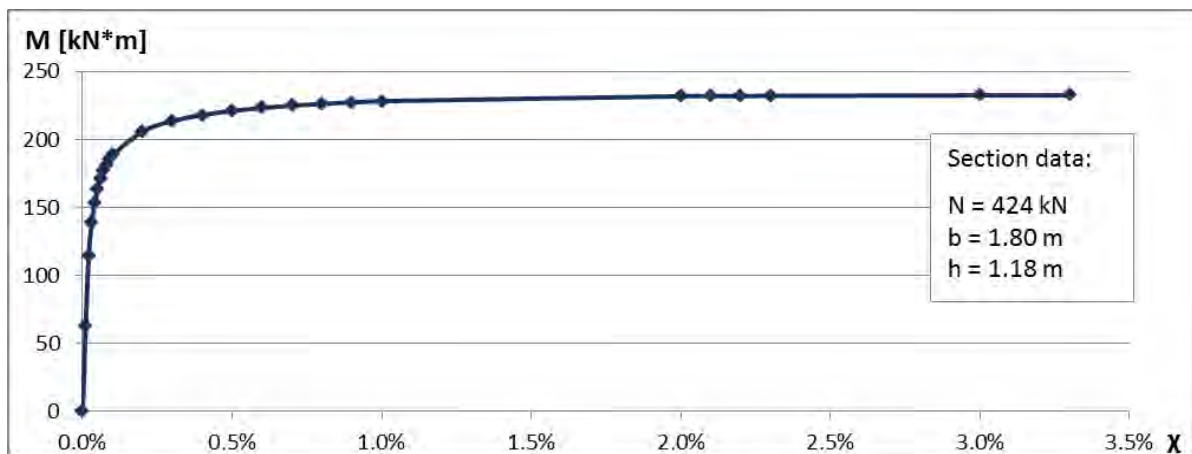


Figure E.1 Moment-curvature diagram corresponding to masonry section n°10

E.2 CALCULATION OF THE DEFORMED CONFIGURATION

Consider the model described in §4.4.5: each layer of the element is subjected to the corresponding self-weight and to a lateral force, F_i , simulating the seismic action; lateral forces are equal to the product of the mass of the layer for its height related to the extrados of the foundation, and for the acceleration of soil, a . The deformed configuration, considering the second order effects, is evaluated by a step-by-step procedure based on the *Finite Differences* method.

The general equation of *Finite Differences* expresses the displacement, y_n , of the n -th section according to the Taylor series, stopped to the third term:

$$y_n = y_{n-1} + q_n \cdot y'_{n-1} + \frac{q_n^2}{2} \cdot y''_{n-1} \quad (\text{E1})$$

where:

- q_n is the distance between n -th and $(n-1)$ -th sections.

Assuming that approximately y''_{n-1} is equal to the curvature of the section

$$y''_{n-1} = \chi_{n-1} \quad (\text{E2})$$

and that approximately:

$$y'_{n-1} = \frac{y_n - y_{n-2}}{q_n + q_{n-1}} \quad (\text{E3})$$

the general equation becomes:

$$y_n = \frac{q_{n-1} + q_n}{q_{n-1}} \cdot \left[y_{n-1} - \frac{q_n}{q_{n-1} + q_n} \cdot y_{n-2} + \frac{q_n^2}{2} \cdot \chi_{n-1} \right] \quad (\text{E4})$$

In the case study, such equations can be written for each layer, allowing to evaluate the horizontal displacement of the centroid of the layers. Initially, for each layer the first order moments are considered and the correspondent values of the curvature, χ , are obtained from the appropriate moment-curvature diagram. Using the equation (E4), the values of the horizontal displacements of the centroid of each layer, y_n , are calculated. At the next steps, the second order moments are considered too. When the displacement of the top section differs less than 10^{-6} m from that found in the previous step, the operation stops and the actual deformed configuration is found.

In fig. E.2 are shown the deformed configurations at each step of the procedure for a given set of lateral forces F_i , i.e. a given value of a .

In fig. E.3 are shown the final deformed configurations related to six different values of a .

E.3 DETERMINATION OF THE CAPACITY CURVE

The procedure described in §E.2 is applied for increasing values of the horizontal acceleration, a , obtaining the corresponding displacements, d , of the control point, placed in the centroid of the key section. The procedure stops when, in a certain layer, the resisting moment is reached, so that, also for little increments of the moment, the curvature increases very much and the procedure does not converge. The method allows to identify the critical section, in which the failure occurs.

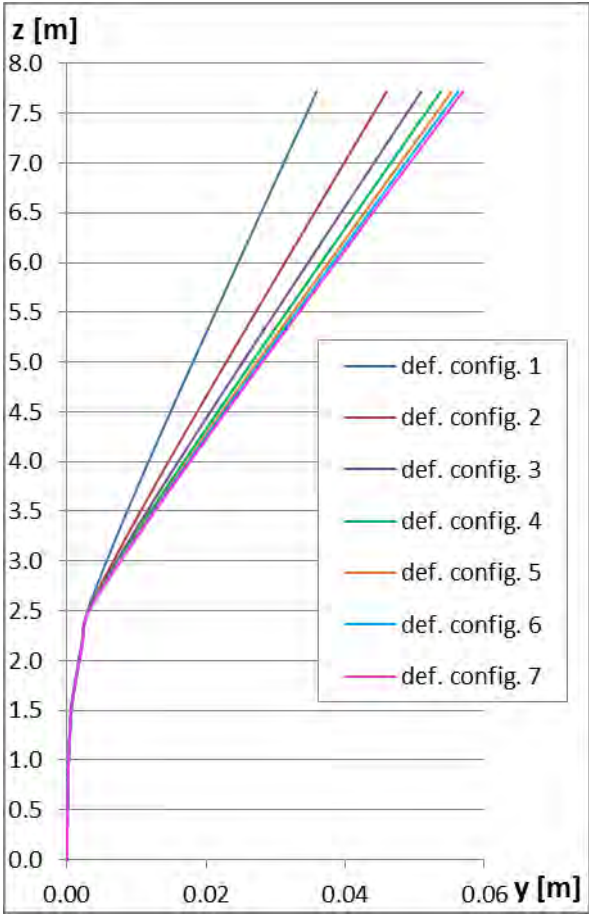


Figure E.2 Deformed configurations at each step for $a = 1,17 \text{ m/s}^2$

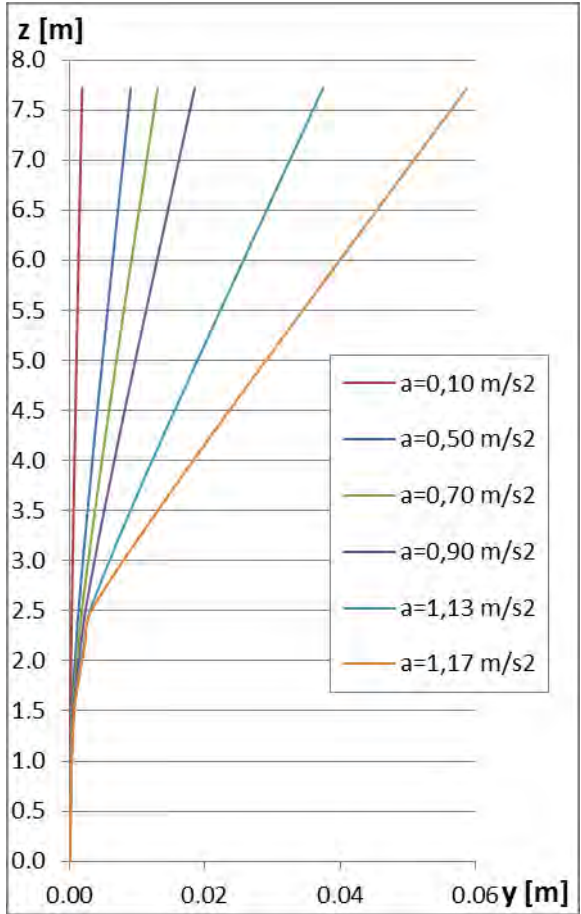


Figure E.3 Final deformed configurations corresponding to different values of a

CHAPTER 9 - ANNEX F

EVALUATION OF STABILIZING FORCES

In fig. F.1 a plan view of the arches, in which each block corresponds to a macro-element separated from the others in correspondence of the arch keys. Due to the out-of-plane rotation at the pillar's foot, the top of the macro-element moves transversely by δ . In the fig. F.1 only half of the interesting portion is represented, given the symmetry of the configuration.

As described in §4.5.2 a sort of arch effect may develop in the horizontal plane; so a compressed band takes place, as indicated by the area highlighted in grey.

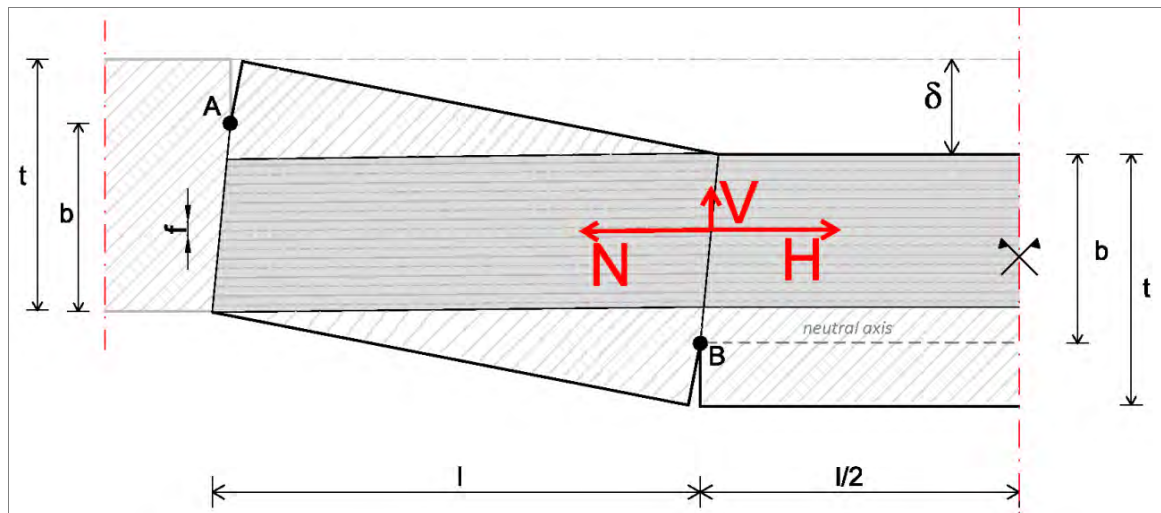


Figure F.1 The arch mechanism

The relationship between the force V acting between the macro-elements at the interface and the displacement δ , may be evaluated assuming the following hypotheses:

- 1) stress-block constitutive law for masonry;
- 2) the deformations are assumed to be zero in the external hinges of the constraint sections ($\epsilon(A) = 0$, $\epsilon(B) = 0$); as a consequence, the line BB' , representing the neutral axis, have constant length;
- 3) the level of stress is assumed to be the same in the constraint sections; therefore, in both sections, the depth of the neutral axis is equal to “ b ”.

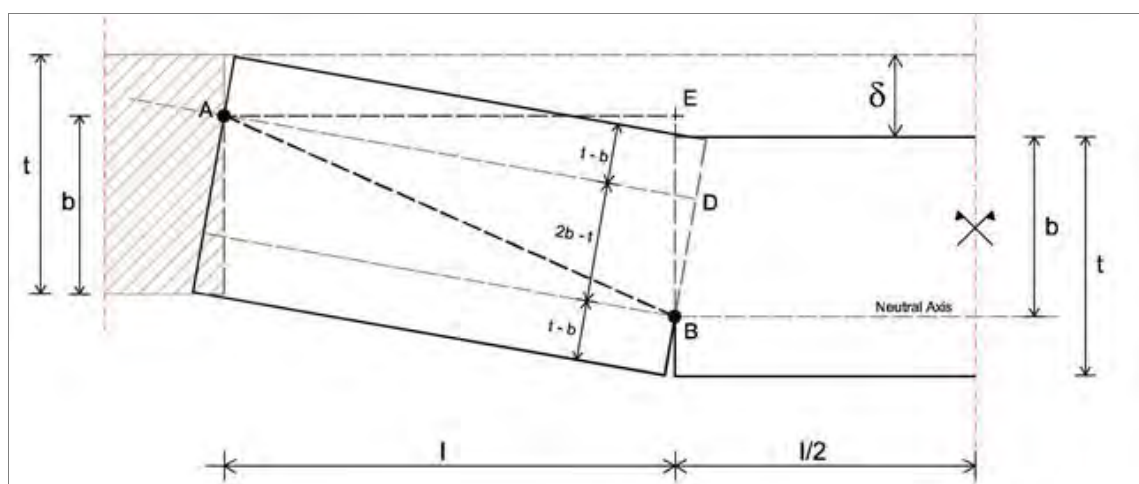


Figure F.2 The arch mechanism

Referring to fig. F.2:

$$\overline{BD} = |t - 2(t - b)| = |2b - t| \quad (\text{F1})$$

$$\overline{AD} = \overline{AE} = l \quad (\text{F2})$$

$$\overline{AB} = \sqrt{l^2 + (2b - t)^2} \quad (\text{F3})$$

$$\overline{EB} = b + \delta - (t - b) = \delta + 2b - t \quad (\text{F4})$$

Considering:

$$\overline{AE}^2 = \overline{AB}^2 - \overline{EB}^2 \quad (\text{F5})$$

$$l^2 = l^2 + (2b - t)^2 - (\delta + 2b - t)^2 \quad (\text{F6})$$

which yields the congruence condition:

$$b = \frac{t}{2} - \frac{\delta}{4} \quad (\text{F7})$$

At the constraint sections, considering a stress-block distribution of tension, the resultant of the compressions is:

$$N = 0,8bsf_m = 0,4\left(t - \frac{\delta}{2}\right)sf_m \quad (\text{F8})$$

where f_m is the compressive strength of the masonry.

Referring to fig. F.1:

$$f = (t - 0,4b) - (0,4b + \delta) = t - 0,8b - \delta \quad (\text{F9})$$

$$H = \frac{VL}{f} \quad (\text{F10})$$

$$N = \sqrt{H^2 + V^2} = V\sqrt{1 + \frac{l^2}{f^2}} \quad (\text{F11})$$

Equating (F8) and (F11), we obtain:

$$0,4\left(t - \frac{\delta}{2}\right)sf_m = V\sqrt{1 + \frac{l^2}{f^2}} \quad (\text{F12})$$

Finally, combining (F7), (F9) and (F12):

$$V(\delta) = \frac{0,04f_mst\left(2 - \frac{\delta}{t}\right)\left(3 - 4\frac{\delta}{t}\right)}{\sqrt{\left(0,6 - 0,8\frac{\delta}{t}\right)^2 + \left(\frac{l}{t}\right)^2}} \quad (\text{F13})$$

Expression (F13) leads to a diagram like that shown in fig. 67 §4.5.2.

It must be noted that, for small values of δ , the compressive force is small, so that the hypothesis of the stress block is not valid. In this case expression (F13) is supposed to be valid for δ greater than the displacement δ_e that determines the achievement of the elastic limit deformation in the most stressed fibre of the arch mechanism.

To preserve the smoothness of the curve itself, the first part of the diagram has been fitted with a cubic curve, passing from the origin, tangent to the curve determined as described above at the point δ_e and characterized by a decreasing slope in the left neighbourhood of δ_e itself, so obtaining the diagram illustrated in fig. 67 (§4.5.2).

CHAPTER 10: COLLAPSE OF THE RIVER VERDE VIADUCT SCAFFOLDING SYSTEM

Peter Tanner¹, Ramon Hingorani¹ and Antonio Menéndez Ondina²

¹Eduardo Torroja Institute for Construction Science, IETcc-CSIC, Madrid, Spain

²Civil Engineering School, University of Granada, Spain

Summary

Explicit risk analysis, a powerful structural safety decision-making tool, was applied to investigate the collapse of a movable scaffolding system (MSS) during construction of the River Verde Viaduct at Almuñécar, Spain in 2005, in which six workers lost their lives. Systematic qualitative risk analysis was conducted to identify the MSS structural safety hazards that may have theoretically caused the collapse. Based on exhaustive experimental and theoretical studies, these hazards were classified by their relevance to the accident. Logical combinations of the hazards were subsequently established to ascertain possible failure scenarios. This was followed by quantitative risk analysis, in which probabilistic methods were deployed to corroborate the likelihood of occurrence of the scenarios envisaged. Without such methods, no credible conclusions could have been drawn.

1 INTRODUCTION

Cost efficiency of the movable scaffolding systems (MSS) used in bridge construction is generally based as fully as possible on automating operating procedures to minimise construction labour costs. Theoretically, automated procedures should also contribute to enhancing on-site safety. The use of sophisticated ancillary equipment generally entails considerable risk, however, as denoted by a number of accidents taking place over a fairly short period of time in recent Spanish history [1]. One such accident involved the collapse of the underslung movable scaffolding used to build the viaduct over River Verde at Almuñécar, Spain, in which six workers plummeted to their death. The severity of the accident and especially its timing contributed to undermining public confidence in the professionals who design and build large-scale civil works and prompted considerable concern in the professional community itself.

The examining magistrate assigned to the case asked an interdisciplinary team of experts from the Eduardo Torroja Institute for Construction Science (IETcc-CSIC), the University of Granada (UGR) and the Polytechnic University of Madrid (UPM) to draw up a forensic report with a dual purpose: on the one hand, to establish the causes of the failure and the mechanism involved, and on the other, to determine whether in spite of the collapse the structure met minimum reliability standards.

The present paper addresses the studies conducted in connection with the first of the aforementioned purposes. The investigation was based on explicit risk analysis, divided into two clearly distinct stages: qualitative and quantitative assessment. The former entailed identifying possible failure scenarios, and the latter calculating the likelihood of those scenarios by means of probabilistic analysis.

2 RIVER VERDE VIADUCT

River Verde Viaduct is located on Mediterranean Highway A7 between Almuñécar-La Herradura and Almuñécar-Taramay. With a curved plan layout (941 m radius) and a total length

of 563.5 m, it is divided into two 51.75 m side spans and 8 centre spans measuring 57.5 m each.

The two mid-spans, located over the river itself, rest on a reinforced concrete arch (Figure 1) whose hollow rectangular cross-section is characterised by variable dimensions: it is 3 to 2 m deep by 6.5 to 4 m wide. The remaining spans are supported by reinforced concrete piers with a maximum height of 67.5 m. The bridge superstructure consists of two parallel, continuous, prestressed concrete box girders with 11.8 m wide decks. Their depth is constant at 2.3 m, except at the supports where it is variable increasing to 3.8 m



Figure 1 River Verde Viaduct in progress (photograph: F. Nederlof)

3 THE MOVABLE SCAFFOLDING SYSTEM

The main components of the underslung MSS used to build the bridge superstructure are shown in Figures 2 and 3. The formwork and its supports rested on two main parallel truss girders, spaced at 9.5 m. Each main girder was subdivided into three parts: the centre, consisting of four parallel trusses, and the front and rear, consisting of two parallel trusses each. The centre was bolted to the front and rear by means of connection frames (Figures 2, 9 and 10) made of welded vertical and horizontal steel profiles and stiffeners (see item 6.4 for further details).

The two main girders were braced transversely by four truss girders (hereafter, the transverse bracing girders) and a double-T beam (Figure 2). The bracing girders were fitted with sliding devices to enable the structure to clear the piers, and the double-T beam was positioned above the pier crowns for the same reason.

The main girders rested on supports fitted with sliding bearings and hydraulic jacks so they could be moved both longitudinally and transversely. These supports stood on a base platform attached to the top of the piers with ties (Figure 3). At pier P-6, positioned at the top of the arch, an ancillary structure consisting of longitudinally and transversely braced parallel steel frames was needed between the base platform and the supports to raise it to the required elevation (Figure 3).

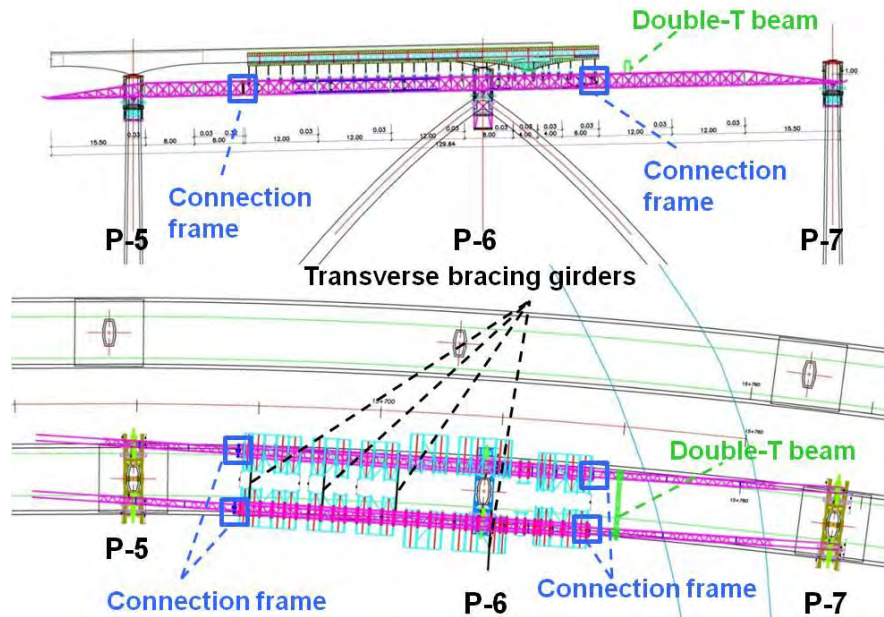


Figure 2 Elevation and plan view of viaduct and MSS

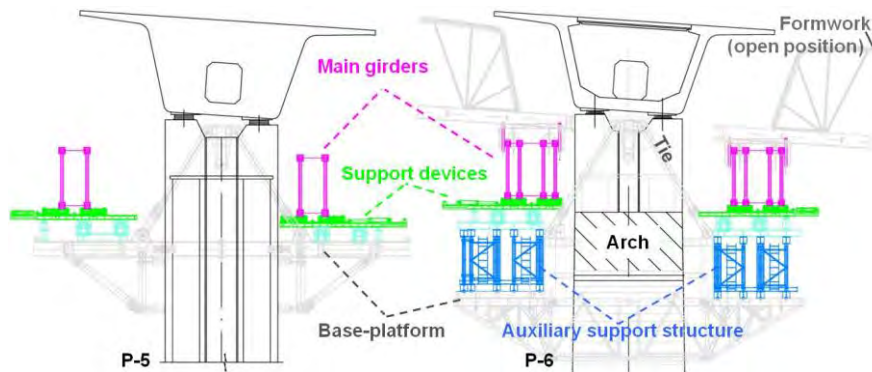


Figure 3 Cross section at pier P-5 (left) and P-6 (right)

4 THE ACCIDENT

After the concrete for span 6 (between piers P-5 and P-6; see Figure 2) had been cast and prestressed, the formwork was folded back and the rear part of the main girders was freed from the bridge deck erected prior to span 6. The MSS was then moved transversely with the hydraulic jacks fitted onto the support devices at piers P-5 and P-6 to align the system with bridge horizontal geometry. Longitudinal launching was subsequently undertaken, for which purpose the front transverse bracing girder had to slid open for the structure to clear pier P-6. Upon arrival at P-7, the launching nose was lifted by a truck crane, as shown in Figure 1. At a distance of about 2 m between the tip of the launching nose and pier P-7, a damaged electric cable caused a power supply outage in the launching equipment that was driving the right main girder (left and right are referred here to the launching direction). Differential travel of the left and right main girders ensued and the launching operation was halted. The approximate position of the MSS at the time is shown in Figures 1 and 2. A few moments later, the structure collapsed (Figure 4). Eye witnesses later reported that the collapse began at the left main girder, while the right girder, to which it was connected by the transverse bracing girders, was dragged down with it in its fall. The accident also induced the collapse of the entire support structure at P-6 (Figure 3).



Figure 4 Collapse of the MSS (photograph: F. Nederlof)

5 EVALUATION PROCEDURE

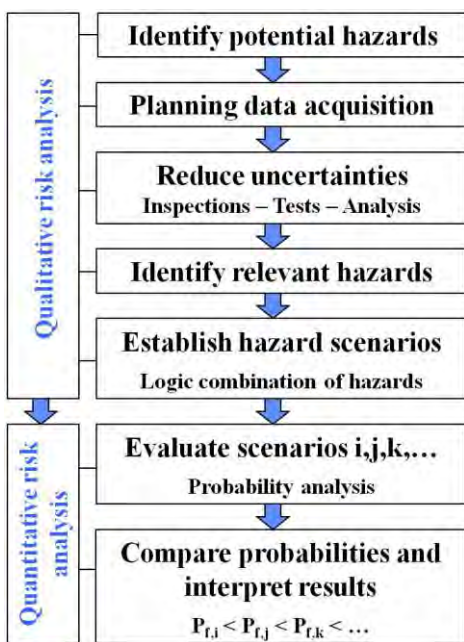


Figure 5 Evaluation flow chart

One of the major differences between assessing existing structures, whether or not they have collapsed, and designing new structures revolves around the information available. In the former, many characteristics can be obtained from inspections and tests on the structure that during the design stage could only be estimated. Nonetheless, today's structural codes and standards still lack suitable methods for including site-specific data in the structural safety evaluation procedure.

An explicit risk analysis procedure (outlined in Figure 5) able to accommodate updated information, was applied to investigate the collapse of the MSS during construction of the River Verde Viaduct. This procedure was divided into two stages: qualitative and quantitative risk analysis. The former aimed primarily to identify the hazards which may have triggered the accident and to combine them logically to establish possible hazard scenarios. The latter was intended to deliver a quantitative, reliability based evaluation of those scenarios with a view to establishing their likelihood. The main steps of the procedure are outlined below.

Evaluating the causes of a structural accident calls, firstly, for identifying all the possible hazards to which the structure may have been exposed prior to when the accident occurred. This step is of crucial importance, since any unidentified relevant hazard necessarily introduces a bias in the decisions adopted during the subsequent evaluation, as a result of which misleading conclusions may be drawn. Moreover, it constitutes the basis for planning subsequent data acquisition. Inspections, tests and analyses may reduce the uncertainties associated with the potential hazards identified and provide grounds for distinguishing between the hazards most and least likely to have been involved in structural collapse.

Several hazards may concur in space and time, giving rise to what is known as a hazard scenario. Such situations normally generate higher risks than any individual hazard separately.

They may be defined with fault tree analysis [2], in which combinations of circumstances that may lead to an undesired event are represented in a logic diagram. Based on the classification of the potential hazards by their relevance to the accident, each scenario is characterised by a combination of leading and accompanying actions and influences.

Once the possible hazard scenarios have been qualitatively established, their associated risk can be quantified. Site-specific data is used to update models for load and resistance variables and probabilistic methods based on reliability theory [3] are then applied to determine the likelihood of the occurrence of a given hazard scenario and a comparison is conducted. Nonetheless, the notional nature of the likelihood of failure precludes any interpretation of the data in absolute terms.

6 QUALITATIVE RISK ANALYSIS

6.1 Situation

As noted in section 4, the MSS used to build River Verde Viaduct collapsed after span 6 of the first of the two parallel bridge decks had been cast and prestressed. The previous spans had been erected using a nominally identical construction procedure. The following two circumstances differed from the conditions prevailing during construction of the first five spans, however:

- The specific geometry of the bridge substructure at pier P-6 (Figure 2), characterised by the presence of the arch, called for an ancillary support structure at that point (Figure 3).
- The power supply outage mentioned above led to differential travel in the left and right main girders (see section 4).

6.2 Hazard identification

The many identified potential hazards to the MSS were related both to the actions and influences to which the structure was exposed and its resistance. Some of these hazards could be immediately ruled out as a possible origin of the accident and were thus disregarded in the course of the investigation. These included, for instance, action effects associated with ground movements resulting from unforeseen settlement or seismic loading and unforeseen wind action effects. The investigative efforts focused primarily on the potential hazards listed below:



Figure 6 Position of the formwork before the accident

- possible deviation of the permanent loads from their nominal position, with the respective rise in the intensity of action effects, particularly as regards the position of the formwork immediately prior to the accident (see Figure 6), which would infer that its support structures had been folded back in their entirety to clear pier P-6, whereas nominally (see Figure 2), the formwork should have been only partially folded back;
- the 0.18-m difference between left and right main girder travel (inferred from the detected difference in the extension of the left and right main girder jacks) and the respective action effects on the MSS;
- possible deviations in MSS support elevations

or main girder precamber from their nominal values and the deformation concomitantly imposed on the structure;

- possible slow motion impact between the MSS and the bridge structure due to their differing (straight and curved, respectively) horizontal geometry, which may have exposed the MSS supports to an unforeseen horizontal force;
- possible deviations from construction tolerances in critical structural members such as the connections between the main girder modules, including highly stressed welded joints in the connection frame between the central and rear main girders (Figure 2), leading to deviations from the design resistance values;
- the effects of load inversion, including dynamic action on the structure, introduced during successive launching and casting cycles and their impact on the resistance of the main girder module interconnecting elements, particularly the connection frame between the central and rear main girders (Figure 2).

6.3 Inspections, tests and analyses

A substantial number of inspections, tests and analyses were conducted to reduce the uncertainties associated with the main hazards described above and ascertain the relevance of each hazard to the accident. Inasmuch as a detailed description of data acquisition lies outside the scope of the present paper, it is discussed only briefly in the following. The key observations and conclusions deriving from these experimental and analytical studies are set out in item 6.4.

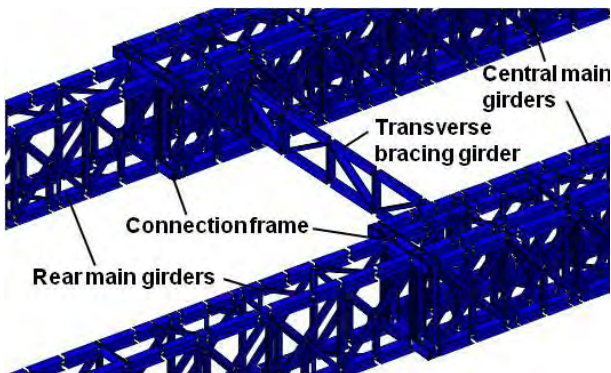


Figure 7 Partial representation of the numerical model used for structural analysis



Figure 8 Testing pier P-6 ancillary support

The MSS was monitored for action effects during the full launch of a system similar to the one that collapsed, used to build nearby River Seco Bridge [4]. Monitoring focused particularly on the action effects due to differential travel in the left and right girders.

A numerical model (Figure 7) was developed to determine the action effects on MSS structural members. Specific on-site circumstances prevailing immediately prior to the collapse, such as the position of the formwork (Figure 6), were taken into consideration in this structural analysis. In addition, the numerical model was applied to study the effects of any support elevation or main girder precamber deviations from the nominal.

The possibility of a slow motion impact between the bridge structure and the MSS and the respective transfer of a horizontal force to the MSS supports was explored by experimental testing. This entailed making laboratory replicas of the on-site supports at piers P-5, P-6 and P-7 (Figure 3) at IETcc-CSIC facilities. Figure 8 depicts the test conducted on the pier P-6 ancillary support. First

vertical loads, V , representing the vertical support reactions in the main girders, and then gradually increasing horizontal loads, H , were applied to the support structure until it failed. The loads applied were recorded during these trials, along with the vertical and horizontal displacements observed in the support devices.

The structural resistance of both the connection frame (Figures 2 and 7) and the joints between it and its adjacent modules was determined from tests run on six replicas, four of which were nominally identical to the frame in place on the collapsed structure [5]. The frames were loaded to failure and the forces applied, strain values and displacements at different characteristic points were recorded. Lastly, the findings were tested statistically to develop updated probabilistic models for the subsequent quantitative assessment (section 7).

The connection frame fracture surfaces were analysed and compared to the surfaces found in the collapsed structure [6]. The main objective was to seek evidence of the possible accumulation of plastic deformation, which could theoretically have been generated by variable load cycles and accentuated by dynamic effects introduced during successive launching and casting. Dynamic effects were also monitored during the aforementioned MSS launch on nearby River Seco Bridge.

6.4 Hazard classification

The inspections, tests and analyses summarised in item 6.3 furnished the grounds for separating the hazards regarded to be relevant to the collapse of the MSS from those esteemed to be only scantily relevant or wholly irrelevant:

Irrelevant hazards

- The increase in load effects attributable to the 0.18 m difference in the distance travelled by the left and right main girders was practically negligible.
- The experimental studies addressing the possibility of a slow motion impact between the MSS and the bridge deck (Figure 8) showed that the occurrence of a horizontal force of the magnitude required to destabilise the support structures was highly unlikely under real circumstances.

Scantily relevant hazards

- The increase in load effects attributable to the deviation from the nominal position of the formwork (Figure 6) was one of the possible causes explored. Since the analysis showed, however, that this alone was unlikely to have triggered the accident, it was regarded as a hazard of minor relevance.
- The possible deviations in MSS support elevations or main girder precamber from their respective nominal values were also regarded as scantily relevant hazards.

Relevant hazards

Fracture surface analysis [6] of both the connection frame positioned at the rear of the left main girder and its adjacent modules (Figures 2 and 7) revealed that the collapse very likely originated in that area, possibly in association with the failure of some of the welds in the downstream connection to the lower chords shown in Figure 9 (hereafter, the critical joint). The evidence supporting this conclusion came from two sources: the fact that this critical joint was also the joint most heavily loaded in the left main girder; and the very brittle structural behaviour observed for this joint during the structural trials conducted on the nominally identical replicas of the connection frame [5] (item 6.3). This theory is, moreover, compatible with the eye witness

accounts of the accident (section 4). Two relevant hazards potentially able to cause the welds to fail were identified:

- resistance loss in one of the welds between the vertical profile and the stiffeners (Figure 9) due to the possible accumulation of plastic deformations;
- alteration of the boundary conditions prevailing around the non-prestressed bolts connecting the connection frame to its adjacent modules (Figure 9), due to the loosening of one or several nuts, with the resulting internal load redistributions and subsequent failure of one of the welds.

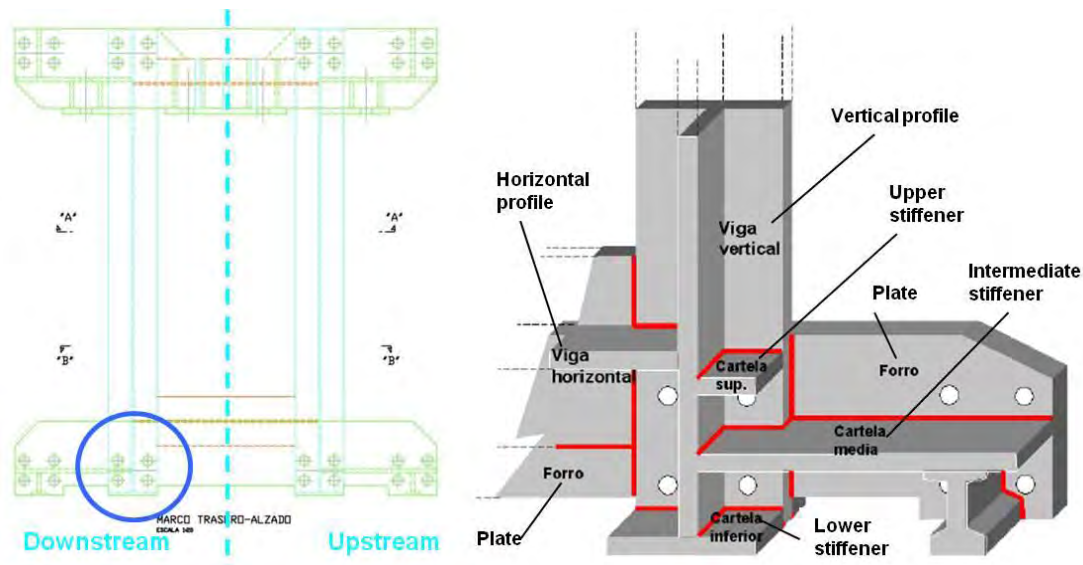


Figure 9 Position of critical joint in the connection frame (left); drawing of frame [6] (right)

While the analysis of the connection frame fracture surface revealed no clear evidence of accumulated plastic deformation-induced failure [6], neither could such a possibility be wholly ruled out on the basis of that analysis. It was consequently explored as one of the potential relevant hazards. The analysis did suggest, however, that weld failure was more probably a result of stress redistributions attributable to prior alteration of the load transfer mechanism in the joint. The loosening of one or several of its bolt nuts may have generated such an alteration, the inference being that the second of the relevant hazards listed above was more likely to have triggered the collapse of the MSS. The use of non-prestressed bolts exposed to variable, sign-changing load cycles accentuated by dynamic effects entails particular risk.

6.5 Hazard scenarios

The most likely hazard scenarios were established on the grounds of hazard classification into three categories depending on their relevance to the collapse of the MSS (item 6.4). The results of that exercise are shown below:

Leading influence

- loosening of at least one bolt nut at the critical joint, *and/or*
- failure in one of the welds between the vertical profile in the connection frame and the intermediate stiffener in the critical joint;

Accompanying actions and influences

- structure self-weight;

- permanent loads, given the actual position of the formwork (Figure 6);
- 0.18 m differential travel between the left and right main girders (although classified as irrelevant, this hazard was observed on site and consequently taken into consideration in the subsequent analysis);
- nominal geometry of the MSS, including precamber;
- actual MSS support elevations.

7 QUANTITATIVE ASSESSMENT

The updated data on action effects and respective resistance values found during inspections, tests and analyses were applied in the quantitative assessment of the hazard scenarios identified in item 6.5. Figure 11 shows the expected value of the tensile force to be transferred by the critical joint (Figure 10), $\mu_{TE,int}$ (red line), versus the distance, x , between the P-5 rear support and the connection frame. Prior to collapse, this value was estimated to be $\mu_{TE,int,acc} = 1477$ kN, i.e., slightly below the maximum value, $\mu_{TE,int,max} = 1493$ kN, which would be reached upon the arrival of the launching nose at P-7 and its elevation by the truck-crane.

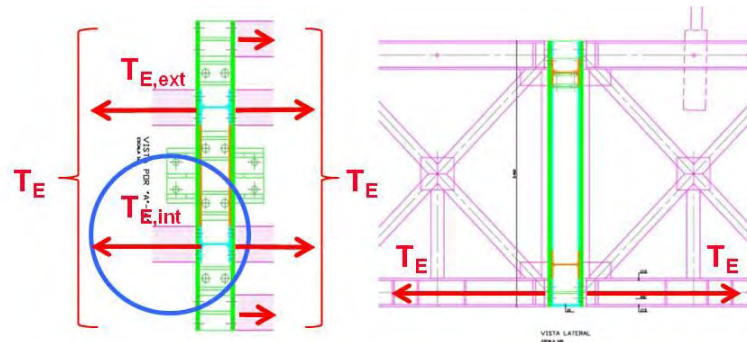


Figure 10 Tensile force transfer at the connection frame (left: plan view, right: elevation)

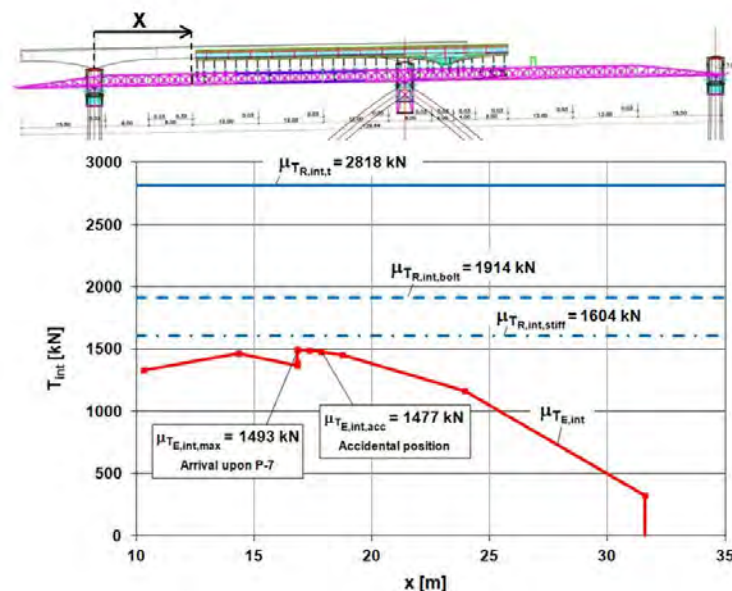


Figure 11 Variations in the expected action effects and resistance values at the critical joint

The expected critical joint resistance was calculated to be $\mu_{TR,int,t} = 2818$ kN (Figure 11). Assuming that the upper right bolt in the critical joint worked loose (Figure 9), estimated resistance would decline to $\mu_{TR,int,bolt} = 1914$ kN. If, in addition, the welded connection between

the vertical profile in the connection frame and the intermediate stiffener failed (Figure 9) under the stress redistributions mentioned in item 6.4, the estimated joint resistance would dip to $\mu_{TR,int,stiff} = 1604$ kN. While this value is still larger than the tensile force expected at the joint, ($\mu_{TE,int,acc} = 1477$ kN), this comparison is based on estimated values. Since the basic variables involved in structural analysis are random and subject to uncertainties, safety evaluation should be conducted in terms of the probability of failure in the context of explicit probabilistic analysis, as outlined in section 5. Updated probabilistic model data for the basic variables involved in both action effects and structural resistance delivered a probability of failure of $p_f = 0.06$, assuming a loose upper right bolt in the critical joint. When weld failure was factored in, the probability of failure for the critical joint rose to approximately $p_f = 0.3$. These values are several orders of magnitude higher than the implicit 10^{-5} to 10^{-7} ceiling for probability of failure accepted by structural design codes (reference period: 50 years) [2]. These computations denote the existence of unstable equilibrium at the critical joint, corroborating the likelihood that bolt nuts loosening in the joint was the event that triggered MSS collapse.

8 CONCLUSIONS

The experimental and analytical analyses conducted on the occasion of the investigation into the collapse of the MSS used to build River Verde Viaduct were able to determine where collapse was triggered and that the first element to fail was very likely the joint between the rear connection frame on the left main girder and the adjacent girder module. The primary cause of joint failure could not be unequivocally established, however. The inspections, tests and analyses run, whose findings were compatible with eye witness accounts, nonetheless suggested that the accident was in all likelihood caused by the loosening of one or several bolt nuts in the aforementioned joint, induced by load inversion and the concomitant dynamic effects generated during previous MSS launch-concrete casting cycles. Stress would then be redistributed and concentrate in certain parts of the joint, all of which would be favoured by the conceptual layout of this detail. Such stress concentration would affect the welds joining the intermediate stiffener to the vertical profile in the connection frame (Figure 9), where initial fracture probably occurred. As a result, the overloaded welds would fail and generate further stress redistribution at the critical joint, whose brittle behaviour would trigger the failure of other connection components. This chain reaction would ultimately lead to failure of the joint and hence of the connection between the frame and its adjacent rear module, inducing MSS collapse.

Such a failure mechanism is associated with unorthodox detailing, particularly as regards the conceptual design of the critical joint. Indeed, failure of this joint was closely related to complex load transfer mechanisms across a number of inefficiently oriented connection elements such as stiffeners and welds. Moreover, no provision was made for high intra-joint stress redistribution capacity, which would have afforded ductile structural behavior and alternative load paths. Finally, the consequences of using non-prestressed bolts in joints exposed to variable load cycles were clearly underestimated.

REFERENCES

- [1] Taner, P., Bellod, J.L., Sanz, D. And Hingorani, R., Lessons from incidents attributable to the uncertainties in bridge launching illustrated by a case study, *Civil Engineering and Environmental Systems*, 2012, DOI:10.1080/10286608.2012.733376.
- [2] Vrouwenvelder, T., Holicky, M., Tanner, P., Lovegrove, R. And Canisius, G., “Risk assessment and risk communication in civil engineering”, International Council for Research and Innovation in Building and Construction, *CIB Publication n° 259*, Rotterdam, 2001. ISBN 90-6363-026-3, 62 pages.

- [3] Hasofer, M. and Lind, N.C., “Exact and Invariant Second-Moment Code Format”, *Journal of Engineering Mechanics*, ASCE, Vol.100, EM1, February 1974, pp.111-121.
- [4] KINESIA, *Autovía del Mediterráneo A-7. Tramo Almuñécar (La Herradura) – Almuñécar (Taramay). Viaducto de Río Seco. Ensayo de autocimbra*, KINESIA Ingeniería de Auscultación, Madrid, 25 de julio de 2006.
- [5] INTEMAC, *Informe de resultados de la monitorización realizada en los cuatro ensayos a escala real efectuados sobre una cimbra similar a la que sufrió el colapso durante la construcción del viaducto sobre el Río Verde en Almuñécar (Granada) el 7 de noviembre de 2005*, Instituto Técnico de Materiales y Construcciones (INTEMAC), Torrejón de Ardoz, 11 de julio de 2006.
- [6] DCM-ETSICCP-UPM y CENIM-CSIC, *Cimbra colapsada del viaducto sobre el Río Verde en la autovía A7. Estudio visual y fractográfico del marco de unión entre las baterías doble y simple del lado izquierdo, de sus pernos de conexión a las baterías, y de los nuevos marcos ensayados*, Departamento de Ciencia de Materiales (ETSICCP-UPM) y Centro Nacional de Investigaciones Metalúrgicas (CSIC), Madrid, 27 de febrero de 2007.

CHAPTER 11: PREDICTING FLOODS AND DAMAGE TO INFRASTRUCTURES

Milan Holický¹, Miroslav Sýkora¹, Dimitris Diamantidis²

¹ Klokner Institute, Czech Technical University in Prague

² OTH Regensburg, Regensburg

Summary

Extreme flooding in Central Europe in August 2002 affected a number of infrastructures. Significant economic losses were related with damage to a subway system. Presented statistical evaluation of the extreme annual flows provides valuable background information for assessments of flooded structures. Based on the obtained experience, recommendations proposed for design and assessment of structures and infrastructures potentially endangered by flooding include analyses of local data, safety measures and structural robustness.

1 INTRODUCTION

Extent of the flooding in Central Europe in August 2002 had been unexpected and, therefore, partly inadequate pre-flood protective measures had been taken. Emergency measures hastily accepted during the flooding included protective barriers, immediate removing floating debris from bridges, additional anchors of ships on rivers and transport of persons from endangered areas. Despite these measures, damage to construction works, road networks and other infrastructures was on an unprecedented scale. Particularly severe consequences were observed in the historic city of Prague where recorded water levels seemed to be exceptionally high. The Vltava River during the flooding is shown in Fig. 1.



Figure 1 The Vltava River in Prague during the flooding in 2002

Significant economic losses were related with damage to a subway system. Although the subway system was protected by several types of barriers, some of them were not activated in due time and others failed under a long-term water pressure [1]. A flooded subway station is shown in Fig. 2.



Figure 2 Flooded station of Prague subway system

Assessments of damaged structures were intended to answer the following questions:

- Was the flooding really so exceptional and unpredictable?
- What were main causes of structural failures?

After the flooding various precautions such as safety barriers and river management including construction of polders, modifications of depth, width and roughness of a river channel have been considered to reduce consequences of future flooding. Decisions concerning these expensive measures should be preferably based on cost optimisation, taking into account potential societal and economic consequences of flooding. However, such an analysis needs a theoretical model suitable for predicting river flows and extents of future flooding.

Available hydrological data are thus statistically evaluated to develop the required model for flows of the Vltava River in Prague and are described in section 2. The method of moments and method of maximum likelihood [4, 12] are applied to analyse the data and to answer frequent questions of forensic experts as well as civil engineers:

- What is the actual return period corresponding to the observed water level?
- Does the measurement recorded in 2002 affect estimates of characteristic and design values of flows?

Note that the prediction of flows is needed also in an insurance sector [2]. These aspects are described in section 3. Findings of extensive investigations of failure causes are also reviewed in section 4 and risk based recommendations for design and assessment of structures endangered by flooding are outlined in section 5. Finally conclusions are drawn in section 6.

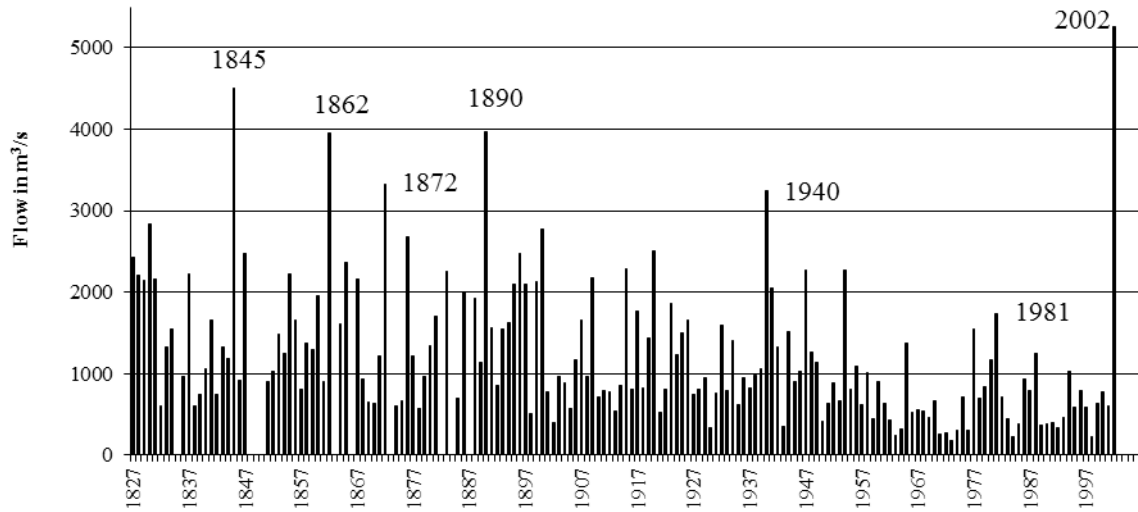


Figure 3 Annual maximum flows of the Vltava River in Prague

2 STATISTICAL MODELLING

2.1 Statistical evaluation of annual maximum flows

Annual maximum flows of the Vltava River in Prague measured by the Czech Hydrometeorological Institute since 1827 are further analysed. A time series of available measurements is indicated in Fig. 3. Sample characteristics are initially estimated by the classical method of moments [4, 12] for which prior information on the type of an underlying distribution is not needed.

Point estimates of the characteristics are given in Table 1 for the sample without and with the observation q_{2002} . It appears that the sample mean, standard deviation and coefficient of variation are influenced by the flow q_{2002} rather insignificantly (the enhancing factor varies in the range from 1.02 up to 1.07). However, the coefficient of skewness seems to be considerably affected by q_{2002} as the enhancing factor is 1.22.

Table 1 Sample characteristics of the annual maxima (sample size $n = 165$ or 166).

Sample characteristic	Relationship	Without q_{2002}	With q_{2002}	Enhancing factor
Mean	$m = \frac{1}{n} \sum_{i=1}^n q_i$	1200 m ³ /s	1220 m ³ /s	1.02
Standard deviation	$s = \sqrt{\frac{1}{n-1} \sum_{i=1}^n (q_i - m)^2}$	790 m ³ /s	850 m ³ /s	1.07
Coefficient of variation	$v = \frac{s}{m}$	0.66	0.69	1.05
Skewness	$w = \frac{n}{(n-1)(n-2)s^3} \sum_{i=1}^n (q_i - m)^3$	1.43	1.74	1.22

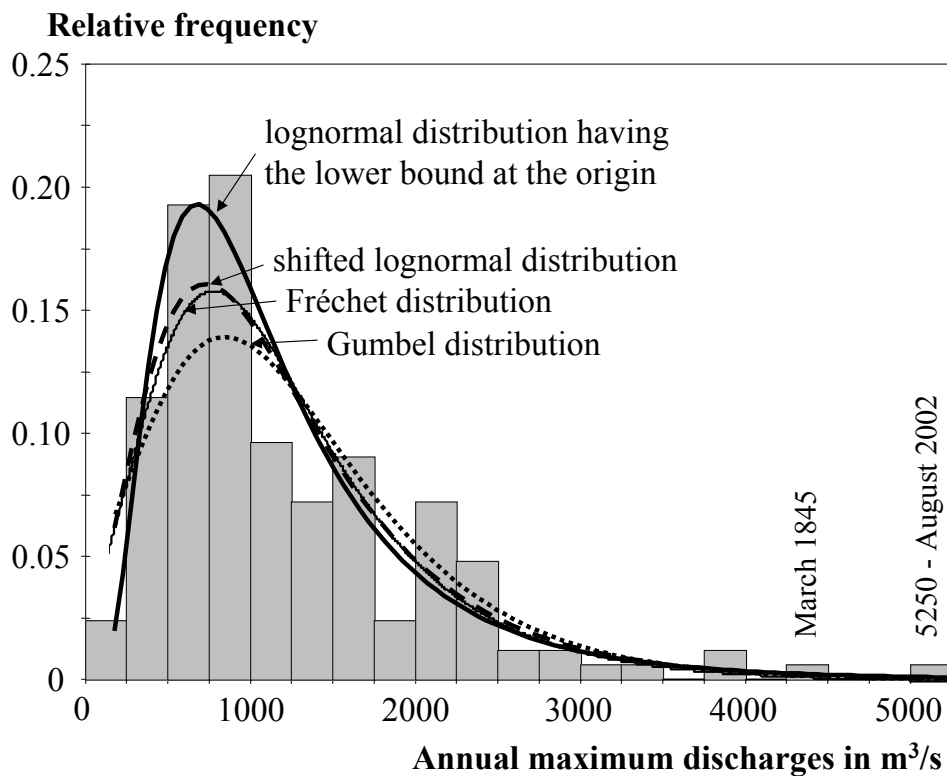


Figure 4 Histogram of the annual maxima and the selected theoretical models.

2.2 Probabilistic models

The sample characteristics provided in Table 1 indicate that the annual maxima might be described by a two-parameter lognormal distribution having the lower bound at the origin (LN0) or by a more general three-parameter shifted lognormal distribution having the lower bound different from zero. Other possible theoretical models are extreme value distributions: the type II called also the Fréchet distribution or type I, a popular Gumbel distribution with the constant skewness 1.14 [12].

Probability density functions of the considered theoretical models and a sample histogram are shown in Fig. 4. It appears that the lognormal distribution LN0 describes well the data.

To compare goodness of fit of the considered distributions, Kolmogorov-Smirnov and chi-square tests [4, 12] are applied. It appears that the lognormal distribution LN0 is the most suitable model. Less favourable test results are observed for the three-parameter shifted lognormal and Fréchet distribution and the worst test results are obtained for the Gumbel distribution as the fixed skewness of 1.14 may be rather small. Numerical results are provided elsewhere [3].

Note that appropriate models should be selected on the basis of the statistical tests taking into account general experience with distributions of flows at other localities. Experience of the Czech Hydrometeorological Institute indicates that the lognormal distribution LN0 might be a suitable model. Therefore, this distribution is considered in estimation of extreme flows only.

2.3 Parameter estimation

The method of moments applied to estimate the sample characteristics is often assumed to be not very efficient as variance of the estimator is often rather greater. Assuming that the

underlying distribution of the sample is the lognormal distribution LN0, the sample characteristics can be improved by the method of maximum likelihood, which is considered as an efficient method for parameter estimation in case of large samples.

Comparison of the distribution parameters estimated by the method of moments and the method of maximum likelihood indicates that the estimates of the mean are nearly independent of the applied method (differences about 1 %). However, the standard deviations estimated by the method of maximum likelihood are systematically greater than those obtained by the method of moments (differences about 10 %). More details can be found in the recent study [3].

3 ESTIMATION OF EXTREMES

Upper fractiles q_p of the lognormal distribution LN0 are further approximated by the estimate $q_{p,\text{cov}}$ that “covers” the fractile q_p (i.e. is greater than the fractile q_p) with a given confidence level γ

$$P(q_{p,\text{cov}} > q_p) = \gamma \quad (1)$$

Details of the so-called coverage method are given e.g. in ISO 12491 [5] that provides general techniques for quality control of building materials and components used in building or other civil engineering works. The confidence level 0.75 is often accepted in civil engineering applications as indicated e.g. in EN 1990 [6] for the basis of structural design. In this document, the characteristic value q_k is obtained as the 0.98 fractile of annual maxima whilst the design value q_d is the fractile of the life-time maxima corresponding to the probability

$$p_d = 1 - \Phi(\alpha_E \times \beta) = 1 - \Phi(-0.7 \times 3.8) = 1 - 0.0039 \quad (2)$$

$\Phi(\)$ is the cumulative distribution function of the standardised normal distribution, the FORM sensitivity factor α_E is approximated by the value -0.7 recommended for the leading action [6] and the target reliability index β is 3.8 for a fifty-year reference period. Assuming statistical independence of the annual maxima, the design value is estimated as follows

$$q_d = F^{-1}\left(\sqrt[50]{p_d}\right) \quad (3)$$

$F^{-1}(\)$ denotes the inverse cumulative distribution function of the underlying distribution of the annual maxima. Note that $F^{-1}(\)$ is sometimes referred to as the quantile or fractile function in statistical literature. Partial factor for flows is consequently obtained as the ratio of the design value over the characteristic value.

Table 2 Estimated extreme flows in m³/s and partial factors.

	Characteristic value		Design value				Partial factor		
	Without q_{2002}		With q_{2002}		Without q_{2002}			With q_{2002}	
	Expect. $\gamma = 0.75$	Expect. $\gamma = 0.75$	Expect. $\gamma = 0.75$	Expect. $\gamma = 0.75$	Expect. $\gamma = 0.75$	Expect. $\gamma = 0.75$		Expect. $\gamma = 0.75$	Expect. $\gamma = 0.75$
Method of moments	3400	3600	3600	3900	9600	10600	10700	11800	2.8 – 3.1
Method of maximum likelihood	3700	4000	3800	4100	11400	12600	12000	13300	3.1 – 3.3

Estimated extreme flows and partial factors summarized in Table 2 indicate that:

- The extreme values predicted from the available data including the flow q_{2002} are greater than those estimated without this flow. The differences are by about 5-10 %.
- The extreme flows predicted by the method of maximum likelihood are greater than those obtained by the method of moments (by about 6-9 % for the characteristic value and 12-19 % for the design value).
- The upper fractiles estimated considering the commonly accepted 0.75 confidence level are greater than the expected upper fractiles (by about 6 % for the characteristic values and 11 % for the design values).
- The partial factor of about 3.0 derived from the data seems to be significantly greater than the recommended value 1.5.

Note that the data recorded since 1827 appears to provide a sufficiently large sample for estimating extreme flows by the method of maximum likelihood or method of moments. However, other available techniques such as the minimum cross-entropy method may be more suitable in case of smaller samples [7,8].

Expected return periods T_R corresponding to the flow q_{2002} are derived using the relationship

$$T_R = 1 / [1 - F(q_{2002})] \quad (4)$$

T_R is in years when F is the cumulative distribution function of annual maxima. Return periods estimated using the characteristics obtained by the method of moments are 350 and 240 years for the samples without and with q_{2002} , respectively. The maximum likelihood method leads to the return periods of 210 and 180 years. Apparently, the return periods are considerably influenced by the fact whether the flow q_{2002} is taken into account or not. Considering the sample without q_{2002} , the observed flow $q_{2002} = 5250 \text{ m}^3/\text{s}$ corresponds to the return period 210 years for the method of maximum likelihood that exceeds the commonly accepted return period 100 years. Note that estimates of a return period may significantly vary with a type of considered probability distribution [9].

It should be mentioned that this analysis is strictly based on the available data. Non-statistical influences that may have developed during the period covered by the measurements (since 1827) are not considered. In particular water flows may be strongly dependent on a river management including construction of polders, modifications of depth, width and roughness of a river channel and removal of vegetation, and local paved areas affecting local flood conditions. Effects of deforestation and other man-made interventions in environment should also be taken into account. It follows that a separate study is necessary to include these aspects in prediction of floods.

4 CAUSES OF STRUCTURAL FAILURES

Valuable experience has also been gained by investigation of structural failures due to flooding in 2002.

Hundreds of flooded structures in Prague including parts of the historic city as well as in countryside in the south and central Bohemia were inspected. These structures include public buildings (schools, office buildings, hotels, and churches), residential buildings (family houses and cottages) and few bridges. Main observed causes of structural damage due to the flooding, determined by visual inspections, can be subdivided into geotechnical and structural aspects. The geotechnical causes include:

- Insufficient foundation (depth, width - consequences indicated in Fig. 5),
- Underground transport of sediments and man-made ground (propagation of caverns),

- Increased earth pressure due to elevated underground water.

The major structural causes cover:

- Insufficient structural robustness (no ring beams as indicated in Fig. 6),
- Use of inadequate construction materials (unfired masonry units as shown in Fig. 7),
- Material property changes caused by moisture (volume, strength).



Figure 5 Damaged residential house with insufficient foundation.



Figure 6 Partial collapse of a residential house without ring beams.



Figure 7 Failure of a structure with unfired masonry units.

Note that multiple causes of failure have been identified in some cases. More detailed information intended to assist operational investigations of damage to flood-affected structures can be found elsewhere [10].

It is emphasized that the post-flood observations of failures are affected not only by flood actions, but also (and in some cases even more significantly) by structural properties. Experience gained from numerous assessments indicates that lack of structural robustness might have led to consequences of failures disproportionate to original causes due to flood actions. In general structural robustness may be improved by adequate:

- System of horizontal and vertical ties,
- Increased resistance of key members (a member essentially important for the structural robustness in the way that failure of this member implies a failure of a whole structure or significant parts of it),
- Secondary protection of key members,
- Invulnerable structural detailing (details insensitive to production quality).

For more details see [11].



Figure 8 construction of protective levees at the Danube river in Regensburg

5 RISK-BASED IMPLEMENTATION OF SAFETY MEASURES

As described in Handbook 1 methodologies of risk are imbedded in the reliability procedures, where concepts such as the consequences of different levels of failure provide the basis for assessment and verification design; or the classification of structures into reliability classes similarly reflect adjustment of performance levels for more important structures, where the consequences of failure are more severe as for example in case of floods.

The initial conceptual application of risk concepts in structural design is gradually being replaced by quantitative procedures, leading up to the application of risk optimization as analyzed in Handbook 1. The nature of a risk based approach is thereby illustrated by providing an outline of risk acceptance criteria and the application of risk concepts in performance based design procedures. The main characteristics of risk acceptance criteria, as shown in Handbook 1, are constant risk limits across the consequence and probability domain and dual upper and lower limits, with the intermediate “as low as reasonably possible” (ALARP) region to be determined by risk optimization. This scheme is conceptually consistent with present practice. Separate optimization procedures are applied for cost optimization and life safety.

It is important to consider the whole structure or system such as dam, port structure or bridge subjected to an extreme environmental hazard for example a storm or flood. From the optimization point of view it is useful to classify structures according to the possible consequences of collapse (i.e. global failure or failure of the main part of the structure).

The consequences include human, environmental and economic consequences. In many cases three consequence classes are proposed according to various standards (see Handbook 1):

- CC3: high consequences
- CC2: medium consequences
- CC1 low consequences

Risk acceptance can be implemented in a simplified way through the performance objectives which specify the acceptable or tolerable response of the structure to the extreme environmental hazard scenarios. They should be defined on a global level, that is, as acceptable extent of collapse of the whole system or of its main part for a hazard with a specified intensity (event size) and an associated return period.

Table 1 illustrates an example for a possible performance matrix in terms of acceptable degree of damage for the three consequence classes. Such a matrix forms the basis of performance-based design, for which global performance objectives are formulated. Local performance criteria can alternatively be used and substitute the aforementioned criteria for achieving global objectives.

Table 1 Performance analysis: Acceptable degree of potential damage

Event size	CC1	CC2	CC3
Very large	Severe	High	Moderate
Large	High	Moderate	Mild
Medium	Moderate	Mild	Mild
Small	Mild	Mild	Mild

Safety measures against floods include for example dams, levees, walls etc. The construction of a levee is shown in Fig 8. Such measures should be designed based on cost-benefit considerations including evaluation of human risk for example through the Implied Cost to Avert a fatality ICAF, the Societal Willingness To Pay SWTP and the Societal Value of Statistical Life SVSL. When conducting a cost-benefit-approach the ICAF value can be for example utilized for evaluating investments; in chapter 7 an expression for the evaluation of each individual safety measure was given as:

$$\frac{(C_{Ik} \delta(T))}{T} + C_{Ak} < ICAF dR_{Hk} + dR_{Ck} \tag{9}$$

where

- C_{Ik} investment cost;
- C_{Ak} annual maintenance/operation costs;
- T desired lifetime of measure;
- dR_{Hk} risk reduction due to measure k related to human risk;
- dR_{Ck} risk reduction due to measure k related to economic risk;
- $\delta(T)$ discount rate.

When the inequity is satisfied it means that the safety measure is beneficial. Note that the parameters entering the inequity are associated to significant variability and in many cases the risk reduction effect cannot be easily quantified. Probabilistic risk optimization based on the comparison of societal and economic consequences may provide valuable background information for a rational decision concerning effective safety measures applied to infrastructure for flood protection.

6 CONCLUSIONS AND RECOMMENDATIONS

The implementation of probabilistic and risk-based methods for the protection of aging infrastructure against floods has been discussed in this chapter. Presented statistical evaluation of the extreme annual flows provides valuable background information for assessments of flooded structures. It is indicated that:

- A lognormal distribution with the lower bound at the origin is a suitable theoretical model for the analysed sample, considering results of statistical tests and experience with distributions of flows in other localities.
- The characteristic and design values of flows predicted using data including the flow in 2002 are greater than those estimated without considering this flow (in most cases by about 5 %).
- Extreme flows predicted by the method of maximum likelihood are greater than those by the method of moments (by about 10 %).
- It follows from investigation of structural failures due to the flooding that:
- The main observed causes of structural damage may be subdivided into geotechnical and structural aspects.
- Lack of structural robustness might have led to failures of flooded structures disproportionate to original causes.

Based on the above conclusions, the following recommendations for design and assessment of structures and infrastructures potentially endangered by flooding are provided:

- Prior to decisions concerning safety of flooded structures, available data on flows should be carefully analysed since extreme flows predicted from measurements may considerably differ from those provided in standards.
- Appropriate safety measures such as levees, dams etc. should be planned based on risk principles and optimization procedures as described in Handbook 1.
- Especially robustness aspects and consideration of global failure should be considered at a design phase to reduce possible damage due to flooding.

REFERENCES

- [1] MACHEK J., TOMÁŠEK T., FOŠUMPAUR P. and SATRAPA L. Pražské metro a povodeň na Vltavě v srpnu v roce 2002 (Prague subway and the Vltava river flood in August 2002 - in Czech). *Inženýrská komora*, 2004, **8**, special issue, 12-26.
- [2] RODDA H. J. E. The Development and Application of a Flood Risk Model for the Czech Republic. *Natural Hazards*, 2005, **36**, No. 1-2, 207-220.
- [3] HOLICKÝ M. and SÝKORA M. Forensic investigation of fluvial flood damage in the Czech Republic. *Proceedings of the Institution of Civil Engineers: Civil Engineering*, 2009, **162**, Number May 2009 – Special issue on forensic engineering, 33-37.
- [4] ANG A. H. S. and TANG W. H. *Probabilistic Concepts in Engineering Emphasis on Applications to Civil and Environmental Engineering*. 2nd Ed. John Wiley & Sons, Inc., 2007.
- [5] ISO (International organization for Standardization). *ISO 12491:1997, Statistical methods for quality control of building materials and components*. 1st Ed. ISO, 1997.
- [6] CEN (European Committee for Standardization). *EN 1990:2002 Eurocode - Basis of structural design*. CEN, 2002.

- [7] LIND N. C., HONG P. and SOLANA V. A cross entropy method for flood frequency analysis. *Stochastic Environmental Research and Risk Assessment*, 1989, **3**, No. 3, 191-202.
- [8] PANDEY M. D. Extreme quantile estimation using order statistics with minimum cross-entropy principle. *Probabilistic Engineering Mechanics*, 2001, **16**, No. 1, 31-42.
- [9] HOLICKÝ M. and SÝKORA M. Probabilistic Evaluation and Prediction of Discharges on the Vltava River in Prague. *CTU Reports (Vol. 8, No. 3), Proceedings of 3rd Czech/Slovak Symposium "Theoretical and Experimental Research in Structural Engineering"*. CTU, 2004, 47-52.
- [10] KELMAN I. and SPENCE R. An overview of flood actions on buildings. *Engineering Geology*, 2004, **73**, No. 3-4, 297-309.
- [11] Canisius T. D. G. (ed.) *COST TU0601 – Structural Robustness Design for Practising Engineers*. JCSS, 2011
- [12] HOLICKY M. *Introduction to Probability and Statistics for Engineers*. 1st ed. Springer, 2013.

